



HAL
open science

Control of the rheological properties of chocolate suspensions by optimizing the morphological properties of the particles

Janine Deou

► **To cite this version:**

Janine Deou. Control of the rheological properties of chocolate suspensions by optimizing the morphological properties of the particles. Materials Science [cond-mat.mtrl-sci]. Université Gustave Eiffel, 2021. English. NNT : 2021UEFL2012 . tel-03546225

HAL Id: tel-03546225

<https://theses.hal.science/tel-03546225>

Submitted on 27 Jan 2022

HAL is a multi-disciplinary open access archive for the deposit and dissemination of scientific research documents, whether they are published or not. The documents may come from teaching and research institutions in France or abroad, or from public or private research centers.

L'archive ouverte pluridisciplinaire **HAL**, est destinée au dépôt et à la diffusion de documents scientifiques de niveau recherche, publiés ou non, émanant des établissements d'enseignement et de recherche français ou étrangers, des laboratoires publics ou privés.



**CONTROL OF THE RHEOLOGICAL
BEHAVIOUR OF CHOCOLATE
SUSPENSIONS BY OPTIMIZING THE
MORPHOLOGICAL PROPERTIES OF THE
PARTICLES**

A THESIS PRESENTED BY

JANINE DEOU

To

UNIVERSITÉ PARIS EST
ÉCOLE DOCTORALE SCIENCES, INGÉNIERIE ET ENVIRONNEMENT

IN PARTIAL FULFILLMENT OF THE REQUIREMENTS FOR THE DEGREE
OF DOCTOR OF PHILOSOPHY IN

MATERIALS SCIENCE

COMMITTEE MEMBERS:

M. XAVIER CHATEAU	JURY PRESIDENT
M. PETER FISCHER	THESIS REVIEWER
M. CHRISTOPHE LANOS	THESIS REVIEWER
M. PAUL SMITH	THESIS EXAMINER
M. JOEL WALLECAN	THESIS EXAMINER
M. FABIEN DECLERCQ	THESIS INVITEE
MME. HELA BESSAIES-BEY	THESIS CO-SUPERVISOR
M. NICOLAS ROUSSEL	THESIS SUPERVISOR

CHAMPS-SUR-MARNE, FRANCE, 5 FEBRUARY 2021

Abstract

The objective of this thesis is the formulation of fat-reduced chocolate and emulsifier free chocolate without affecting the viscosity and yield stress of the melt chocolate. To achieve these objectives, we control the rheological behaviour of chocolate suspensions by optimizing the morphological properties (particle size distribution, particle shape and maximum packing fraction) of sugar and cocoa powders.

First, we develop appropriate protocols for the characterization of the morphological and rheological properties of chocolate suspensions.

Then, we study the effect of the production process on the rheological and morphological properties of chocolate and show that viscosity depends on relative solid volume fraction (i.e., solid volume fraction to maximum packing fraction ratio) while yield stress depends on relative solid volume fraction and is inversely proportional to the particle mean size. Our experimental results show that the viscosity of melt chocolate suspension (i.e., sugar, cocoa, sugar and cocoa suspensions) can be related to the solid volume fraction and the maximum packing fraction by the phenomenological Krieger-Dougherty type equation.

Moreover, we show that the maximum packing fraction of cocoa and sugar powders can be well predicted by the compressive packing model developed for the optimization of the mineral powdery materials used in construction materials.

Finally, we exploit these results and models to attain the objectives of this thesis. We show that an accurate control of maximum packing fraction by adding “fine” cocoa particles allows for the decrease of the amount of fat in chocolate without affecting viscosity and chocolate solid composition. We moreover show that an accurate control of particle average size and maximum packing fraction by adding “coarse” sugar particles allows for the removal of the emulsifiers from chocolate without increasing the fat content of the suspension and affecting the viscosity and yield stress.

Keywords: viscosity, yield stress, maximum packing fraction, particle size distribution optimization.

Résumé

L'objectif de cette thèse est de formuler du chocolat à faible taux de matières grasses et du chocolat sans additives sans affecter les propriétés rhéologiques (viscosité et seuil) du chocolat fondu. Pour atteindre ces objectifs, nous contrôlons le comportement rhéologique des suspensions de chocolat en optimisant les propriétés morphologiques (granulométrie, forme des particules et fraction de garnissage maximale) des poudres de sucre et de cacao.

Tout d'abord, nous développons des protocoles appropriés pour la caractérisation des propriétés morphologiques et rhéologiques des suspensions de chocolat.

Ensuite, nous étudions l'effet du procédé de production sur les propriétés rhéologiques et morphologiques du chocolat et montrons que la viscosité dépend de la fraction volumique solide relative (c'est-à-dire le rapport fraction volumique solide / compacité maximale) tandis que le seuil dépend de la fraction volumique solide relative et est inversement proportionnelle à la taille moyenne des particules. Nos résultats expérimentaux montrent que la viscosité de la suspension de chocolat fondu peut être liée à la fraction volumique solide et à la compacité maximale par l'équation phénoménologique de type Krieger-Dougherty.

De plus, nous montrons que la compacité maximale des poudres de cacao et de sucre peut être bien prédite par le « Compressible Packing Model » développé pour l'optimisation des matériaux de construction.

Enfin, nous exploitons ces résultats et modèles pour atteindre les objectifs de cette thèse. Nous montrons qu'un contrôle précis de la compacité maximale en ajoutant des particules de cacao « fines » permet de diminuer la quantité de matière grasse dans le chocolat sans affecter la viscosité et la composition solide du chocolat. Nous montrons en outre qu'un contrôle précis de la taille moyenne des particules et de la compacité maximale par l'ajout de particules de sucre « grossières » permet d'éliminer les additives présents dans la suspension de chocolat sans augmenter la teneur en matière grasse de la suspension et affecter la viscosité et le seuil.

Mots clés : viscosité, seuil, compacité maximale, optimisation de la distribution de taille des particules.

Introduction

Introduction

In our society, offering food products containing less calories and less additives are a long-term trend in response to consumer's demand. Even though chocolate cannot be considered as a staple food, it remains one of the most consumed food products in the world, especially in Europe. In 2017, 8.8 kg of chocolate are consumed per capita in Switzerland, and 5.1 kg in the Netherlands [1]. Melt chocolate can be defined as a suspension of sugar, cocoa and milk solid particles in fat continuous medium that is mainly cocoa butter [2, 3]. Depending upon the industrial application, between 27% to 40% by total mass of chocolate consists of fat that corresponds both to the highest caloric ingredient [4] and to the most expensive one. The caloric amount varies between 510 and 530 kcal per 100 g [5]. Therefore, reduced-fat chocolate will provide an attractive alternative for consumers. However, reducing the fat amount is equivalent to taking out a fraction of the continuous fluid phase of chocolate. It therefore causes an increase in chocolate rheological properties (i.e., yield stress and viscosity) [6, 7]. This, in turn, may lead to difficulties in processing for operations like moulding or enrobing, for instance [4]. An increase of yield stress and viscosity may also lead to an unpleasant, pasty mouthfeel [8].

In literature, there are several approaches to decrease the amount of fat in chocolate while keeping desirable flow properties. One of them is the use of emulsifier blends to increase emulsifier levels in chocolate [9]. Do et al. [10] have used polymers as stabilizer in fat-based food suspensions as an example of reduced-fat chocolate. Another method is the replacement of the fat continuous phase by a water-in-oil emulsion. Hulgelshofer [11] has demonstrated that emulsion-based chocolates show similar sensory properties to conventional ones. However, these chocolates exhibit poor stability (sugar bloom on their surface) and cannot be manufactured using the existing assets of chocolate plants. Fat replacers can also be used even though their level of addition is restricted due their non-digestibility by the consumer [12]. The optimization of the particle size distribution of sugar and cocoa allows for a control of rheology without modifying the composition of chocolate [5, 13-15]. Feichtinger et al. [5] have showed that it is possible to decrease the fat amount of chocolate by using model chocolates with varying particle size distribution and size ratios. They have showed that bimodal particle size distribution (specific blend of fine and coarse particles) leads to a higher maximum packing fraction, and thus lower viscosity. The same observation is highlighted by the studies of [13-15] on chocolate and those of [16, 17] on mustard and nut paste respectively.

The objective of this thesis is therefore the formulation of fat-reduced chocolate and emulsifier-free chocolate without affecting the rheological properties (viscosity and yield stress) of the suspensions. To achieve these objectives, we aim at controlling the rheological behaviour of melt chocolate suspensions by optimizing the morphological properties (size distribution, shape and maximum packing fraction) of both sugar and cocoa particles. We

optimize the maximum packing fraction using a compressive packing model from literature, which has been developed for the optimization of cement-based materials in the construction industry.

To the best of our knowledge, unlike reduced-fat chocolate, the particle size optimization has never been used as a method to formulate emulsifier-free chocolate. It is also important to note that, for the sake of simplicity, we deliberately choose here to only study dark chocolate. Indeed, the two other types of chocolate (milk and white) contain soft and deformable particles of dairy products, which are outside the scope of most rigid particles packing optimization models.

In a first chapter, we present a review of literature on chocolate and its rheological behaviour. We describe the interactions between cocoa and sugar particles in oil, the parameters governing the rheological behaviour of chocolate suspensions and the effect of other components such as water and emulsifier on the rheological behaviour. We also describe the main production processes influencing chocolate rheological (viscosity and yield stress) and morphological (particle size distribution, particle shape, maximum packing fraction) properties.

In a second chapter, we describe the experimental protocols developed to characterize the morphological, physical and rheological properties of the chocolate suspensions studied in this thesis. We highlight the problems encountered, the choices made and, therefore, the reasoning followed, in order to develop protocols deemed suitable for observation and analysis of the studied materials.

In a third chapter, we present the chocolate suspensions studied in this thesis and the processes followed to produce them. We assess the evolution of the morphological and rheological properties of these chocolate suspensions over the production process and qualitatively analyse our results.

In a fourth chapter, we highlight the fact that the suspensions studied in this thesis are following the theoretical predictions about the principle of the rheology of concentrated suspensions. We show that the viscosity of the suspensions depends only on their relative solid volume fraction (i.e., solid volume fraction to maximum packing fraction ratio) and seems therefore to be mainly governed by hydrodynamics viscous dissipations. We also highlight a dependency of yield stress on the relative solid volume fraction, but also on the average particle size.

In a fifth chapter, we show that the Compressive packing Model [18], a packing model initially developed for cement-based materials, can be used to predict and optimize the maximum packing fraction of sugar and cocoa particles.

Finally, in the sixth and last chapter, we exploit these results and models to get closer to the objectives of this thesis. We show that an accurate control of maximum packing fraction by adding “fine” cocoa particles allows for the decrease in the amount of fat in chocolate without affecting viscosity and chocolate solid composition. We moreover show that an accurate control of particle mean size and maximum packing fraction by adding “coarse” sugar particles allows for the removal of the emulsifiers from chocolate without increasing the fat content of the suspension and without affecting viscosity and yield stress.

References

- [1] Statista, <https://www.statista.com/statistics/819288/world-wide-chocolate-consumption-by-country/>, (accessed October 2018).
- [2] Beckett, S.T. *The science of chocolate*, Royal Society of Chemistry, 2018.
- [3] Servais, C.; Jones, R.; Roberts, I. *J. Food Eng.* 2002, 51, 201–208.
- [4] Schakel, S.F.; Jasthi, B.; Van Heel, N.; Harnack, L. *J. Food Compos. Anal.* 2009, 22, S32–S36.
- [5] Feichtinger, A.; Scholten, E.; Sala, G. *Food Func.* 2020, 11, 9547-9559.
- [6] Hartel, R.W.; Joachim, H.; Hofberger, R. *Confectionery science and technology*, Springer, 2018.
- [7] Beckett, S.T. *Industrial chocolate manufacture and use*, John Wiley & Sons, 2011.
- [8] Gonçalves, E.V.; Lannes, S. C. d. S *Food Sci. Technol.* 2010, 30, 845–851.
- [9] Kaiser, J.M.; Gestel, A.V.; Vercauteren, J. U.S. Patent WO 99/45790, 1999.
- [10] Do, T-A.L.; Mitchell, J.R.; Wolf, B.; Vieira, J. *Reactive & Functional Polymers* 2010, 70, 856-862.
- [11] Hugelshofer, D. Structural and rheological properties of concentrated suspensions mixed with an emulsion. Ph.D. Dissertation, Zurich, ETH, 2000.
- [12] Beckett, S.T. *Industrial Chocolate Manufacture and Use*, 3rd edition, Blackwell Science, Oxford, 1999.
- [13] Do, T.A.L.; Hargreaves, J.M.; Wolf, B.; Mitchell, J.R. *J. Food Sci.* 2007, 72, 541-552.
- [14] Mongia, G.; Ziegler, G.R. *Int. J. Food Properties* 2000, 3, 137-147.
- [15] Kaiser, J.M.; Purwo, S. U.S. Patent WO 99/45790.
- [16] Aguilar, C.A.; Rizvi, S.S.H.; Ramirez, J.F.; Inda, A. *J Texture Stud.* 1991, 22, 59–84.
- [17] Villagran, F.V.; McCabe, G.M.; Wong, V.Y.L. U.S. Patent 5490999, 1996.
- [18] de Larrard, F. *Concrete Mixture Proportioning: a scientific approach*, E&FN SPON: An imprint of Routledge, London and New-York, 1999.

Chapter 1: Review of literature

Table of contents

1.1	Chocolate history.....	10
1.2	Chocolate ingredients.....	11
1.2.1	Cocoa beans, cocoa powder and cocoa butter.....	11
1.2.2	Sugar and its derivatives.....	12
1.2.3	Milk and other dairy components	13
1.2.4	Other ingredients	14
1.3	Chocolate production process.....	15
1.3.1	Mixing	1616
1.3.2	Refining.....	17
1.3.3	Conching.....	1818
1.4	Interaction within chocolate suspension.....	1919
1.4.1	Interactions occurring between sugar particles	19
1.4.1.1	Attractive forces	19
1.4.1.2	Repulsive forces.....	20
1.4.1.2.1	Effect of emulsifier: steric forces	21
1.4.1.2.2	Structural forces.....	21
1.4.2	Interactions occurring between cocoa particles.....	24
1.5	Chocolate rheology.....	24
1.5.1	Typical rheological behaviour of chocolate suspension	24
1.5.2	Effect of inter-particle interactions	28
1.5.3	Effect of particle size distribution.....	31
1.5.4	Effect of solid volume fraction.....	32
1.5.5	Understanding the microscopic origin of the rheological behaviour of chocolate suspension during production.....	33
1.6	Chocolate particle size distribution optimization	34
1.6.1	Principle of concentrated suspensions rheology.....	35
1.6.2	Parameters influencing the maximum packing fraction.....	36
1.7	Conclusion	39
	References.....	40

1.1 Chocolate history

Chocolate is well-known fat-based food product of the 21st century. In order to enhance its popularity amongst the different civilisations, it has undergone various changes in production process and flavour throughout its history. Originated from the Maya civilisation in Southern and Central America, chocolate comes from the cocoa bean produced by *Theobroma cacao* trees and was first produced in Mexico and Peru [1, 2]. Chocolate was mainly mixed with cold water and consumed as a drink by the Mayans [3-5].

The conquistadors, Christopher Columbus and Herman Cortès bought back some cocoa beans to Europe especially in Spain as a curiosity in the 1520s [6]. Here sugar was added to overcome the bitterness of the Mayan's drink. The drink remained virtually unknown in the rest of Europe for almost a hundred years, coming to Italy in 1606 and France in 1657. It was very expensive and, being a drink for the aristocracy, its spread was often through connections between powerful families. In 1727, milk was being added to the drink. This invention is generally attributed to Nicholas Sanders [7].

One problem with the chocolate drink was its fattiness [6]. Over half of the cocoa bean being made up of cocoa butter, this will melt in hot water making the cocoa particles hard to disperse as well as looking unpleasant, because of fat coming to the surface. The Dutch, however, found a way of improving the drink by removing part of this cocoa butter. In 1828, Van Houten developed a quite remarkable technique known as the Dutching process [6]. This technique is a hydraulic press based on the process of boiling and skimming the beans that would remove most of the cocoa butter and produce a "cake". The "cake" was then ground into a powder used to produce much less fatty drink.

In 1847, Fry had the idea of blending cocoa powder and sugar with melted cocoa butter instead of warm water [6]. By adding additional cocoa butter to the blends, the first chocolate bar was formed. Meanwhile in Switzerland, Sanders formulated the first drinkable milk chocolate by mixing hot chocolate liquor and hot milk. By using Sanders and Fry's processes, Nestlé created the first milk chocolate bar in 1879. Further improvements were made to this chocolate bar in order to extend its shelf life (longer than 3 months) and its quality. Lindt, in 1879, invented the conching process, which pushed the warm chocolate backwards and forwards for a certain length of time. This process led to a glossy appearance on the material surface and a tastier chocolate. Along the centuries, three main and different types of chocolates involving different production processes and ingredients were created: dried chocolate also known as cocoa powder, dark chocolate, white chocolate and milk chocolate.

1.2 Chocolate ingredients

Chocolate is a suspension mainly composed of cocoa powder, sugar particles, and eventually milk powder suspended in cocoa butter. Cocoa powder and cocoa butter are produced from the drying, grinding and roasting of the cocoa beans. Sugar and its derivatives are required for the chocolate sweetness and milk, for the making of milk chocolate.

1.2.1 Cocoa beans, cocoa powder and cocoa butter

The production of cocoa beans is mainly carried out in Western Africa, South East Asia and Latin America. These continents have the proper climate (relatively high humidity and temperature) required for the maturation of the cocoa pods and nuts of cocoa trees. Up to 6 months are required to mature a pod, and it contains approximately 40 cocoa beans after full maturation. Cocoa pods are generally 20 cm long and 15 cm wide. Once the beans are removed from the pods, they contain about 55% fat, and 45% moisture. In order to use these beans for the production of chocolate, several process treatments are required. The most important one being the decrease of the moisture content. Indeed, a raw cocoa bean is differentiated from a bean ready for chocolate production by its moisture content. Two processes need to be carried out in order to decrease the moisture content: fermentation and drying.

Fermentation is usually carried out by piling the beans in wooden boxes or baskets covered by banana or plantain leaves. The purposes of this process are the liquefaction of the pulp surrounding the beans, the avoidance of seed germination and the development of the final flavour of chocolate. It should be specified that it is not the beans that are fermented but the pulp that surrounds them. Drying allows decreasing the moisture content in the beans from 60% to 7%. This reduction of moisture content to 7% is essential in order to avoid the growth of moulds within the beans (when moisture content is above 7%) or a brittleness of the beans (when moisture content is under 7%) during storage. Drying also allows some of the chemical changes, which occur during fermentation to continue and improve flavour development. There exist various methods of drying that can be classified in two classes: natural or sun-drying and artificial drying [8]. At this stage, beans are ready for further processing such as grinding, milling and roasting leading to the production of cocoa mass, which is the paste, produced when the beans are roasted and ground. This paste is then ground with hydraulic press (Dutching process) or expeller extrusion to produce cocoa powder and cocoa butter.

Most cocoa powders contain 20-22% fat by mass, but lower fat range can also be found (15-17% or 10-12%). A defatted (i.e., fat-free) cocoa powder can also be produced. Cocoa butter is composed of triacylglycerols, commonly called triglycerides (i.e., they have three fatty acids attached to a glycerol backbone). Cocoa butter can exist and crystallize in six different crystalline and polymorphic forms (often denoted by Roman numbers I-IV), each of which exhibits different thermodynamic stability and melting temperatures [9, 10]. This confers to

chocolate its most interesting sensory property and is what makes it melt relatively rapidly in the mouth without becoming grainy. The overall production process of cocoa powder and cocoa butter is represented in Figure 1-1 [11].

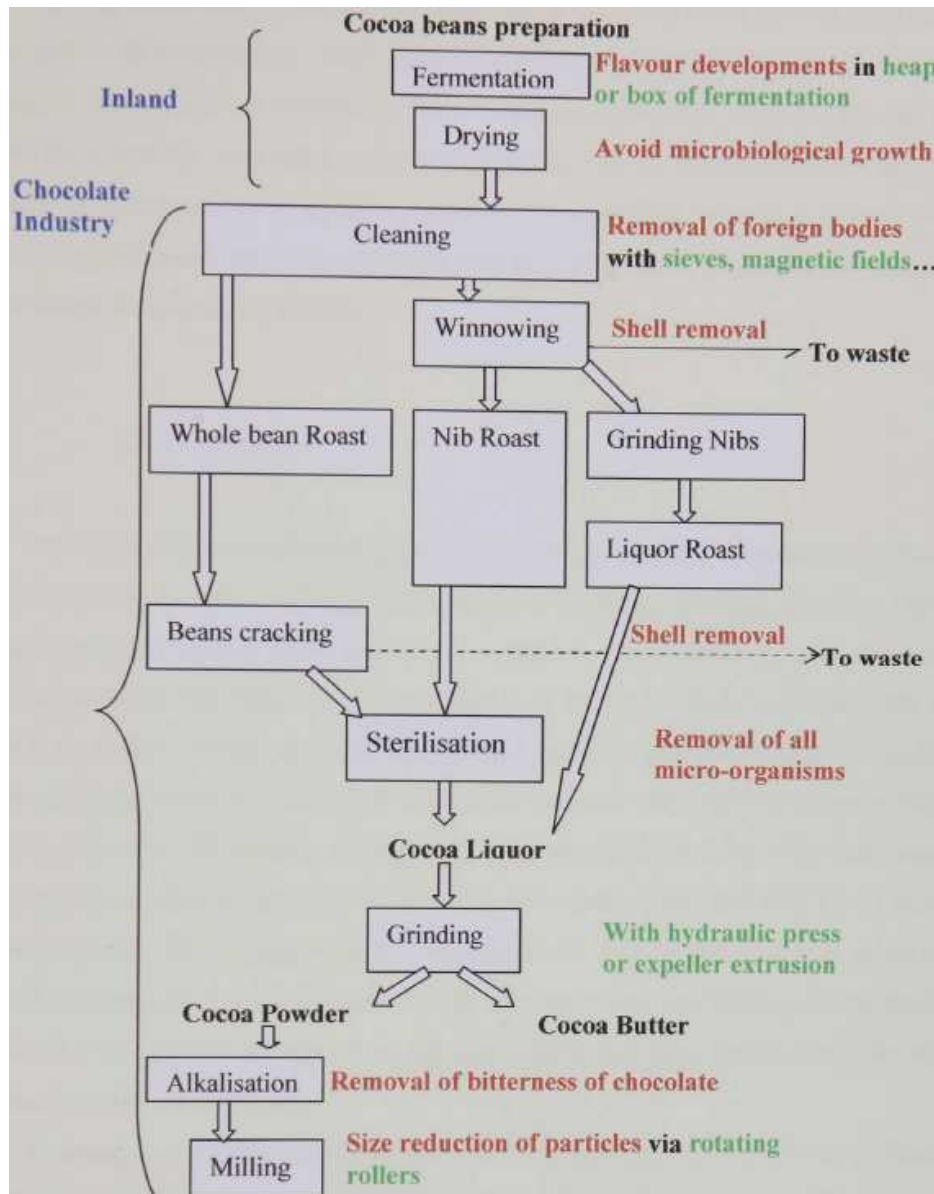


Figure 1-1. Schematic representation of the production processes of cocoa butter and cocoa powder extracted from [11].

1.2.2 Sugar and its derivatives

Sugar accounts for about 50% by mass of chocolate [12]. The sugar used to produce chocolate is mainly sucrose (also known as saccharose), but lactose originated from dairy products is also present in milk chocolate. Sucrose, a disaccharide molecule composed of two single sugars (monosaccharide) chemically linked together is produced from both sugar beet and sugar cane. Both give the same natural crystalline disaccharide material. The monosaccharides

are glucose and fructose, and they are present in the same proportion in sucrose. Lactose is also a disaccharide and is made up of a combination of glucose and galactose. Sugar alcohols, like sorbitol, can also be used as sugar substitutes in the making of chocolate. In the present study, the sugar particles studied are only sucrose since we only study dark chocolate. The chemical formula of sucrose is shown in Figure 1-2.

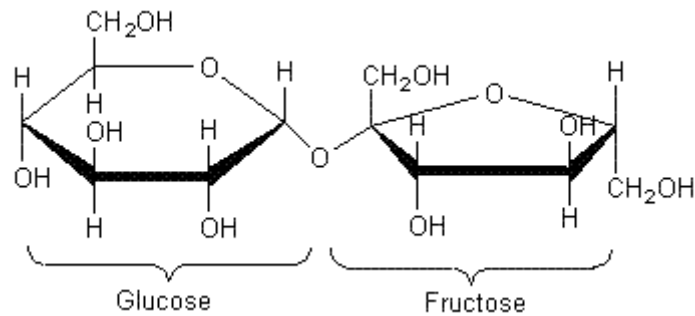


Figure 1-2. Chemical formula of sucrose.

The particle size distribution of sucrose is extremely important as it substantially alters the sensorial qualities of the final chocolate product [13]. The size of sugar particles decreases during process. The particle size decreases from 1000-600 μm to 100-200 μm during pre-refining and from 100-200 μm to 18-45 μm during refining.

1.2.3 Milk and other dairy components

The most consumed chocolate worldwide is milk chocolate. Usually used in its dehydrated form, milk represents 13.5% by mass of milk chocolate. In this 13.5%, we have around 5% of lactose, 4.3% of milk fat, approximately 3.5% of proteins, and about 0.7% minerals, of which calcium, in particular, is considered beneficial to health.

Milk fat is essentially composed of 98% of triglycerides. The other 2% is made up of diglycerides (2 fatty acids + glycerol), sterols and phosphoglycerides (primarily lecithin). It plays an important role as a texture and flavor enhancer and improves the flowability of chocolate. Moreover, milk fat also allows slowing down the setting rate of the liquid chocolate at the end of production.

The proteins provide nutrients, but also impart flavor, texture and the flow properties of chocolate: low amounts of proteins make the products grainier, and if they are exposed to high temperatures, the Maillard reaction [6, 14] may take place giving a cooked flavor to the chocolate. The most common protein found in milk is casein, which has emulsifying and water-binding properties beneficial to the flowability of chocolate [6].

Skimmed milk powder (SMP) is the most common dairy powder used in chocolate. Spray drying or roller drying can be used to produce SMP. Despite the skimming, this milk always contains at least 1% fat content. This fat is important as it helps decreasing the viscosity and

yield stress of chocolate during production. Spray-dried powders are spherical (with a median particle size of 30-80 μm) and the fat is contained within them. In roller drying, the particles are larger (about 150 μm), and most of the fat remains on the surface of the particles. Rolled dried milk powder is usually preferred because of its high free-fat (i.e., fat not enclosed into the particles) level, greater than 95% by total mass of fat in the milk powder [15]. This high level of free fat allows to not add some additional cocoa butter in order to decrease viscosity during production. When spray dried milk powder is used, 2 to 2.5% additional cocoa butter by mass of chocolate is required to provide the same flow properties as roller dried powder [8]. In addition to SMP, there is other types of milk powders that can be used: the whole milk powder (WMP) and the high-fat milk powder.

1.2.4 Other ingredients

There are other various additional ingredients such as emulsifiers [16, 17], water [18], and minor surface-active components present in cocoa butter [19]. Emulsifiers are used to improve the flow properties of the melted chocolate (i.e., decrease the viscosity and yield stress of melted chocolate) and stabilize the suspension throughout its shelf life. Besides the flow properties, emulsifiers also influence the microstructural properties of chocolate as well as its sensitivity to moisture and temperature. Two emulsifiers are mainly used in chocolate recipe: soy lecithin and polyglycerol polyricinoleate (PGPR).

Lecithin is naturally occurring surface-active molecules that is extracted from a variety of sources, including soybeans, milk, rapeseed, and egg [20-23]. Lecithin isolated from natural sources contain a complex mixture of different types of phospholipids and other lipids. The most common phospholipids in lecithin are phosphatidylcholine (PC), phosphatidylethanolamine (PE), and phosphatidylinositol (PI). The hydrophilic head of these molecules are either anionic (PI) or zwitterionic (PC and PE), whereas the lipophilic tail consists of two fatty acids (see Figure 1-3).

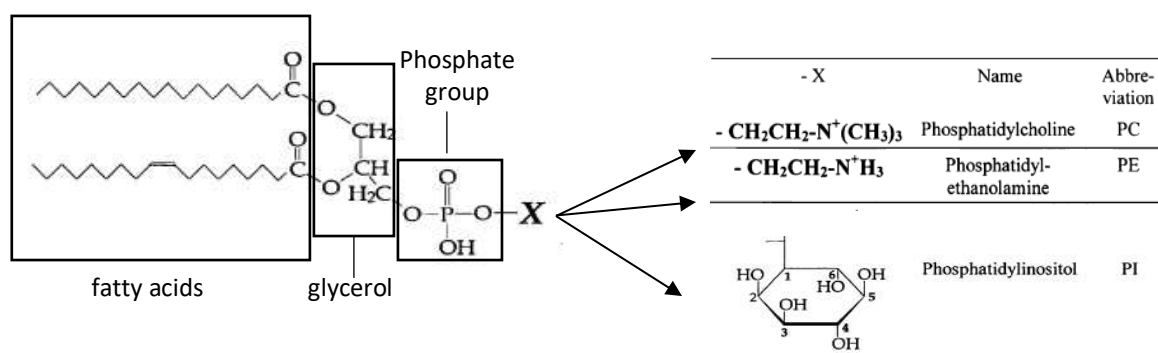


Figure 1-3. General structural formula of Lecithin.

Generally, soybean lecithin is used in chocolate production. The structure of soybean lecithin is represented in Figure 1-4. Glycerol, which contains three carbon atoms, serves as the backbone of the lecithin molecule. The two fatty acids are linked to glycerol at carbon atoms 1 and 2 and the phosphate group is linked to carbon atom 3. Choline is linked to the phosphate group. Typically, though not always, the fatty acid attached to carbon 1 of glycerol is saturated, while that attached to carbon 2 is unsaturated. The molar mass of soy lecithin is 759 g/mol.

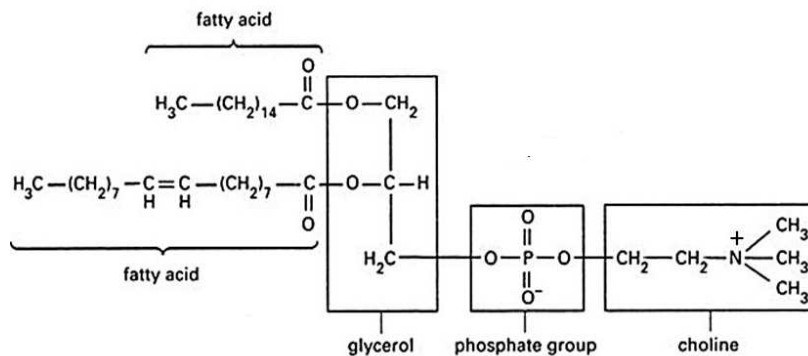


Figure 1-4. Chemical structure of soybean lecithin.

Unlike lecithin that is extracted naturally, polyglycerol polyricinoleate (PGPR) is a synthetic molecule produced by the esterification reaction of polymerized glycerol with condensed castor oil fatty acids [24]. Most commercial samples are far from being monodisperse, and include a variety of hydrogen, fatty acid and polyricinoleic acid esters of polyglycerol [25]. PGPR is commonly used in chocolate production, due to its excellent water-binding properties that inhibit the thickening of chocolate in the presence of undesired inclusions of water [24]. The general chemical formula is shown in Figure 1-5.

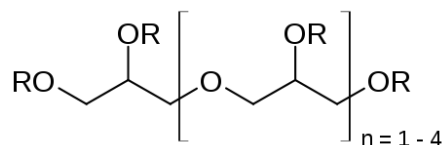


Figure 1-5. General chemical formula of PGPR, subjected to production process. R can be hydrogen atoms, ricinoleic acid and/or poly-ricinoleic acid residues. If $n=1$ and R is poly-ricinoleic acid, the molar mass of PGPR is 1356 g/mol, and if $n=4$, the molar mass is 2472 g/mol.

1.3 Chocolate production process

Since in this thesis, we are only interested in studying the morphological and rheological properties of the final chocolate product, we will only focus on the production steps (mixing,

refining and conching) influencing these properties on an industrial scale. Figure 1-6 represents the overall industrial production process.

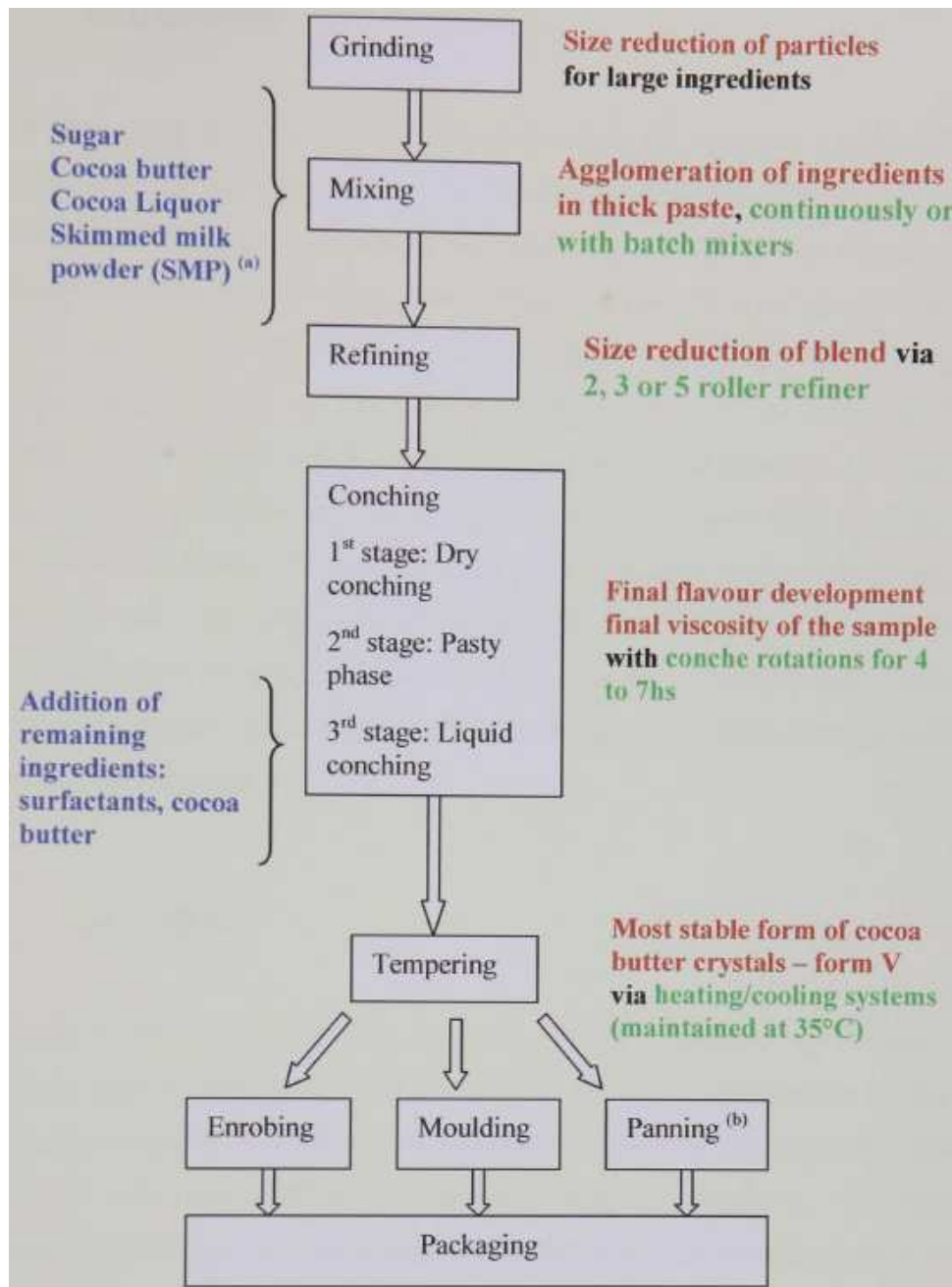


Figure 1-6. Chocolate industrial production process extracted from [11].

1.3.1 Mixing

The first step of chocolate production on an industrial scale is mixing. Mixing is a fundamental operation employed using time–temperature combinations in a continuous or batch mixer to obtain constant formulation consistency. In batch mixing, chocolate containing cocoa liquor, sugar, cocoa butter, milk fat and milk powder (depending on product category) is thoroughly

mixed normally for 12 to 15 minutes at 40–50°C. At the end of this step, we should obtain a thick paste, which is crucial for the rest of the production process. Beckett [13] stated that this thick paste should possess a rough texture and have a plastic consistency.

1.3.2 Refining

Refining of chocolate is important as it allows for the production of the smooth texture that is desirable in chocolate confectionery. The principle is to push the thick paste obtained after mixing through rollers with defined gap in order to decrease the particle size below 30 μm normally using a combination of two- and five-roll refiners. Final particle size critically influences the rheological and sensory properties. A five-roll refiner (Figure 1-7) consists of a vertical array of four hollow cylinders, temperature controlled by internal water flow, held together by hydraulic pressure. A thin film of chocolate is attracted to increasingly faster rollers, travelling up the refiner until removed by a knife blade. Roller shearing fragments solid particles, coating new surfaces with lipid so that these become active, absorbing volatile flavour compounds from cocoa components.

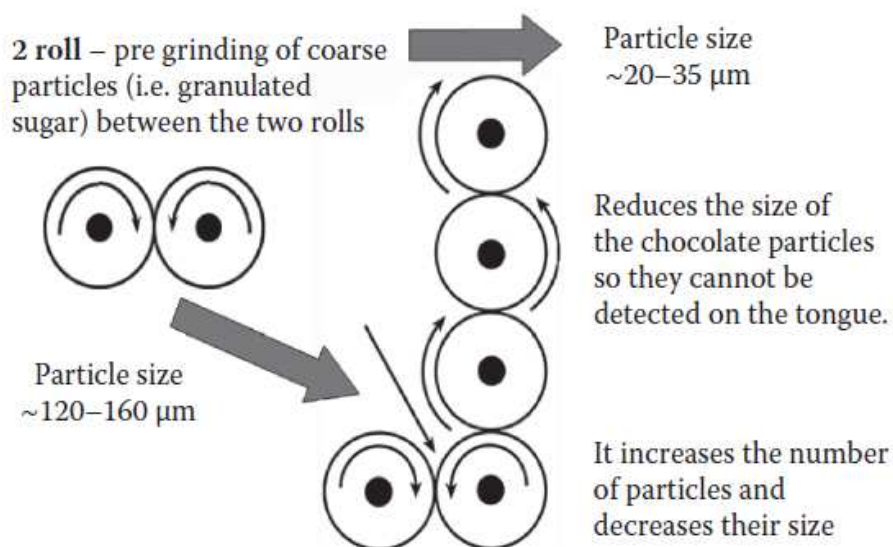


Figure 1-7. Two- and five-roll refining processes extracted from [8].

Each roller is thermostatically controlled via inner cooling/heating systems. The temperature plays an important role. For instance, if the roller is too cold, the fat will crystallize on it. The average size of the particles obtained in the final production step depends greatly on the gap between rollers, the speed of the refining rollers, and the original size of the particles [26, 12, 13]. Refiners, in summary, not only lead to particle size reduction and agglomerate breakdown but also allow for the distribution particles through the continuous phase, coating each with lipid.

1.3.3 Conching

Conching, generally considered to be the final step in chocolate production, is an essential process that contributes to the decrease in viscosity, the change in flavor of the chocolate as well as the way it melts in the mouth [12]. Conching is normally carried out at a temperature above 50 ° C for a few hours. As explained by Beckett [6], the conching process can be divided into two distinct processes. The first is flavour development. The fermentation and roasting processes produce the flavour components required to give chocolate its pleasant taste, but they also result in some unwanted flavoring volatiles such as acetic acid that need to be removed. The second process is to turn the chocolate from a powder or thick dry paste into a liquid chocolate. Afoakwa [8] stated that in addition to the removal of volatile acids, the first process also allows the evaporation of moisture and favors the interactions between the dispersed particles and the continuous fat phase and the second process also leads to a reduction in the viscosity as well as a reduction in particle size and the elimination of particle edges.

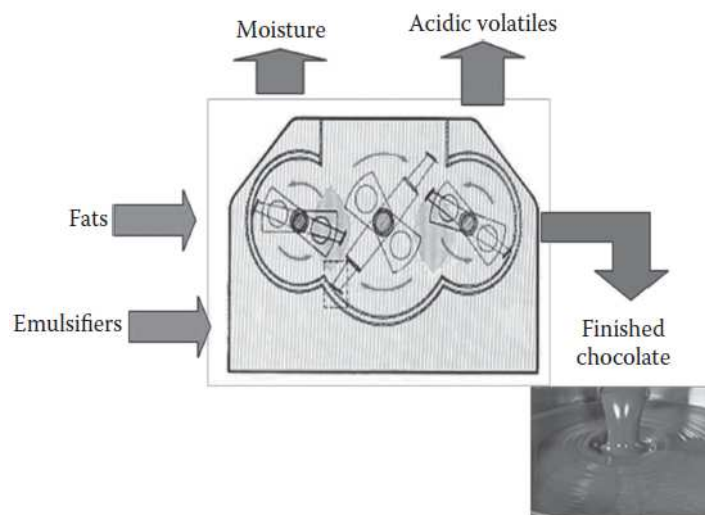


Figure 1-8. Internal mechanics of the Frisse conche extracted from [8].

The name of the machine, the “conche”, is derived from the Latin word for ‘shell’, as the traditional conche used in chocolate manufacture resembled the shape of a shell. Figure 1-8 is an illustration of the Frisse conche. The Frisse conche is a typical example of an overhead conche used in chocolate industry. It consists of a large tank with three powerful inter-meshing mixer blades, providing shearing and mixing action. To give chocolate a suitable viscosity, additional cocoa butter and lecithin can be added at the end of conching to thin or liquefy the chocolate prior to tempering [12, 27].

1.4 Interaction within chocolate suspension

1.4.1 Interactions occurring between sugar particles

Sugar surfaces being hydrophilic (i.e., attract water and repel fat), they tend to agglomerate in cocoa butter. In literature, studies were carried out to highlight the attractive forces occurring between sugar particles in an oil media by using Atomic Force Microscopy (AFM) [28-32]. These studies highlighted the existence of adhesive forces [28] and capillary forces [29-32] between surfaces. However, they also show that emulsifiers are at the origin of repulsive interactions between the particles.

1.4.1.1 Attractive forces

Arnold et al. studied the interaction between sugar particles in different food oils using Atomic Force Microscopy (AFM) [28]. Their results show that no attractive force is detected until the sugar particles are brought into contact, and they remain in contact until a detachment force F_D is reached. This detachment force corresponds to the adhesive force between the particles when they are in contact. They concluded from their results that adhesive forces of magnitude 2.5 nN dominate the interactions between sugars particles in oil-based suspensions. Figure 1-9 shows their results.

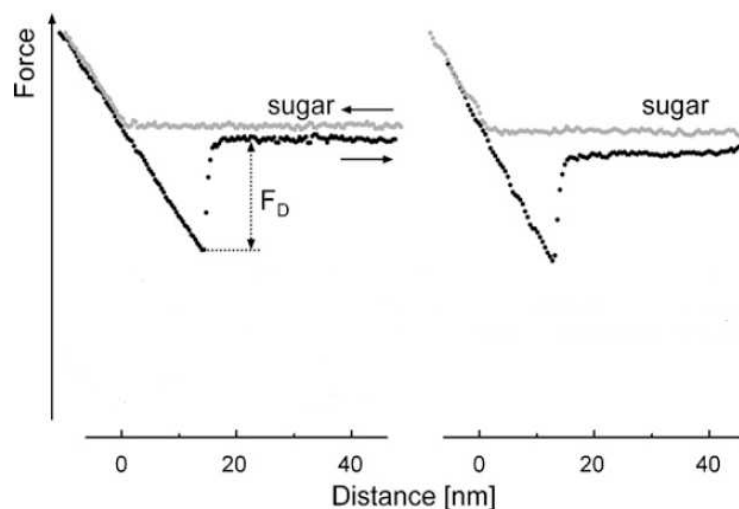


Figure 1-9. Force as function of surface separation between particles in soybean oil (left) and Medium Chain Triglycerides (right). Grey line, approach; black line, retreat of the AFM cantilever. F_D indicates detachment forces of 2.7 ± 1.6 nN (between sugar surfaces in soybean oil) and of 2.5 ± 2.1 nN (between sugar surfaces in medium chain triglycerides) [28].

Cleasson et al. [32] studied the interactions occurring in a system composed of mica surfaces suspended in anhydrous triolein. The system mica surfaces/triolein is used as sugar suspension model system to investigate the possible interactions occurring between sugar particles in chocolate suspension. Indeed, Triolein is a food oil composed of triglyceride as

cocoa butter, and mica surfaces have the same surfaces properties than sugar particles. Their results showed that in absence of water in the system, a strong detachment forces F_D is measured. Indeed, they showed that the magnitude of the detachment force required to separate the surfaces in absence of water is of 3 mN/m. Similar detachment forces were measured between mica surfaces in other anhydrous non-polar liquids [33].

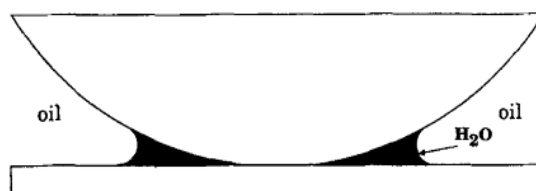


Figure 1-10. A drawing of a water capillary formed between two hydrophilic surfaces in a non-polar medium. The attractive adhesion force arises from the pressure drop across the curved oil-water interface [32].

The adhesive forces measured in the two studies described above may find their origin in van der Waals forces (which are always present and arise from induced and permanent dipole-dipole interactions between molecules or particles [34, 35]) according to some authors [36, 11], or in capillary forces according to others [37, 38]. Indeed, oil-continuous food systems are never completely free of water since the latter can accumulate at the particle surfaces and strongly change their interactions [37]. The presence of water affects interactions between hydrophilic particles in non-polar media such as oil-continuous systems. In those systems, water preferentially adsorbs on the hydrophilic surfaces, as shown by the low water contact angle (assumed to be equal to 0°) in the oil (see Figure 1-10). However, since Cleasson et al. [32] measured adhesive forces also in a water-free system, it suggests that in absence of capillary forces there exist other attractive forces at the origin of adhesive forces. Indeed, another probable source of interactions lies in the local polar interaction (hydrogen bonds) at contact. Hydrogen bonds are common between polar particles such as sugar particles [11].

1.4.1.2 Repulsive forces

1.4.1.2.1 Effect of emulsifier: steric forces

Arnold et al. [39] showed that the presence of lecithin in sugar/oil suspensions leads to a clear decrease of the attractive forces between the particles related to the adsorption of lecithin on sugar surfaces, which prevent the sugar particles to attract themselves. Indeed, their results (Figure 1-11) highlighted that AFM detachment force F_D in sugar/oil suspensions decreased when lecithin is added as surfactant. This repulsive effect of lecithin was also highlighted by [31, 40-46]. Johansson and Bergenståhl [40, 41] stated that this repulsive effect is also responsible for the decrease in yield stress observed in presence of lecithin. In other

words, by adsorbing at the sugar surfaces, lecithin prevents contact between particles and increases the inter-particle distance.

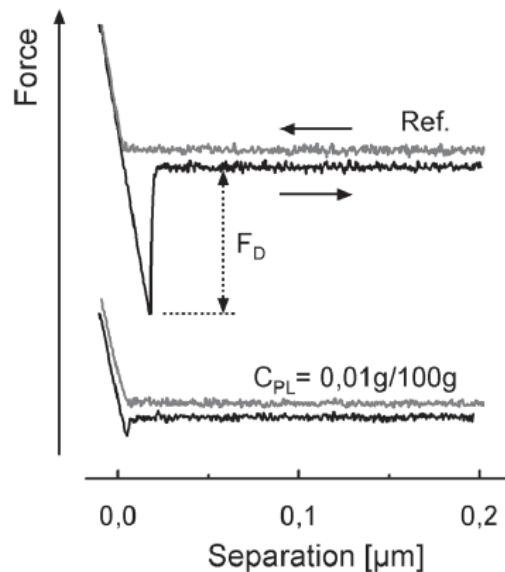


Figure 1-11. Force/separation function between sugar surfaces in soybean oil without lecithin (Ref.) and a lecithin/soybean oil dispersion ($C_{PL} = 0.01 \text{ g}/100 \text{ g}$) [39].

Studies of the effect of PGPR on chocolate processing showed that it also decreases the attractive forces between particles by adsorbing on the particle surfaces [30, 47-49]. However, little is known about its adsorption mechanism even if some suggestions were made in literature. Rousset et al. [49] suggested that the adsorption of PGPR increases the lipophilic nature of sugar particles via a decrease of their surfaces acidic character, and consequently the degree of attractive forces decreases. As a consequence, the fluidity of oil-based suspensions increases.

1.4.1.2.2 Structural forces

Structural forces [34, 35] arise from the molecular nature of the solvent and are especially important for the solvents consisting of large and rigid molecules. They are short distance interactions with a range of a few molecular diameters and oscillate with a wavelength equal to the solvent molecular diameter. With more flexible solvent molecules (as unsaturated triglyceride molecules), the structural forces are reduced, and the structure do not extend beyond a couple of molecular diameters [35]. To highlight the influence of these forces on particle interactions in sugar/oil suspensions, we focused on Cleasson and al. [29] work. They used the interferometric surface force apparatus (SFA) to study the interactions between hydrophilic mica surfaces immersed in triolein media. The Force/Distance curve obtained from their measurements highlighted the existence of two barrier forces to overcome in order to get the surfaces into contact. Barrier forces appear when the interparticle separation distances are 60-50 Å and 30-20 Å respectively (see Figure 1-12).

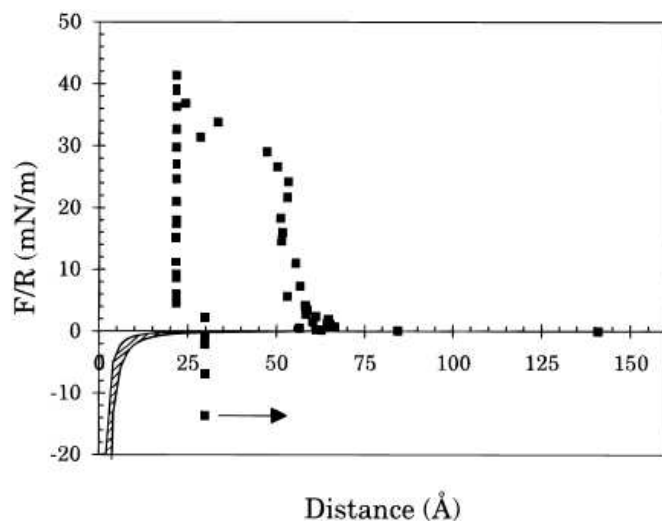


Figure 1-12. Force normalized by radius as a function of surface separation between mica surfaces immersed in anhydrous triolein. The arrow represents an outward jump occurring upon separation. The shaded area indicates the magnitude of the non-retarded van der Waals force [29].

The apparition of these forces' barrier is related to a change in conformation of the oleic acid chains of triolein. Indeed, they showed that at a distant of 60-50 Å (Figure 1-13(a)), there are two triolein molecular layers between the surfaces and one molecular layer at a distance of 30-20 Å (Figure 1-13(b)). This layering may be favored by the possibility of dipolar interactions between mica and ester groups of the triglyceride. Hence, a significant compaction of the layers takes place under the action of an external compressive force.

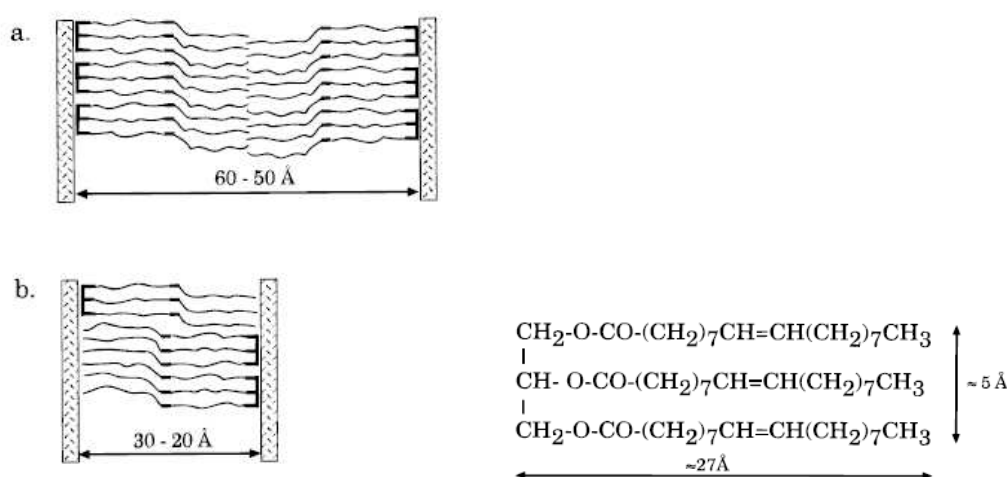


Figure 1-13. Proposed layering of triolein molecules at a hydrophilic mica surface: (a) the case of anhydrous triolein at a separation of 60-50 Å and (b) at a separation of 30-20 Å; (c) chemical structure of the triolein molecule [29].

The repulsive barrier can gradually be overcome in this case when the compressive force reaches 30 mN/m. The second barrier observed, is impossible to overcome, even under very strong compressive forces. It means that the surfaces cannot be brought closer than 20 Å even under very strong compressive forces. The barrier forces measured are due to repulsive forces occurring between mica surfaces across triolein. These forces are called structural forces because they are related to the conformation adopted by the triglyceride's molecules between the surfaces.

When water is present, it preferentially adsorbs onto the mica surface. At low water activities the triolein layering is disturbed, and the repulsive branch of the oscillating force becomes weaker. Close to saturation a water capillary forms around the contact position, removing the oscillating structural force and giving rise to a strong adhesive force (see Figure 1-14) [32]. The long-range force measured in this case is purely attractive, and the surfaces jumped directly into contact from a distance of approximately 100 Å. The same phenomenon has been observed in simpler liquids, such as in the nearly spherical OMCTS, where an increased water content also reduces the range and strength of the structural forces [50].

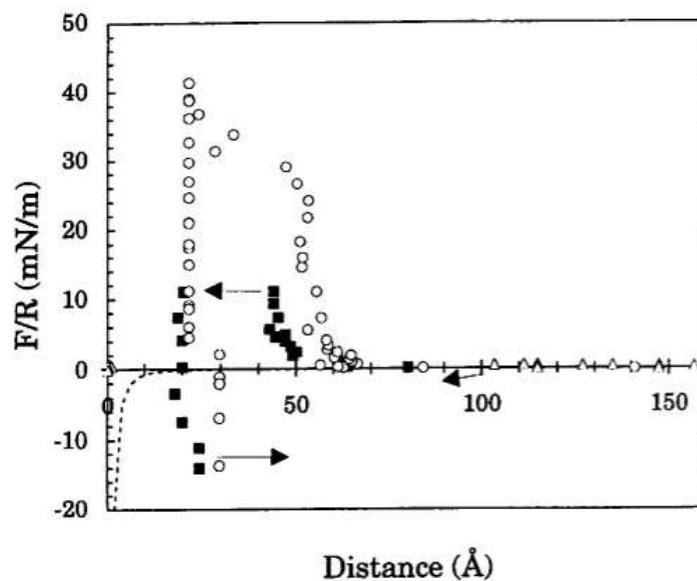


Figure 1-14. Force normalized by radius as a function of surface separation between mica interacting across anhydrous triolein (unfilled circles), triolein containing water with an activity of 0.47 (solid squares) and saturated with water (unfilled triangles). The arrows show 'jumps' of the surfaces caused by attractive forces. The dashed line represents the theoretically calculated attractive van der Waals force for the system mica-triolein-mica [32].

The effect of water on the structural forces for instance, is the reason why it is important that as much water is removed as possible during production process. Very approximately, for every 0.3% extra moisture that is left within the chocolate at the end of conching, an extra 1%

of fat must be added [6]. The strong affinity with sugar particles causes the increase of the viscosity of chocolate during manufacture. However, the viscosity decreases when an emulsifier is added to the mixture because the emulsifier interacts with the layer of water at the particle surfaces and facilitate the coating of particles by the oil molecules.

1.4.2 Interactions occurring between cocoa particles

To our knowledge, the interactions occurring between cocoa particles or cocoa and sugar particles within chocolate suspensions appear to not have been studied extensively, or, at least, only little information is available in the open literature. However, it was highlighted by Hoffmann et al. [51] that the presence of water in a cocoa/oil suspension leads to the formation of capillary bridges between the particles even when no sugar is present. They concluded that cocoa particles form networks and maintain a smooth texture but do not cause large agglomerates in presence of water as it has been reported for sugar/oil suspensions [52]. The transition of cocoa/oil suspension from a weakly elastic fluid to a gel upon addition of water is shown in Figure 1-15. This capillary bridging phenomenon has also been highlighted in [53, 54].

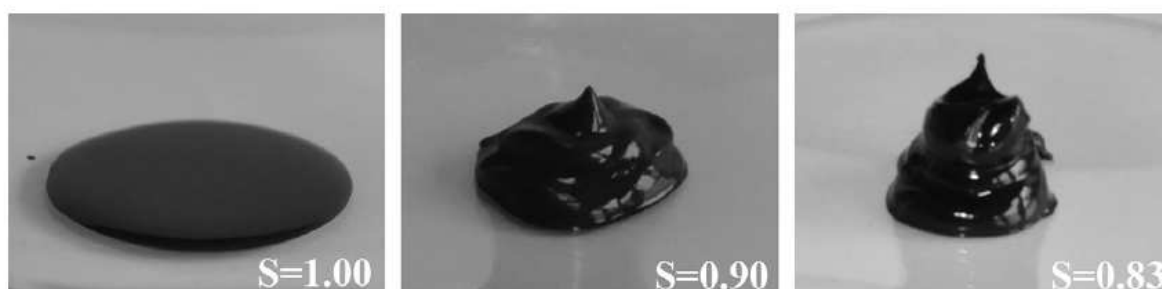


Figure 1-15. Suspension of cocoa solids in oil suspension at solid volume fraction $\phi = 0.35$ without added water ($S = 1$, left) and with added water in two different amounts ($S = 0.90$, middle and $S = 0.83$, right). S represents the saturation of the preferentially wetting fluid and equals to the volume of the preferentially wetting fluid to the total volume ratio. The preferentially wetting fluid is cocoa butter, and the secondary fluid is water [51].

1.5 Chocolate rheology

1.5.1 Typical rheological behaviour of chocolate suspension

The rheological behaviour of the 3 type of chocolate suspensions (milk, white and dark) measured by Glycerina et al. [55] is shown in Figure 1-16.

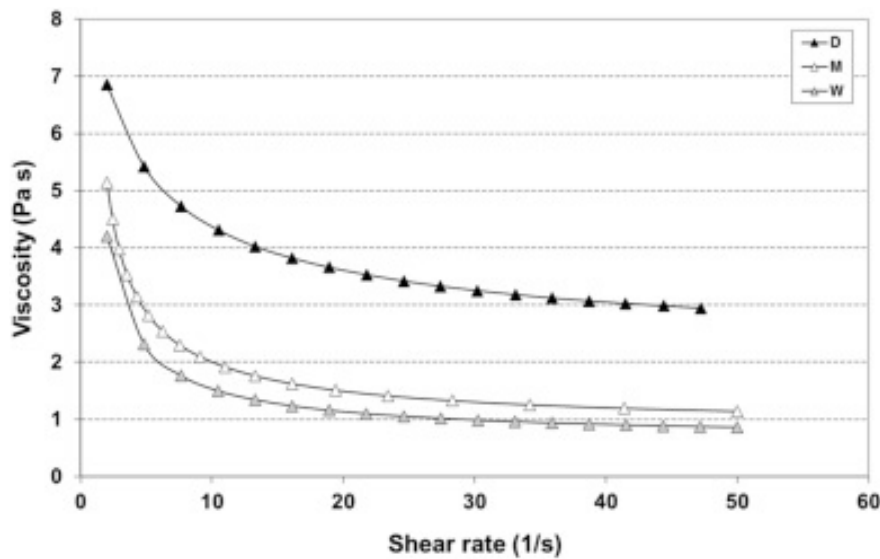


Figure 1-16. Flow curves of chocolate samples: dark (D), milk (M) and white (W) [55].

For all 3 chocolate suspensions, viscosity decreases with the increase of the shear rate, underlining the presence of a shear thinning behaviour. This behaviour has been also highlighted by [56, 57]. According to [58, 56] this behaviour can be explained by the structural breakdown of the molecules due to the generated hydrodynamic forces and to the increased alignment of the same molecules. Moreover, we also observe from this flow curves a Newtonian plateau (more pronounced for milk and white chocolates) at high shear rate. We should also specify herein that at low shear rate, all chocolate suspensions exhibit a yield value (known as yield stress) corresponding to the minimum stress required to achieve flow. To explain the origin of this yield value, we recall that to predict the flow behaviour of materials, it is necessary to derive from experimental measurements, a tensional relationship between the deviatoric stress tensor and the strain rate tensor [59]. However, these tensional relationships been hard to derive, it is common to simplify them by considering a simple shear of fluid between two plates as illustrated in Figure 1-17.

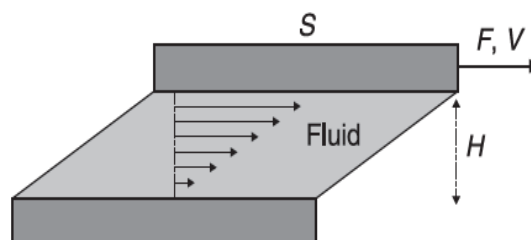


Figure 1-17. Schematic representation of a simple shear measurement adapted from [59].

In this interpretation, a sample of the material is sheared between two infinite parallel plates separated by a distance H and between which a difference of velocity V is imposed. F is the force that has to be applied to enforce a flow characterized by the velocity V . S represents the plates' surface supposed to tend to infinity. In these ideal conditions, the relationship between shear stress (τ) and the shear rate ($\dot{\gamma}$) can describe by the flow behaviour. The shear stress (τ) can be defined as the force divided by the area parallel to the force direction (Equation 1-1), while the shear rate ($\dot{\gamma}$) is defined as the velocity gradient or deformation rate (Equation 1-2). The viscosity (μ) can be expressed as a constant linking stress and shear rate (Equation 1-3).

$$\dot{\gamma} = V/H \quad (1 - 1)$$

$$\tau = F/S \quad (1 - 2)$$

$$\mu = \tau/\dot{\gamma} \quad (1 - 3)$$

For a Newtonian fluid such as cocoa butter, shear stress and shear rate have a linear dependence, but in concentrated suspensions exhibiting a non-Newtonian behaviour such as chocolate, these two parameters are not linear related anymore [60]. These non-Newtonian fluids are characterized in particular by the presence of a yield stress and this is the reason why a yield value can be observed for milk, dark and white chocolate at low shear rates. When the stress applied to a material is below the yield stress, the material exhibits little or no deformation. When the stress exceeds the yield stress, the material begins to flow. The yield stress is related to the strength of the network structure, which in turn results from attractive particle- particle interactions [61, 62]. The magnitude of the yield stress is affected by a number of factors, such as the density of the network, solid volume fraction and particle size [63]. The yield stress (τ_o) and viscosity (μ) are usually the parameters used to evaluate the flow properties of the molten chocolate during production process [64].

Several models were developed in order to describe the flow behaviour of chocolate suspensions and estimate the yield stress and the viscosity of these suspensions on the basis of the experimental flow curves obtained. The most used models are the Power Law model [65, 66], the model of Casson [67], the model of Windhab [68], and the model of Bingham [69].

The equation of the Power Law model is the following one:

$$\tau = K * \dot{\gamma}^n \quad (1 - 4)$$

Where τ is the shear stress (Pa), K is the consistency index (Pa sⁿ), $\dot{\gamma}$ is the shear rate (s⁻¹) and n is the dimensionless flow behaviour index. For instance, $n < 1$ for shear thinning suspensions such as chocolate whereas $n = 1$ for Newtonian fluid such as cocoa butter.

The equation of the Casson model is the following one:

$$\tau^{0.5} = \tau_0^{0.5} + \mu_{PL}\dot{\gamma}^{0.5} \quad (1 - 5)$$

Where τ_0 is the yield stress and μ_{PL} is the so-called “plastic viscosity”.

The model of Casson was originally introduced to describe the rheological behaviour of suspension of pigments [70]. The Casson model is the most known and used to study the rheological behaviour of chocolate suspensions because in 1973, the International Confectionery Association (ICA) recommended the use of Casson model for shear rates between 5 and 60 s^{-1} . However, according to Weipert et al. [71], this model does not always reflect in accurate way the flow behaviour of chocolate because its rheological properties do not fit exactly to the Casson equation. For this reason, further models modifying the Casson model were developed such as the Chevalley model [72] and the Windhab model [68].

The equation of the Windhab model is the following one:

$$\tau = \tau_0 + \mu_\infty\dot{\gamma} + (\tau_1 - \tau_0)(1 - e^{-\dot{\gamma}/\dot{\gamma}^*}) \quad (1 - 6)$$

This model has been recommended for shear rates in the range between 2 and 50 s^{-1} at 40°C. It assumes that when molten chocolate is put under shear, there is a change in its structure highlighting by a decrease in viscosity from an initial value (structure of no shear) to a steady state value. When the shear stress is increased further, an equilibrium viscosity is reached which no longer decrease, and a final viscosity μ_∞ is reached. In the region of this final viscosity μ_∞ , there is a straight line with a constant slope in the flow curve. This straight line can be extrapolated back to the point of zero shear rate in order to find the intercept. This intercept would give the parameter τ_1 which is a hypothetical yield stress [73]. The schematic diagram of the Windhab model extracted from [73] is represented in Figure 1-18.

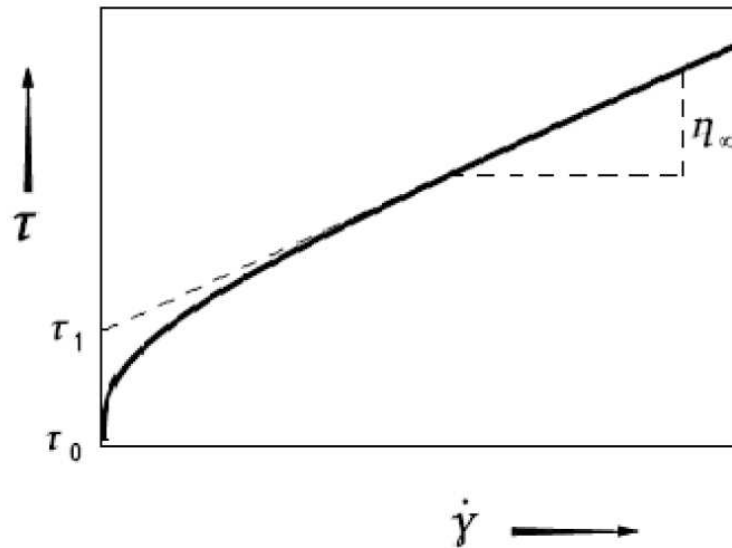


Figure 1-18. Schematic diagram of the Windhab model extracted from [73].

In order to find the point on the curve where the final viscosity μ_∞ is reached, the *Windhab* model uses a second parameter $\tau^* = \tau(\dot{\gamma}^*)$ indicating that the shear-induced loss of structure is at a maximum when $\dot{\gamma} = \dot{\gamma}^*$ is reached. For shear rates higher than $\dot{\gamma}^*$ the material behaves like a plastic fluid and the Bingham equation would apply.

The Bingham equation is the following one:

$$\tau = \tau_0 + \mu\dot{\gamma} \quad (1 - 7)$$

where τ is the shear stress (Pa), τ_0 is the yield stress (Pa), μ is the plastic viscosity (Pa. s) and $\dot{\gamma}$ is the shear rate (s^{-1}). This model, widely used to describe the flow behaviour of many types of fluid, estimates that the apparent viscosity of a colloidal suspension is the sum of the colloidal and hydrodynamic forces.

Furthermore, chocolate exhibits time-dependent behaviour; in other words, a thixotropic behaviour [74, 75]. This behaviour corresponds to a decrease of viscosity with time of shearing, followed by recovery of the structure when the stress is removed.

1.5.2 Effect of inter-particle interactions

As previously mentioned, lecithin reduces the strength of the adhesive forces between sugar particles in sugar/oil suspensions [39]. Arnold et al. [28] studied the effect of lecithin on flow properties of sugar/oil suspensions and their results are showed in Figure 1-19. The flow properties were measured by applying a decrease shear rate from $1000 s^{-1}$ to $0.01 s^{-1}$ in a logarithmic ramp within 990 s. They used the viscosity at shear rate $\dot{\gamma} = 1000 s^{-1}$ to analyze the effect of lecithin at the Newtonian plateau, while the viscosity at shear rate $\dot{\gamma} = 10 s^{-1}$ was

used to characterize the effect in the shear thinning region. Their results highlighted that the highest impact of lecithin addition is observed for yield stress which exhibits an important decrease. Whilst a less pronounced decrease of the viscosity at high shear rates $\dot{\gamma} = 1000 \text{ s}^{-1}$ (i.e., Newtonian plateau). They related the decrease of yield stress to the reduction of the adhesive forces in presence of lecithin measured via AFM. Regarding the Newtonian plateau, the less pronounced decrease could be explained by the fact that hydrodynamic forces become more important than particle interactions at high shear rate [76].

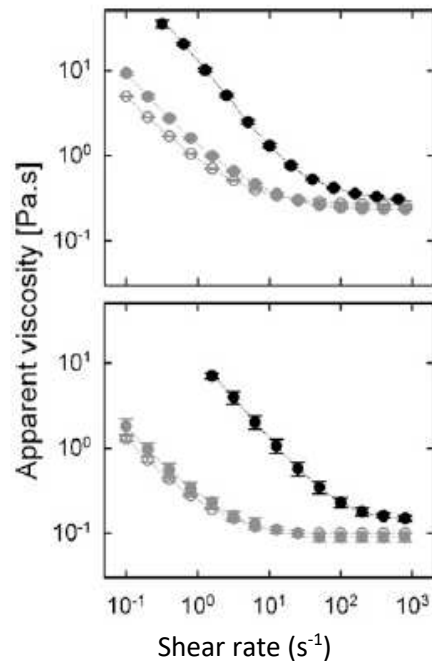


Figure 1-19. Viscosity functions of sugar/oil suspensions as affected by the continuous phase (top, soybean oil; bottom, MCT) and the addition of soybean lecithin. The total amount of phospholipids per unit of solid surface in suspension was black circle, 0 mg/m^2 ; grey circle, 3.25 mg/m^2 ; unfilled circle, 16.26 mg/m^2 . Data represent arithmetic mean \pm half range of 2 independent measurements. Only a reduced number of data points is displayed in the chart [28].

It has also been shown in the literature [6] that beyond a certain concentration ($> 0.3\%$), lecithin can be detrimental to flow properties. Indeed, as can be seen in Figure 1-20, the casson yield stress increases while the casson viscosity remains constant. Beckett [6] suggested that the increase of yield stress observed may be due to the formation of lecithin micelles or lecithin bilayer around the sugar.

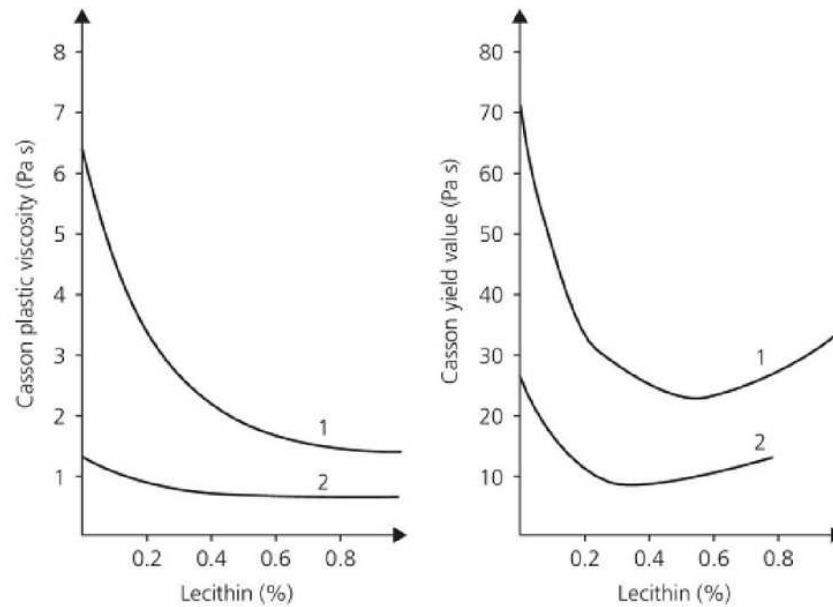


Figure 1-20. Influence of soya lecithin on the rheological parameters of two dark chocolates: (1) 33.5% fat and 1.1% moisture; (2) 39.5% fat and 0.8% moisture [6].

Schantz and Rohm [47] studied the flow curves of dark chocolate in presence of lecithin and PGPR. Their results are shown in Figure 1-21. Their results showed that PGPR has a greater influence on dark chocolate rheology than lecithin which is in accordance with other studies [42, 6].

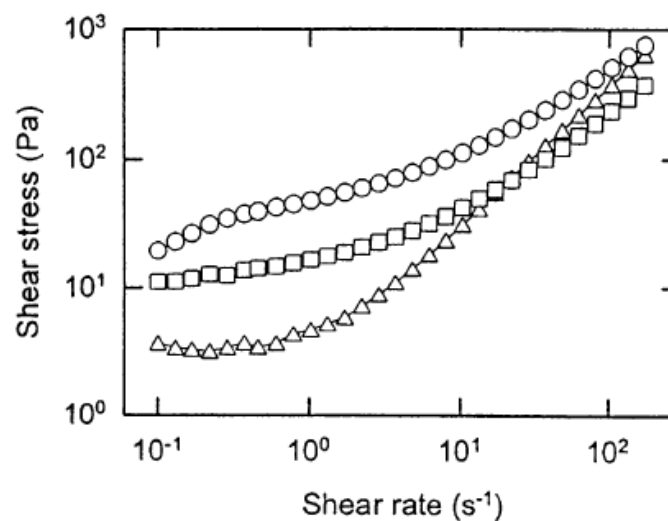


Figure 1-21. Flow curves of dark chocolate suspensions (40°C) without emulsifier (circles) and with addition of 4g/kg lecithin (squares) and 4g/kg PGPR (triangles). Only every fifth data point is depicted in the graph [47].

Regarding the capillary bridges highlighted by [51] previously mentioned in section 1.4.2, the authors showed that the presence of these capillary bridges between the particles causing an increase of the rheological parameters of cocoa suspensions. They highlighted the effect of

water content on yield stress by plotting the relative yield stress (i.e., the yield stress measured when the system contains water to the one measured when the system does not contain water ratio) as a function of a parameter $S = \frac{Volume_{preferentially\ wetting\ fluid}}{Volume_{total\ fluid}}$ which characterize the saturation of the preferentially wetting fluid (i.e., cocoa butter). When there is no water in the suspension, $S = 1$. Their results are showed in Figure 1-22.

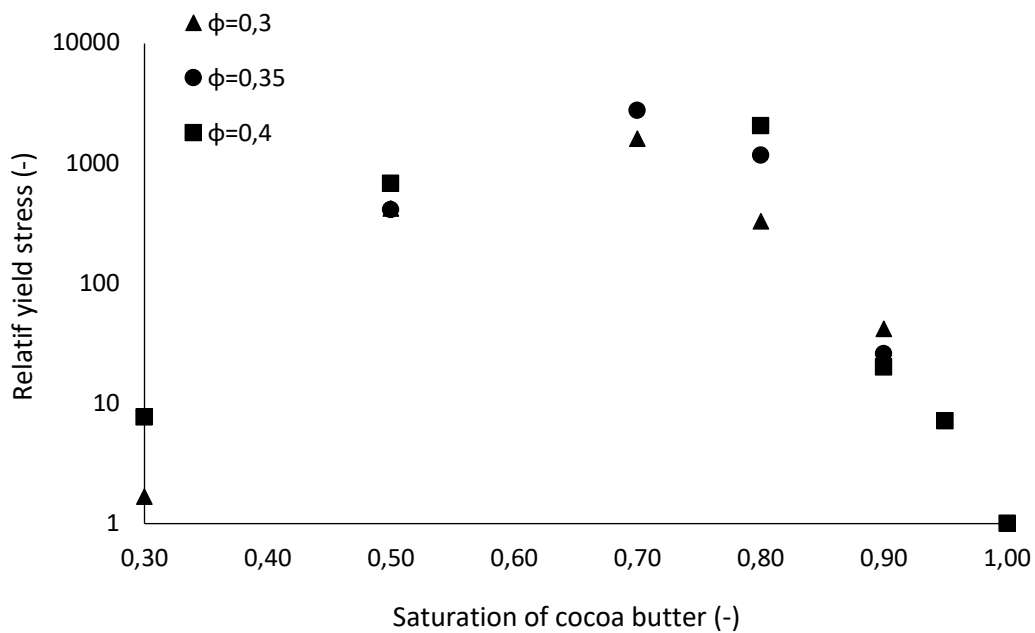


Figure 1-22. Normalized yield stress as a function of saturation of the preferentially wetting fluid for cocoa suspensions at 3 different solid volume fractions extracted from [51].

1.5.3 Effect of particle size distribution

Figure 1-23 shows the yield stress and plastic viscosity as a function of particle size [6]. These results show that the yield stress increases dramatically as the particles become finer. Viscosity is almost not affected by the size of the particle and exhibits a moderate increase as the mean particle diameter is below 10 μm . The authors suggested that the increase of yield stress is owed to the increase in the number of contacts between particles.

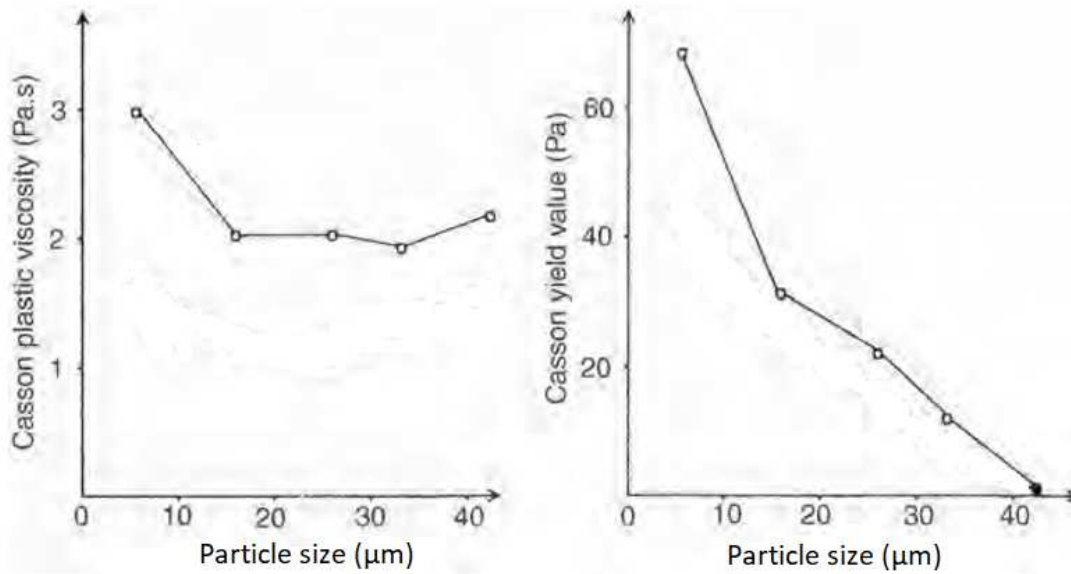


Figure 1-23. Influence of particle fineness on the rheological parameters milk chocolate [6].

1.5.4 Effect of solid volume fraction

Concentrated suspension such as chocolate can be defined as a fluid in which particles of size much larger than the size of the molecules of the suspending the fluid. The parameter allowing to describe the behaviour of suspensions is the solid volume fraction (ϕ) which corresponds to the ratio of the volume occupied by the solid particles to the total volume (see Equation 1-8).

$$\phi = \frac{\text{Volume}_{\text{occupied by the particles}}}{\text{Volume}_{\text{occupied by the particles}} + \text{Volume}_{\text{occupied by the fluid}}} \quad (1 - 8)$$

Literature [6, 77] shows that the decrease of the solid volume fraction of chocolate (i.e., increase of its fat content) leads to the decrease of apparent viscosity as illustrated in Figure 1-24. More details about the effect of this parameter on suspension rheology can be found in section 1.6.1.

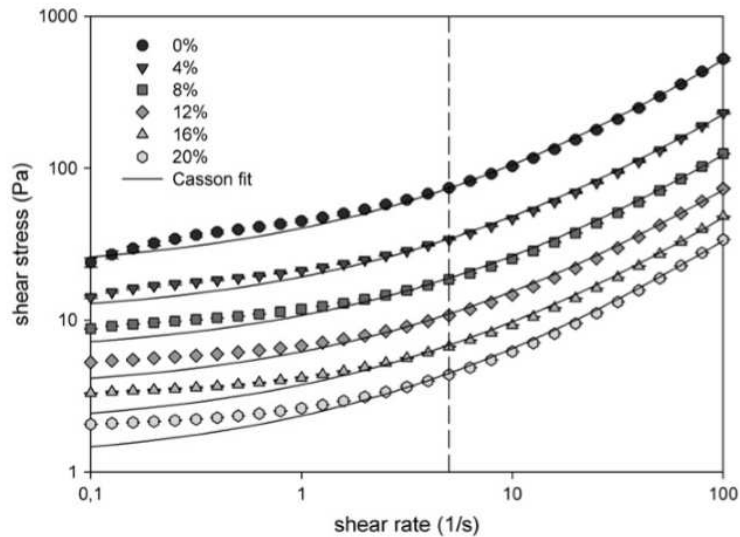


Figure 1-24. Flow curves of chocolate samples with increasing fat content (legend: % of added fat) (average of three measurements). The Casson fit to the data is also included [6].

1.5.5 Understanding the microscopic origin of the rheological behaviour of chocolate suspension during production

From a rheological point of view the most important chocolate production steps are refining, conching and tempering. The effect of these production steps on chocolate rheology was studied in literature [78-80]. Figure 1-25 shows the rheological behaviour of dark chocolate during production process [80].

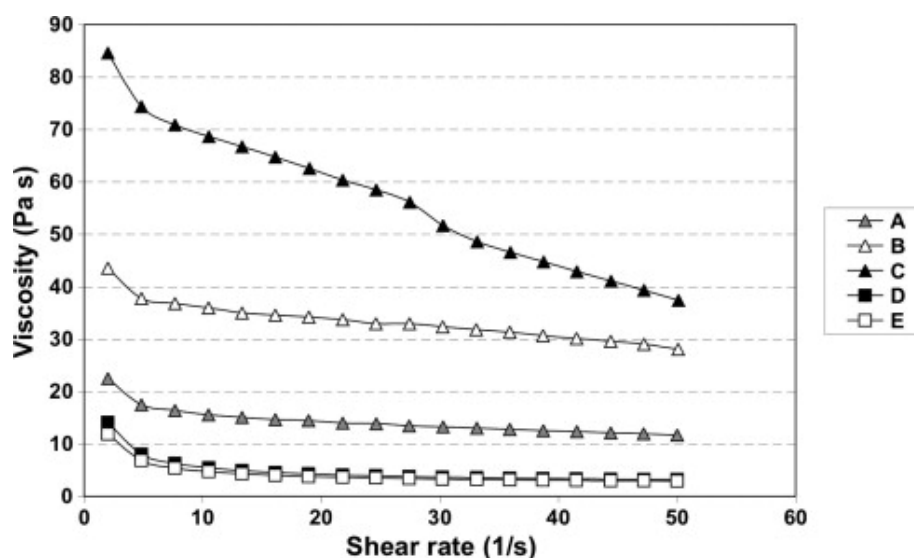


Figure 1-25. Changes of apparent viscosity of dark chocolate samples during mixing (A), pre-refining (B), refining (C), conching (D) and tempering (E) steps [80].

The highest plastic viscosity and yield stress are observed for the pre-refining and refining steps whereas the lowest values are measured for the two last production steps (conching and tempering). It is concluded that the highest values measured from the mixing step through the pre-refining (B) and refining (C) ones are related to a reduction in the particle size that causing an increase in the contact points between them and thus, an increase of the formation of aggregate. Whilst the lowest values of viscosity of conching and tempering sample are probably related with their less aggregate packing structure network. In these steps, in fact the addition of lecithin and further cocoa butter reduce the particle–particle interactions.

Furthermore, while studying the effect of conching on chocolate rheology, Blanco et al. [81] interestingly found that by adding PGPR together with lecithin at the beginning of conching, the yield stress is dramatically lowered, revealing shear thickening behaviour. This suggests that, in the sample conched with lecithin only, shear thickening is masked. This is in accordance with other studies [82-84]. Blanco et al. [81] also highlighted that conching reduces the aggregate size and leads to an increase of the maximum packing fraction.

1.6 Chocolate particle size distribution optimization

We recall that our study aims to decrease fat content and remove emulsifier of chocolate suspension while controlling the viscosity. In literature, there are several approaches used to decrease the fat amount of chocolate while keeping desirable flow properties. One of them is the use of emulsifier blends to increase emulsifier levels in chocolate [85]. Another method is the replacement of the fat continuous phase by a water-in-oil emulsion. Hugelshofer [66] demonstrated that emulsion-based chocolates show similar sensory properties to conventional ones. However, these chocolates exhibit poor stability (sugar bloom on their surface) and could not be manufactured using the existing assets of chocolate plants. Fat replacers can also be used even though their level of addition is restricted due to side effects as their non-digestibility by the consumer [13]. Do et al. used polymers as stabilizer in fat-based food suspensions as an example of reduced-fat chocolate [86]. However, the most method used to decrease the fat content without considerably increase the viscosity is the optimization of the particle size distribution of chocolate [87-90]. Feichtinger et al. [87] showed that it is possible to decrease the fat amount of chocolate by using model chocolates with varying particle size distribution and size ratios. They showed that bimodal particle size distribution (specific blend of small and large particles) leads to a higher maximum packing fraction, and thus lower viscosity. The same observation is highlighted by the studies of [88-90] on chocolate and those of [91, 92] on mustard and nut paste respectively. The use of this last method is based on theoretical predictions about the principles of the rheology of concentrated suspensions [93] and the fact that the viscosity of a suspension depends on the solid volume fraction of suspended particles.

1.6.1 Principle of concentrated suspensions rheology

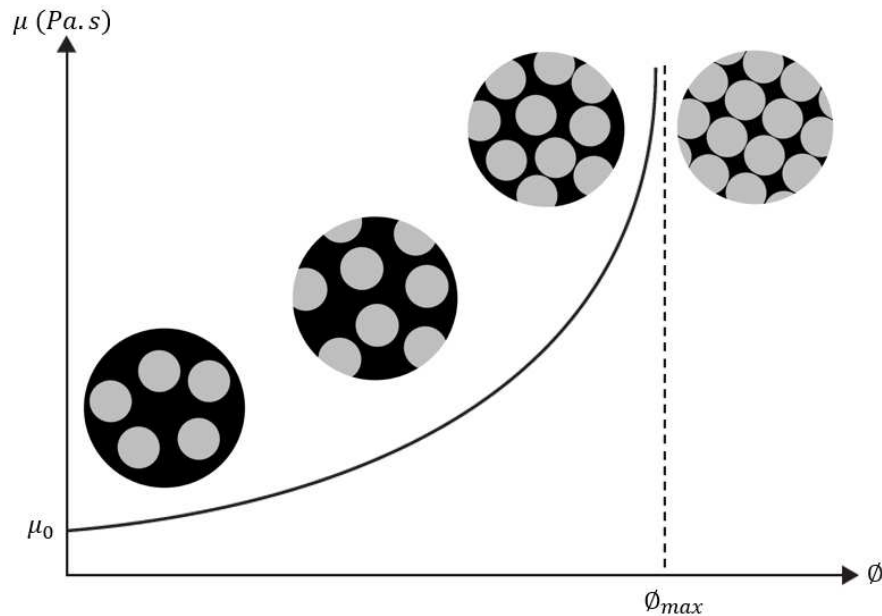


Figure 1-26. Viscosity of a suspension of uniform spheres in a Newtonian fluid as a function of the solid volume fraction. The schemes correspond to the different regimes of concentration (from left to right): dilute, semi-dilute, concentrated, compact.

The rheological behaviour of dilute suspensions, similar to that of the suspending fluid (possibly with slightly larger rheological parameters) since it is assumed in these suspensions that there are no hydrodynamic interactions between the particles (see Figure 1-26), is well described by the well-known Einstein equation [94] that stated that the viscosity of a dilute suspension of hard spheres ($\phi < 2\%$), can be defined as:

$$\mu = \mu_0 (1 + [\mu]\phi) \quad (1 - 9)$$

With μ the suspension viscosity, μ_0 is the viscosity of the suspending fluid and $[\mu]$ the intrinsic viscosity, which is equal to 2.5 for spherical particles. This equation is only valid for spherical and non-interacting particles.

In highly concentrated suspensions, as in the case of chocolate suspensions, the interaction between particles dominates over the hydrodynamic forces (see Figure 1-26), especially at low shear rates, and the material exhibit a complex flow behaviour. Therefore, Equation 1-9 cannot be used anymore to describe the viscosity since particle-particle interactions need to be taken into account. It was shown in literature [95, 96] that the empirical equation describing well the experimental viscosity of these suspensions is the one of Krieger Dougherty [93]:

$$\mu = \mu_0 \left(1 - \frac{\phi}{\phi_{\max}}\right)^{-q} \quad (1 - 10)$$

Where μ is the suspension viscosity, μ_0 is the viscosity of the suspending fluid and ϕ_{\max} is the maximum packing fraction. The maximum packing fraction corresponds to the maximum solid volume fraction that can be reached by a suspension. The viscosity tends to infinity as the particle solid volume fraction approaches its maximum, ϕ_{\max} (see Figure 1-26). At the maximum packing fraction ϕ_{\max} , the particles are in a 3-dimensional contact throughout the suspension, thus making flow impossible. The relative solid volume fraction (ϕ/ϕ_{\max}), corresponding to a normalized concentration [97], was thus reported to be a relevant parameter to reflect particle interactions.

Equation 1-10 suggests that it is possible to decrease the viscosity of chocolate suspension at a given solid volume fraction ϕ by increasing the maximum packing fraction, ϕ_{\max} . Conversely, increasing the maximum packing fraction will allow an increase of the solid volume fraction (i.e., decreasing the fat content) without affecting the viscosity of the suspension.

1.6.2 Parameters influencing the maximum packing fraction

The optimization of a system particle size distribution usually leads to an increase of its maximum packing fraction (ϕ_{\max}). The maximum packing fraction is an intrinsic geometric property of the particle system and shall depend only on two morphological parameters namely the particle size distribution and the particle shape [98]. The maximum packing fraction ϕ_{\max} is an intrinsic geometric property that depends on the particle shape, and particle size distribution (PSD).

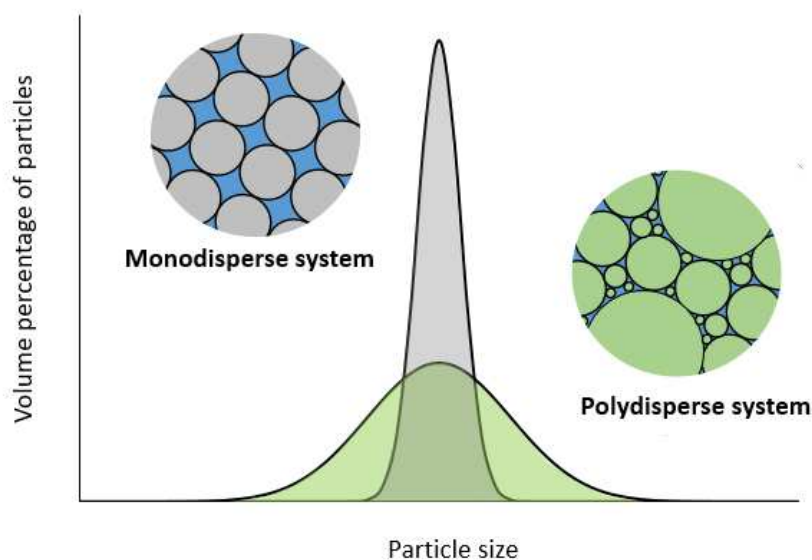


Figure 1-27. Effect of particle size distribution on packing density for spheres. Polydisperse system have a higher packing density than monodisperse system.

Polydisperse suspensions have generally a higher packing density compared to monodisperse suspensions because particles with variable size can fill more efficiently the space (see Figure 1-27). However, it should be kept in mind that this is not always true, as geometrical interactions between particles of different size must be taken into account [99]. First, inserting a fine particle between coarser ones may lead to a loosening of the packing of the system if the fine particle size is larger than the typical size of the empty space between coarse particles. Similarly, when a coarse particle is inserted into a packing of fine particle, it will lead to a decrease of the packing density of the fine particles near the coarse particle. This effect is referred to as wall effect. The influence of these effects on maximum packing fraction will be detailed in chapter 5.

Particle shape	Random close packing density
Spheres	0.60–0.64
Cubes	0.76
Parallelepiped ($4.0 < L/D < 8.0$)	0.51–0.67
Disks ($L/D = 1$)	0.63
Spheroids ($0.6 < L/D < 1.3$)	0.58–0.61
Rounded aggregates	0.59–0.63
Crushed aggregates	0.50–0.57
Fibres ($L/D = 10$)	0.48
Fibres ($L/D = 167$)	0.03

Table 1-1. Random close packing density for particle of different shapes [100].

Particle shape considerably affects the maximum packing fraction. As shown in Table 1-1, spheres do not arrange themselves as cubes, crushed aggregates or fibbers [100]. Previous studies have shown that particles with regular shapes and flat surfaces locally arrange themselves better than particles with irregular shapes [101-103]. It is shown in Figure 1-28 that particles having the same apparent size, but different roughness does not have the same maximum packing fraction. Spheres have therefore higher packing density than irregular particles. Roughness is defined here as the ratio between the surface area of a sphere having the same volume of the particle and the surface area of the particle. De Larrard [99] showed that crushed mineral aggregates have lower density than rounded aggregates corroborating the effect of roundness (see Table 1-1). Moreover, particle size ratio or aspect ratio is considered to be one of the most dominant morphological parameters governing maximum packing fraction. Aspect ratio is defined as the ratio between the maximum diameter and the minimum diameter of a particle. Good correlations have been found in literature between packing density and aspect ratio [104], (see Figure 1-29). Moreover, it should be kept in mind that particle roughness also could play a role when the particle volume fractions reach values

of the order of the dense packing fraction. For all these reasons, neglecting the shape or assuming all particles are spherical in a mixture can lead to a wrong prediction of the packing fraction. The overall shape of the particles (i.e., roundness, aspect ratio, surface roughness...) are the dominant morphological parameters conditioning the packing.

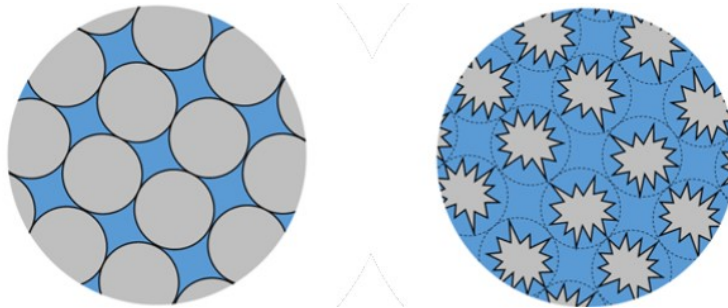


Figure 1-28. Effect of particle shape (i.e., roundness) on packing density of two particles having the same size. Spheres have higher packing density than irregular particles.

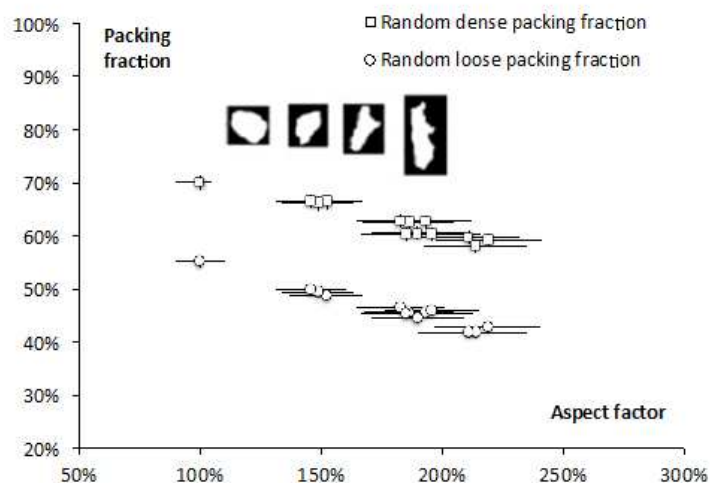


Figure 1-29. Random dense packing fraction and random loose packing fraction as a function of aspect ratio of sand having the same size distribution [104].

1.7 Conclusion

This review of literature highlighted the fact that chocolate suspension exhibits a shear thinning behaviour with a transition to a Newtonian plateau at high shear. This rheological behaviour is influenced by the particles interactions, particle size, the solid volume fraction, the production process, and the presence of water and emulsifier in the system.

We also learnt from literature that there are adhesion forces between sugar particles due to the capillary forces when water is present in the system or to the presence of polar interactions (hydrogen bonds) between surfaces. Structural forces prevent the formation of agglomerates by increasing the particle-particle separation distance. All these forces are influenced by the presence of lecithin and water. Regarding cocoa particles, the presence of water also leads to the apparition of capillary forces in the system.

The presence of water in the system leads to an increase of the rheological parameters whereas lecithin causes a decrease of the rheological parameters. The effect of lecithin is more pronounced on yield stress and seems less important on viscosity at the Newtonian plateau.

We finally learnt from literature that there are theoretical predictions that allow the control of the viscosity of a suspension and thus, can be used to achieve the objective of this thesis.

References:

- [1] Alvim, P.D.T. Flowering of cacao. *Cocoa Growers' Bulletin* 1984, 35, 23–31.
- [2] Anon, History of chocolates 2008. <http://www.barry-callebaut.com/1589> (accessed October 20, 2011).
- [3] Nair, K.P. Cocoa (*Theobroma cacao* L.). In: *The Agronomy and Economy of Important Tree Crops of the Developing World*. The Hague, Netherlands: Elsevier, 2010, Chapter 5, 131–180.
- [4] Purdy, L.H.; Schmidt, R.A. Status of cacao witches' broom: Biology, epidemiology, and management. *Annual Review of Phytopathology* 1986, 34, 573–594.
- [5] Anon, Cocoa 2011. http://www.theice.com/publicdocs/ICE_Cocoa_Brochure.pdf (accessed August 7, 2011).
- [6] Beckett, S.T. *The Science of Chocolate*: 2nd ed.; Royal Society of Chemistry: Cambridge, 2008.
- [7] Cook, L.R. (revised Meursing, E.H.), *Chocolate Production and Use*, Hardcourt Brace, New York, 1984.
- [8] Afoakwa, E.O. Chocolate manufacturing and processing technology. In: *Cocoa production and processing technology* Taylor and Francis Group, Boca Raton, 2015, 183-195.
- [9] Rousseau, D. Understanding and Controlling the Microstructure of Complex Foods Physical Properties: Structural and Physical Characteristics, McClements, D.J. (Ed.); Woodhead Publishing: Cambridge, 2007, 648-690.
- [10] Svanberg, L.; Ahrné, L.; Lorén, N.; Windhab, E. *J.Food Eng.* 2011, 104, 70-80.
- [11] Babin, H. Colloidal properties of sugar particle dispersions in food oil with relevance to chocolate processing. Thesis. University of Leeds, 2005.
- [12] Beckett, S.T. *The Science of Chocolate*, The royal Society of Chemistry, Cambridge, 2000.
- [13] Beckett, S.T. *Industrial Chocolate Manufacture and Use*, 3rd edition, Blackwell Science, Oxford, 1999.
- [14] Scharma, A.; Jana, A.H.; Chavan, R.S. *Comprehensive Reviews in Food Science and Food Safety* 2012, 5, 518-528.
- [15] Haylock, S.J.; Dodds, T.M. Ingredient from Milk, *Industrial Chocolate Manufacture and Use*. Beckett, S.T. (Ed.), Blackwell Science, Oxford, 2009, 76-99.
- [16] Aronhime, J. S.; Sarig, S.; Garti, N. *Journal of the American Oil Chemists Society*, 1988a, 65, 1140-1143.
- [17] Johansson, D.; Bergenstahl, B. *Journal of the American Oil Chemists Society*, 1992c, 69, 128-733.
- [18] Gaonkar, A. G. *Journal of the American Oil Chemists Society*, 1989, 66, 1090-1092.
- [19] Kawaguchi, M.; Okuno, M.; Kato, T. *Langmuir*, 2001, 17, 6041-6044.
- [20] Bueschelberger, H.G. Lecithins in Emulsifiers in Food Technology, Whitehurst, R.J. (ed.), Blackwell Publishing: Oxford, U.K. 2004, 1-39.
- [21] Padley, F.B.; Gunstone, F.D.; Harwood, J.L. Occurrence and Characteristics of Oils and Fats. In: *The Lipid Handbook* (2nd ed.), Chapman & Hall: London, 1994, 47.

- [22] Wendel, A. Lecithin. In Kirk-Othmer Encyclopedia of Chemical Technology (4th ed.), John Wiley & Sons: New York, 1995, 15, 192.
- [23] Kuksis, A. Animal Lecithins. In Lecithins, Szuhaj, B.F., Ed. The American Oil Chemists' Society: Champaign, Illinois, 1985, 105.
- [24] Wilson, R.; Van Schie, B. J.; Howes, D. Food and Chemical Toxicology 1998, 36, 711-718.
- [25] Dedinaite, A.; Campbell, B. Langmuir 2000, 16, 2248-2253.
- [26] Minifie, B.W. Chocolate, Cocoa and Confectionery – Science and Technology. London: Chapman & Hall, 1989.
- [27] Whitefield, R. 2005. *Making Chocolates in the Factory*. London, UK: Kennedy's.
- WHO/FAO. 2009. Definition of Pesticide.
- [28] Arnold, G.; Schuldt, S.; Schneider, Y.; Friedrichs, J.; Babick, F.; Werner, C.; Rohm, H. *Colloids and Surfaces A: Physicochem. Eng. Aspects*, 2013, 418, 147-156.
- [29] Claesson, P.M.; Dedinaite, A.; Bergenståhl, B.; Campbell, B.; Christenson, H. *Langmuir*, 1997, 13, 1682-1688.
- [30] Dedinaite, A.; Campbell, B. *Langmuir*, 2000, 16, 2248-2253.
- [31] Dedinaite, A.; Claesson, P.M.; Campbell, B.; Mays, H. *Langmuir*, 1998, 14, 5546-5554.
- [32] Dedinaite, A.; Claesson, P.M.; Bergenståhl, B.; Campbell, B. *Food Hydrocolloids*, 1997, 11, 7-12.
- [33] Christenson, H. K. *J. Phys. Chem.* 1993, 97, 12034-12041.
- [34] Dickinson, E.; Stainsby, G. Colloids in Food, Applied Science Publishing, London, 1982, p.123.
- [35] Israelachvili, J.N. Intermolecular and Surface Forces: Solvation, Structural and Hydration Forces, 3rd ed.; Academic Press: London, 1985, 341-380.
- [36] Van den Temple, M. *J. Colloid. Sci.* 1964, 16, 284.
- [37] Shubert, H. In Kapillarität in Feststoff Systemen, Fisher Verlag, Berlin, 1981.
- [38] Shubert, H. *Int. Chem. Eng.* 1981, 21, 363.
- [39] Arnold, G.; Schneider, Y.; Friedrichs, J.; Babick, F.; Rohm, H. *Annual Transactions of The Nordic Rheology Society*, 2013, 21, 199-203.
- [40] Johansson, D.; Bergenståhl, B. *J. Am. Oil Chem. Soc.* 1992, 69, 705-717.
- [41] Johansson, D.; Bergenståhl, B. *J. Am. Oil Chem. Soc.* 1992, 69, 718-727.
- [42] Middendorf, D.; Bindrich, U.; Mischnick, P.; Juadjur, A.; Franke, K.; Heinz, V. *Colloids and Surfaces A: Physicochemical and Engineering Aspects* 2016, 499, 60-68.
- [43] Bueschelberger, H.G. Lecithins in Emulsifiers in Food Technology, Whitehurst, R.J. (ed.), Blackwell Publishing: Oxford, U.K. 2004, 1-39.
- [44] Beckett, S.T. Chocolate flow properties in Beckett, S.T. (ed.), *Industrial Chocolate: Manufacture and Use*, Wiley Blackwell: UK, 2009, 224-246.
- [45] Nieuwenhuyzen, W.V.; Tomás, M.C. *Eur. J. Lipid Sci. Technol.* 2008, 110, 427-486.
- [46] Weyland, M.; Hartel, R.W. Emulsifiers in confectionery in Hasenhuettl, G.L.; Hartel, R.W. (Eds), *Food Emulsifiers and their Applications*, Springer: New York, 2008, 285-305.
- [47] Schantz, H.; Rohm, H. *Lebensm.-Wiss. u.- Technol.* 2005, 38, 41-45.

- [48] Ghorbel, D.; Saidi, I.; Slema, M.; Ben Gharsallah, M. *Journal of Food Process Engineering* 2011, 34, 317-331.
- [49] Rousset, Ph.; Sellapan, P.; Daoud, P. *Journal of Chromatography A* 2002, 969, 97-101.
- [50] Christenson, H. K.; Blom, C. E. *J. Chem. Phys.* 1987, 86, 419-424.
- [51] Hoffmann, S.; Koos, E.; Willenbacher, N. *Food Hydrocolloids* 2014, 40, 44-52.
- [52] Storz, T.; Marangoni, A.G. *Trends in Food Science & Technology* 2011, 22, 201-214.
- [53] Galet, L.; Vu, T.; Oulahna, D.; Fages, J. *Food and Bioproducts Processing* 2004, 82, 298–303.
- [54] Koos, E.; Willenbacher, N. Capillary forces in suspension rheology. *Science*. 2011, 80, 897–900. 6091. [PubMed: 21330542].
- [55] Glicerina, V.; Balestra, F.; Dalla Rosa, M.; Romani, S. *Journal of Food Engineering*, 2016, 169, 165-171.
- [56] Izidoro, D.R.; Scheer, A.P.; Sierakowski, M.R.; Haminiuk, C.W.I. Influence of green banana pulp on the rheological behaviour and chemical characteristics of emulsion (mayonnaises). *LWT* 2008, 41, 1018-1028.
- [57] Chhabra, R. P. Non-Newtonian Fluid behaviour. *Bubbles, Drops, and Particles in Non-Newtonian Fluids*. 2^{ed}, Chapter 2: 9-48. CRC Press, Boca Raton.
- [58] Juszczak, L.; Witczak, M.; Fortuna, T.; Banys, A. *Journal of Food Engineering* 2004, 63, 209-271.
- [59] Ovarlez, G. Introduction to the rheometry of complex suspensions. In: *Understanding the rheology of concrete*. Woodhead Publishing Limited. 2012, 23-59.
- [60] Babin, H.; Dickinson, E.; Chrisholm, H.; Beckett, S. *Food Hydrocolloids* 2004, 19, 513-520.
- [61] Larsson, R.G. *The Structure and Rheology of Complex Fluids*. New York, Oxford University Press. 1999.
- [62] Coussot, P.; Ancey, A. *Physical Review E* 1999, 59, 4445-4457.
- [63] Dzuy, N. Q.; Boger D. V. *Journal of Rheology* 1983, 27, 321-349.
- [64] Afoakwa, E.O. *Chocolate Science and Technology*. Oxford, UK: Wiley- Blackwell, 2010, 3–82.
- [65] Holdsworth S. D. Rheological model used for the prediction of the flow properties of food products. *Institution of Chemical Engineering*. 1993, 71, Part C.
- [66] Hugelshofer, D. Structural and rheological properties of concentrated suspensions mixed with an emulsion. Doctoral Thesis – Swiss Federal Institute of Technology (ETH) Zürich–Switzerland. 2000.
- [67] International Confectionery Association (ICA), 1973. Viscosity of chocolate. Determination of Casson yield value and Casson plastic viscosity. London: OICC, p. 10
- [68] IOCCC, (2000). Viscosity of cocoa and chocolate products. Analytical Method 46-2000. Geneva: International Office of Cocoa, Chocolate and Confectionary.
- [69] Bingham, E.C., Fluidity and plasticity, McGraw-Hill, New York, 1922.
- [70] Bolenz, S.; Tischer, T. *International Journal of Food Science and Technology* 2013, 48, 2408–2416.
- [71] Weipert, Tscheuschner and Windhab. *Rheologie der Lebensmittel*, 1993, 452-457.

- [72] Chevalley, J. J. *Texture Stud.* 1991, 22, 219-229.
- [73] Ludger, O. F.; Teixeira, A. A. *Food Physics-Physical properties Measurements and Applications.* Springer -Verlag Berlin Heidelberg. 2007.
- [74] Roopa, B.S.; Bhattacharya, S. *International Journal of Food Science and Technology* 2009, 44, 2583– 2589.
- [75] Dolz, M.; González, F.; Delegido, J.; Hernández, M.J.; Pellicer, J. *Journal of Pharmaceutical Sciences* 2009, 89, 790–797.
- [76] Windhab, E.J. Rheology in food processing. In: S.T. Beckett (Ed.) *Physico-chemical Aspects of Food Processing*, Blackie Academic and Professional, Glasgow, 1995, 80-116.
- [77] De Graef, V.; Depypere, F.; Minnaert, M.; Dewettinck, K. *Food Research International*, 2011, 44, 2660-2665.
- [78] Glicerina, V.; Balestra, F.; Dalla Rosa, M.; Romani, S. *Food Bioprocess. Technol.* 2015, 8, 770-776.
- [79] Glicerina, V.; Balestra, F.; Dalla Rosa, M.; Romani, S. *Journal of Food Engineering*, 2015, 145, 45-50.
- [80] Glicerina, V.; Balestra, F.; Dalla Rosa, M.; Romani, S. *Journal on Processing and Energy in Agriculture Food Engineering*, 2013, 17, 59-63.
- [81] Blanco, E.; Hodgson, D.J.M.; Hermes, M.; Besseling, R.; Hunter, G.L.; Chaikin, P.M.; Cates, E.M.; Van Damme, I.; Poon, W.C.K. *PNAS* 2019, 116, 10303-10308.
- [82] Guy, B.M.; Richards, J.A.; Hodgson, D.J.M.; Blanco, E.; Poon, W.C.K. *Phys Rev Lett* 2018, 121:128001.
- [83] Gopalakrishnan, V.; Zukoski, C. J. *Rheology* 2004, 48, 1321–1344.
- [84] Brown, E. et al. Generality of shear thickening in dense suspensions. *Nat Mater* 2010, 9, 220–224.
- [85] Kaiser, J.M.; Gestel, A.V.; Vercauteren, J. U.S. Patent WO 99/45790, 1999.
- [86] Do, T-A.L.; Mitchell, J.R.; Wolf, B.; Vieira, J. *Reactive & Functional Polymers* 2010, 70, 856-862.
- [87] Feichtinger, A.; Scholten, E.; Sala, G. *Food Func.* 2020, 11, 9547-9559.
- [88] Do, T.A.L.; Hargreaves, J.M.; Wolf, B.; Mitchell, J.R. *J. Food Sci.* 2007, 72, 541-552.
- [89] Mongia, G.; Ziegler, G.R. *Int. J. Food Properties* 2000, 3, 137-147.
- [90] Kaiser, J.M.; Purwo, S. U.S. Patent WO 99/45790.
- [91] Aguilar, C.A.; Rizvi, S.S.H.; Ramirez, J.F.; Inda, A. *J Texture Stud.* 1991, 22, 59–84.
- [92] Villagran, F.V.; McCabe, G.M.; Wong, V.Y.L. U.S. Patent 5490999, 1996.
- [93] Krieger, I.M.; Dougherty, T.J. *Trans. Soc. Rheol.* 1959, 3, 137–152.
- [94] Einstein, A. *Ann. Physik* 1906, 19, 289-306.
- [95] Fang, T.N.; Tiu, C.; Wu, X.; Dong, S. *Journal of Texture Studies* 1995, 26, 203-205.
- [96] Taylor, J.E.; Vandamme, I.; Johns, M.L.; Routh, A.F; Wilson, D.I. *Journal of Food Science* 2009, 74(2), 55-61.
- [97] Barnes HA, Hutton JF, Walters K. 1993. An introduction to rheology. Amsterdam: Elsevier.
- [98] Barnes, H. A.; Hutton, J.F.; Walters, K. An introduction to rheology, Elsevier, New York, 1989.

- [99] De Larrard, F. Concrete Mixture Proportioning: a scientific approach, E&FN SPON: An imprint of Routledge, London and New-York, 1999.
- [100] Chateau, X. Particle packing and the rheology of concrete. In: Roussel, N. (Ed.), Understanding the Rheology of Concrete, Woodhead Publishing, 2012.
- [101] Cumberland, D.J.; Crawford, R.J. The packing of particles, Elsevier, Amsterdam, 1987.
- [102] German, R. M. Particle packing characteristics, Princeton, Metal Powder Industry Federation, 1989.
- [103] Aste, T.; Weaire, D. The pursuit of perfect packing, Bristol, Institute of Physics, 2000.
- [104] Hafid, H.; Ovarlez, G.; Toussaint, F.; Jezequel, P.H.; Roussel, N. *Cement and Concrete Research* 2016, 80, 44-51.

Chapter 2: Development of experimental protocols

Table of contents

2.1	Materials.....	48
2.2	Mixing protocol	48
2.3	Density measurements.....	49
2.3.1	Introduction.....	49
2.3.2	Gas pycnometer: AccuPyc II 1345.....	50
2.3.2.1	Presentation of the device.....	50
2.3.2.2	Description of the test protocol	50
2.3.3	Water pycnometer	52
2.3.4	Drying tunnel	52
2.3.4.1	Presentation of the device.....	52
2.3.4.2	Description of the test protocol	53
2.4	Morphological properties.....	57
2.4.1	Particle size distribution.....	57
2.4.1.1	Introduction.....	57
2.4.1.2	Theoretical considerations	58
2.4.1.2.1	Equivalent spherical diameter.....	58
2.4.1.2.2	Parameters influencing the particle size distribution measurement by laser granulometry	59
2.4.1.3	Description of the measuring device	60
2.4.1.3.1	Malvern Mastersizer 3000: presentation and working principle.....	60
2.4.1.3.2	Mie Scattering Theory	61
2.4.1.4	Steps followed to develop the particle size distribution protocol of a suspension composed of one powder.....	61
2.4.1.4.1	Sampling.....	61
2.4.1.4.2	Dispersion	62
2.4.1.4.3	Optical indexes	65
2.4.1.5	Steps followed to develop the particle size distribution protocol of a suspension composed of two or more powders.....	67
2.4.1.6	Particle size distribution: developed protocols	70
2.4.2	Maximum Packing Fraction	71
2.4.2.1	Introduction.....	71
2.4.2.2	Compressive Yield Stress	72
2.4.2.3	Measuring device: Centrifuge 3-16PK	74
2.4.2.4	Steps followed to develop the protocol	74
2.4.2.4.1	Deflocculation.....	74
2.4.2.4.2	Multiple speeds technique	75
2.4.2.4.3	Initial solid volume fraction.....	76

2.4.2.5	Maximum packing fraction: developed protocol.....	77
2.5	Rheological properties.....	78
2.5.1	Introduction.....	78
2.5.2	Measuring device: Bohlin C-VOR.....	78
2.5.3	Steps followed to develop the protocol.....	80
2.5.3.1	Rheological behaviour of the interstitial fluid.....	80
2.5.3.2	Thixotropic behaviour.....	81
2.5.3.3	Suspension stability.....	86
2.5.4	Rheological measurements protocol.....	86
2.6	Conclusion.....	87
	References.....	88

This chapter is entirely dedicated to the description of the experimental protocols developed to study the morphological, physical and rheological properties of chocolate suspensions. We first assess in this chapter the envelope density of cocoa and sugar particles. We use a gas pycnometer to determine the density of sugar particles whereas we combine gas pycnometer and a drying procedure to determine the one of porous cocoa particles. By means of laser diffractometry and compressive centrifugation, we measure the particle size distribution and the maximum packing fraction of each material respectively. Rheological measurements are conducted using a rheometer equipped with a vane-in-cup geometry.

This chapter also aims to highlight the problems encountered, the choices made, and therefore the reasoning followed, in order to develop the final protocols deemed suitable for our observation and analysis. In general, when we talk about protocols, it takes into account the test protocol, that is to say the measurement procedure once the system to be studied is ready, but also the sample preparation protocol meaning the steps carried out before the test starts.

2.1 Materials

To develop the different protocols, we use as materials: fatted cocoa particles (Cocoa ($D_{50} = 9.2 \mu\text{m}$)), defatted cocoa particles (Cocoa ($D_{50} = 10.2 \mu\text{m}$)), sugar particles (Sugar ($D_{50} = 436 \mu\text{m}$) and Sugar ($D_{50} = 58.6 \mu\text{m}$)), siliceous sand, cocoa butter, sunflower oil and emulsifiers (soy lecithin and PGPR). In this thesis, since the only solid particles studied are cocoa and sugar particles, we choose to name them with their mean diameter (D_{50}) in brackets to differentiate them. Fatted cocoa particles that contain 10-12% fat by total mass and cocoa butter of density 0.89 from West Africa are provided by Cargill NV (Wormer, Netherlands). The defatted cocoa particles (less than 1% fat by mass) are purchased from Skinny Body (United Kingdom). Sugar ($D_{50} = 58.6 \mu\text{m}$) is purchased from Frank Vereecke NV (Menen, Belgium) and Sugar ($D_{50} = 436 \mu\text{m}$) is provided by Cargill (Mouscron, Belgium). Soybean lecithin is supplied by Cargill whereas PGPR is purchased from Palsgaard (Belgium). Sunflower oil is purchased from a local supermarket (AUCHAN, France). The siliceous sand used here has a particle size ranging from 0.06 mm to 4 mm and is supplied by Palvadeau Challan sandpits. It is a yellow sand of alluvial origin, crushed and washed, with a density equals to 2.64.

2.1 Mixing protocol

The same mixing protocol is used to develop the morphological and rheological measurements protocols of chocolate. The chocolate suspensions are mixed for 5 min using a Turbo-Test Rayneri VMI mixer at 840 rpm. The mixing is carried out in a hot water bath to keep the temperature of the sample constant and equal to 40°C.

2.2 Density measurements

2.2.1 Introduction

Density is one of the most important physical properties, which allows for the characterization of a material. For a given mass, evaluating a sample's density consists into measuring its volume. The volume of homogeneous solids with well-defined geometry can be readily calculated from their dimensions. However, most solids consist of heterogeneous combinations of particles with varying sizes and shapes. In such cases, volumes are most accurately measured by fluid displacement, following Archimedes' principle. Gas pycnometry is recognized as one of the most reliable techniques for obtaining true, absolute, skeletal, and apparent density. This technique provides non-destructive volume measurements with extremely high precision and speed. Both these parameters are of utmost importance for applications, for which sample purity, buoyancy, or packaging are key. Inert gases, such as helium or nitrogen, are used as the displacement medium. Helium gas is the preferred displacement fluid because of its small molecular dimensions and ideal gas behaviour. Density calculations using the gas displacement method are much more accurate and reproducible than the traditional Archimedes water displacement method.

In this thesis, we are interested in determining the envelope density (see Figure 2-1) of the solid particles composing dark chocolate. Sometimes also called the particle density, the envelope density is an expression of the bulk density of an individual particle rather than an assembly of many particles. It is determined from the volume of the solid particles, open pores and closed pores. This density is of interest for our study because it will allow to define a solid volume fraction that dominates the rheological behaviour of dark chocolate. Since sugar particles do not contain open and closed pores, their envelope density corresponds to their true density and therefore, can be determined by gas pycnometry. Conversely, for porous particles such as cocoa, the gas pycnometry technique gives an apparent density. The apparent density corresponds to ratio of mass to the volume of the solid particles and the closed pores. To be able to measure the envelope density of cocoa particles, we first consider using water as displacement fluid instead of helium since it is usually assumed that cocoa particle surface is hydrophobic, and therefore, water is expected not to penetrate into pores. However, as it will be demonstrated later in this chapter, this technique cannot be used either because our results suggest that water can also penetrate into cocoa particles pores like helium. After noticing that water can penetrate into the pores, we then decide to saturate the cocoa particles with water and then dry them to estimate the volume occupied by the open pores using drying technique. This technique has already been used in literature to determine the density of food products [1]. It is also used to measure water absorption of porous aggregates in the construction industry [2]. By knowing the volume of the open pores and the apparent density, we can therefore estimate the envelope density. True, apparent and envelope density are illustrated in Figure 2-1.

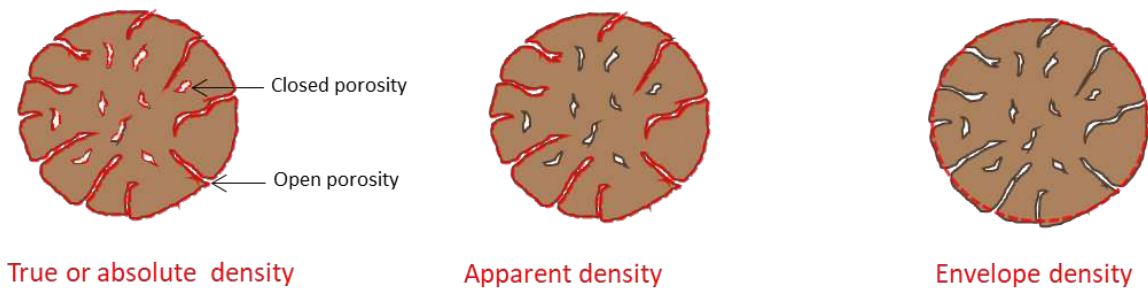


Figure 2-1. Schematic representation of true, apparent and envelope density of a porous material. The area surrounded in red corresponds to the volume measured in each case.

2.2.2 Gas pycnometer: AccuPyc II 1345

2.2.2.1 Presentation of the device

The AccuPyc II 1345 is an instrument used for measuring volume and calculating true density. The instrument is composed of two chambers (a sample or filling chamber and an expansion chamber) and three valves as shown in Figure 2-2.

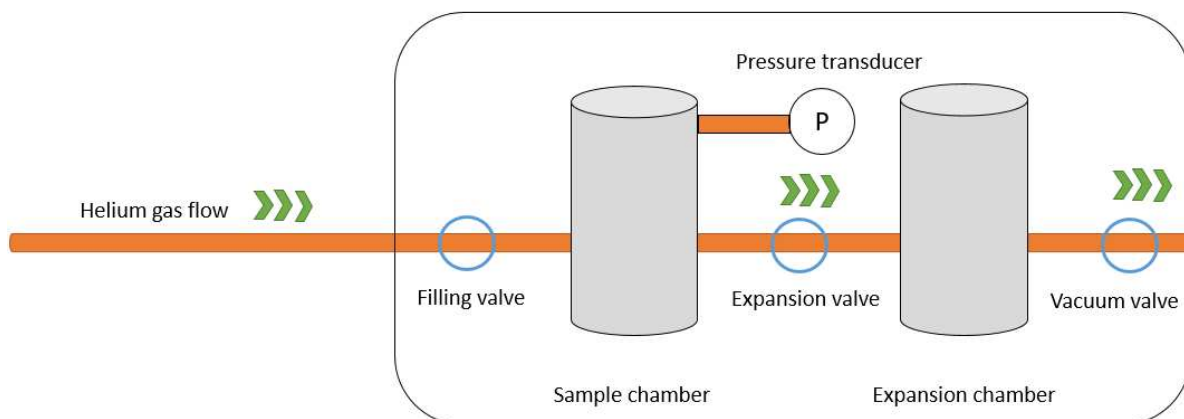


Figure 2-2. Schematic representation of AccuPyc II 1345 device.

2.2.2.2 Description of the test protocol

A sample of known mass (m_{sample}) is poured in a sealed cell of known volume ($V_{cell} = 10 \text{ cm}^3$) before being placed in the sample chamber. To allow for the displacement of Helium into the sample chamber, the filling valve opens, and the chamber is pressurized up to a target pressure of 1.35 bar. Once this pressure is stabilized, the expansion valve is then opened allowing the gas to expand into the expansion chamber. Finally, the last valve opens, and the pressure vent off to open atmosphere. This process is repeated 10 times before starting analysis in order to purge the system. We then start the analysis by choosing the same filling

and venting cycle with cycle duration allowing for pressure equilibrium. During the analysis, the instrument automatically records the pressure of the first filling chamber (P_1) and then the filling and expansion chamber (P_2). The volume of gas displaced which corresponds to the sample volume (V_{sample}) is then calculated (Equation 2-1). Dividing this volume by the sample mass gives the true density.

$$V_{sample} = V_{sample\ chamber} - \frac{V_{expansion\ chamber}}{\frac{P_1}{P_2} - 1} \quad (2 - 1)$$

The density of sugar and cocoa particles are assessed using this test protocol. The same amount of powder ($m_{sample} = 4\text{ g}$) is placed into the cell for each measurement and for each material studied, the measurement is repeated 3 times. The measured densities are gathered in Table 2-1. We recall that the densities measured for sugar particles are their true densities that also correspond to their envelope densities since they are no porous (Cf. Figure 2-1.). While, for cocoa particles, the densities determined correspond to some apparent densities. The density of 1.59 measured for both sugar particles is in good agreement with the one found in literature [3].

	Sugar ($D_{50} = 436\ \mu\text{m}$)	Sugar ($D_{50} = 58.6\ \mu\text{m}$)	Fatted Cocoa ($D_{50} = 9.2\ \mu\text{m}$)	Defatted Cocoa ($D_{50} = 10.2\ \mu\text{m}$)
Density	1.59 ± 0.001	1.59 ± 0.007	1.53 ± 0.007	1.42 ± 0.005

Table 2-1. Apparent densities of cocoa particles and envelope densities of sugar particles determined by helium pycnometry.

Regarding cocoa particles, it is possible to calculate the apparent density of fatted cocoa knowing the one of defatted cocoa and vice versa. Indeed, knowing the fat proportion of each of them (1% and 11% for defatted and fatted cocoa respectively), the density of fatted cocoa particles can be calculated by the following formula:

$$d_{fatted\ cocoa} = \frac{m_{fatted\ cocoa\ without\ fat} + m_{fat\ in\ fatted\ cocoa}}{m_{fatted\ cocoa\ without\ fat} / d_{defatted\ cocoa} + m_{fat\ in\ fatted\ cocoa} / d_{fat}} \quad (2 - 2)$$

Let's consider that the mass of fatted cocoa particles is 1 g. This means that 11% of this mass correspond to $m_{fat\ in\ fatted\ cocoa}$ and 89% to $m_{fatted\ cocoa\ without\ fat}$. We also recall here that the density of cocoa butter $d_{fat} = 0.89$. Therefore:

$$d_{fatted\ cocoa} = \frac{0.89+0.11}{0.89/1.53+0.11/0.89} = 1.42$$

This result confirms that the densities measured by gas pycnometer are reliable.

2.2.3 Water pycnometer

The measurement by water pycnometer is carried out using a borosilicate glass pycnometer having a capacity of 100 ml and an accuracy of 0.001 cm³ supplied by VWR (France).

The glass pycnometer is first weighed with its cap and a mass m_1 is obtained. After filling the pycnometer with deionized water, a mass m_2 is weighed. The volume occupied by the water (V_1) that also corresponds to the volume of the glass pycnometer is calculated as follows:

$$V_1 = \frac{m_2 - m_1}{\rho_{water}} \quad (2 - 3)$$

with ρ_{water} corresponding to the density of water and equals to 1.

Then, 10 g of cocoa particles is added in the glass pycnometer followed by 70 g of deionized water. The suspension is mixed during 5 min with a spatula. Knowing the mass of water $m_3 = 70$ g and the mass of cocoa particles $m_1 = 10$ g, the density of cocoa particles can be calculated as follow:

$$\rho_{cocoa\ particles} = \frac{m_4}{V_1 - \left(\frac{m_3}{\rho_{water}}\right)} \quad (2 - 4)$$

The density is found to be 1.32 and 1.46 for fatted and defatted cocoa particles respectively. However, these results are not reliable because the presence of air bubbles and lumps in the glass pycnometer is observed during the measurement. This suggests that mixing by hand with a spatula is not sufficient to have a homogeneous suspension. Ultrasonic bath is therefore used to get rid of the lumps and bubbles formed when cocoa is mixed with water. 15 min of ultrasonic bath is sufficient. After repeating the test 3 times for both cocoa particles, the densities obtained are the same as those determined previously by helium pycnometry (i.e., 1.53 and 1.42 for defatted and fatted cocoa respectively). It can be concluded from these results that water can fill the open pores of cocoa particles and that neither helium nor water pycnometer can be used to determine the envelope density of cocoa particles.

2.2.4 Drying tunnel

2.2.4.1 Presentation of the device

We recall that drying tests are conducted in order to estimate the volume occupied by open pores in cocoa particles, and therefore the envelope density of cocoa particles. We perform the drying tests on defatted cocoa particles. These tests are carried out in a drying tunnel with

a cross section of 50x70 cm². Within this tunnel circulates a flow of dry air at a constant flow rate of 60 L.min⁻¹, or 0.01 m. s⁻¹ (Figure 2-3). Such a flow rate made it possible to ensure that the air flow is laminar, and that the free surface of the sample is therefore not disturbed. In the tunnel, the temperature and humidity conditions are as follows: 24.5 ° C ± 0.1 ° C, and 3% ± 1% relative humidity.

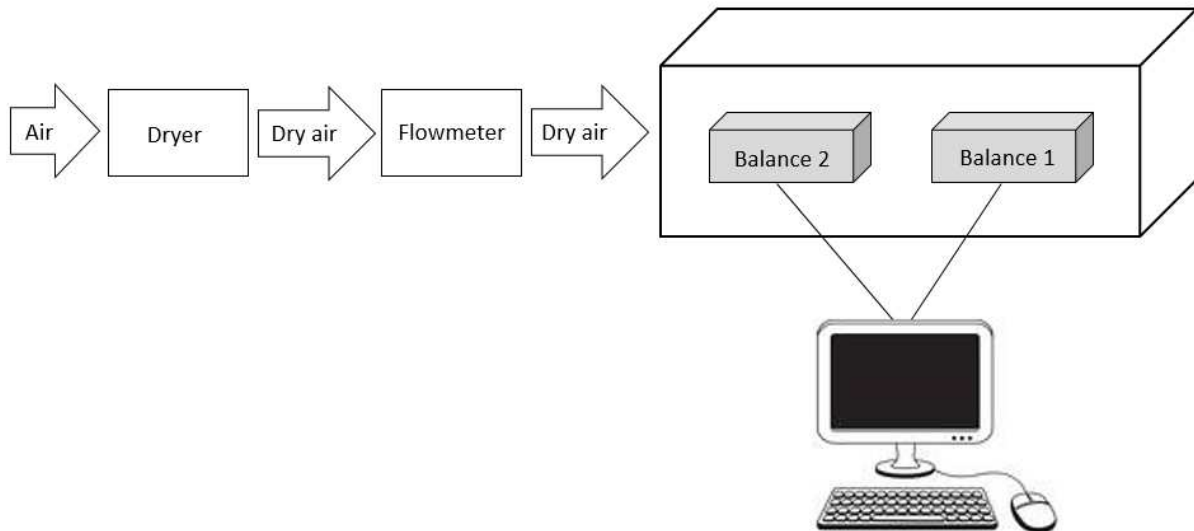


Figure 2-3. Representation of the drying experimental setup.

The experimental set up makes it possible to control the air flow entering the drying tunnel. The flow rate is the same whatever the balance on which the sample is placed in the tunnel and to avoid any influence of the sample thickness, all drying tests are carried out using petri dishes of the same dimensions: 100 mm diameter and 16 mm thickness. This test is based on the fact that the drying rate of an initially saturated granular sample in constant drying conditions drops when all the water located between the grains has evaporated as the evaporation of the water contained in the grains porosity has a longer characteristic time.

2.2.4.2 Description of the test protocol

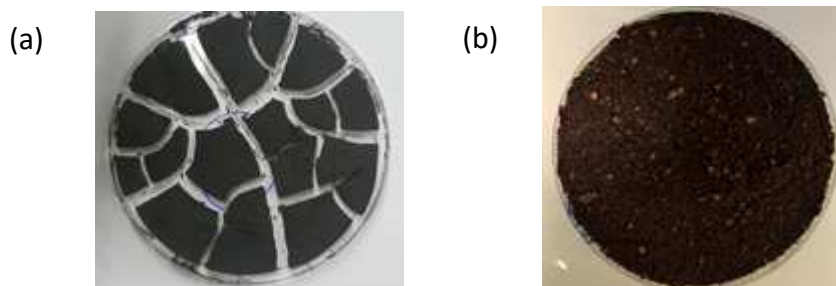


Figure 2-4. Cracks formed after drying in (a) absence and (b) presence of sand.

As shown in Figure 2-4 (a), a problem is encountered during the drying of defatted cocoa particles suspension. Indeed, cracks formation during drying is a ubiquitous phenomenon important in soil science [4] as well as industrial material and processing development [5-7]. Understanding crack formation in particle films and developing strategies to suppress crack formation is an important field of research, as desired product properties generally decline with the occurrence of cracks. Drying a dispersion of colloidal particles such as the suspension we are studying here can lead to the formation of a porous matrix saturated with solvent [6]. During evaporation, high mechanical stresses are generated. When these stresses exceed the strength of the material, they can be released through the formation of cracks. This process strongly depends on both the mechanical properties of the material and on the way the porous matrix consolidates. It is shown in [6] that, for colloidal dispersions, the number of cracks formed depends mainly on the drying rate, the nature of the solvent and the mechanical properties of the colloidal particles. We decide to add coarse particles in the suspension in order to make it thicker and stronger. As shown in Figure 2-4 (b), this technique allows to significantly decrease the number of cracks. The coarse particles added are non-porous siliceous sand particles. The composition of the suspension studied is detailed in Table 2-2.

	Water	Siliceous sand	Defatted cocoa particles
Mass (g)	25.02	57.55	12.51

Table 2-2. Composition of the suspension studied.

Defatted cocoa particles suspended in deionized water are first mixed by hand for 5 minutes using a spatula before being placed in ultrasonic bath for 1 hour to ensure that water penetrates in the open pores. Water pycnometry is then used to measure density and ensure that it is equal to 1.53 as expected. Siliceous sand is then added, and the overall suspension is mixed by hand. Finally, the suspension is poured in a petri dish of 100 mm diameter and 16 mm thickness. The tests are performed 3 times on both balances (1 and 2) and the same drying kinetic is obtained whatever the balance used.

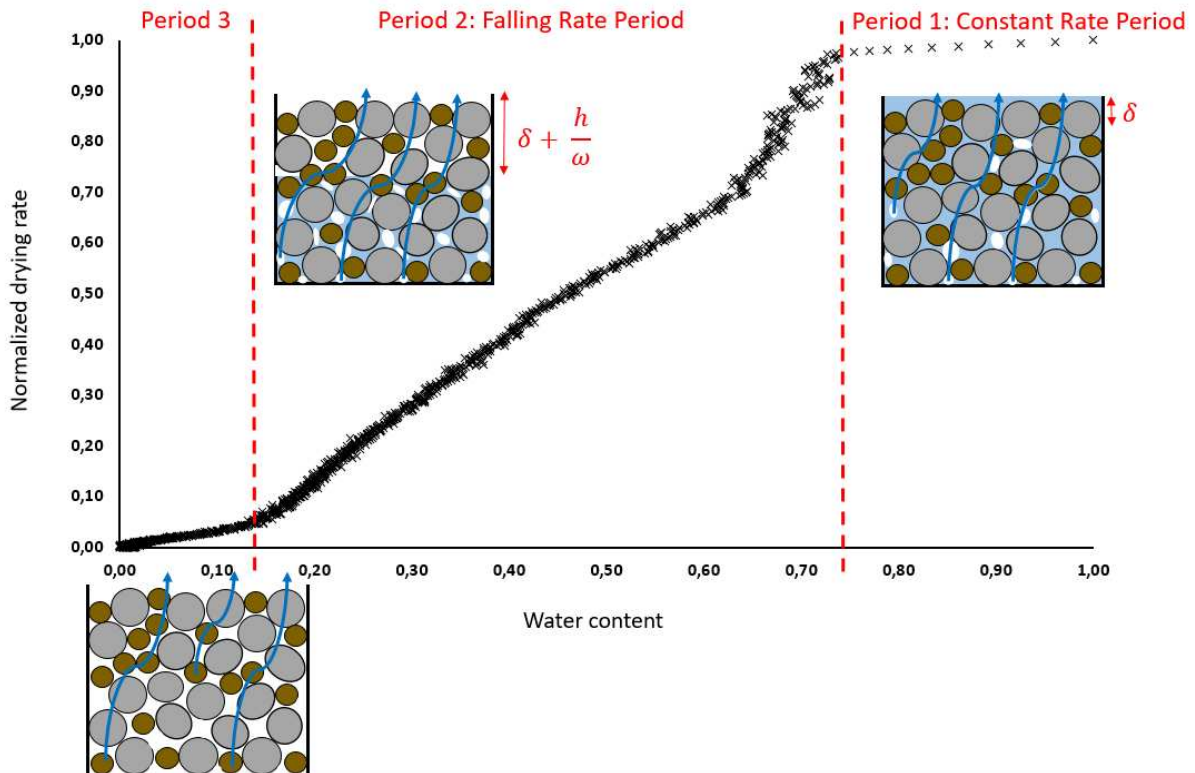


Figure 2-5. Drying rates normalized by initial constant drying rate as a function of water content (ratio of water mass evaporated and initial water mass) of cocoa and sand suspension. The arrows represent the water vapor evaporation; the sand particles are represented by the grey circle and the cocoa particles are represented by the brown circles. The white voids represent the capillarity.

We plot in Figure 2-5 the drying rate normalized by the initial constant drying rate (ratio of the derivative of water mass evaporated and derivative of evaporation time) as a function of water content (ratio of evaporated water mass and initial water mass). We observe that the drying kinetic of defatted cocoa and sand suspension is divided into 3 periods.

In the first period (right part in Figure 2-5), called the “constant rate period”, around 30% of water is evaporated at a constant drying rate of 1.3 g/h corresponding to a uniform but decreasing water distribution in the sample. In this stage, air inside the sample is saturated by water vapor preventing any evaporation, thus drying occurs only at the sample surface. As there is always water at the sample surface, this implies that water flows inside the porous medium. The capacity of the porous media to provide water to the surface depends on the capillary forces [8-10]. In our experiment, these forces order of magnitude is around 10 kPa, i.e., 100 times greater than gravity forces (see Equation 2-5 and 2-6). Therefore, water flows in the porous medium according to Darcy’s law with a pressure gradient dominated by capillary forces. From the measured drying rate, we can calculate a diffusion length of water vapor (Equation 2-7) above the sample, δ , considering that water vapor diffuses along one

direction according to Fick's law and that the air flux in the tunnel is dry, which sets the external vapor density at $n_0 = 0 \text{ g/m}^3$. At the sample surface, air is saturated with water vapor i.e., $n_{sat} = 23.4 \text{ g/m}^3$ (at 25 °C). The computed diffusion length is equal to 8 mm.

$$F_{Capillary} = \frac{\gamma}{r} \quad (2 - 5)$$

$$F_{Gravity} = \rho gh \quad (2 - 6)$$

$$\delta = \frac{D n_{sat} S}{(dm/dt)_{initial}} \quad (2 - 7)$$

With $\gamma = 70 \text{ nM/m}$ is the surface tension, $r = 10 \text{ }\mu\text{m}$ is the size of the particles, $\rho = 1$ is the density of water, $g = 9.8 \text{ m/s}^2$ is the acceleration, and $h = 1.6 \text{ cm}$ is the height of the petri dish. $D = 2.7 \times 10^{-5} \text{ m}^2/\text{s}$ is the water vapor diffusion coefficient in the air, $S = 6.4 \times 10^{-3} \text{ m}^2$ is the sample surface area, and $(dm/dt)_{initial} = 1.4 \text{ g/h}$ is the initial drying rate.

In the second period (center of Figure 2-5), called the "falling rate period", the evaporation of water from the surface of the sample by the tunnel flux being too high (or too fast), there is not enough water in the sample to replace the water evaporated at the surface. This leads to the progression of a dry front inside the porous medium. Then, the water vapor must diffuse inside the sample over an increasing diffusion length of water vapor, δ^* , which slows down the drying rate. The diffusion length is now $\delta^* = \delta + h/w$ ($h = 1.6 \text{ cm}$ being the height of the petri dish and $w = 25\%$ being the porosity (i.e., the volume occupied by the water in the petri dish)) and the drying rate is decreased by a factor 10 approximately.

Generally, the two periods described above that are the only ones encountered in the drying kinetics of a permeable non-deformable porous media [8, 11]. However, we observe a third period in our study, and we suggest, similarly to [12], that this period is related to the evaporation of the water accumulated in the cocoa particles' porosity. In order to verify this assumption, we calculate the water height evaporated from our experimental data (drying rates and water vapor diffusion length). Indeed, if the height of water evaporated at the end of falling rate period is equal to the initial height of the sample (that is also the height of the petri dish ($h = 1.6 \text{ cm}$)), we can conclude that all the water in the petri dish has been evaporated.

$$\frac{(dm/dt)_{end\ of\ falling\ rate\ period}}{(dm/dt)_{initial}} = \frac{\delta + h/w}{\delta} \quad (2 - 8)$$

$$h = 9\delta w \quad (2 - 9)$$

Knowing that the drying rate decreased by a factor 10 from the beginning to the end of the falling rate period, we estimate the water height evaporated to be $h = 1.8$ cm, which is approximately equivalent to the height of the petri dish. This result confirms that, indeed, all the water between the particles is removed at the end of the falling rate period, and thus the further decrease of the drying rate is related to presence of water in the cocoa particles. Therefore, knowing the proportion of water remained in the cocoa particle's pores at the end of falling rate period, porosity and envelope density of cocoa particles can be estimated as follows:

$$\text{Porosity} = \frac{\text{Volume occupied by the remaining water}}{\text{Volume occupied by cocoa particle} + \text{Volume occupied by the remaining water}} \quad (2 - 10)$$

$$\text{Density} = \frac{\text{Volume occupied by the cocoa particle}}{\text{Volume occupied by cocoa particle} + \text{Volume occupied by the remaining water}} \quad (2 - 11)$$

We find an envelope density of 1.20 and a porosity of 21% for cocoa particles. In the following, 1.59 and 1.20 will therefore be used as sugar and cocoa particles envelope density respectively.

2.4 Morphological properties

2.4.1 Particle size distribution

2.4.1.1 Introduction

Particle size distribution (PSD) is a geometric feature that is usually used to describe polydisperse materials (i.e., material containing various size range of particles). Measurements of PSD are important for research and development in many industries, including pharmaceuticals, cements, ceramics, paints and foods.

There is a wide range of techniques that can be used to measure the PSD of a material and they can be divided into 4 groups: counters (Coulter counter...), separation methods (sieving, sedimentation...), light scattering methods (laser diffraction, dynamic light scattering...) and microscopic methods (Imaging particle analysis...). All of these methods rely on the measurement of a certain property of a material, and then compute the PSD from the measured raw data using an appropriate theory. There are several mathematical theories that can be used, and which are described in detail in Van de Hulst's book [13].

In this thesis, we use a light scattering method, namely laser diffraction, to determine the PSD of the sample. Even though determining the PSD of a powder is quite easy using this method knowing the optical indexes of the latter, it becomes more difficult when it is question of a

suspension of two or more powders as one has in chocolate. Indeed, the optical indexes being specific to each material, it is difficult to determine the right one to use when two or more powders are mixed together. Therefore, developing an appropriate method allowing to have a representative PSD of cocoa and sugar suspensions was one of the biggest difficulties encountered during this thesis. In the following, we discuss in detail how this problem can be solved as well as the chosen measurement method and important parameters studied in the framework of this thesis to measure the particle size distributions.

2.4.1.2 Theoretical considerations

2.4.1.2.1 Equivalent spherical diameter

The problem commonly encountered in particle size distribution measurement is the non-sphericity of most particles. Indeed, it is very difficult to directly determine the size of a non-spherical particle unlike a spherical particle. The size of a spherical particle can be represented by only one parameter: its diameter. For non-spherical particles such as the ones of chocolate, there is no single diameter that can be defined, therefore, it is often convenient to define the particle size using the concept of equivalent spheres [14]. In this case, the particle size is defined by the diameter of an equivalent sphere having the same property as the actual particle such as volume or mass for example. The equivalent spherical diameter (ESD) concept depends on the method used to measure the particle size distribution and each of the methods give a characteristic diameter as illustrated in Figure 2-6.

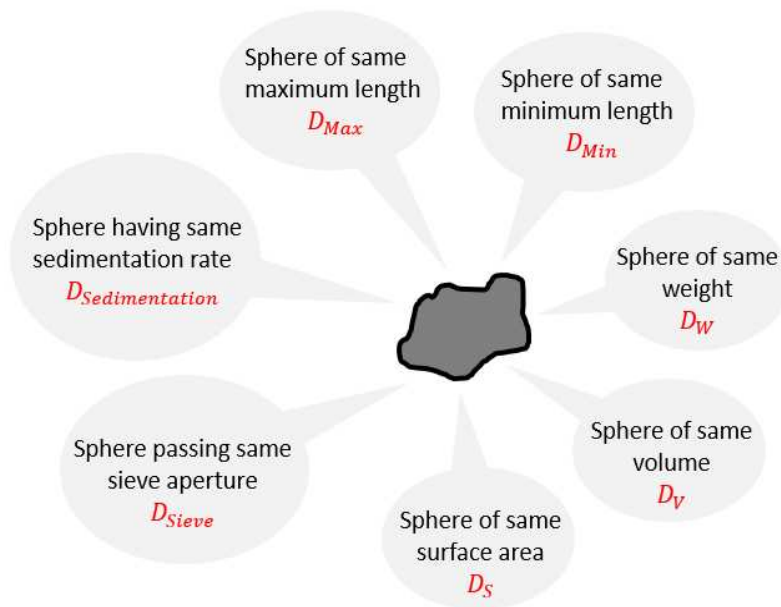


Figure 2-6. The different equivalent spherical diameters of a non-spherical particle.

Each method has its relative strengths and limitations and there is no universally applicable technique for all samples and all situations. However, as shown in Table 2-3, laser diffraction is the commonly used technique, which allows to measure PSD over the widest range. Based on this feature, a laser granulometer is used to measure the size distribution of chocolate's particles during this thesis. Within the frame described above, the diameter measured by laser diffraction is the equivalent diameter of the sphere (D_v) having the same volume as the particle.

Particle size range	0.1nm	1nm	10nm	100nm	1 μ m	10 μ m	100 μ m	1mm	10mm
Laser diffraction			7 decades						
Dynamic Light Scattering	6 decades								
Electrophoretic Light Scattering		5 decades							
Automated Imaging			6 decades						
Sedimentation			4 decades						
Sieving						4 decades			

Table 2-3. List of the commonly used techniques and their particle size ranges [15].

2.4.1.2.2 Parameters influencing the particle size distribution measurement by laser granulometry

For analytical measurements such as PSD, it is important to ensure that the amount of sample used is representative of the whole material PSD. Therefore, a good sampling is of utter importance as highlighted by many authors in literature [16-21]. A second important parameter to consider is the sample dispersion. Indeed, a poor dispersion of the particles leads to the formation of agglomerates and, therefore, an erroneous measurement of the PSD. To avoid agglomeration, additives can be used or sometimes a simple ultrasonic treatment is sufficient to break all agglomerates. The latest important parameter is the mathematical theory used to interpret the results. These theories must take into account the shape of the particle. Indeed, non-spherical particles can be modeled as spheres described by a complex number (n) which is commonly called refractive index (RI). It can be defined mathematically as follows:

$$n = A + iB$$

A is the real component of the complex number and represents the refractive index of the material. The real part is responsible of the light deviation when the latter penetrates the particle. The imaginary component B, usually called the absorption index, represents the absorption of the light beam by the particle crossed.

2.4.1.3 Description of the measuring device

2.4.1.3.1 Malvern Mastersizer 3000: presentation and working principle

Malvern Mastersizer 3000 Laser Particle Size Analyzer is designed to measure the distribution of different sizes within a sample by volume. The Mastersizer 3000 allows the measurement of a wide size range (ranging from 0.01 μm to 3.5 mm). It is composed of a main optical unit, a dispersion unit, a measurement cell and a software which runs on a computer (see Figure 2-7).

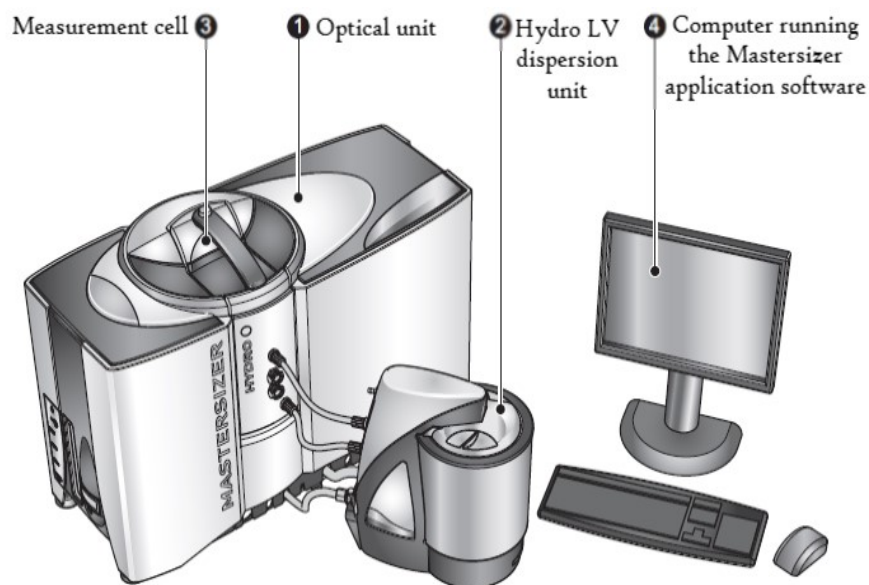


Figure 2-7. A schematic representation of the Mastersizer 3000 Laser Analyzer extracted from Malvern Mastersizer 3000 User Manual.

There are two types of dispersion unit: wet and dry. Wet units control the dispersion of a sample suspended within a liquid dispersant whereas dry units ensure that a dry sample is dispersed and evenly fed to the measurement cell within a continuous stream of air. For materials such as chocolate that are used or produced wet in the manufacturing process, a wet unit is needed to achieve a reproducible dispersion. Therefore, we choose the Hydro LV wet unit from Malvern to measure chocolate particle size distributions. The purpose of the optical unit is to transmit red laser light with a wavelength of 632.8 nm through a sample and then use its detectors to generate data about the light scattering pattern generated by the particles in the sample. The data is then interpreted by the Mastersizer application software to provide accurate particle size information. The measurement cell is the interface between

the dispersion unit and the optical unit. The sample is routed between measurement windows in the cell so that the laser can pass through it in order to make a measurement. This application controls the optical unit and dispersion unit hardware, and also processes the raw data gathered by the system, providing flexible data analysis and reporting features.

2.4.1.3.2 Mie Scattering Theory

In 1905, by working on Maxwell's equations, Gustav Mie proposes a generalized solution to the problem of light diffraction on a sphere. In other words, Mie theory allows to describe the light scattering by homogeneous spherical particles present in a transparent medium which does not absorb. More details on the theory can be found in Bohren and Huffman's book [22]. As previously said, most sizing techniques using a mathematical model (Mie, Fraunhofer, Rayleigh...) [14] to determine a material size distribution, assume that the particles being characterized are spherical and report the particle size as the diameter of the "equivalent sphere", which would show the same response as particles that are being measured. This assumption can only work with the Mie Theory if the material refractive and absorption indexes are known [14]. The use of Mie theory makes it possible to calculate a scattering image very close to that obtained experimentally. The scattering image can be modeled for a known size, wavelength and optical indexes in order to obtain the particle size distribution of the material.

2.4.1.4 Steps followed to develop the particle size distribution protocol of a suspension composed of one powder

2.4.1.4.1 Sampling

Based on Malvern recommendations, we use Gy's sampling theory to estimate the mass of sample required to have a good representativeness. Pierre Gy's theory [17, 18] is usually applied for the sampling of particulate materials of vegetable and mineral origin, including cereals, oil seeds, sugar beets, slags or ingots. A crucial part of Gy's theory deals with the estimation, prediction and minimization of the variance of the Fundamental Sampling Error (FSE) using a formula known as "Gy's formula" (Equation 2-12). The FSE, also called standard error, is defined by Petersen and al. [23] as the only error that can be estimated before measuring a material's PSD.

$$Var_{Gy}(FSE) = \frac{Kd^3}{M_{Sample}} \quad (2 - 12)$$

Where $Var_{Gy}(FSE)$ is the prediction of FSE variance defined by Gy, K is a constant that represents the material intrinsic properties, d is the maximum particle size, and M_{Sample} is the mass of sample.

As predicted by Gy, to reach a standard error of 1%, 5% and 10%, the sample must contain 10000, 400 and 100 particles respectively. Besides, Gy's formula can also be used to calculate the "minimum sample mass" to be incorporated into the measurement cell to have a good representativeness of the particle size distribution of a material (Equation 2-13).

$$M_{min}(sample) = FSE \times GF \times \frac{\pi d^3}{6} \times d_{material} \quad (2 - 13)$$

Where GF is the granulometric factor, $\frac{\pi d^3}{6}$ represents the volume of 1 particle (cm^3) and $d_{material}$ is the density of material ($\text{g}\cdot\text{cm}^{-3}$).

When calculating the variance of FSE, it is presumed that it is proportional to the third power of the maximum particle size (d) as shown in Equation 2-12. However, given that all particles of a material do not have the same size, a correcting factor called granulometric factor is generally used. Gy defined this factor to be equal to 10 when the maximum particle size measured is $D_v(90)$ as it is the case in this thesis. Based on $D_v(90)$ values of fatted cocoa powder and Sugar ($D_{50} = 58.6 \mu\text{m}$) provided by Cargill, the minimum sample masses are calculated with 1% of FSE as follows:

$$M_{min}(fatted\ cocoa\ powder) = 10 \times 10000 \times \frac{\pi \times (55.10^{-4})^3}{6} \times 1.2 = 0.01\text{ g}$$

$$M_{min}(\text{Sugar } (D_{50} = 58.6 \mu\text{m})) = 10 \times 10000 \times \frac{\pi \times (150.10^{-4})^3}{6} \times 1.59 = 0.28\text{ g}$$

2.4.1.4.2 Dispersion

We recall that sugar particles being hydrophilic, they tend to agglomerate in sunflower oil, which is hydrophobic. As mentioned above, these agglomerates may be broken with ultrasonic treatment or by the use of additives. In this thesis, we choose to use additives to disperse the sugar particles in sunflower oil. As additives, we use emulsifiers that are usually found in chocolate: soy lecithin and PGPR. To determine which one will have a greater influence on deflocculating the suspension (i.e., break the agglomerates), the yield stress of the latter is measured after adding different proportions of each emulsifier. Indeed, a dense (i.e., above the percolation critical solid fraction) attractive-particles system is considered deflocculated when it no longer exhibits a yield stress (i.e., no interaction occurring between the particles). The proportions of each emulsifier added ranged from 0 to 2% (with an increment of 0.5%) per total mass of sugar particles. The rheological measurements are carried out using the mixing and rheological protocols described in sections 2.2 and 2.5 respectively.

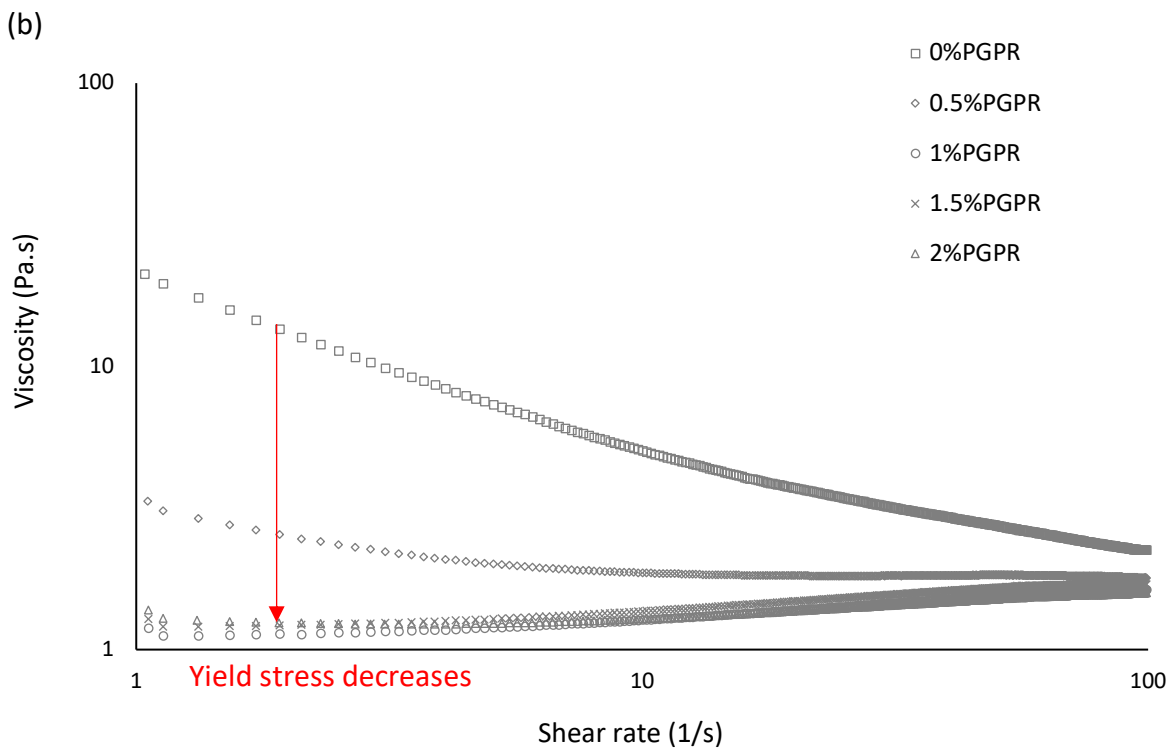
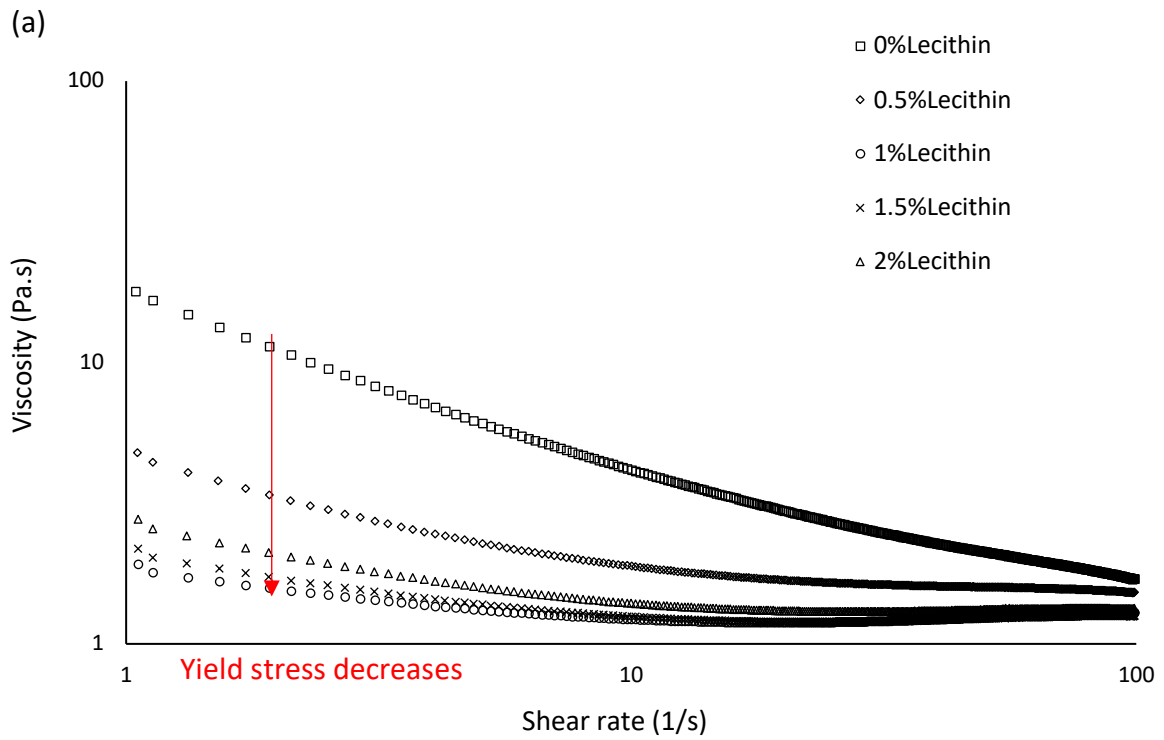
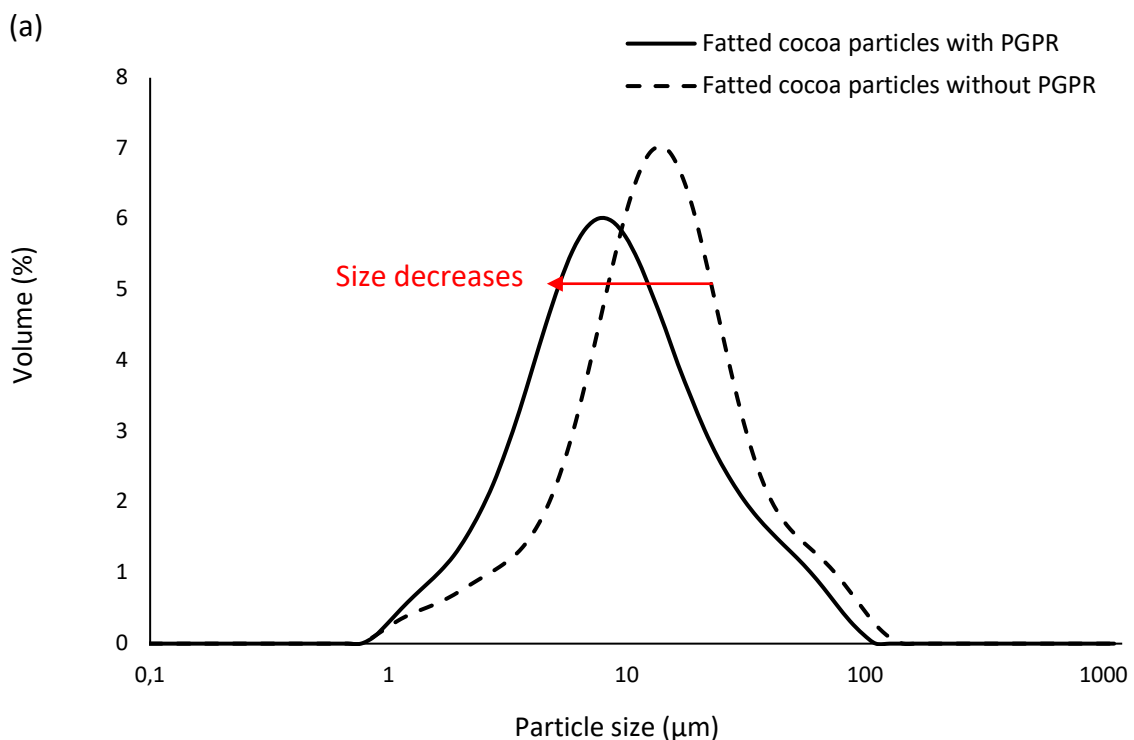


Figure 2-8. Estimation of the amount of (a) Lecithin and (b) PGPR by total mass of Sugar ($D_{50} = 58.6 \mu\text{m}$) required to deflocculate Sugar ($D_{50} = 58.6 \mu\text{m}$) suspension. The solid volume fraction is set at $\phi = 0.53$.

We plot in Figure 2-8 the viscosity as a function of the shear rate for a suspension of Sugar ($D_{50} = 58.6 \mu\text{m}$) in cocoa butter using both emulsifiers. We observe that, in both cases, the lowest value of yield stress is reached when 1% of emulsifier by total mass of sugar particles is added. By fitting the flow curves with Bingham equation, this observation is confirmed, and the yield stress is equal to 1.25 Pa and 0.87 Pa when the emulsifier used is lecithin and PGPR respectively. We conclude from these observations that PGPR must be used as emulsifier to ensure a good dispersion of sugar particles in sunflower oil. By applying the same method to fatted cocoa particles (Cocoa ($D_{50} = 9.2 \mu\text{m}$)), we also find that 1% PGPR is sufficient to deflocculate a system composed of Cocoa ($D_{50} = 9.2 \mu\text{m}$) suspended in cocoa butter. Sugar ($D_{50} = 58.6 \mu\text{m}$) suspension and Cocoa ($D_{50} = 9.2 \mu\text{m}$) suspension are formulated at a solid volume fraction, ϕ of 0.53.

We then measure the particle size distribution of Sugar ($D_{50} = 58.6 \mu\text{m}$) with and without PGPR. We prepare two suspensions. The first one is composed of 10 g of Sugar ($D_{50} = 58.6 \mu\text{m}$) suspended in 8 g of solution containing 7 g of sunflower oil and 1 g of PGPR. The second one is composed of 10 g of Sugar ($D_{50} = 58.6 \mu\text{m}$) suspended in 8 g of sunflower oil. The measurement is performed after mixing. The same procedure is followed to measure the particle size distribution of Cocoa ($D_{50} = 9.2 \mu\text{m}$). For the measurement, 0.30 g of the suspension (when the latter is composed of sugar particles) is placed in the unit cell to reach an obscuration of 10-15% whereas only 0.05 g of the suspension is required when the latter is composed of cocoa particles. This obscuration range is chosen following Malvern recommendations. Moreover, we note that this range of obscuration allows for a good measurement repeatability and no multiple diffractions.



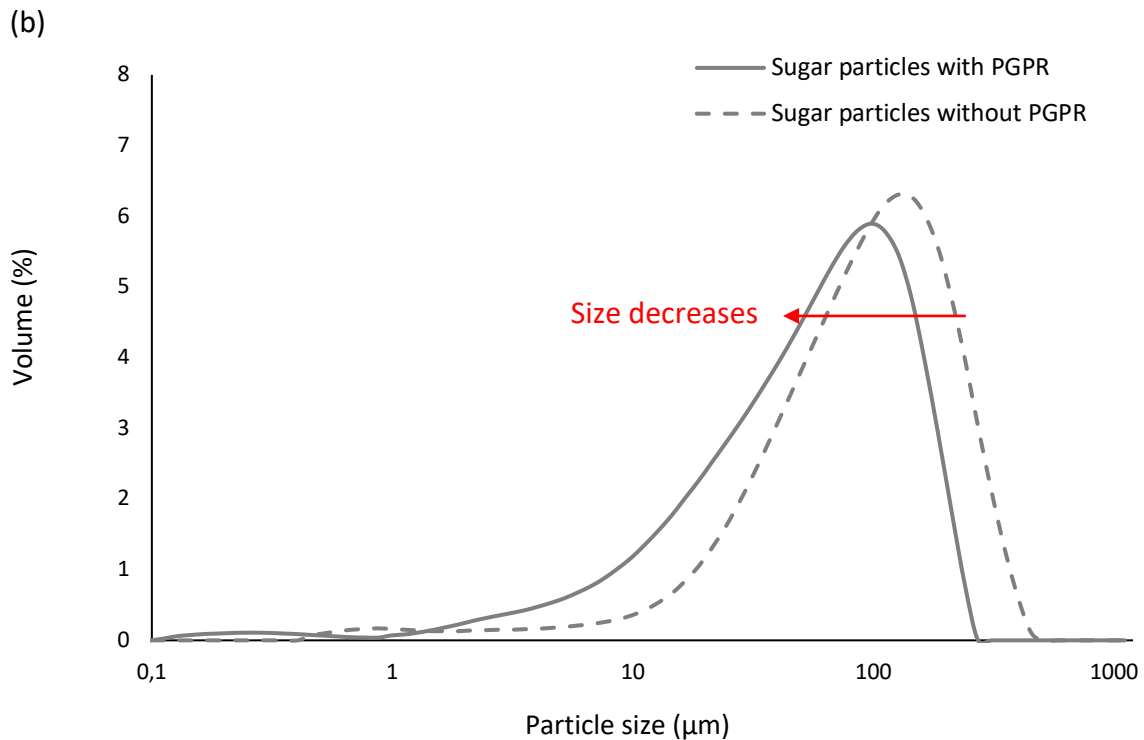


Figure 2-9. Particle size distribution of (a) Cocoa ($D_{50} = 9.2 \mu\text{m}$) and (b) Sugar ($D_{50} = 58.6 \mu\text{m}$) particles in presence and absence of PGPR.

We plot in Figure 2-9 the volume proportion as a function of the particle size for both particles. We observe that, in both cases, there is a shift of the particle size distribution to the left (i.e., particle size decreases) when PGPR is present in the system. This confirms that the PSD measured in absence of PGPR is distorted by the presence of agglomerates in the system, and therefore, the use of PGPR is required to get rid of this artifact preventing from the assessment of true geometrical PSD.

2.4.1.4.3 Optical indexes

Based on Malvern recommendation (see Table 2-4), the absorption indexes (AI) of cocoa and sugar particles can be, in a first step, roughly estimated. Sugar particles being crystalline, their AI shall be around 0.01 whereas cocoa particle shall have an AI around 0.1 since cocoa is a slightly colored powder.






Appearance	Imaginary RI	Example
	0	Latices
	0.001	Emulsions
	0.01	Crystalline milled powders
	0.1	Slightly coloured powders
	1.0 +	Highly coloured powders

Table 2-4. Absorption indexes based on particle's appearance provided by Malvern.

As suggested by Cargill, we use a refractive index (RI = 1.59) for cocoa. For sugar, the RI is usually assumed to be between 1.51-1.54. To optimize the choice of this refractive index, we use a fit as recommended by Malvern. The fit is between the raw data measured and the data calculated from the optical model that we recall is derived from Mie theory. The distribution curves obtained from these two data must be stackable. A residual is then calculated from these data. There are two kind of residual: weighted and unweighted residual. The unweighted residual corresponds to the raw data and the weighted one to the data calculated with the optical model. If the optical indexes used are right, the values of these residuals shall be equivalent and as low as possible. By measuring the PSD of Sugar ($D_{50} = 58.6 \mu\text{m}$) at RI = 1.51, RI = 1.52, RI = 1.53 and RI = 1.54 and comparing the fit and residuals, the lowest residuals are obtained when a RI of 1.54 is used.

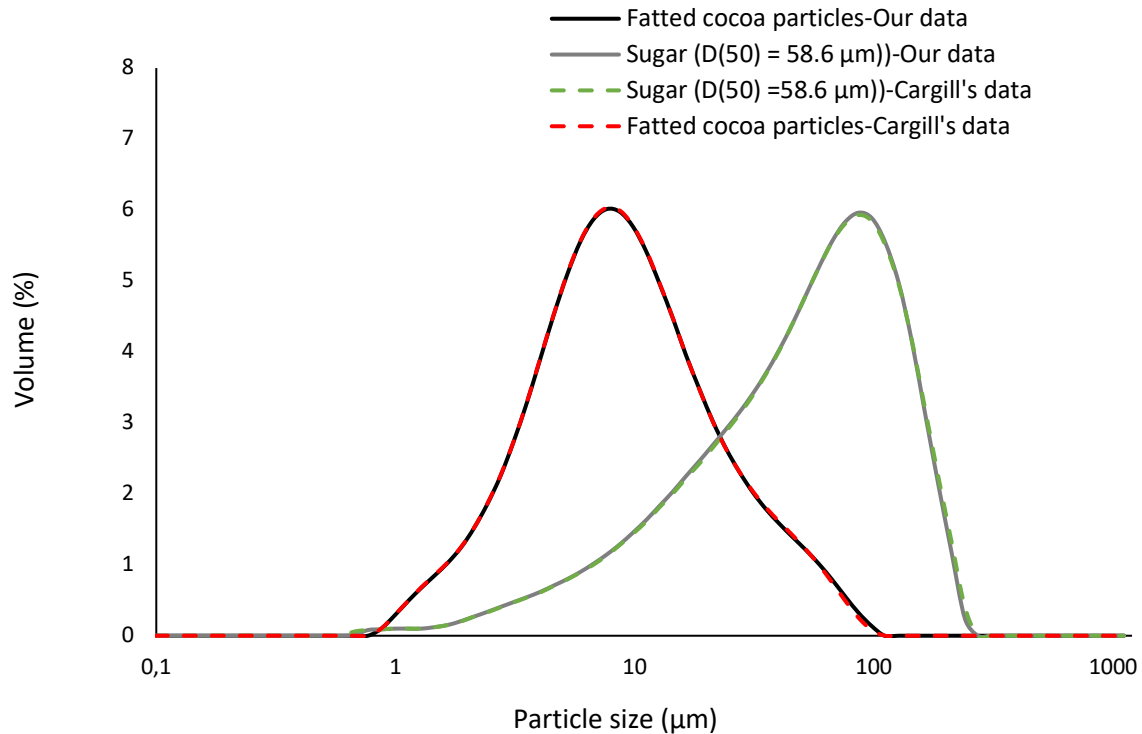


Figure 2-10. Particle size distribution of Cocoa ($D_{50} = 9.2 \mu\text{m}$) and Sugar ($D_{50} = 58.6 \mu\text{m}$) particles.

The particle size distribution measurements of Cocoa ($D_{50} = 9.2 \mu\text{m}$) particles and Sugar ($D_{50} = 58.6 \mu\text{m}$) particles are also carried out by Cargill using the optical indexes and dispersion procedure described previously. However, they use a Malvern apparatus composed of a Hydro SM unit cell instead of a Hydro LV. Figure 2-10 shows that their results that are in good agreement with ours. This suggests that the protocol developed to measure the particle size distribution is reliable.

2.4.1.5 Steps followed to develop the particle size distribution protocol of a suspension composed of two or more powders

As previously mentioned, it is usually difficult to measure the particle size distribution of a suspension composed of two or more powders as they have different optical indexes. We develop here a method, which allows to moderate the error generated by the optical indexes' variation.

First of all, we calculate the PSD we must have if we formulate a suspension composed of 40% of Cocoa ($D_{50} = 9.2 \mu\text{m}$) (i.e., 47% by total volume of solid particles) and 60% of Sugar ($D_{50} = 58.6 \mu\text{m}$) (i.e., 53% by total volume of solid particles) by total mass of solid particles. The particle size distribution by volume of this suspension is obtained by averaging the average particle size distribution by volume obtained with the optical indexes of cocoa and sugar according to their respective volume proportion. Then, the PSD is measured experimentally

by using both cocoa and sugar optical indexes. By applying sugar’s optical indexes to the mixture, we observe the appearance of a peak around 0.8 μm whereas there is no peak when cocoa’s optical indexes are applied (Figure 2-11). As shown in Figure 2-12, this peak appears when sugar’s optical indexes are applied to cocoa particles whereas cocoa’s optical indexes have no influence on Sugar ($D_{50} = 58.6 \mu\text{m}$) PSD. Finally, we find that by averaging the average PSDs obtained using each optical index, we have an experimental PSD that minimizes the error on the volume proportion of fine particles, and which is close to the PSD calculated. We summarize in Table 2-5 the diameters measured for each PSD curve represented in Figure 2-11.

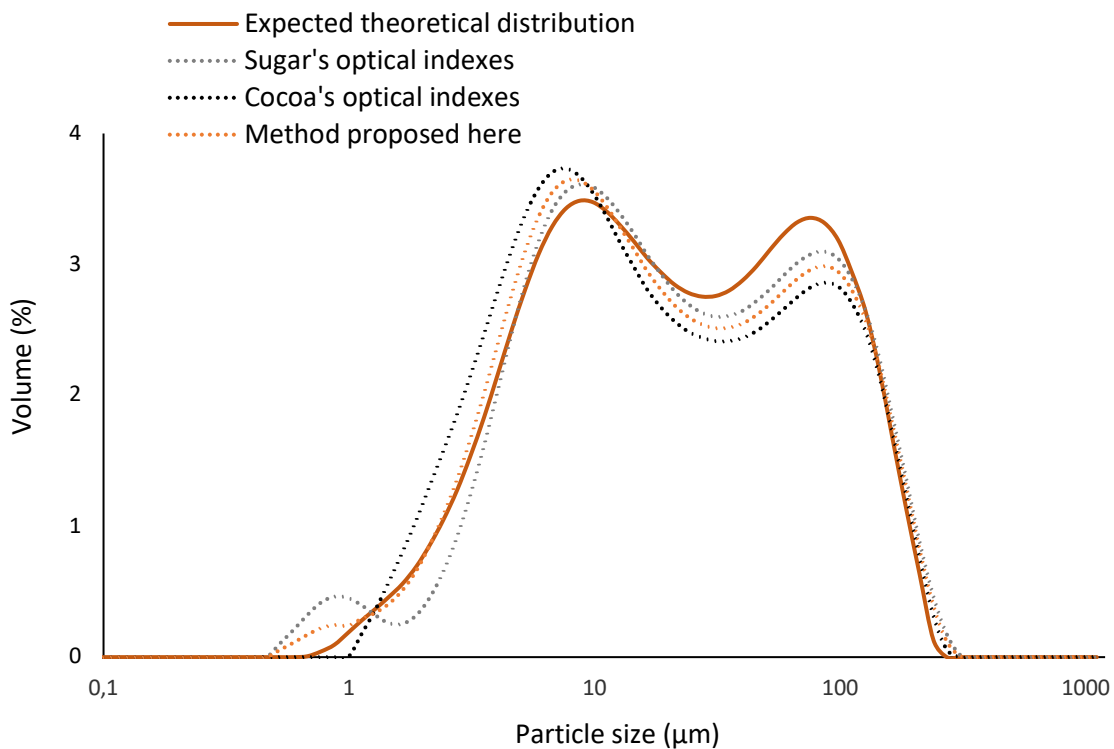


Figure 2-11. Particle size distribution of Cocoa ($D_{50} = 9.2 \mu\text{m}$) particles, Sugar ($D_{50} = 58.6 \mu\text{m}$) particles and Cocoa ($D_{50} = 9.2 \mu\text{m}$) + Sugar ($D_{50} = 58.6 \mu\text{m}$) particles.

	$D_{10}(\pm 0.15\mu\text{m})$	$D_{50}(\pm 0.09\mu\text{m})$	$D_{90}(\pm 0.25\mu\text{m})$
Expected theoretical distribution	6.93	35.44	93.72
Cocoa’s optical indexes	3.57	16.9	124
Sugar’s optical indexes	4.04	19.61	121.8
Method proposed here	4.46	22.02	119

Table 2-5. Particle diameters measured while applying sugar’s optical indexes, cocoa’s optical indexes and both optical indexes to a suspension of 47% of Cocoa ($D_{50} = 9.2 \mu\text{m}$) and 53% of Sugar ($D_{50} = 58.6 \mu\text{m}$) by total volume of solid particles.

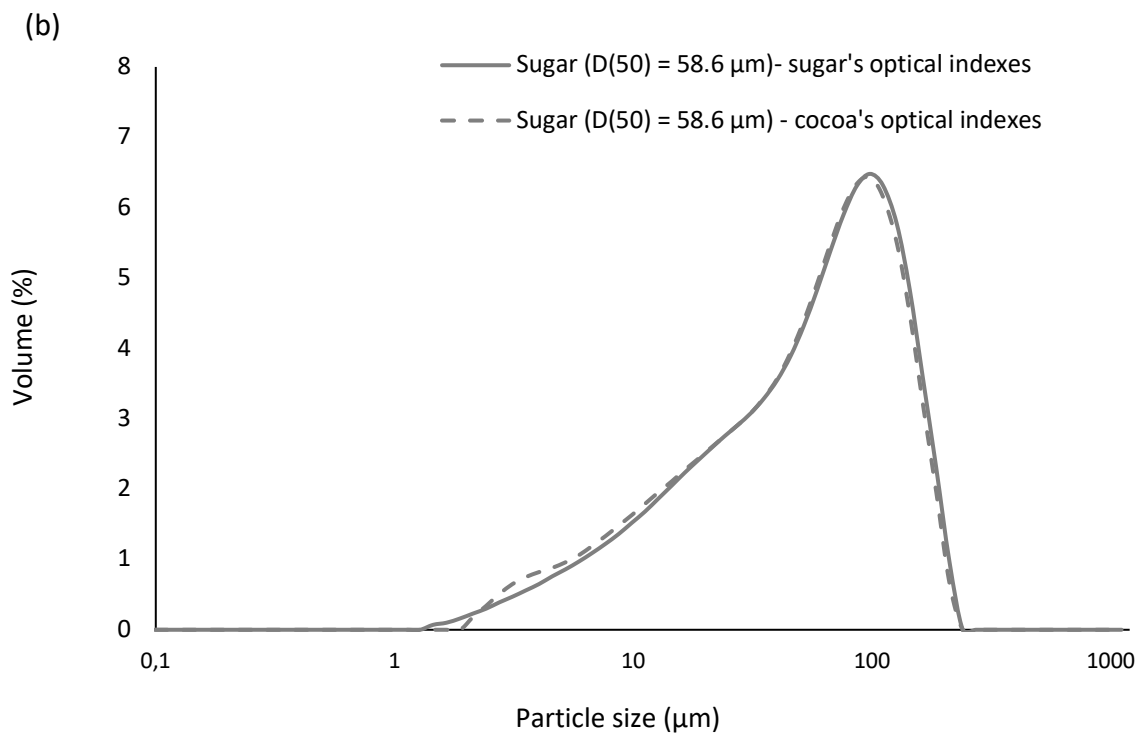
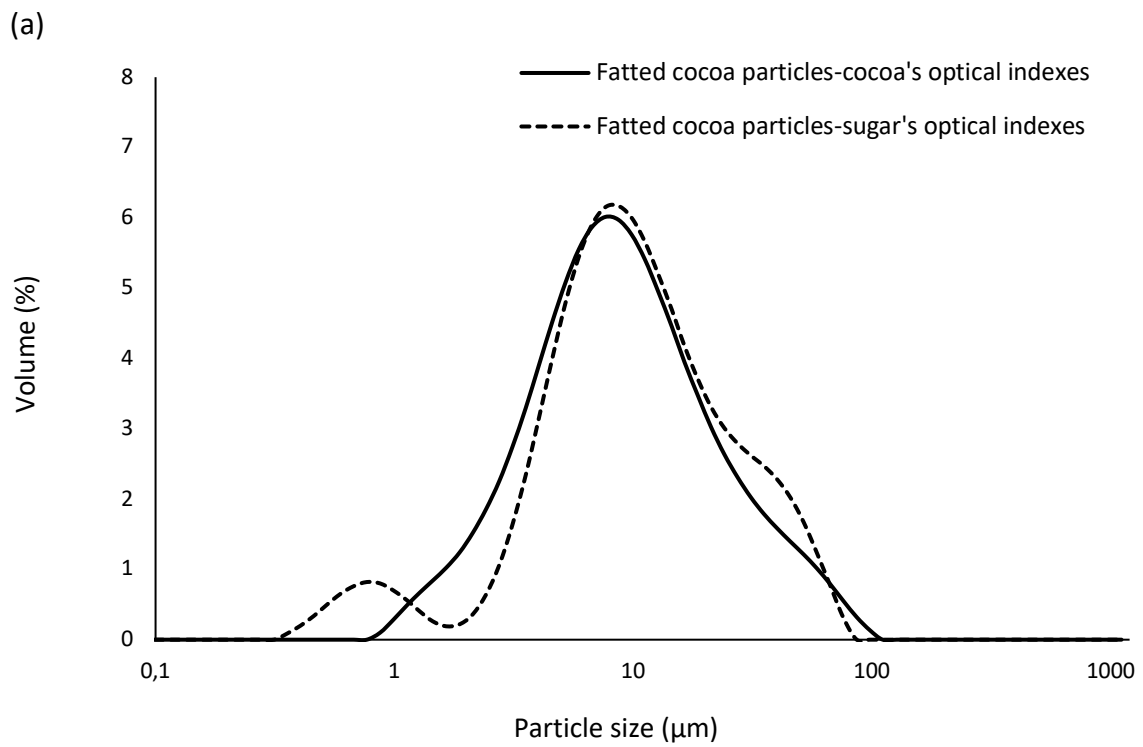


Figure 2-12. Particle size distribution of (a) Cocoa ($D_{50} = 9.2 \mu\text{m}$) and (b) Sugar ($D_{50} = 58.6 \mu\text{m}$) particles while applying both optical indexes.

2.4.1.6 Particle size distribution: developed protocols

We summarize in this section the steps of the developed protocol.

For a suspension composed of one powder:

- Prepare a suspension composed of 10 g of the solid particles dispersed in a solution made of 7 g of sunflower oil and 1 g of PGPR
- Mix the suspension by following the mixing protocol described in section 2-2
- Enter the particle's optical indexes in the apparatus software

	Refractive index	Absorption index
Cocoa particles	1.59	0.1
Sugar particles	1.54	0.01
Sunflower oil	1.46	-

- Place 0.30 g of the suspension (when the latter is composed of sugar particles) in the unit cell and only 0.05 g when the suspension is made of cocoa particles.
- Verify that the obscuration is between 10-15%
- Measure the PSD

For a suspension of known composition made of two or more powders (sugar and cocoa in the example below):

- Prepare a suspension composed of 10 g of the solid particles (40% cocoa and 60% sugar by total mass of solid particles) dispersed in a solution made of 7 g of sunflower oil and 1 g of PGPR
- Mix the suspension by following the mixing protocol described in section 2-2
- Place the suspension in the oven at 45-50°C overnight
- Place 0.30 g of the suspension in the unit cell and verify that the obscuration is between 10-15%
- Enter sugar's optical indexes in the apparatus software
- Measure the particle size distribution (PSD (1))
- Enter cocoa's optical indexes in the apparatus software
- Measure the particle size distribution (PSD (2))
- Estimate the experimental particle size distribution by volume of this suspension as follows:

Volume proportion of dark chocolate (γ):

$$\gamma = (\alpha \times \text{PSD (2)}) + (\beta \times \text{PSD (1)})$$

With:

Volume proportion of sugar particles (α):

$$\alpha = \frac{\text{Volume of sugar}}{\text{Volume of sugar} + \text{Volume of cocoa particles}}$$

Volume proportion of cocoa particles (β):

$$\beta = \frac{\text{Volume of cocoa particles}}{\text{Volume of sugar} + \text{Volume of cocoa particles}}$$

We recall that:

$$\text{Volume of sugar} = \frac{\text{Mass of sugar}}{\text{Density of sugar}}$$

$$\text{Volume of cocoa particles} = \frac{\text{Mass of cocoa particles}}{\text{Density of cocoa particles}}$$

2.4.2 Maximum Packing Fraction

2.4.2.1 Introduction

We recall first that the maximum packing fraction (ϕ_{max}) is an important parameter to study since, as explained in chapter 1, it allows for the control of the viscosity of a suspension. Three types of packing can be defined. Ordered or dense packing corresponds to the highest geometrically admissible packing. It is, for spheres or cubes, a crystallized state (i.e., displaying a periodic structure). For highly elongated particles, it is an asymptotic state that is rarely reached in practice and not relevant for viscosity prediction. Random loose packing is another asymptotic packing state, which corresponds to particles packed without any external energy. It corresponds therefore to the absolute minimum solid volume fraction required for contact percolation between particles. It is highly relevant for viscosity prediction, but it is extremely delicate to measure experimentally as any vibration or gravity effect will force the particles to pack more than in this critical state. Finally, random close packing corresponds to the packing of particles pile under a given amount of compaction energy. The higher the energy, the closer random packing gets to dense packing. In most experiments, it is such a value that is measured. As a consequence, random close packing measurement are dependent on the amount of energy brought to the system and therefore on the experiment itself. We choose however here to measure a random close packing value because it is easy to measure it experimentally, and it is relevant for viscosity prediction.

Several methods allow for the assessment of the random close packing. These include the solid bed density (SBD) technique [24], pressure filtration, centrifugation and osmotic consolidation technique [25] or the water demand method [26]. To compare the packing density of different systems it is necessary to follow the same experimental method. It must also be kept in mind that inter-particle forces can affect the maximum packing fraction measurement of colloidal suspensions [27, 28]. Therefore, it is necessary to suppress these

forces in order to measure a geometrical maximum packing fraction, which, we recall, only depends on the size and shape of the particles [29].

2.4.2.2 Compressive Yield Stress

When mechanical loads such as artificially generated by centrifugation are applied directly to a suspension, the latter consolidates into a denser system. In order to predict how much compaction will occur under a given mechanical load, several models for the compressive constitutive response (i.e., the degree of compaction) of a suspension can be found in literature. Some of those models, analogous to the Bingham model for the shear response of a fluid, describes the constitutive response through a compressive yield stress and a compressive viscosity [30, 31]. However, literature shows that a compressive yield stress model with negligible compressive viscosity can successfully describe the consolidation response under mechanical loads in many systems [31, 32-34]. The compressive yield stress, $P_y(\phi)$, is typically a strong function of solid volume fraction, ϕ , which is often describe using power-law [35, 36], exponential [35, 37, 38], or other mathematical equations [30-32, 39, 40].

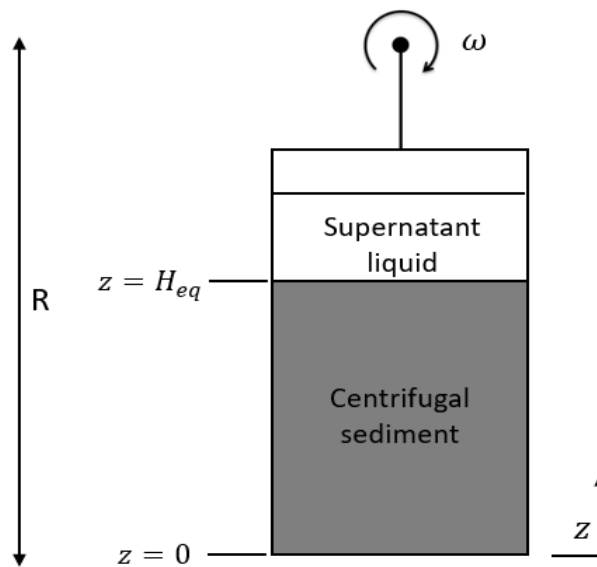


Figure 2-13. Schematic of centrifugation coordinate systems.

To determine $P_y(\phi)$ from centrifuge experiments, two techniques can be used: multiple speed technique [30, 31, 41, 42] and volume fraction profile technique [31, 32]. Equilibrium is considered achieved when fluid flow ceases and the sediment height no longer change with time. At equilibrium, the pressure acting upon any point in the system is merely the cumulative weight of all particles above that point [30, 32]:

$$P_y[\phi(z)] = \int_z^{H_{eq}} \Delta\rho g(z) \phi(z) dz \quad (2 - 14)$$

Where z is the height, measured from the bottom of the centrifuge tube (see Figure 2-13), $P_y[\phi(z)]$ the pressure acting upon the suspension, H_{eq} the equilibrium sediment height, $\Delta\rho$ the difference in density between the solid and liquid phases, g the gravitational or centrifugal acceleration, and ϕ the solid volume fraction. The acceleration g is a function of both spinning speed and height up the column:

$$g(z) = \omega^2 R (1 - z/R) = g_0 (1 - z/R) \quad (2 - 15)$$

Where ω is the angular velocity of the rotor, R is the distance from the rotor center to the bottom of the sediment column, and g_0 is the acceleration at the base of the sediment column.

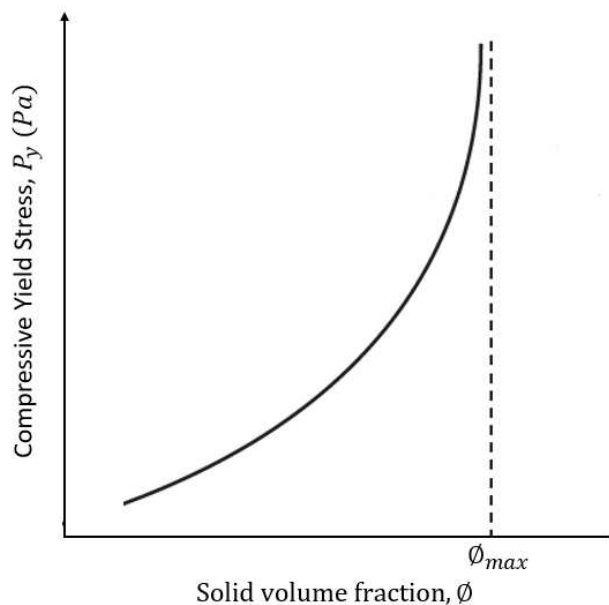


Figure 2-14: Representation of a Compressive Yield Stress curve.

From knowledge of the equilibrium heights measured at each speed, the pressure, $P_y(\phi)$, and the solid volume fraction, ϕ , a compressive yield curve can be determined (see [25] for more details). A representation of the shape of this curve is shown in Figure 2-14. We can observe from this figure that above a critical solid volume fraction ϕ , $P_y(\phi)$ diverges. This critical solid volume fraction is assumed to correspond to the maximum packing fraction, ϕ_{max} .

In this work, we consolidate a suspension of chocolate by applying the highest speed allowed by our device (i.e., 4500 rpm). We measure the height at equilibrium and compute a mean volume fraction along the tube using the following equation [30, 41]:

$$\phi_{max} = \phi_0 \cdot \frac{H_0}{H_{eq}} \quad (2 - 16)$$

Where ϕ_0 is the initial solid volume fraction and H_0 is the initial height.

Our centrifugation method requires to:

- accurately determine the initial and equilibrium heights
- work on deflocculated system in order to avoid particle-particle interactions that can mislead the estimation of the maximum packing fraction ϕ_{max}
- work on homogeneous system (i.e., no particle size separation due to difference in density)

In the following, we detail the steps followed to determine all these key parameters.

2.4.2.3 Measuring device: Centrifuge 3-16PK

Centrifugal loads are applied using a Sigma 3-16 PK laboratory centrifuge (Sigma Laborzentrifugen GmbH, Germany) to measure the maximum packing fraction. The centrifuge is equipped with a swing-out rotor, which has a speed range from 102 to 4500 rpm. The distance from the center of rotation to the bottom of the suspension in such tubes is approximately 153 mm. The centrifuge temperature is set up at 40°C throughout the measurement.

2.4.2.4 Steps followed to develop the protocol

2.4.2.4.1 Deflocculation

We recall here that it is important to deflocculate a system when determining its maximum packing fraction because the latter shall only depend on particle size distribution and particle shape and the presence of inter-particle interactions can affect the measurement. Sugar ($D_{50} = 58.6 \mu\text{m}$) + Cocoa ($D_{50} = 9.2 \mu\text{m}$) particles suspended in cocoa butter compose the system studied in this section. The initial solid volume fraction is $\phi_0 = 0.53$. The proportion of PGPR required to deflocculate the system is determined by following the same procedure than in section 2.4.1.4.2. Indeed, by adding a proportion of PGPR ranging from 0.5 to 2% by total mass of solid particles to Sugar ($D_{50} = 58.6 \mu\text{m}$) + Cocoa ($D_{50} = 9.2 \mu\text{m}$) particles suspension, we find that 1.5% PGPR by total mass of solid particles is sufficient to entirely deflocculate the suspension.

Knowing that, the highest speed of the rotor (i.e., 4500 rpm) is applied to determine the maximum packing fraction of flocculated and deflocculated Sugar ($D_{50} = 58.6 \mu\text{m}$) + Cocoa ($D_{50} = 9.2 \mu\text{m}$) suspensions. After mixing, the suspension is poured in 50 ml polypropylene conical-bottom tubes. Initial suspension heights measured after filling the tubes are 84 mm. However, by measuring again the initial height at the end of centrifugation, we find $H_0 = 82$ mm. We suggest that after mixing, there are entrapped air bubbles in the suspension, what distort the measurement of the initial height at the beginning. In the following, the initial height will always be measured at the end of centrifugation for all studied suspensions. After

spinning for 1 hour, the sample is removed from the centrifuge and the sediment height is measured; the sample is then spun further, and the height is again measured. This cycle is repeated until there is no change in the height. The initial and equilibrium heights are measured using a steel ruler to a precision of 0.1 mm.

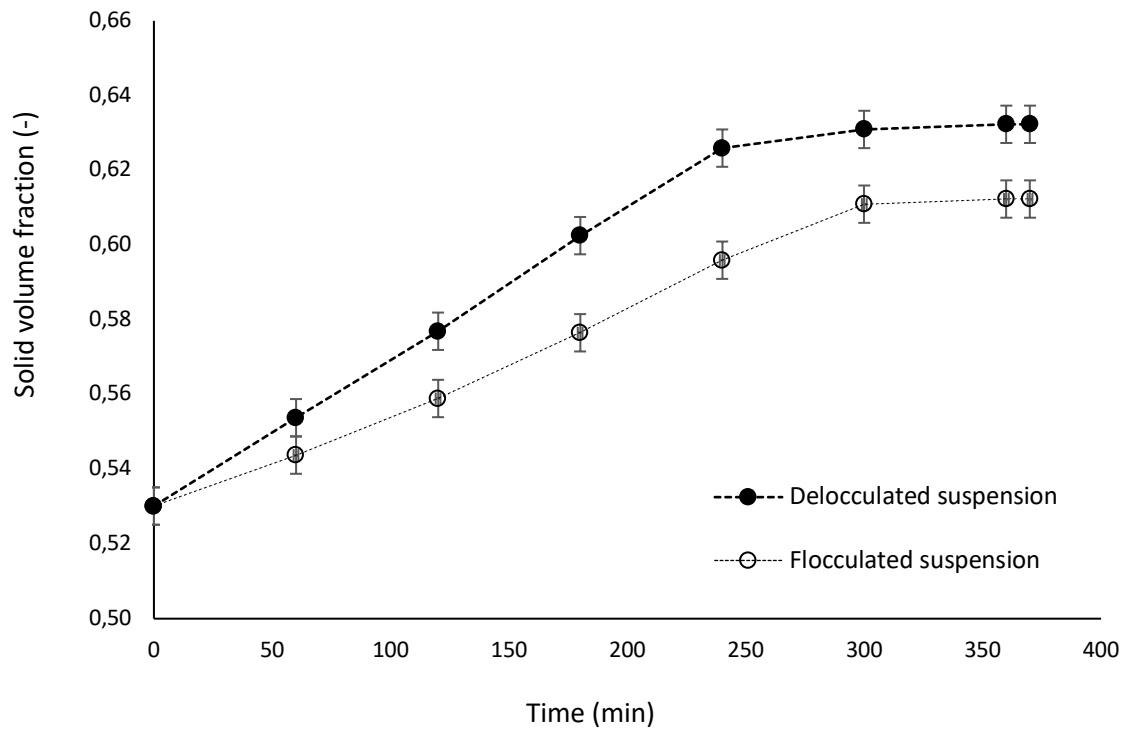


Figure 2-15. Solid volume fractions calculated while applying the highest speed in flocculated (unfilled circles) and deflocculated (filled circles) Sugar ($D_{50} = 58.6 \mu\text{m}$) + Cocoa ($D_{50} = 9.2 \mu\text{m}$) suspensions. The initial solid volume fraction and height are $\phi_0 = 0.53$ and $H_0 = 82 \text{ mm}$ respectively.

We plot in Figure 2-15 the evolution of the solid volume fraction as a function of the centrifugation time. We recall here that these solid volume fractions are calculated from Equation 2-11. We observe that the highest solid volume fraction is reached for the deflocculated suspension ($\phi_{max} = 0.63$ instead of 0.61 for the flocculated suspension) after 5 hours of centrifugation. This result confirms that maximum packing fraction must be measured in deflocculated state.

2.4.2.4.2 Multiple speeds technique

Increasing successively the speed applied allows to avoid particle size separation between Sugar ($D_{50} = 58.6 \mu\text{m}$) + Cocoa ($D_{50} = 9.2 \mu\text{m}$) particles. Indeed, since there is an important difference between their densities (1.59 for sugar and 1.2 for cocoa) and sizes, applying the highest speed directly can affect the suspension homogeneity and lead to a loose packing of the system. Four speeds (1613, 2280, 2593 and 4500 rpm) are therefore used, chosen over

the rotor's range to give the wanted gravitational field. We start at a speed of 1613 rpm because we observe that below this speed, the sugar particles are on the bottom of the centrifuge tube whereas cocoa particles are on the top.

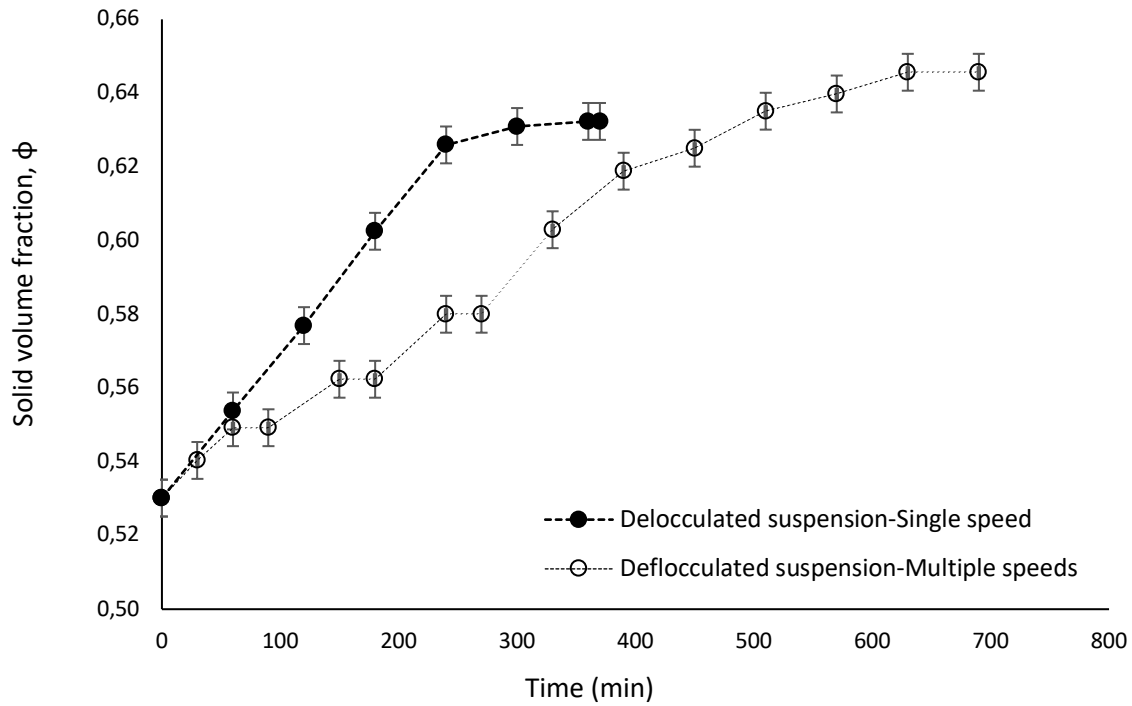


Figure 2-16. Solid volume fractions evolution while applying multiple speeds and single speed techniques to deflocculated Sugar ($D_{50} = 58.6 \mu\text{m}$) + Cocoa ($D_{50} = 9.2 \mu\text{m}$) suspension. The initial solid volume fraction and height are $\phi_0 = 0.53$ and $H_0 = 82 \text{ mm}$ respectively.

We measure the maximum packing fraction at deflocculated state for Sugar ($D_{50} = 58.6 \mu\text{m}$) + Cocoa ($D_{50} = 9.2 \mu\text{m}$) suspension at solid volume fraction, $\phi_0 = 0.53$ and initial height, $H_0 = 82 \text{ mm}$ while applying multiple speed technique. We plot in Figure 2-16 the solid volume fraction as a function of the centrifugation time. We observe that for the first three speeds the equilibrium height is reached after 1 hour of centrifugation since the solid volume fraction remains constant whereas it took 6 hours to reach the equilibrium height for the last speed. The maximum packing fraction measured is 0.65 which is higher than the one measured by single speed technique (see Figure 2-16). This suggests that the multiple speed technique is more accurate for maximum packing fraction measurements.

2.4.2.4.3 Initial solid volume fraction

Increase the compressive yield stress of a material and therefore its maximum packing fraction require to either increase the centrifugation speed or increase the initial solid volume fraction of the sample. Since in this thesis, we choose rather to increase gradually the centrifugation speed, it is important to ensure that an increase of the initial volume fraction will not have

any influence on the maximum packing fraction. It is therefore necessary to determine the initial volume fraction at which one must work to always achieve the real maximum packing fraction of a material. To that end, the maximum packing fractions of suspensions of Sugar ($D_{50} = 58.6 \mu\text{m}$) + Cocoa ($D_{50} = 9.2 \mu\text{m}$) prepared at different solid volume fractions, ϕ_0 (0.35, 0.45, 0.49, 0.53 and 0.57) are determined by applying multiple speeds technique.

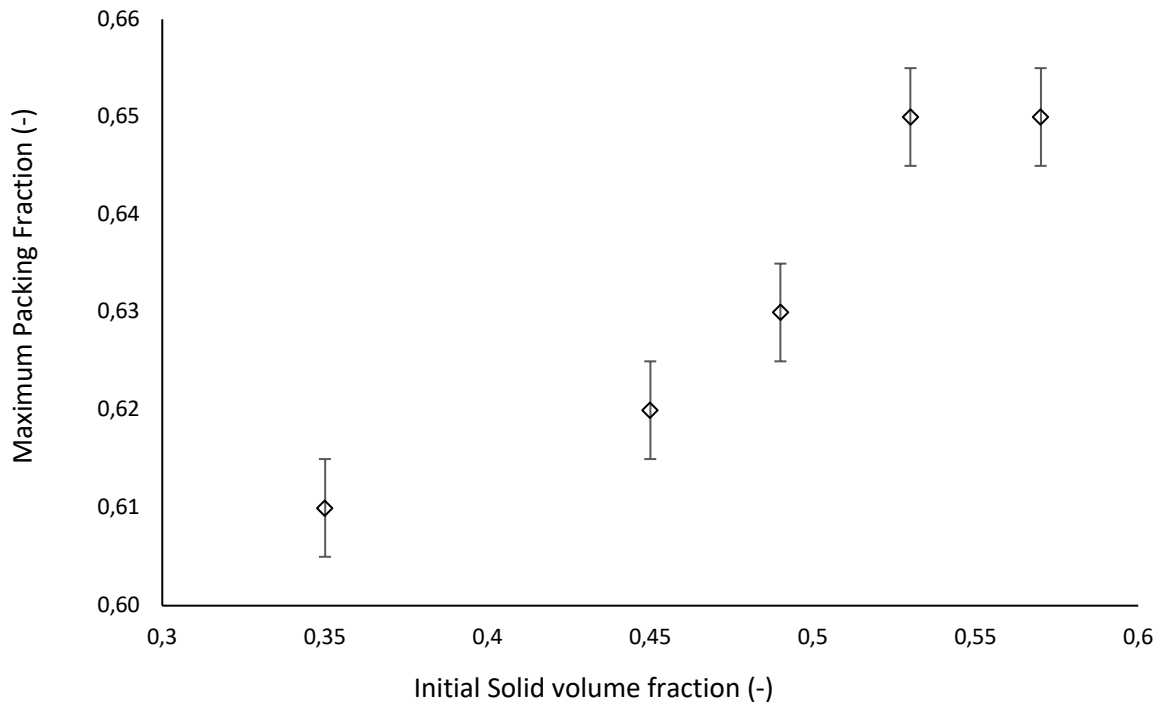


Figure 2-17. Maximum packing fractions measured by centrifugation at different solid volume fractions for Sugar ($D_{50} = 58.6 \mu\text{m}$) + Cocoa ($D_{50} = 9.2 \mu\text{m}$) suspension while applying multiple speeds technique. The initial solid volume fraction and height are $\phi_0 = 0.53$ and $H_0 = 82 \text{ mm}$ respectively.

We plot in Figure 2-17 the maximum packing fraction as a function of the initial solid volume fraction. We observe that the highest maximum packing fraction is obtained for solid volume fractions $\phi_0 = 0.53$ and $\phi_0 = 0.57$. We can conclude from these results that the suspension must be prepared at $\phi_0 = 0.53$ in order to reach the material real maximum packing fraction.

2.4.2.5 Maximum packing fraction: developed protocol

We summarize in this section the developed protocol into the following steps:

- Deflocculate the suspension by adding 1.5% PGPR by total mass of solid particles and make sure to work at initial solid volume fraction higher than $\phi_0 = 0.53$
- Mix the suspension by following the mixing protocol described in section 2.2
- Fill the centrifuge tubes

- Place the tubes in the apparatus and set the temperature at 40°C
- Centrifuge at 1613 rpm for 1 hour
- Centrifuge at 2280 rpm for 1 hour
- Centrifuge at 2593 rpm for 1 hour
- Centrifuge at 4500 rpm for 6 hours
- Remove the tubes from the apparatus and measure the initial and equilibrium heights with a precise steel ruler.
- Use Equation 2-11 to calculate the maximum packing fraction

2.5 Rheological properties

2.5.1 Introduction

As already explained in chapter 1, chocolate suspension displays a shear-thinning behaviour at low shear rate while at high shear rate a Newtonian behavior is observed. We recall that the shear thinning behaviour mainly depends on the magnitude of the attractive forces, solid volume fraction and maximum packing fraction. Viscosity at the Newtonian plateau is owed to the hydrodynamic interactions between particles. It mainly depends on the viscosity of the suspending fluid, the volume fraction of the solid particles, and their maximum packing fraction. In this work, the rheological measurements are conducted with a rheometer equipped with a Vane geometry. In industry, the Couette geometry is often used to determine the rheological behavior of chocolate.

Chocolate suspensions are yield stress fluids (i.e., the suspension flows beyond some critical stress) and thixotropic fluids (i.e., its rheological behaviors evolve upon time and depends on the flow history). Their characterization implies rigorous procedures to ensure reproducibility. Another parameter that has to be controlled during the measurement is the stability of the suspension (i.e., there is no sedimentation observed in the suspension) especially while working in deflocculated state.

In the following, after describing the measuring device, the steps followed to control the key parameters listed above will be presented.

2.5.2 Measuring device: Bohlin C-VOR

Rheometric measurements are performed on chocolate suspensions using a Bohlin C-VOR rheometer equipped with a Vane type geometry [43]. In a Vane geometry, the material is placed between the fin and the vessel (see Figure 2-18). The Vane geometry used here consists of a 4-blade fin centered on a rod. The radius of the fin is $R_f = 12.5$ mm, the radius of the cup $R_0 = 25$ mm and the height $h = 60$ mm.

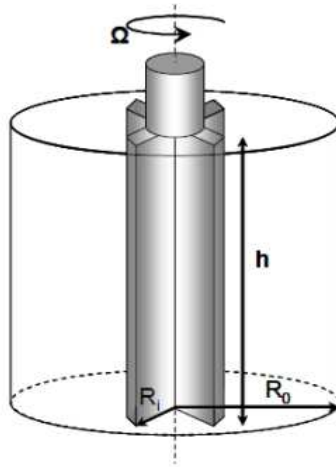


Figure 2-18. Representation of Vane geometry [43].

This geometry allows for the study of systems containing particles covering a wide range of sizes [44]. The outer cylinder is fixed, and the shear is imposed by the rotation of the fin around the symmetry axis at a speed Ω . The flow of material induces a torque C on the fin. The shear stress (τ) in the entire air gap can be determined from the following equation:

$$\tau(r) = \frac{C}{2\pi hr^2} \text{ avec } R_i \ll R_o \quad (2-17)$$

Assuming that there is no slip and that the material is sheared throughout the air gap, the shear rate ($\dot{\gamma}$) and the shear stress (τ) are determined in the middle of the air gap ($R_{average} = \frac{R_o + R_i}{2}$) from the defined equations 2-18 and 2-19 for Couette geometry by analogy [45-47].

$$\dot{\gamma} = \Omega \frac{R_o^2 R_i^2}{R_{average}(R_o - R_i)} \quad (2-18)$$

$$\tau = \frac{C}{2\pi h R_{average}^2} \quad (2-19)$$

To determine the rheological behaviour of the suspending fluid namely cocoa butter, the rheometer is equipped with a striated plane/plane geometry. The cocoa butter is deposited between the two disks, having the same axis of symmetry and the same radius $r = 2$ cm. They are separated by a distance h_e (air gap). The shear is imposed by the rotation of the upper disc around the axis of symmetry at a speed Ω . The flow of material then generates a torque on the C axis (see Figure 2-19).

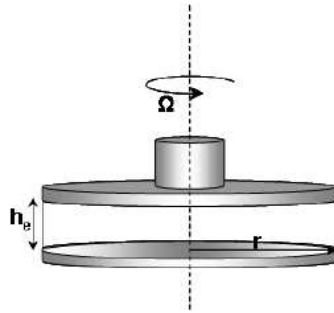


Figure 2-19. Representation of a plane/plane geometry [43].

It is possible to relate the measured rotational speed and the torque to the shear speed and the stress and thus to characterize the behaviour of the material:

$$\dot{\gamma} = \frac{3 \Omega r}{4 h_e} \quad (2 - 20)$$

$$\tau = \frac{3 C}{2 \pi r^3} \quad (2 - 21)$$

We also specify that we keep the rheometer temperature constant at 40°C for all rheological measurements carried out in this thesis.

2.5.3 Steps followed to develop the protocol

2.5.3.1 Rheological behaviour of the interstitial fluid

We first study the rheological behaviour of chocolate interstitial fluid namely cocoa butter. The rheological behaviour of the latter is measured by placing it on the lower disk of the plane/plane geometry and lowering the upper disk until reaching $h_e = 500 \mu\text{m}$. A logarithmic shear ramp increasing from 10 s^{-1} to 1000 s^{-1} followed by a decreasing ramp from 1000 s^{-1} to 10 s^{-1} is applied for 1000 s. We plot in Figure 2-20 the viscosity as a function of the shear rate. We can observe that as expected the cocoa butter exhibits a Newtonian behaviour and its viscosity is 0.05 Pa.s.

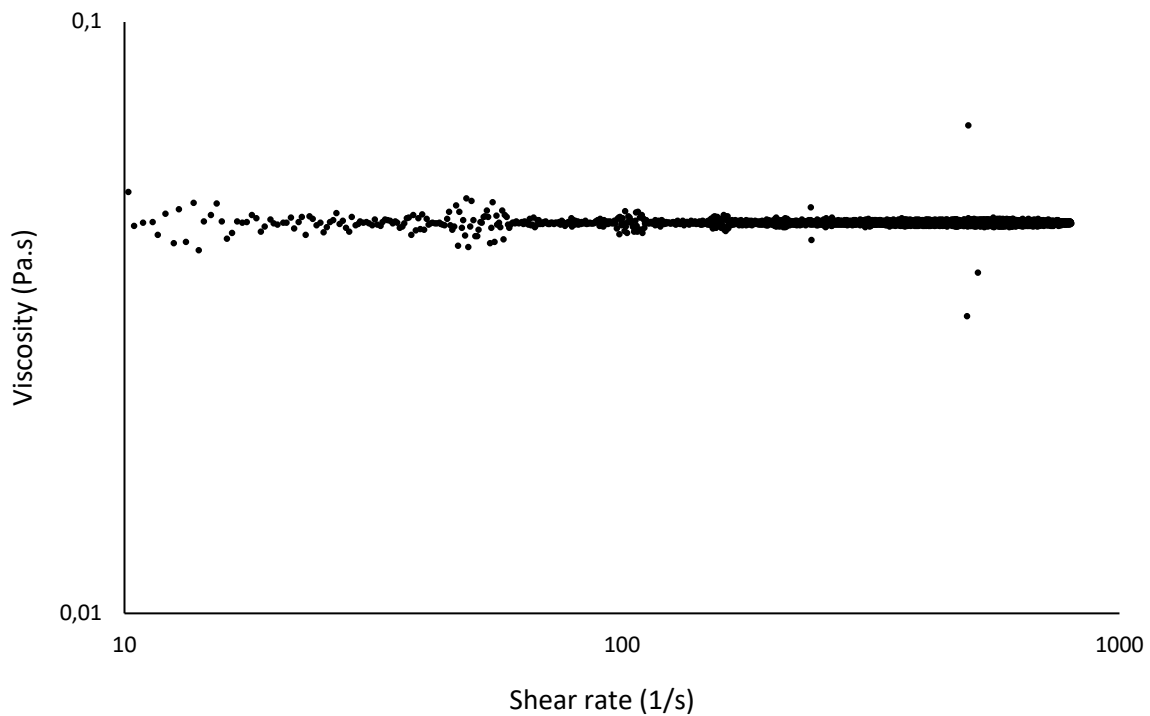


Figure 2-20. Flow curve of cocoa butter.

2.5.3.2 Thixotropic behaviour

To develop a protocol allowing to neglect the thixotropic nature of chocolate, we study the influence of thixotropy on cocoa and sugar suspensions. We formulate two suspensions: Cocoa ($D_{50} = 9.2 \mu\text{m}$) particles suspended in cocoa butter and Sugar ($D_{50} = 58.6 \mu\text{m}$) particles suspended in cocoa butter. Both suspensions are formulated at solid volume fraction of $\phi = 0.53$. After mixing, both suspensions are pre-sheared at 177 s^{-1} during 180 min. After resting for 3 s, the suspension is subjected to a ramp of decreasing shear rates from 100 s^{-1} to 1 s^{-1} for 500 s then a ramp of increasing shear rates from 1 s^{-1} to 100 s^{-1} for 500 s. It is the sequence of decreasing then increasing ramps that allows to verify the influence of thixotropy on the system. Indeed, if the flow curves obtained during the increasing and decreasing ramps are superimposable, it means that the thixotropic nature of the system is negligible within this range of shear rates.

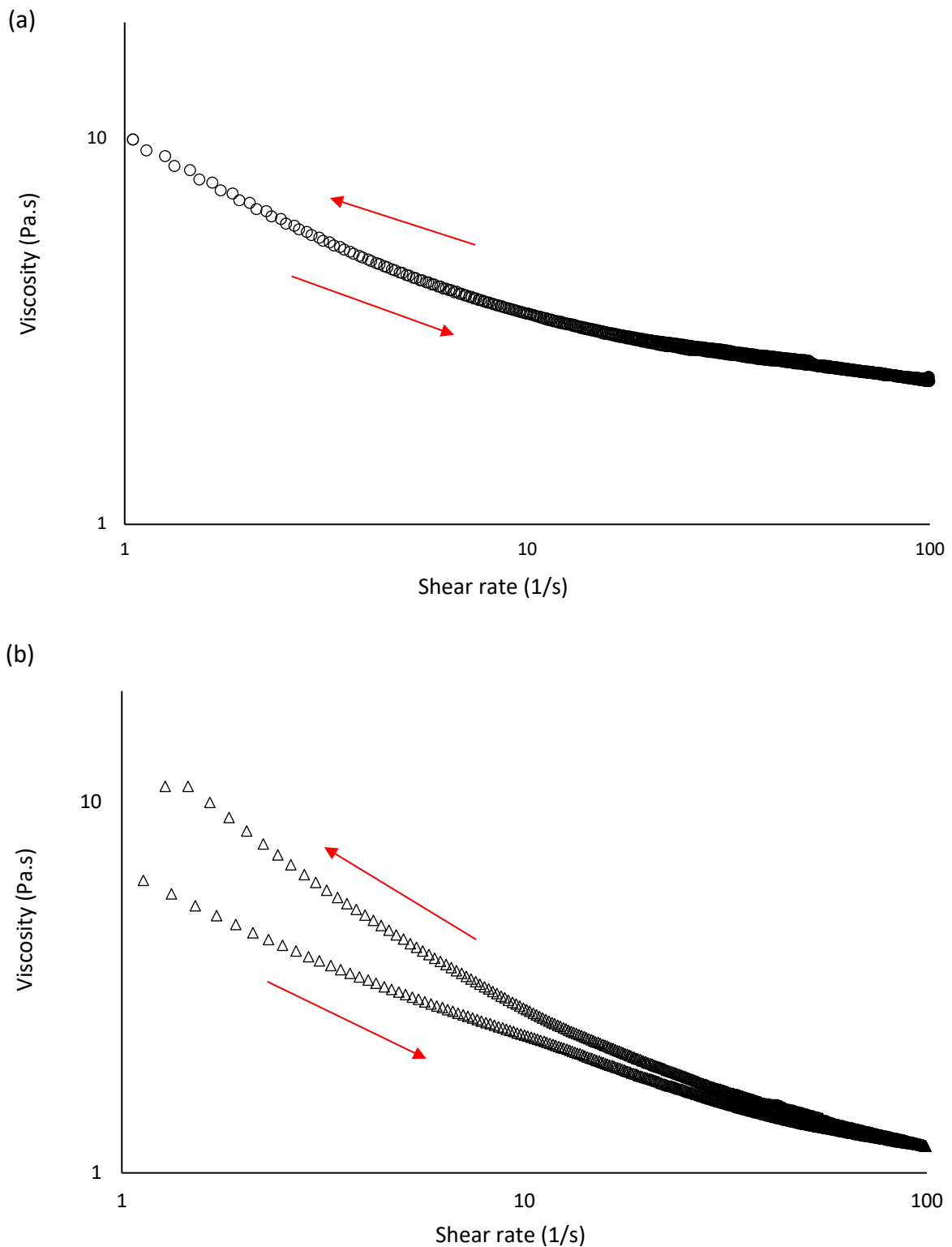
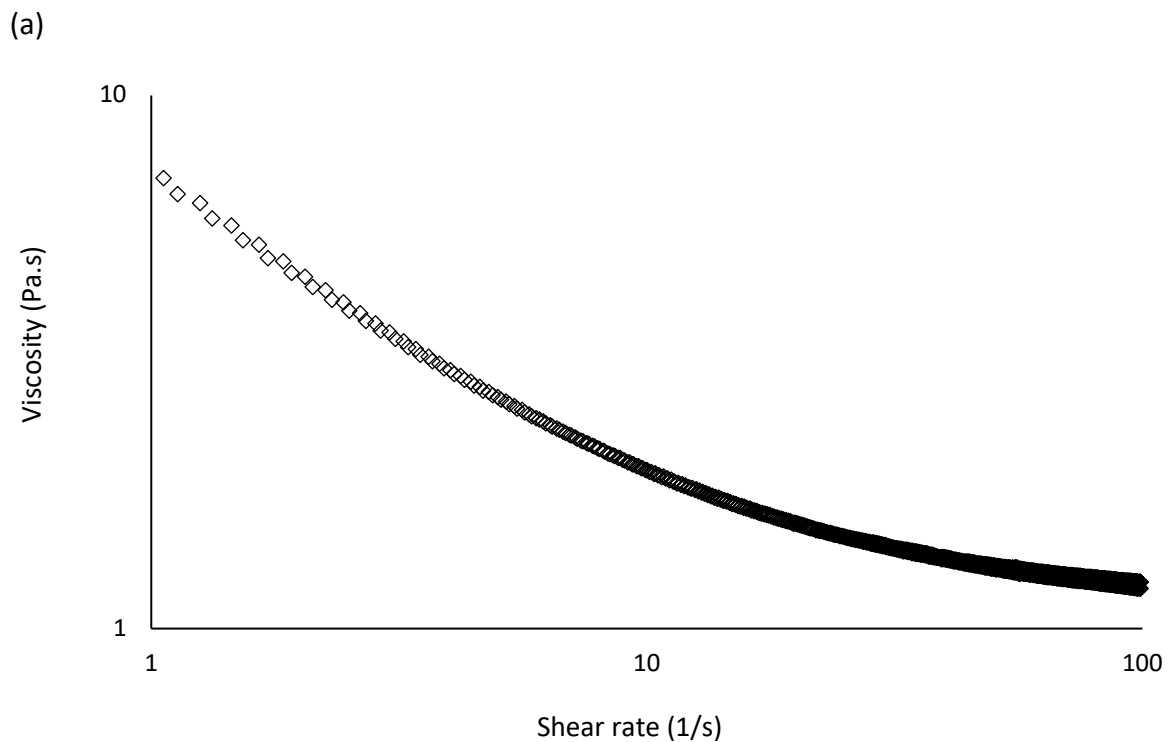


Figure 2-21. Flow curves of (a) Cocoa ($D_{50} = 9.2 \mu\text{m}$) particles suspension and (b) Sugar ($D_{50} = 58.6 \mu\text{m}$) suspension. The pre-shear speed and time are 177 s^{-1} and 2 min respectively. Resting time = 3 s. Decreasing ramp: from 100 to 1 s^{-1} during 500 s. Increasing ramp: from 1 to 100 s^{-1} during 500 s. The solid volume fraction is 0.53.

We plot in Figure 2-21 the viscosity as a function of shear rate for both suspensions. We observe from Figure 2-21 that both suspensions are non-Newtonian fluids and exhibit a shear-thinning behaviour. Figure 2-21 (a) shows that the increasing and decreasing flow curves of fatted cocoa particles suspension are superimposable. For sugar suspension, Figure 2-21 (b) shows the presence of a thixotropic loop at low shear rates (i.e., the hysteretic response obtained when a material is subjected to a series of increasing and decreasing shear rates). To decrease the effect of thixotropy on sugar suspensions, we work at different pre-shear time until we find the one needed to minimize the influence of flow history on the rheological behaviour of sugar suspensions. The pre-shear time required is 300 s. We plot in Figure 2-22 (a) the viscosity as a function of the shear rate for a pre-shear time of 300 s. We observe the disappearance of the thixotropic loop. To verify the reproducibility of the measurement at this pre-shear time, the same procedure is performed on a new formulated Sugar ($D_{50} = 58.6 \mu\text{m}$) suspension. We can observe in Figure 2-22 (b) that the flow curves of both sugar suspensions are superimposable. These results confirm that the thixotropic effect of chocolate can be neglected if we applied a pre-shear time of 300 s.



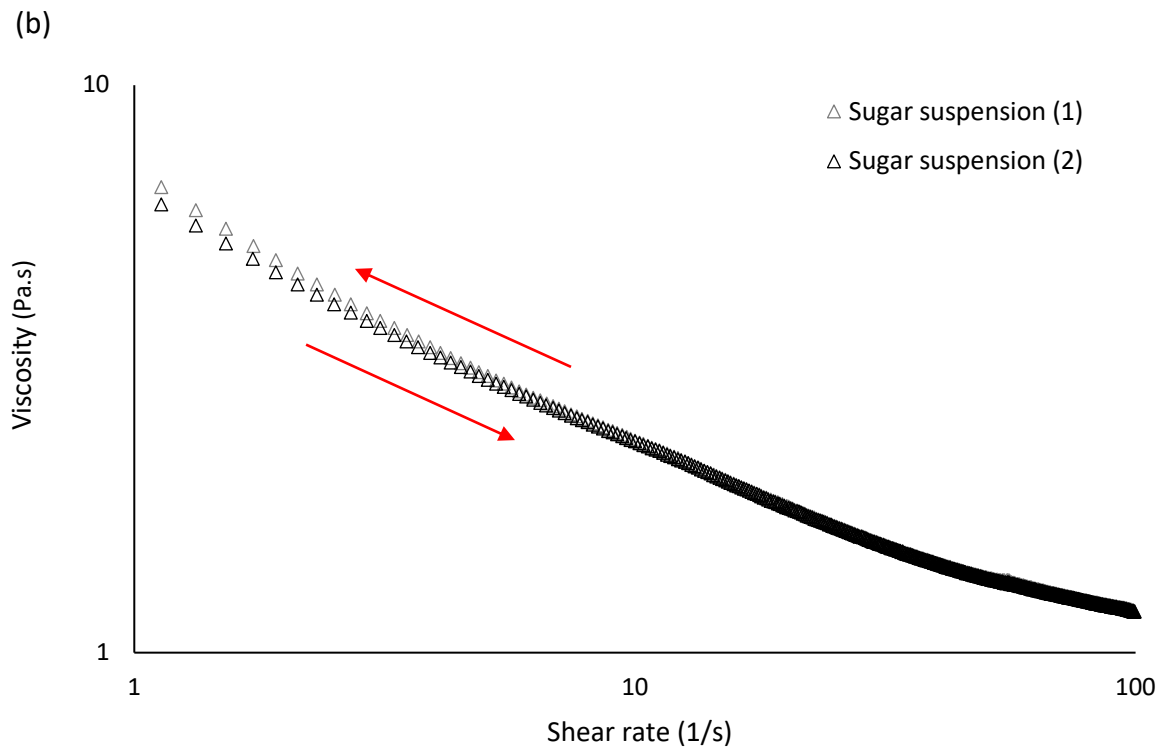


Figure 2-22. Flow curves of (a) Sugar ($D_{50} = 58.6 \mu\text{m}$) suspension (1) and (b) comparison of the flow curves of both Sugar ($D_{50} = 58.6 \mu\text{m}$) suspensions used for reproducibility. Pre-shear time: 300 s at 177 s^{-1} . Resting time = 3 s. Decreasing ramp: from 100 to 1 s^{-1} during 500 s. Increasing ramp: from 1 to 100 s^{-1} during 500 s. The solid volume fraction is 0.53.

To validate the protocol, we demonstrate that we must measure the rheological behaviour directly after mixing and by applying a pre-shear time of 5 min in order to neglect the influence of thixotropy and mechanical history. We therefore apply this protocol to a chocolate suspension made of defatted cocoa particles and Sugar ($D_{50} = 58.6 \mu\text{m}$) in cocoa butter. We work at $\phi = 0.53$. We can observe from Figure 2-23 (a) as expected the thixotropic effect of chocolate suspension is negligible with this protocol.

In order to have access to some plastic viscosity and yield stress values, the flow curves are fitted with a Bingham model [47] that is usually used to describe the rheological behaviour of yield stress fluids:

$$\tau = \tau_0 + \mu\dot{\gamma} \quad (2 - 22)$$

where τ is the shear stress (Pa), τ_0 is the yield stress (Pa), μ is the viscosity (Pa. s) and $\dot{\gamma}$ is the shear rate (s^{-1}).

This model estimates that the apparent viscosity of a colloidal suspension is the sum of the colloidal and hydrodynamic forces contribution. The decreasing flow curve of the chocolate suspension made of defatted cocoa particles and Sugar ($D_{50} = 58.6 \mu\text{m}$) in cocoa butter is

fitted by this equation and as shown in Figure 2-23 (b), there is an accuracy of 99% between the fitted curve and the experimental one. It must also be specified that only the decreasing part of the flow curve of the samples studied in this thesis will be analysed.

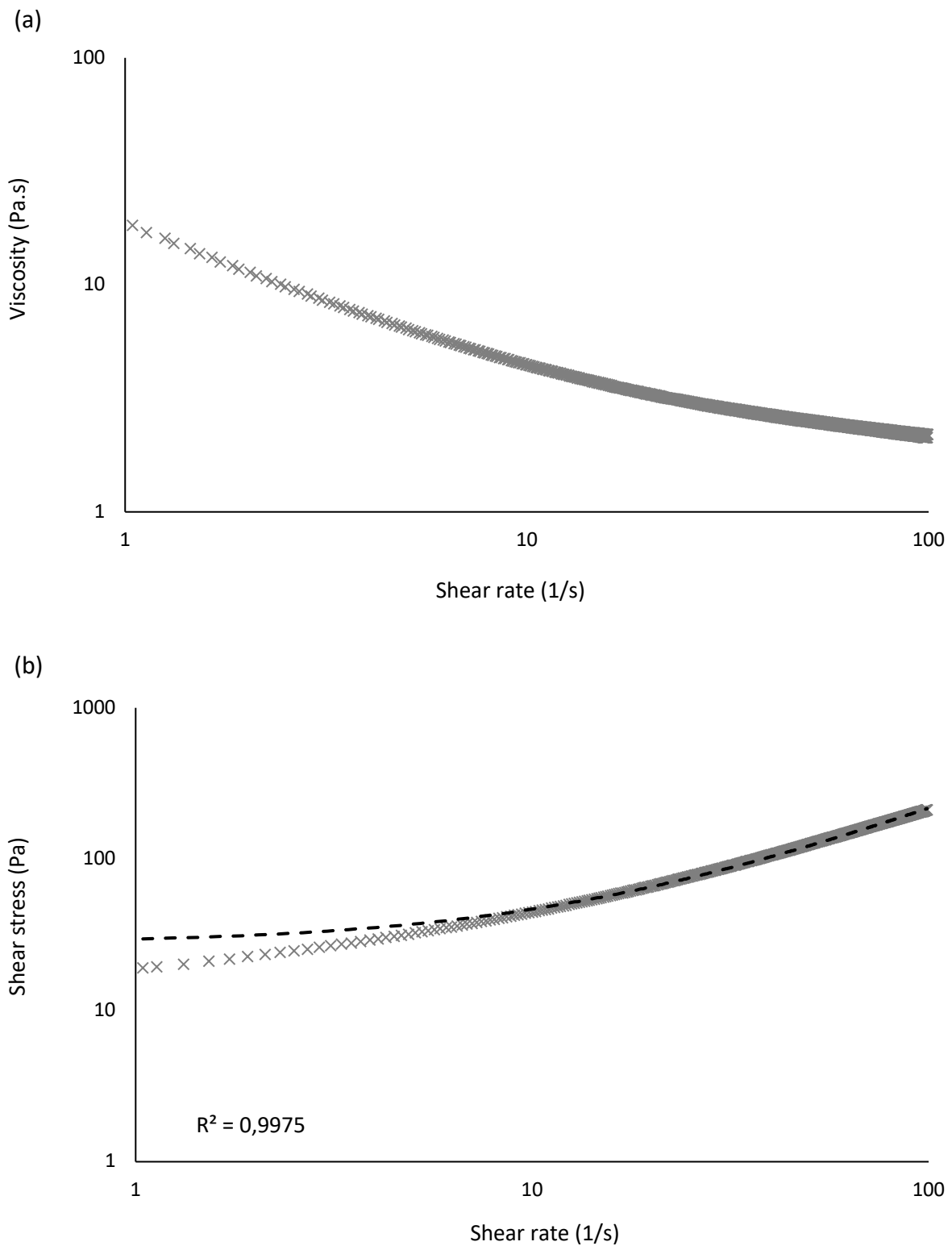


Figure 2-23. Flow curve of (a) defatted cocoa particles and Sugar ($D_{50} = 58.6 \mu\text{m}$) suspension and (b) its corresponding Bingham fit.

2.5.3.3 Suspension stability

During the rheological measurement, the stability of all suspensions studied throughout this thesis are controlled visually. We have not noted any sedimentation either in a flocculated or deflocculated state except when we study suspensions composed of solid particles having a mean diameter D_{50} greater than or equal to 400 μm , that is to say well beyond the size of conventional chocolate (see Chapter 3). Therefore, the rheological behaviour of those suspensions is not studied in this thesis.

2.5.4 Rheological measurements protocol

We can divide the developed protocol into the following steps:

- Mix the chocolate suspension by following the mixing protocol detailed in section 2.2
- Fill the rheometer cup directly after mixing and check that the rheometer temperature is 40°C.
- Pre-shear at 177 s^{-1} for 5 min
- Shear from 100 to 1 s^{-1} for 500 s
- Shear from 1 to 100 s^{-1} for 500 s
- Verify that the decreasing and increasing part of the flow curve are superimposable
- Fit the decreasing part of the curve with Bingham equation to estimate the viscosity and yield stress

2.6 Conclusion

After the description of the material and the devices used, we have presented all the experimental protocols developed during this thesis that allow us to characterize the morphological and rheological properties of the chocolate suspensions studied in the following chapter. We have also described in detail the different steps as well as the key parameters that allowed the development of each protocol.

We have showed that the envelope density of cocoa particles can be determined by a drying-protocol measurement. By means of laser granulometry, we have also showed that the particle size distribution of binary mixture such as chocolate suspensions must be measured using an average of the optical indexes of both cocoa and sugar solid particles and only in a deflocculated state. Moreover, we have used centrifugational loading to measure the maximum packing fraction of our deflocculated materials and proposed a protocol, which limits the particle size separation artefact. Finally, we have showed that the thixotropic behavior of chocolate suspensions can be neglected with the developed rheological protocol and that Bingham equation can be used to accurately fit the measured flow curves.

References

- [1] Rodriguez-Ramirez, J.; Mendez-Lagunas, L.; Lopez-Ortiz, A.; Sandoval Torres, S. *Journal of Food Science* 2012, 77, 145-154.
- [2] Cement and Concrete Research, Volume 104, February 2018, Pages 61-67.
- [3] William, J. Colonna, Upasiri Samaraweera, *Kirk-Othmer Encyclopedia of Chemical Technology: Properties of sucrose*, vol. 23, John Wiley & Sons., 4^e éd., p. 4.
- [4] Morris, P.H. *CAN. GEOTECH. J.* 1992, 29, 263-277.
- [5] Schneider, M.; Maurath, J.; Fischer, S.B.; Weiß, M.; Willenbacher, N.; Koos, E. *ACS Apply. Mater Interfaces* 2017, 12, 11095-11105.
- [6] Prosser, J.H.; Brugarolas, T.; Lee, S.; Nolte, A.J.; Daeyeon, L. *ACS NanoLetters* 2012, 12, 5287-5291.
- [7] Dufresne, E.R.; Stark, D.J.; Greenblatt, N.A.; Cheng, J.X.; Hutchinson, J.W.; Mahadavan, L.; Weitz, D.A. *Langmuir*, 2006, 22, 7144-7147.
- [8] Coussot, P. *Eur.Phys. J. B* 2000, 15, 557-566.
- [9] Yiotis, A. G.; Salin, D.; Tajer, E. S.; Yortsos, Y. C. *Phys. Rev. E* 2012, 86, 026310.
- [10] Chauvet, F.; Duru, P.; Geoffroy, S.; Prat, M. *Phys. Rev. Lett.* 2009, 103, 124502.
- [11] Chauvet, F.; Duru, P.; Geoffroy, S.; Prat, M. *Phys. Rev. Lett.* 2009, 103, 1-4.
- [12] Nael-Redolfi, J.; Keita, E.; Roussel, N. *Cement and Concrete Research* 2018, 104, 61-67.
- [13] Van de Hulst H.C. *Light Scattering by Small Particles*, Wiley, New York, 1957.
- [14] Jennings, B.R., Parslow, K. (1988) 'Particle Size Measurement: The Equivalent Spherical Diameter'. *Proceedings of the Royal Society of London A: Mathematical, Physical and Engineering Sciences* 419 (1856) 137-149.
- [15] Palacios, M.; Kazemi-Kamyad, H.; Mantellato, S.; Bowen, P. Laser diffraction and gas adsorption techniques. In: *A Practical Guide to Microstructural Analysis of Cementitious Materials*, Edited by Scrivener, K.; Snellings, R.; Lothenbach, B., CRC Press.
- [16] Allen, T. *Particle Size Measurement*. Fifth edition. New York: Chapman and Hall, 1997.
- [17] Gy, P. *Sampling of Particulate Materials. Theory and Practice*. Elsevier, Amsterdam. pp 431, 1979.
- [18] Gy, P. *Heterogeneite, Echantillonnage, Homogeneisation*. Masson, Paris. pp 607, 1988.
- [19] Hart, J.R.; Zhu, Y.; Pirard, E. « Advances in the characterization of industrial minerals- Particle size and shape characterization: Current technology and practice” *EMU Notes in Mineralogy*-Volume 9, 2010.
- [20] Masuda, H.; Higashitani, K.; Yoshida, H. *Powder Technology Handbook*, CRC Press, Boca Raton, 2006.
- [21] Petersen, L.; Minkkinen, P.; Esbensen, K.H. “Representative sampling for reliable data analysis: Theory of sampling” *Chemometrics and Intelligent Laboratory Systems* 77(1-2): 261-277, 2005.
- [22] Bohren, C.F.; Huffman, D.R. *Absorption and scattering of light by small particles*, Wiley-Interscience, ISBN 0-471-29340-7 (1983).

- [23] Petersen, L.; Dahl, C.K.; Esbensen, K.H. ACABS Research Group. Correct Sampling—A Fundamental Prerequisite for Proper Chemical Analysis—I. ACABS Posters. www.acabs.dk. 2002.
- [24] Mongia, G.; Ziegler, G.R. *Int. J. Food Properties* 2000, 3, 137-147.
- [25] Miller, K.T.; Melant, R.M.; Zukoski, C.F. *J. Am. Ceram. Soc.* 1996, 79, 2545-2556.
- [26] De Larrard, F. Concrete Mixture Proportioning: a scientific approach, E&FN SPON: An imprint of Routledge, London and New-York, 1999.
- [27] Bournonville, B. Influence de la granulométrie des particules sur la rhéologie des suspensions concentrées, Rapport interne, LMSGC, Champs sur Marne, 2003.
- [28] Kjeldsen, A.M.; Flatt, R.J.; Bergström, L. *Cement and Concrete Research* 2006, 36, 1231-1239.
- [29] Chateau, X. Particle packing and the rheology of concrete. In: Roussel, N. (Ed.), *Understanding the Rheology of Concrete*, Woodhead Publishing, 2012.
- [30] Buscall, R.; White, L.R. *J. Chem. Soc. Faraday Trans. 1* 1987, 83, 873-891.
- [31] Landman, K.A.; White, L.R. *Adv. Colloid Interface Sci.* 1994, 51, 175-246.
- [32] Bergström, L.; Schilling, C.H.; Aksay, I.A. *J. Am. Ceram. Soc.* 1994, 75, 3305-3314.
- [33] Buscall, R.; McGowan, I.J.; Mills, P.D.A.; Stewart, R.F.; Sutton, D.; White, L.R.; Yates, G.E. *J. Non-Newtonian Fluid Mech.* 1987, 24, 183-202.
- [34] Buscall, R.; Mills, P.D.A.; Goodwin, J.W.; Lawson, D.W. *J. Chem. Soc. Faraday Trans. 1* 1988, 84, 4249-4260.
- [35] Meeten, G.H. *Colloids Surf. A: Physiochem. Eng. Aspects* 1994, 82, 77-83.
- [36] Shih, W.H.; Kim, S.I.; Shih, W.Y.; Schilling, C.H.; Aksay, I.A. Consolidation of Colloidal Suspensions. In: *Better Ceramics through Chemistry IV*, Edited by Zelinski, B.J.J.; Brinker, C.J.; Clark, D.E.; Ulrich, D.R., Material Research Society, Pittsburgh, PA, 1990.
- [37] Shih, W.H.; Kim, S.I.; Shih, W.Y.; Aksay, I.A. *J. Am. Ceram. Soc.* 1994, 77, 540-546.
- [38] Lange, F.F.; Miller, K.T. *Am. Ceram. Soc. Bull.* 1987, 66, 1498-1504.
- [39] Chang, J.C.; Lange, F.F.; Pearson, D.S.; Pollinger, J.P. *J. Am. Ceram. Soc.* 1994, 77, 1357-1360.
- [40] Scherwood, J.D.; Meeten, G.H.; Farrow, C.A.; Alderman, N.J. *J. Chem. Soc. Faraday Trans. 1* 1991, 87, 611-618.
- [41] Green, M.D.; Eberl, M.; Landman, K.A. "Compressive Yield Stress of Flocculated Suspensions: Determination via Experiment" *AICHE J.*, in press.
- [42] Buscall, R. *Colloids Surf.* 1982, 5, 269-283.
- [42] Nguyen, Q.D.; Boger, D.V. *Journal of Rheology* 1985, 29, 335-347.
- [43] Bessaies-Bey, H. « Polymères et propriétés rhéologiques d'une pâte de ciment : approche physique générique ». PhD Thesis, University Paris-Est, 2015.
- [44] Ovarlez, G.; Bertrand, F.; Rodts, F. *Journal of Rheology* 2006, 50, 259-292.
- [45] Baravian, C.; Lalante, A.; Parker, A. *Applied Rheology* 2002, 12, 81-87.
- [46] Bousmina, M.; Ait-Kadi, A.; Faisant, J.B. *Journal of Rheology* 1999, 43, 415-433.
- [47] Estelle, P.; Lanos, C.; Perrot, A.; Amziane, S. *Applied Rheology* 2008, 18, 34037-34481.
- [48] Bingham, E.C., Fluidity and plasticity, McGraw-Hill, New York, 1922.

Chapter 3: Effect of chocolate production process on the morphological properties of the particles and rheological properties of the suspension

Table of contents

3.1	Materials and production process.....	92
3.2	Production process.....	93
3.2.1	Mixing, refining and conching processes.....	93
3.2.1.1	Production process devices.....	93
3.2.1.2	Production process steps.....	94
3.2.2	Grinding process.....	97
3.3	Evolution of the morphological properties over production process.....	98
3.3.1	Particle size distribution.....	98
3.3.1.1	Sugar suspension (sweet fat (SF)) samples.....	98
3.3.1.2	Sugar and cocoa suspension (dark chocolate (DC)) samples.....	100
3.3.1.3	Ground and non-ground cocoa masses.....	105
3.3.2	Maximum packing fraction.....	105
3.3.2.1	Sugar suspension (sweet fat (SF)) and sugar and cocoa suspension (dark chocolate (DC)) samples.....	110
3.3.2.2	Ground and non-ground cocoa masses.....	
3.3.3	Particle shape.....	108
3.3.4	Correlation between particle size distribution, particle shape and maximum packing fraction.....	110
3.3.5	Effect of lecithin on maximum packing fraction.....	115
3.4	Evolution of the rheological properties over the production process.....	112
3.4.1	Sugar suspension (sweet fat (SF)) samples.....	112
3.4.2	Sugar and cocoa suspension (dark chocolate (DC)) samples.....	115
3.4.3	Effect of moisture on the rheological behaviour of sugar and cocoa suspension.....	117
3.4.4	Ground and non-ground cocoa masses.....	120
3.5	Conclusion.....	121

Chapter 3: Effect of chocolate production process on the morphological properties of the particles and rheological properties of the suspension

The study of the rheological and morphological properties of fat-based foods such as chocolate is important because they are governing other properties such as texture, consistency and mouth feel of the final product. The rheological properties of these foods are known to depend on many factors such as composition and production conditions [1, 2]. Since the aim of this thesis is to control the rheological behaviour by optimizing the morphological parameters (particle size distribution, particle shape and maximum packing fraction), a better understanding of how processing conditions can influence rheological and morphological properties is necessary. Understanding how each step can affect the final rheological and morphological properties of chocolate cannot just be useful in order to predict and control the viscosity of the final product, but also to manipulate and optimize the production process. To the best of our knowledge, studies have been conducted on the influence of production process on rheological properties in literature, but no study has been conducted on the influence of production process on the morphological properties.

We focus on sugar suspensions and sugar and cocoa suspensions and studied the influence of the production process on their rheological and morphological properties. Sugar and cocoa suspensions and sugar suspensions are produced by following three production processes (mixing, refining, conching) described in chapter 1. We also study the effect of grinding on the morphological and rheological properties of cocoa suspensions. We recall that the particle size distributions, maximum packing fractions and rheological parameters measured in this chapter are determined by following the protocols described in chapter 2.

We devote the first part of this chapter to presenting the chocolate suspensions studied and to the detailed description of the production process followed. Then, in a second part, we analyse the evolution of particle size distribution and maximum packing fraction throughout processing. Finally, in a third part, we study the evolution of the rheological parameters during manufacturing and underline the role of emulsifier and moisture on the resulting rheological behavior. From these experimental results and from other results drawn from literature, we show that the evolution of the rheological and morphological parameters throughout production process is mainly following the same trend for the two suspensions studied.

3.1 Materials and production process

Sugar and cocoa suspension (also refer as dark chocolate (DC)) consists of 50% crystal sugar of unknown mean diameter and 20% fatted cocoa powder (Cocoa ($D_{50}= 9.2 \mu\text{m}$)) suspended in 29.5% cocoa butter by total mass. Sugar suspension (also refer as sweet fat (SF)) is made of 50% Sugar ($D_{50}= 502 \mu\text{m}$) suspended in 29.5% cocoa butter by total mass. Sugar ($D_{50}= 502 \mu\text{m}$) is purchased from Franck Vereecke NV (Menen, Belgium) and Cocoa ($D_{50}= 9.2 \mu\text{m}$) is provided by Cargill NV (Wormer, Netherlands). We recall that we assign to each sugar and cocoa particles that we use their mean diameter in brackets to differentiate them since cocoa

and sugar are the only solid particles studied in this thesis. Sugar and cocoa suspension and sugar suspension are produced by Cargill following the main production processes (mixing, refining and conching) that influence the morphological and rheological properties of melted chocolate. 0.5% soy lecithin is added in both suspensions during conching. For sake of simplicity, we decide to not study milk or white chocolates which contain dairy products. Indeed, dairy products contain soft particles, generally proteins that are very complex to study. Moreover, even if there are some studies on flow properties of milk and white chocolate in literature, little is known on the specific effect of dairy particles on morphological and rheological properties of chocolate [2, 3]. It is known that the rheological behaviour of concentrated suspensions such as chocolate is influenced by the presence of various additional compounds that include moisture [4, 5]. Range of moisture content in food begins with fraction of 1% and reaches even more than 98%. In chocolate, the amount of water is around 1-1.5% by mass of chocolate [6, 7]. The water within chocolate usually comes from cocoa powder. That is why we choose as second suspension to study a water-free system such as sugar suspensions (sweet fat). The comparison of both suspensions rheological behaviour will be useful for the understanding of the influence of water on rheological properties over the process.

West African cocoa mass (Cocoa ($D_{50}= 11.2 \mu\text{m}$)) provided by Cargill NV (Wormer, Netherlands) is also studied. (Cocoa ($D_{50}= 11.2 \mu\text{m}$) is ground for 6 hours to give (Cocoa ($D_{50}= 3.4 \mu\text{m}$)). We recall that cocoa mass is a suspension made up of 46% cocoa particles and 54% cocoa butter by total mass. The interest being to study the effect of grinding on the morphological and rheological properties of the ground and non-ground cocoa masses.

3.2 Production process

3.2.1 Mixing, refining and conching processes

3.2.1.1 Production process devices

Both suspensions are produced by Cargill in Mouscron confectionery factory (Belgium) using a pilot line, ideal for the production of small batches of chocolate such as the ones studied in this thesis. The pilot line is composed of a mixer, a refiner and a conching machine. The devices of the pilot line are shown in Figure 3-1.



Stephan mixer



Collette conche



Bühler SDY-300 refiner



ELK'olino conche

Figure 3-1. Devices composing the pilot line.

The mixer is a Stephan cutter mixer (Stephan Machinery GmbH, Germany) having a capacity of 40 L. A 3-roll refiner called SDY-300 and supplied by Bühler (Switzerland) is used to refine the particles. The SDY-300 has centrifugally cast rolls, comprises a continuous flow cooling system and is driven by a 2.2 kW motor. The gap between each roll is set manually. Regarding the conching step, two different machines are used to conche dark chocolate (DC) and sweet fat (SF) suspensions. A Collette machine having 15 kg of capacity, supplied by GEA Pharma Systems-Collette (Belgium), is used to conche SF model. Whilst for DC recipe, the conching machine is ELK'olino supplied by Bühler. The ELK'olino conche has a capacity of 5 kg.

3.2.1.2 Production process steps

All ingredients are first mixed for 5 minutes. The obtained mixture is then refined for 15 minutes. This first refining involves two passages through the 3-roll refiner. The gaps settled at each passage between each roll are shown in Figure 3-2. At the end of this first grinding, the mixture turned into flakes (see Figure 3-3). The flakes are ground a second time for 15 minutes using the same 3-roll refiner. This second grinding also implies two passages through the Bühler refiner following the same gap settlement than the one shown in Figure 3-2. The

Chapter 3: Effect of chocolate production process on the morphological properties of the particles and rheological properties of the suspension

temperature is around 50°C during the grinding. At this stage of production, three samples (SF1, SF2, SF3 for sugar suspension (sweet fat (SF)) samples and DC1, DC2, DC3 for sugar and cocoa suspension (dark chocolate (DC)) samples (see Figure 3-3)) are collected for each suspension.

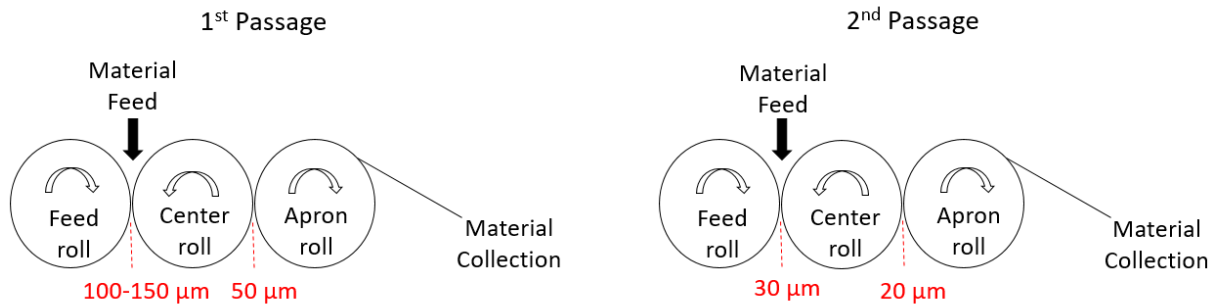


Figure 3-2. Schematic diagram of a 3-roll refiner showing the gap set manually during refining.

During chocolate industrial production, it is difficult to estimate the exact beginning and/or duration of the conching phase as the conche is progressively filled while the refining progresses still goes on. This leads to an overall filling time that can exceed 1 hour. Therefore, in order to have a precise estimation of the beginning and end of our samples conching, the conche is filled instantaneously by the flakes obtained after the 2nd refining. The conching starts immediately after 1% cocoa butter by total mass is added into the conche. The conching is done at 60°C and lasts for 6 hours. Soy lecithin is added after 5 hours of conching and its addition allows for passing from what we can call a thick paste (see Figure 3-3) to a liquid suspension for both studied suspensions. Three samples (DC4(0), DC4(5) and DC4(6)) are collected during sugar and cocoa suspension (dark chocolate) conching. The first one is taken at the beginning of conching, more precisely 5 minutes after the beginning. The second sample is collected after 5 hours of conching before the addition of soy lecithin. The last sample is levied at the end of the sixth hour of conching. Whilst for sugar suspension (sweet fat), 6 samples (SF4(1) to SF4(6)) are collected after each hour of conching. The timeline of the production process and pictures of the samples collected are shown in Figure 3-3. The numbers 1 to 4 in the sample's label designate the successive production steps, 1 being Mixing and 4 being Conching. Whilst the number in brackets represents the hour of conching at which the sample is collected. At the end of production, the samples are stored at 20°C in plastic buckets. The composition and solid volume fraction ϕ of each sample are summarized in Table 3-1.

Chapter 3: Effect of chocolate production process on the morphological properties of the particles and rheological properties of the suspension

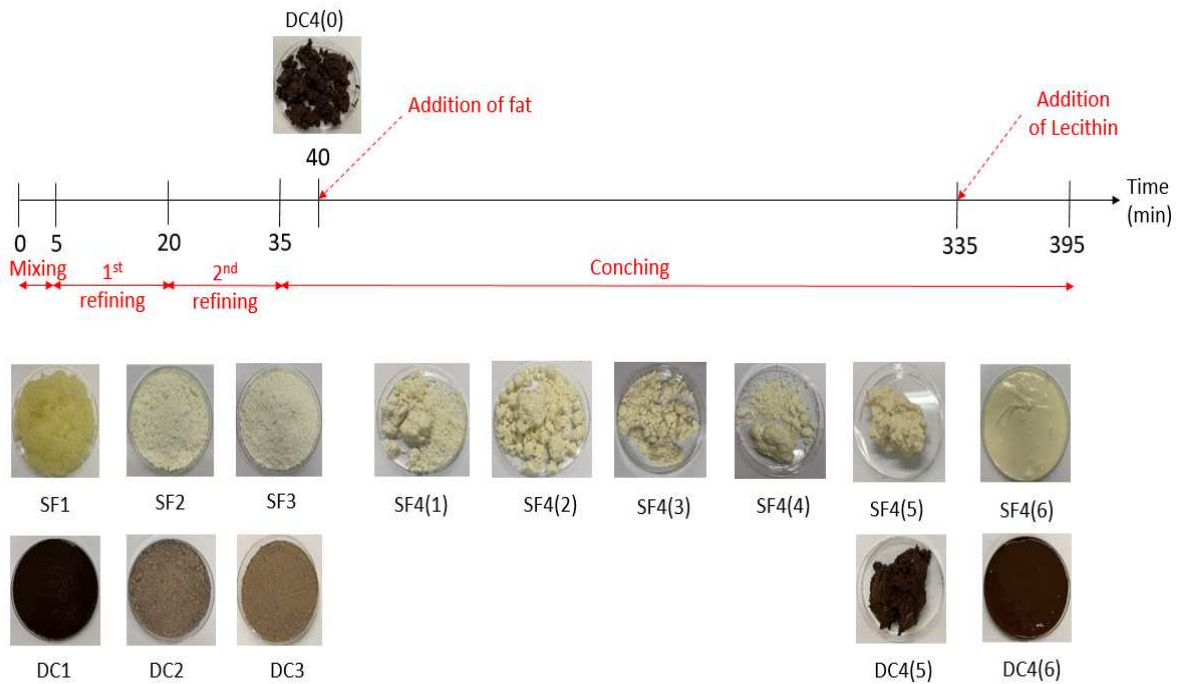


Figure 3-3. Timeline of the production process and pictures of the samples collected during sugar suspensions (sweet fat (SF)) and sugar and cocoa suspensions (dark chocolate (DC)) production.

(a)

	Sugar ($D_{50} = 502 \mu\text{m}$) (% mass)	Cocoa butter (% mass)	Lecithin (% mass)	Solid volume fraction ϕ
SF1-After mixing	79	21	0	0.68
SF2-After 1 st refining	79	21	0	0.68
SF3-After 2 nd refining	79	21	0	0.68
SF4(1)-After 1h of conching	78.20	21.80	0	0.67
SF4(2)-After 2h of conching	78.20	21.80	0	0.67
SF4(3)-After 3h of conching	78.20	21.80	0	0.67
SF4(4)-After 4h of conching	78.20	21.80	0	0.67
SF4(5)-After 5h of conching	78.20	21.80	0	0.67
SF4(6)-End of conching	77.80	21.70	0.5	0.66

(b)

	Sugar (% mass)	Cocoa (D_{50} = 9.2 μm) (% mass)	Cocoa butter (% mass)	Lecithin (% mass)	Solid volume fraction \emptyset
DC1-After mixing	55.55	22.22	22.22	0	0.65
DC2-After 1 st refining	55.55	22.22	22.22	0	0.65
DC3-After 2 nd refining	55.55	22.22	22.22	0	0.65
DC4(0)-Beginning of conching	54.35	21.74	23.91	0	0.63
DC4(5)-After 5h of conching	54.35	21.74	23.91	0	0.63
DC4(6)-End of conching	50	20	29.50	0.5	0.56

Table 3-1. Composition of (a) sugar suspension (sweet fat) samples and (b) sugar and cocoa suspension (dark chocolate) samples.

3.2.2 Grinding process

The grinder used is the LMZ Zeta[®] High Speed Grinding System purchased from NETZSCH (see Figure 3-4). The high-speed ZETA[®] circulation system is a grinding system with many different applications. It is equally suitable for processing products with very low viscosity and grinding products with a high concentration of solids and a correspondingly high viscosity. NETZSCH-BEADS[®] are grinding media ideally tailored to the ZETA[®] grinding system and are available in various materials and sizes ranging from 0.09 mm to 3 mm diameter. The beads size used to grind Cocoa (D_{50} = 11.2 μm) for 6 hours is 1 mm.



Figure 3-4. LMZ Zeta[®] High Speed Grinding System.

3.3 Evolution of the morphological properties over production process

3.3.1 Particle size distribution

3.3.1.1 Sugar suspension (sweet fat (SF)) samples

We plot in Figure 3-5 the particle size distribution by volume of sugar suspension samples. We summarize in Table 3-2 the characteristic diameters (D_{10} , D_{50} , D_{90}) and the ratio D_{90}/D_{10} of each sample. We recall that D_{10} , D_{50} and D_{90} are the volume-based diameters below which 10%, 50% and 90% of the particles are undersized, respectively. The ratio D_{90}/D_{10} is an indicator of the polydispersity of the samples.

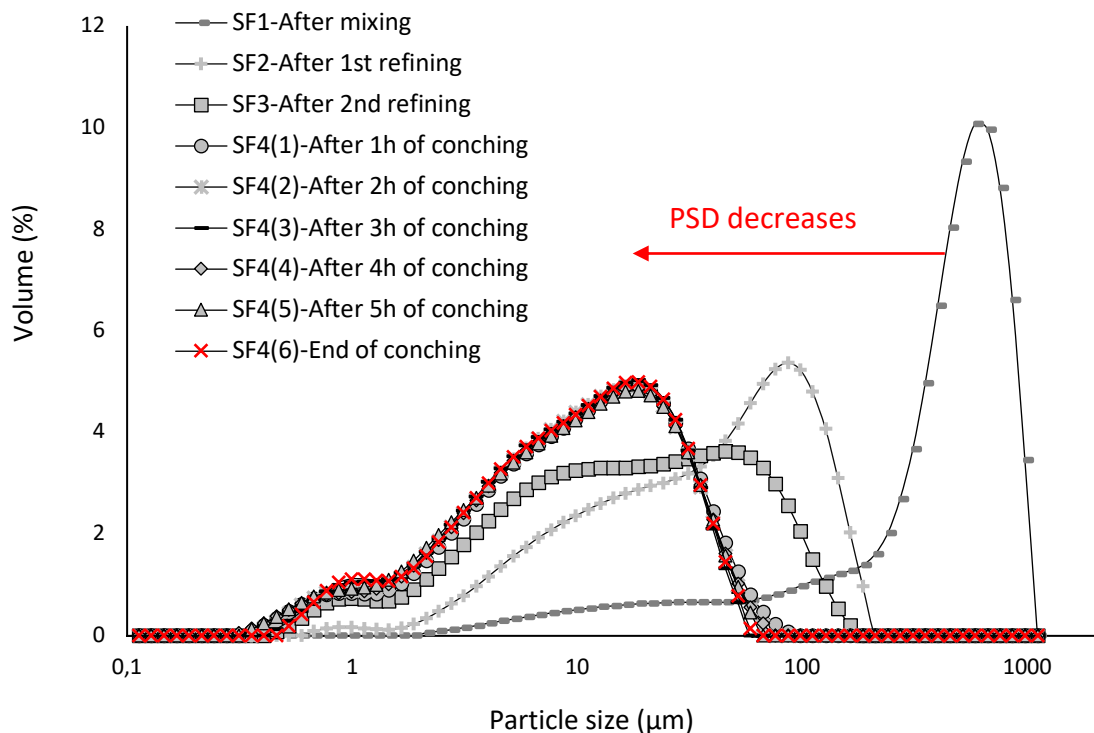


Figure 3-5. Evolution of the particle size distribution of sugar suspension (sweet fat (SF)) samples over the production process. The data in red correspond to the sample containing lecithin.

We observe in Figure 3-5 that the particle size decreases from SF1 to SF4(1) and seems to remain constant from SF4(1) to SF4(6). We also observe the presence of fine particles of size ranging from 0.3 to 1 μm in refining and conching samples PSD curves. From Table 3-2, a significant decrease in particle diameter is observed from sample SF1 to SF4(1) with a simultaneous decrease of the ratio D_{90}/D_{10} (i.e., the polydispersity). However, we note that from sample SF4(1) to SF4(6), the diameters and ratio remain constant. All of these

Chapter 3: Effect of chocolate production process on the morphological properties of the particles and rheological properties of the suspension

observations suggest that the particle size distribution of sugar suspension samples is influenced by the two refining processes and the first hour of conching.

	D_{10} (μm)	D_{50} (μm)	D_{90} (μm)	D_{90}/D_{10}
SF1-After mixing	40.4 ± 12.51	502 ± 13.43	861 ± 7.07	21.31
SF2-After 1 st refining	6.51 ± 0.06	43 ± 0.85	127 ± 1.15	19.51
SF3-After 2 nd refining	4.14 ± 0.21	18 ± 0.42	74.9 ± 0.75	18.1
SF4(1)-After 1h of conching	2.17 ± 0.13	11.6 ± 0.35	35.7 ± 1.61	16.45
SF4(2)-After 2h of conching	2.07 ± 0.12	11 ± 0.46	33.9 ± 0.81	16.37
SF4(3)-After 3h of conching	2.06 ± 0.01	10.7 ± 0.15	31.8 ± 0.98	15.44
SF4(4)-After 4h of conching	2.02 ± 0.01	11 ± 0.10	33.7 ± 0.10	16.68
SF4(5)-After 5h of conching	2.06 ± 0.09	10.9 ± 0.14	33.3 ± 0.07	16.17
SF4(6)-End of conching	2.10 ± 0.03	10.9 ± 0.07	32.5 ± 0.42	15.48

Table 3-2. Characteristic diameters (value \pm standard deviation) of sugar suspension (sweet fat (SF)) samples.

In order to estimate the volume proportion of fine particles generated from SF1 to SF4(6), we calculate the area under the curve of each distribution from 0.3 to 1 μm approximately using the trapezoidal rule [8]. We plot in Figure 3-6 the volume proportion of fines particles as a function of the sample tested. We observe that fine particles appear after the first refining and that their proportion increases from SF2 to SF4(1) and remains unchanged from SF4(1) to SF4(6). These observations confirm the previous suggestion that the particle size distribution is influenced by refining processes and first hour of conching.

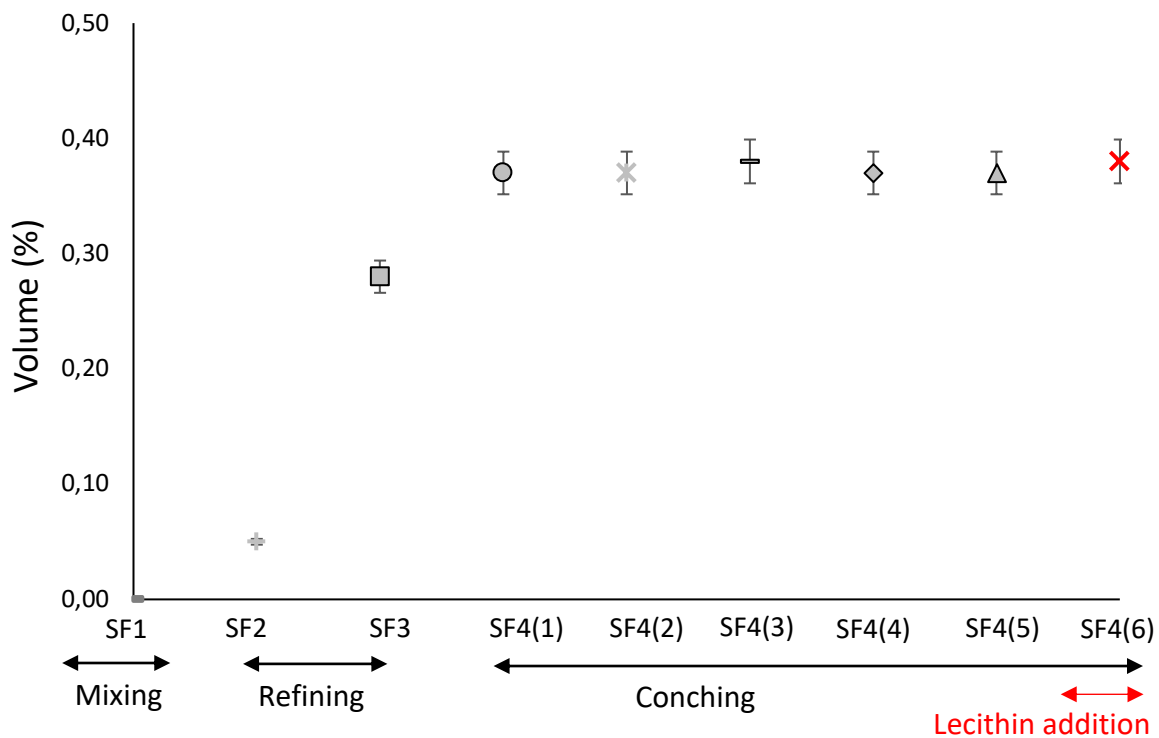


Figure 3-6. Proportion of fine particles (0.3 μm-1 μm) generated during the production process of sugar suspension (sweet fat (SF)) samples. The data in red correspond to the sample containing lecithin.

3.3.1.2 Sugar and cocoa suspension (dark chocolate (DC)) samples

We plot in Figure 3-7 the particle size distribution by volume of sugar and cocoa suspension (dark chocolate (DC)) samples. We summarize in Table 3-3 the characteristic diameters (D_{10} , D_{50} , D_{90}) and the ratio D_{90}/D_{10} of each sample.

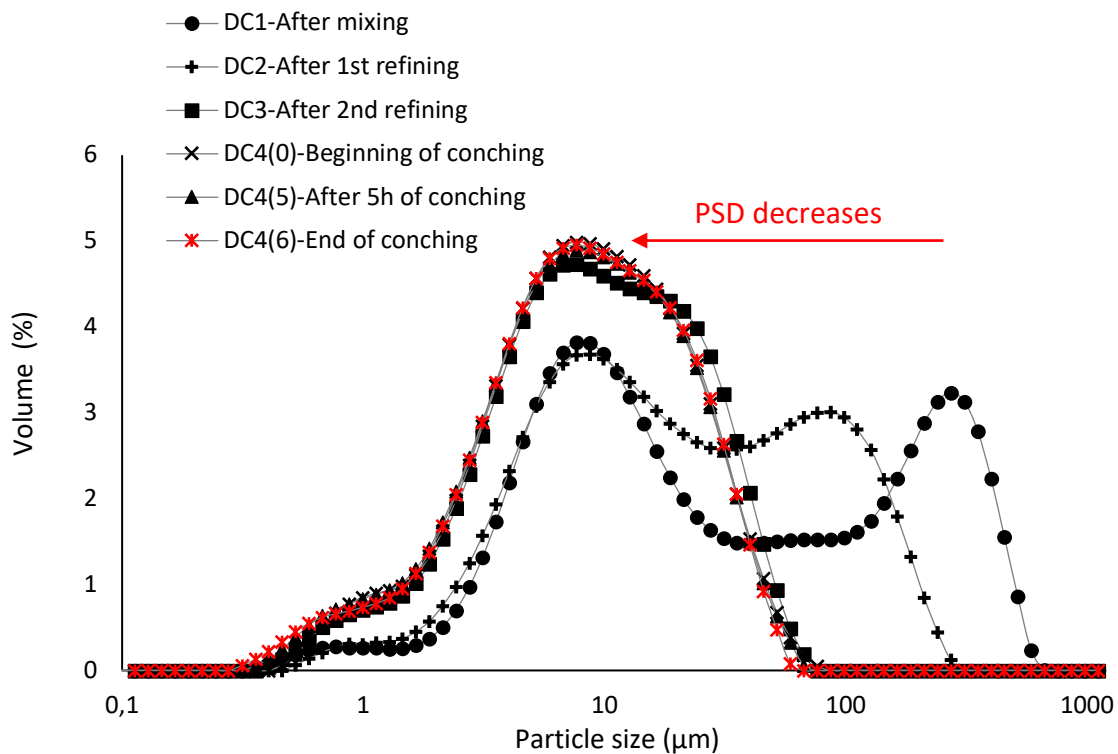


Figure 3-7. Evolution of the particle size distribution of sugar and cocoa suspension (dark chocolate) samples over the production process. The data in red correspond to the sample containing lecithin.

We observe that the particle size distribution and polydispersity decrease from mixing sample (DC1) to 2nd refining sample (DC3) and remains unchanged during conching (from DC3 to DC4(6)). Two peaks of high intensity are observed from DC1 and DC2 PSD curves. The former is around 10 μm for both samples whereas the latter is around 240 μm and 100 μm for DC1 and DC2 respectively. The samples DC3, DC4(0), DC4(5) and DC4(6) exhibit one peak of high intensity around 10 μm . We also observe the presence of fine particles of size ranging from 0.3 to 1 μm in the sample's PSD. The peak of these particles is less intense than the others. Table 3-3 shows that the diameters and polydispersity do not change after the 2nd refining. These observations suggest that only the refining processes influence the particle size distribution of DC samples.

Chapter 3: Effect of chocolate production process on the morphological properties of the particles and rheological properties of the suspension

	D_{10} (μm)	D_{50} (μm)	D_{90} (μm)	D_{90}/D_{10}
DC1-After mixing	4.51 ± 0.60	22.8 ± 3.11	320 ± 6.87	71.1
DC2-After 1 st refining	3.58 ± 0.16	15.2 ± 2.47	123 ± 4.95	34.4
DC3-After 2 nd refining	2.48 ± 0.15	9.73 ± 1.15	32.4 ± 1.27	13.1
DC4(0)-Beginning of conching	2.22 ± 0.25	9.11 ± 0.99	29.3 ± 1.27	13.2
DC4(5)-After 5h of conching	2.07 ± 0.43	8.86 ± 0.86	28.6 ± 0.71	13.8
DC4(6)-End of conching	2.09 ± 0.45	8.86 ± 0.85	28.3 ± 0.85	13.5

Table 3-3. Characteristic diameters (value \pm standard deviation) of cocoa and sugar suspension (dark chocolate) samples.

To estimate the proportion of fine particles in these samples, the trapezoid's method is used to calculate the area under the PSD curve from 0.3 to 1 μm . The results are plotted in Figure 3-8. We observe that the proportion of fine particles increase from DC1 to DC3 and do not change from DC3 to DC4(6).

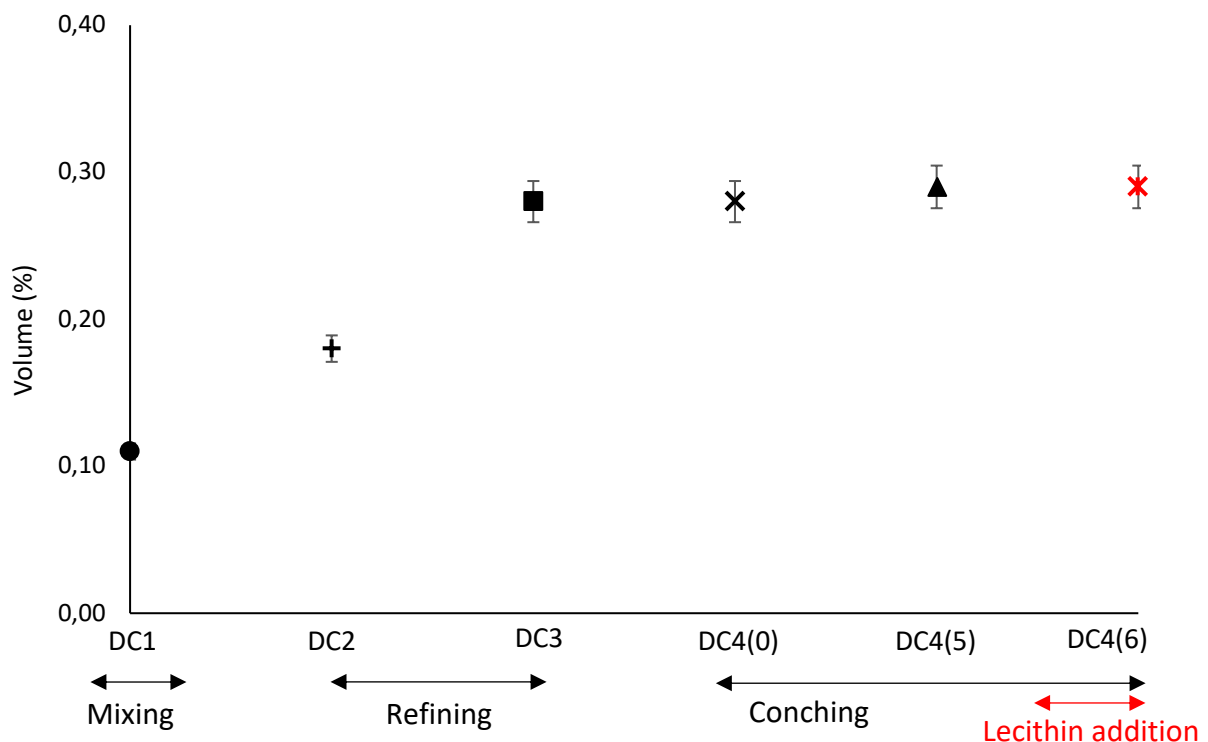


Figure 3-8. Proportion of fine particles (0.3 μm -1 μm) generated during the production process of sugar and cocoa suspension (dark chocolate) samples. The data in red correspond to the sample containing lecithin.

Chapter 3: Effect of chocolate production process on the morphological properties of the particles and rheological properties of the suspension

To know if these fine particles are cocoa and sugar particles or only sugar particles as in the case of sugar suspension samples, we first calculate the particle size distribution of sugar and cocoa suspension samples from the particle size distributions of fatted cocoa powder and sugar suspension samples by considering that the PSD of fatted cocoa powder remains unchanged over the production process contrary to the PSD of sugar particles in sugar suspension samples. We then compare the calculated particle size distributions and the experimental ones. We recall that the particle size distribution shown in Figure 3-9 corresponds to the particle size distribution of fatted cocoa powder used to produce sugar and cocoa suspension. It must also be mentioned that it is not possible to calculate the particle size distribution of DC4(0) sample because there are no sweet fat samples collected at the beginning of conching.

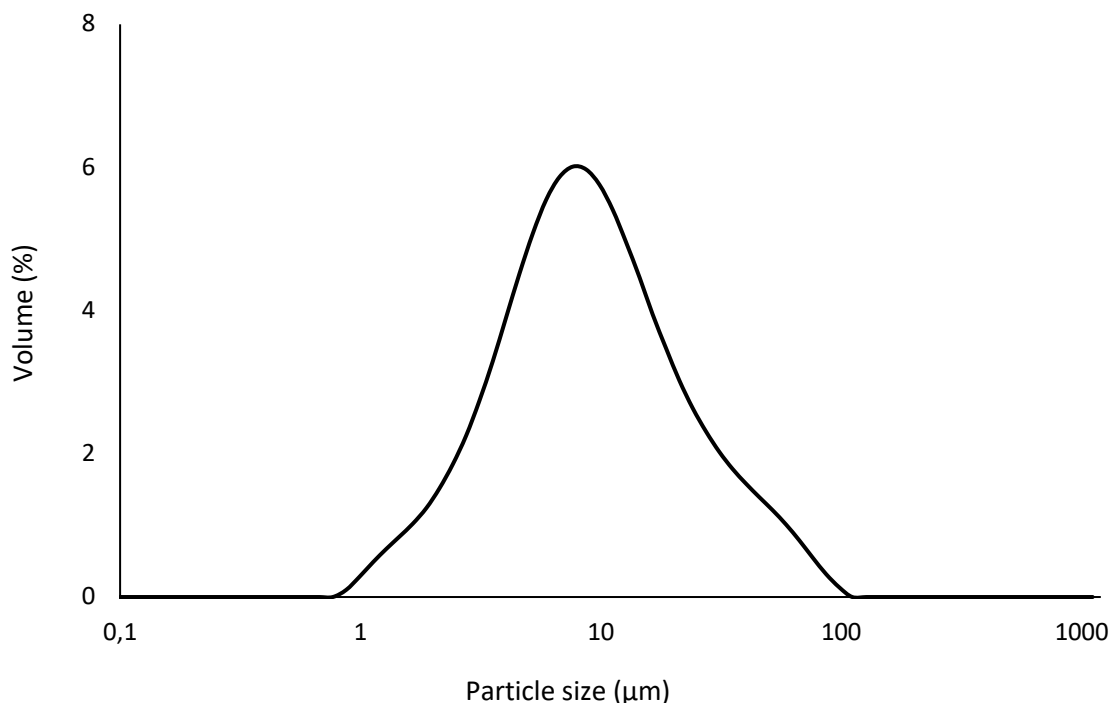


Figure 3-9. Particle size distribution of fatted cocoa powder (Cocoa ($D_{50}= 9.2 \mu\text{m}$)) used to produce sugar and cocoa (dark chocolate) samples.

We plot in Figure 3-10 the particle size distribution by volume of the calculated and measured sugar and cocoa suspension samples. We observe from DC1's particle size distribution that the sugar particles used to produce sugar and cocoa suspension and sugar suspension samples are not the same. However, we also observe from DC4(5) and DC4(6) that the calculated and measured particle size distributions are the same at the end of the production process. These observations suggest that it is mainly sugar particle size distribution that is changing over the production process and therefore, the fine particles are probably fine sugar particles. Moreover, these results suggest that, independently of the particle size distribution of the

Chapter 3: Effect of chocolate production process on the morphological properties of the particles and rheological properties of the suspension

sugar used at the beginning of the production process, the particle size distribution of sugar and cocoa suspension at the end of production will be the same.

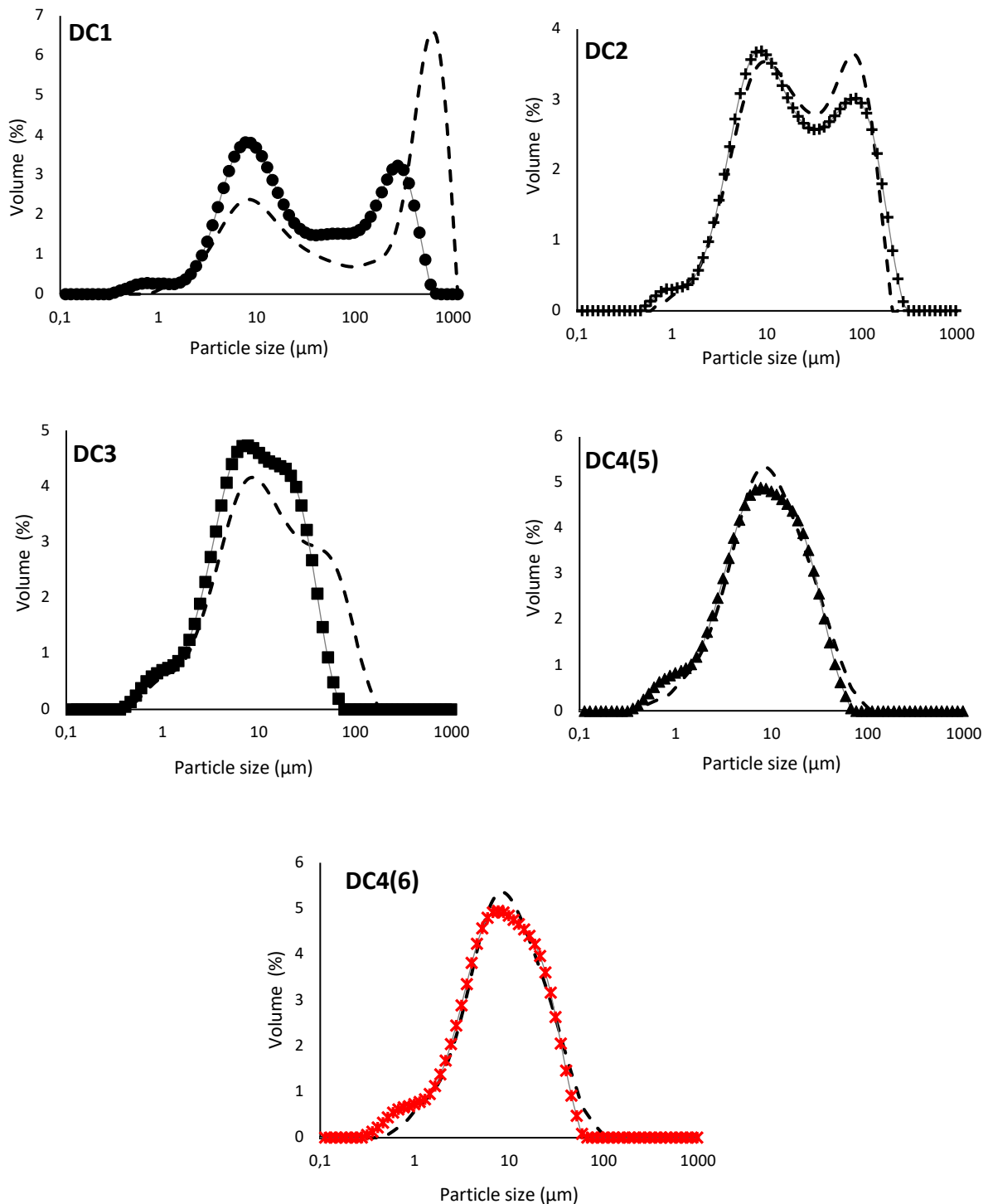


Figure 3-10. Calculated (dash line in black) and experimental (full line) particle size distributions of sugar and cocoa suspension samples. The data in red correspond to the sample containing lecithin.

3.3.1.3 Ground and non-ground cocoa masses

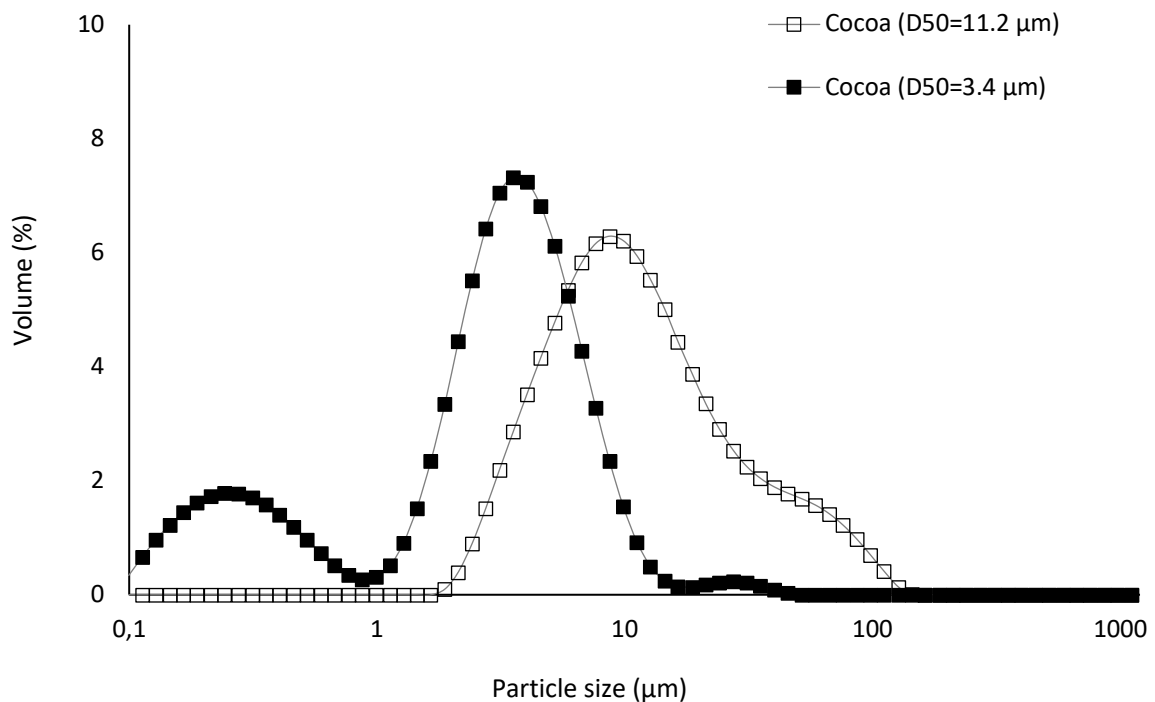


Figure 3-11. Particle size distribution of the ground (Cocoa ($D_{50}= 11.2 \mu\text{m}$)) and non-ground (Cocoa ($D_{50}= 3.4 \mu\text{m}$)) cocoa particles.

We plot in Figure 3-11 the particle size distribution by volume of Cocoa ($D_{50}= 11.2 \mu\text{m}$) and Cocoa ($D_{50}= 3.4 \mu\text{m}$). We summarize in Table 3-4 the characteristic diameters and the polydispersity ratio. As expected, we observe that the grinding decreases the particle size and increases the polydispersity by generating fine cocoa particles of size below $1 \mu\text{m}$.

	D_{10} (μm)	D_{50} (μm)	D_{90} (μm)	D_{90}/D_{10}
Cocoa ($D_{50}= 11.2 \mu\text{m}$)	4.34 ± 0.65	11.2 ± 0.82	45.4 ± 1.65	10.5
Cocoa ($D_{50}= 3.4 \mu\text{m}$)	0.28 ± 0.75	3.4 ± 0.29	7.71 ± 0.95	27.5

Table 3-4. Characteristic diameters and polydispersity ratio of the non-ground and ground cocoa masses.

3.3.2 Maximum packing fraction

3.3.2.1 Sugar suspension (sweet fat (SF)) and sugar and cocoa suspension (dark chocolate (DC)) samples

Before measuring the maximum packing fraction of the samples, we determine the proportion of PGPR required to deflocculate the particles using the procedure described in chapter 2. We

Chapter 3: Effect of chocolate production process on the morphological properties of the particles and rheological properties of the suspension

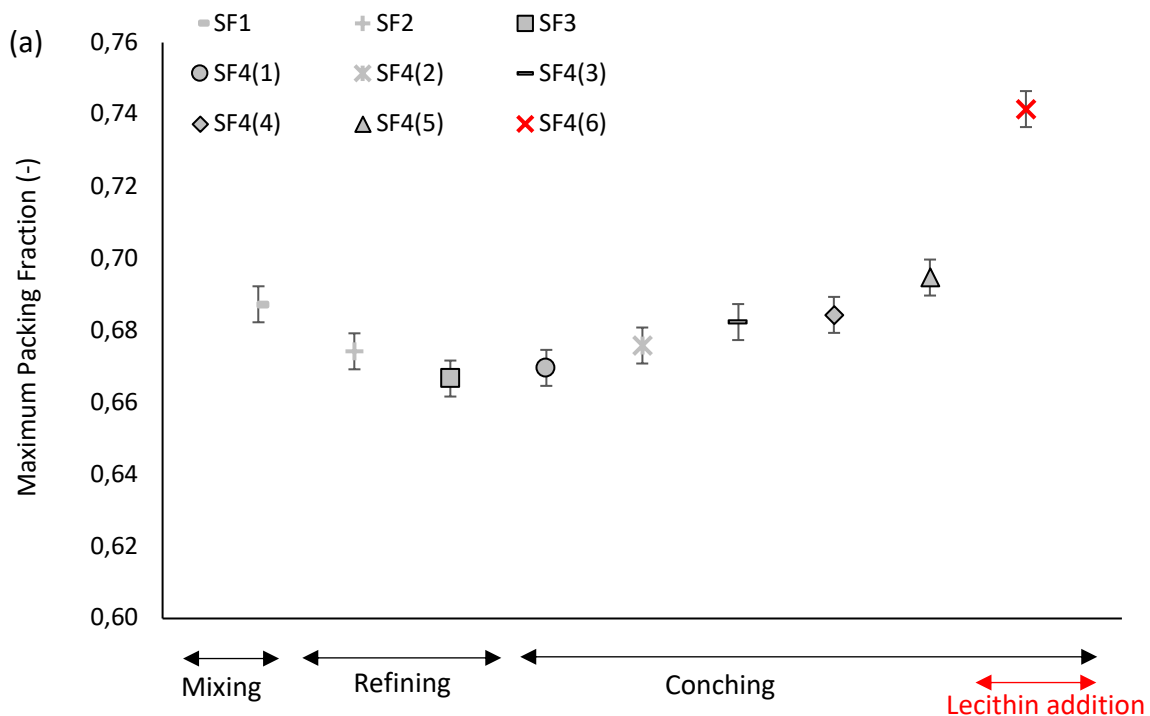
recall that the proportion of PGPR added in this procedure range from 0 to 2% (with an increment of 0.5%) per total mass of solid particles. We also recall that the reduction of particle size leads to an increase of the magnitude of attractive forces and therefore, to an increase of the yield stress. This implies that the quantity of PGPR needed to get rid of attractive forces increases with the decrease of particle size and thus, the required proportion must be determined from a sample collected at the end of the production process rather than at the beginning.

As previously demonstrated, the particle size distribution remains unchanged from SF4(1) to SF4(6) for sugar suspension samples and from DC3 to DC4 (6) for sugar and cocoa suspension samples i.e., we can use any sample collected during conching to determine the proportion of PGPR. We choose SF4(5) and DC4(5). However, SF4(6) and DC4(6) containing lecithin beforehand, we assume that the proportion of PGPR needed will be lower than the one required for samples without lecithin. Therefore, the proportion of PGPR is estimated for the 4 samples. We present in Table 3-5 the viscosity and yield stress values of the 4 samples when different proportions of PGPR are added. The lowest value of yield stress is measured when 1.5% PGPR by the total mass of solid particles is added to SF4(5) and DC4(5). For SF4(6) and DC4(6), the lowest value of yield stress is measured when 1% PGPR by the total mass of solid particles is added. In conclusion, 1.5% PGPR by total mass of solid particles should be used to deflocculate samples that do not contain lecithin whereas 1% PGPR by total mass of solid particles is sufficient for those containing lecithin.

	%PGPR by total mass of solid particles	Viscosity (value \pm 8%) (Pa.s)	Yield stress (value \pm 12%) (Pa)
DC4(5)	0	1.94	35.1
	0.5	1.69	3.50
	1	1.27	1.45
	1.5	1.28	1.25
	2	1.38	1.35
DC4(6)	0	1.10	9.09
	0.5	1.09	1.53
	1	1.03	1
	1.5	1.05	1.08
SF4(5)	0	1.47	29.5
	0.5	1.50	4.1
	1	1.28	1.73
	1.5	1.14	0.87
	2	1.39	1.17
SF4(6)	0	0.78	15.3
	0.5	0.81	2.42
	1	0.79	0.42
	1.5	0.76	0.88

Chapter 3: Effect of chocolate production process on the morphological properties of the particles and rheological properties of the suspension

Table 3-5. Viscosity and yield stress values measured for different proportions of PGPR. We plot in Figure 3-12 the maximum packing fraction as a function of the production process for sugar and cocoa suspension and sugar suspension samples. We observe that both suspensions exhibit the same evolution of maximum packing fraction over the production process i.e., the maximum packing fraction decreases from mixing to the end of refining and increases during conching. From mixing to the end of refining, the maximum packing fraction decreases from 0.69 (SF1) to 0.66 (SF3) for sugar suspension and from 0.68 (DC1) to 0.65 (DC3) for sugar and cocoa suspension. During conching, the maximum packing fraction increases from 0.67 (SF4(1)) to 0.74 (SF4(6)) and from 0.65 (DC4(0)) to 0.70 (DC4(6)). We also observe that the increase of the maximum packing fraction during conching is more pronounced for samples containing lecithin especially for sugar suspension in which the maximum packing fraction goes from 0.70 (SF4(5)) to 0.74 (SF4(6)) while it goes from 0.67 (DC4(5)) to 0.70 (DC4(6)) for sugar and cocoa suspension. We finally observe that the maximum packing fractions of DC3 and DC4(0) are the same.



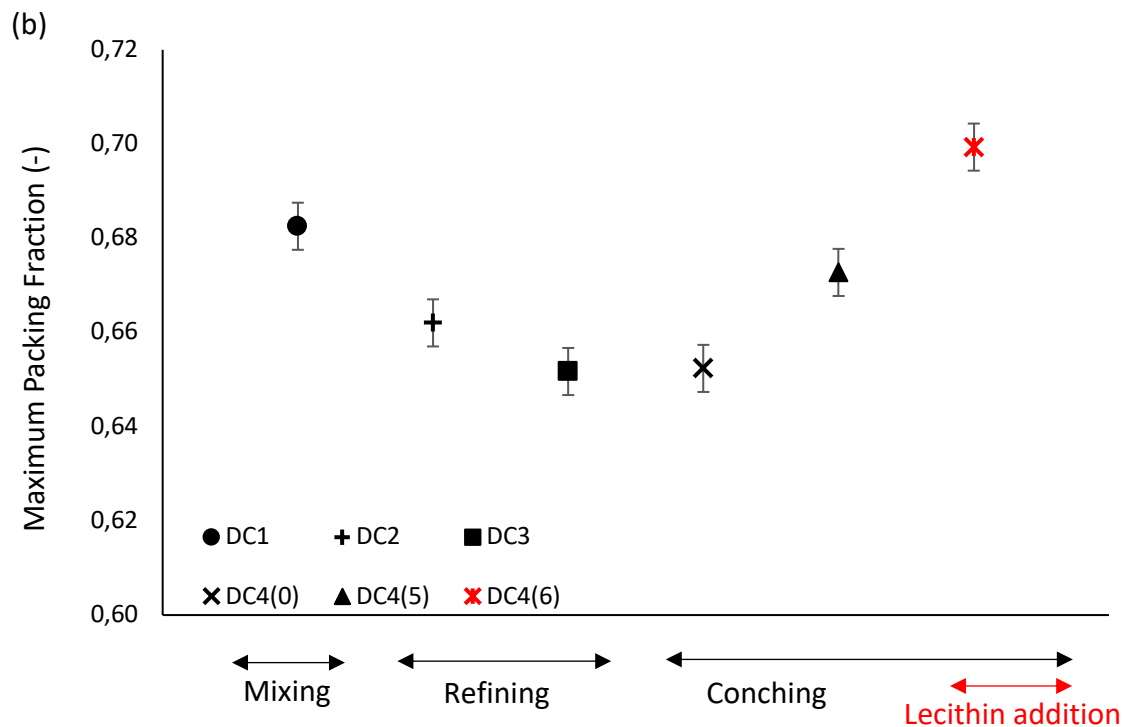


Figure 3-12. Evolution of the maximum packing fraction of (a) sugar suspension samples and (b) sugar and cocoa suspension samples over the production process. The data in red correspond to the sample containing lecithin.

3.3.2.2 Ground and non-ground cocoa masses

The maximum packing fraction goes from 0.49 (Cocoa ($D_{50} = 11.2 \mu\text{m}$)) to 0.59 (Cocoa ($D_{50} = 3.4 \mu\text{m}$)) at the end of grinding. This result suggests that the grinding causes an increase of the maximum packing fraction of the cocoa mass.

3.3.3 Particle shape

The Compressible Packing Model developed by François de Larrard [9] allows for a computation of a shape parameter β describing the shape of particles. It corresponds to the maximum packing fraction of each particle size class constituting a powder. It is calculated from the particle size distribution and maximum packing fraction of a powder. This shape parameter increases when the aspect ratio decreases and/or the sphericity of the particles increases. For more details about the model see chapter 5.

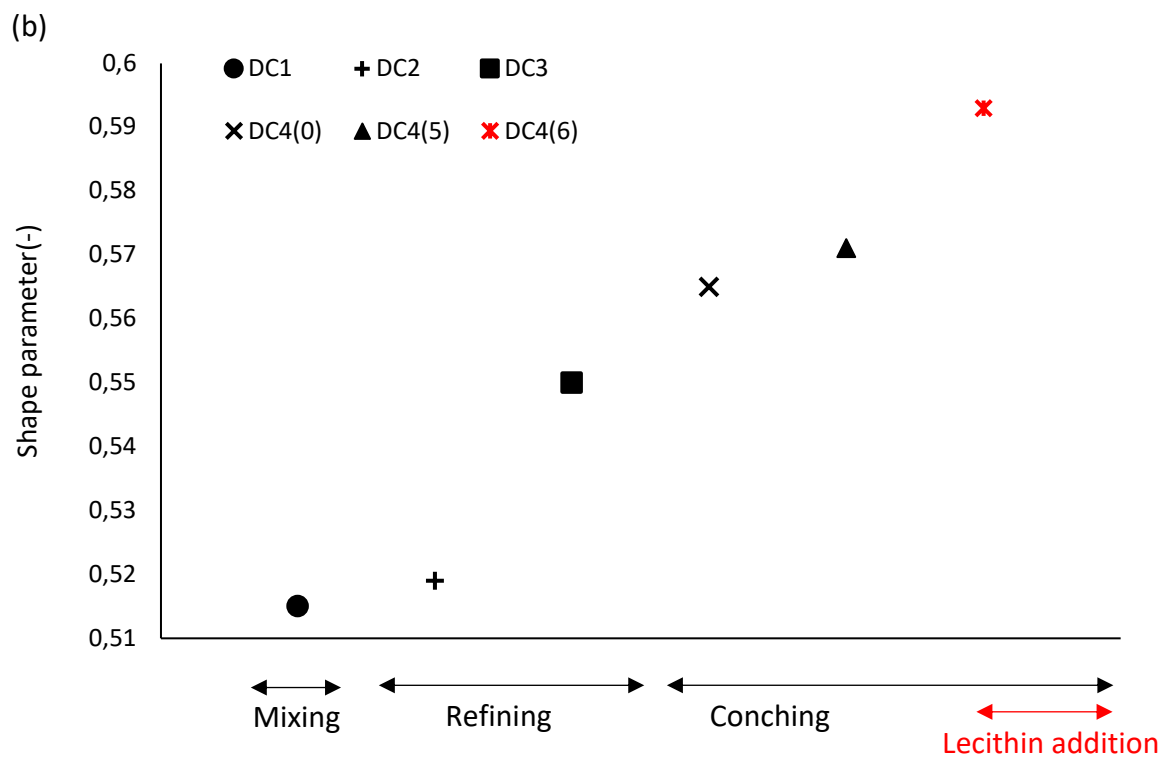
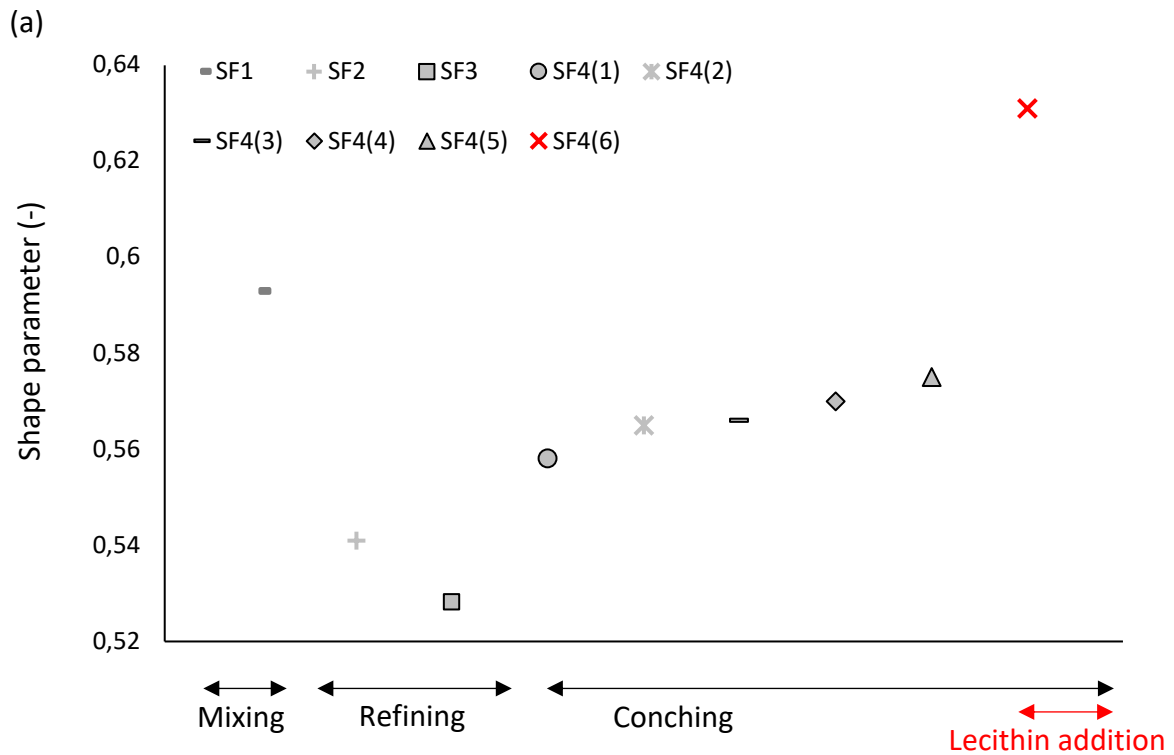


Figure 3-15. Evolution of the shape parameter β of (a) sweet fat and (b) dark chocolate samples over the production process. The data in red correspond to the samples containing lecithin.

Knowing the particle size distribution and maximum packing fraction of each sample, the shape parameter of their particles is calculated. We plot in Figure 3-15 the evolution of the particle shape parameter as a function of the production process. We observe that the shape parameter decreases from SF1 to SF3 and then increases from SF3 to SF4(6) for sugar suspension samples whereas it increases from DC1 to DC4(6) for sugar and cocoa suspension samples. During conching, the highest increase is observed for the samples containing lecithin for both suspensions. A decrease of the shape parameter suggests that the sphericity of the particles decreases and/or the aspect ratio of the particles increases whilst an increase of this parameter suggests that the sphericity increases and/or the aspect ratio decreases. These results imply that all the production steps influence the particle shape of both suspensions.

Regarding the cocoa suspensions, we find a shape parameter of 42% for the non-ground cocoa suspension which only contains Cocoa ($D_{50} = 11.2 \mu\text{m}$) and 48% for the ground cocoa suspension which contains Cocoa ($D_{50} = 3.4 \mu\text{m}$). This suggests that grinding influence the shape of cocoa particles by increasing their sphericity and/or decreasing their aspect ratio.

3.3.4 Correlation between particle size distribution, particle shape and maximum packing fraction

As shown in chapter 1, the maximum packing fraction is controlled by the particle's size (i.e., polydispersity) and shape. We know from literature [10] that polydisperse samples have generally a higher maximum packing fraction than monodisperse samples because particles with variable size can fill more efficiently the space. Therefore, the evolution of the maximum packing fraction of sugar suspension samples, sugar and cocoa suspension samples and cocoa suspensions can be explained by the evolution of their particle size distribution and shape parameter over the production process.

For sugar suspension samples, we suggest that the decrease of maximum packing fraction occurring from mixing to the end of refining can be related to the decrease in polydispersity and the decrease of particle sphericity (and/or increase of particle aspect ratio) whereas the increase of maximum packing fraction during conching shall only be related to the increase of the particle sphericity (and/or decrease of particle aspect ratio) since we show that the sample's polydispersity do not change. In conclusion, the particle size and/or particle shape control the maximum packing fraction during mixing and refining processes whereas only the particle shape seems to control the maximum packing fraction during conching.

For sugar and cocoa suspension samples, the decrease of maximum packing fraction from mixing to the end of refining must mainly be due to the decrease of the sample polydispersity

whereas the increase occurring during conching can be explained by the decrease of the particle aspect ratio (and/or the increase of the particle sphericity). The same maximum packing fraction measured for DC3 and DC4(0) can be explained by the fact that they have the same particle size distribution and the same shape parameter. In conclusion, we suggest that the maximum packing fraction is controlled by the particle size during the mixing and refining processes and the particle shape is governing the maximum packing fraction during the conching process.

For the cocoa masses, the increase of polydispersity and shape parameter during the grinding can explained the increase of maximum packing fraction from the beginning to the end of grinding.

3.3.5 Effect of lecithin on maximum packing fraction

To explain the significant increase of the maximum packing fraction of both suspensions in presence of lecithin, we suggest that the presence of lecithin in the system causes an alignment of the particles leading to an ordered packing of SF4(6) and DC4(6) allowing to reach higher values of maximum packing fraction. We study the effect of lecithin on cocoa and sugar particles maximum packing fraction to verify that as supposed lecithin only influences sugar particles. We measure the maximum packing fraction of Cocoa ($D_{50} = 9.2 \mu\text{m}$), SF1 that contains coarse sugar particles and SF4(5) that contains smaller sugar particles using lecithin as deflocculant. We compare the results to those obtained with PGPR. We observe from Figure 3-14 that Cocoa ($D_{50} = 9.2 \mu\text{m}$) has the same maximum packing fraction ($\phi_{max} = 0.49$) independently of the emulsifier used whereas the addition of lecithin leads to higher maximum packing fraction for sugar powders SF1 and SF4(5). Additionally, we observe that the increase of maximum packing fraction in presence of lecithin is more important for smaller sugar particles than coarse sugar particles. However, although these results seem to confirm our suggestion, further investigations are needed to confirm the possible alignment of sugar particles in presence of lecithin since to our knowledge, this possible alignment of sugar particles by lecithin has not been demonstrated in literature yet.

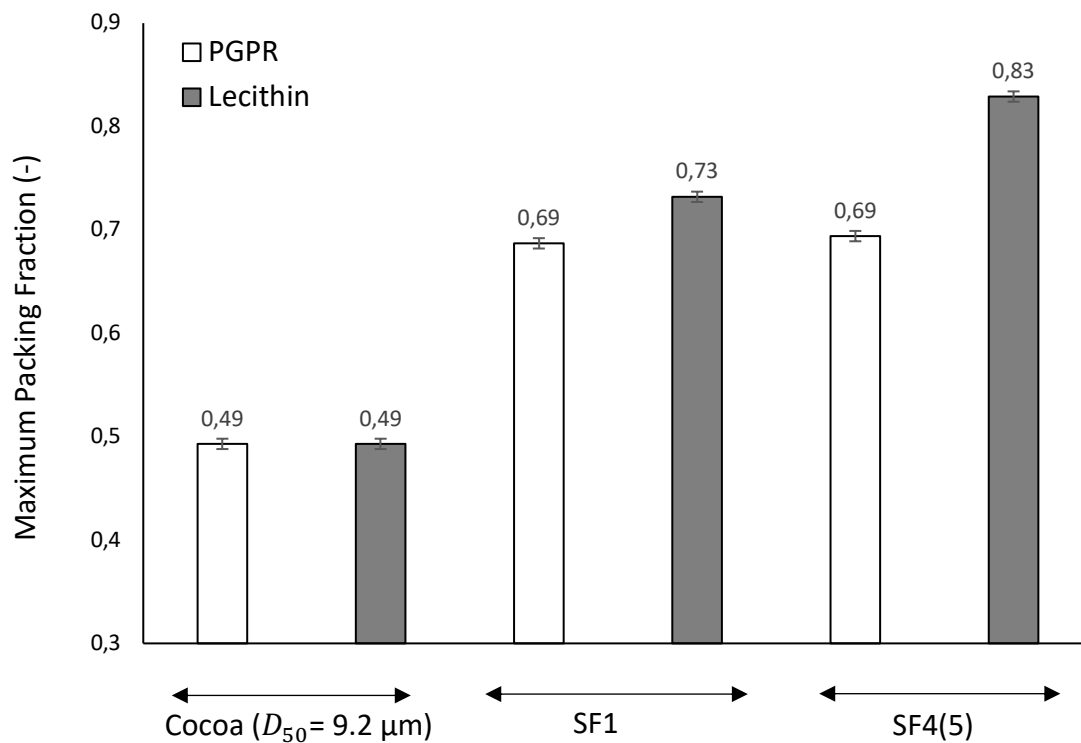


Figure 3-14. Maximum packing fractions measured using PGPR and Lecithin as deflocculant. 1.5% Lecithin by total mass of solid particles is used to deflocculated Cocoa ($D_{50} = 9.2 \mu\text{m}$) and SF1 whereas 1% Lecithin by total mass of solid particles is used to deflocculated SF4(5). The same proportion of PGPR is used to deflocculate these samples.

3.4 Evolution of the rheological properties over the production process

3.4.1 Sugar suspension (sweet fat (SF)) samples

We study in this section the evolution of the rheological behaviour over the production process. In order to study the effect of particles morphological parameters, we set the solid volume fraction of the suspensions at $\phi = 0.53$. Cocoa butter is added to each sample in order to reach this desired solid volume fraction.

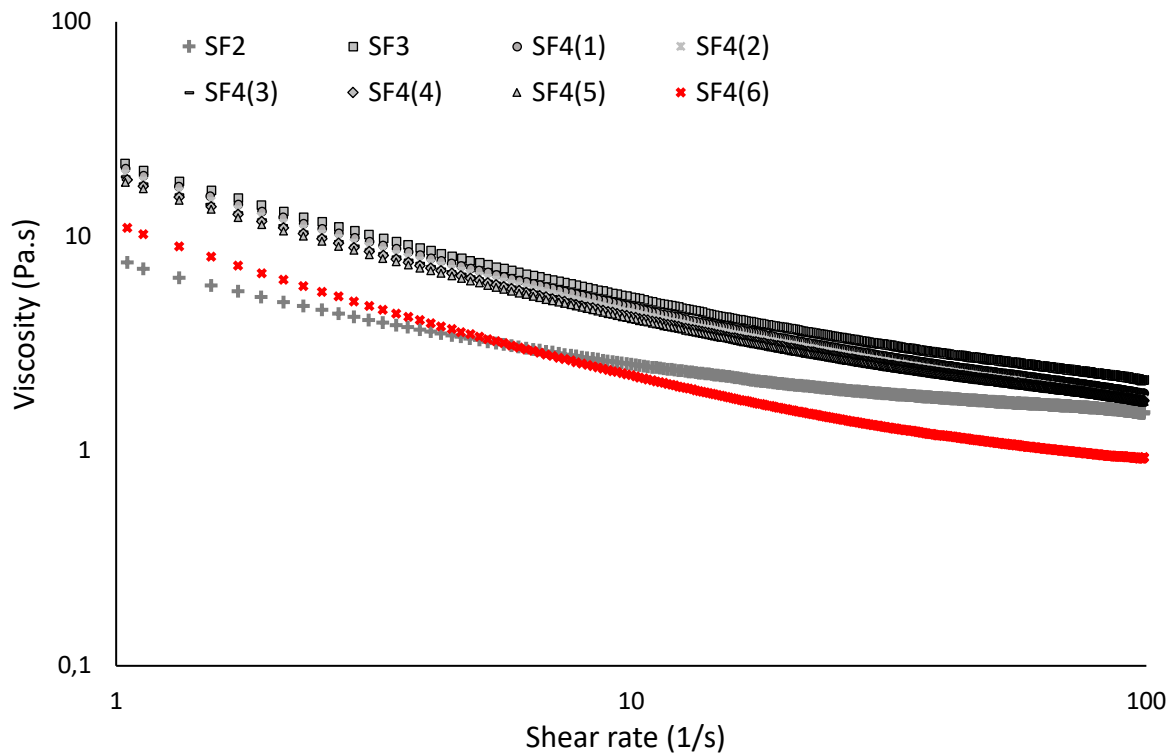


Figure 3-16. Flow curves of sugar suspension (sweet fat) samples. The data in red correspond to the sample containing lecithin.

We plot in Figure 3-16 the measured viscosity as a function of the shear rate for each sugar suspension samples except SF1. During the rheological measurement of the latter, the suspension is unstable (i.e., the sugar particles settle at the bottom of the rheometer cup instead of being homogeneously dispersed in the interstitial fluid) which means that the flow curve measured is not reliable. We observe a shear thinning behaviour (i.e., viscosity decreasing with shear rate) for all samples. After fitting these flow curves with Bingham equation, we plot in Figure 3-17 the rheological parameters (viscosity and yield stress) as a function of the production process. We observe the same evolution of the rheological parameters over the production process: both parameters increase during refining (from 1.4 Pa.s to 1.9 Pa.s for viscosity and from 12.4 Pa to 36.9 Pa for yield stress) and then decrease during conching (from 1.6 Pa.s to 0.8 Pa.s for viscosity and 33.4 Pa to 15.3 Pa for yield stress). The lowest value of both parameters is reached when lecithin is added.

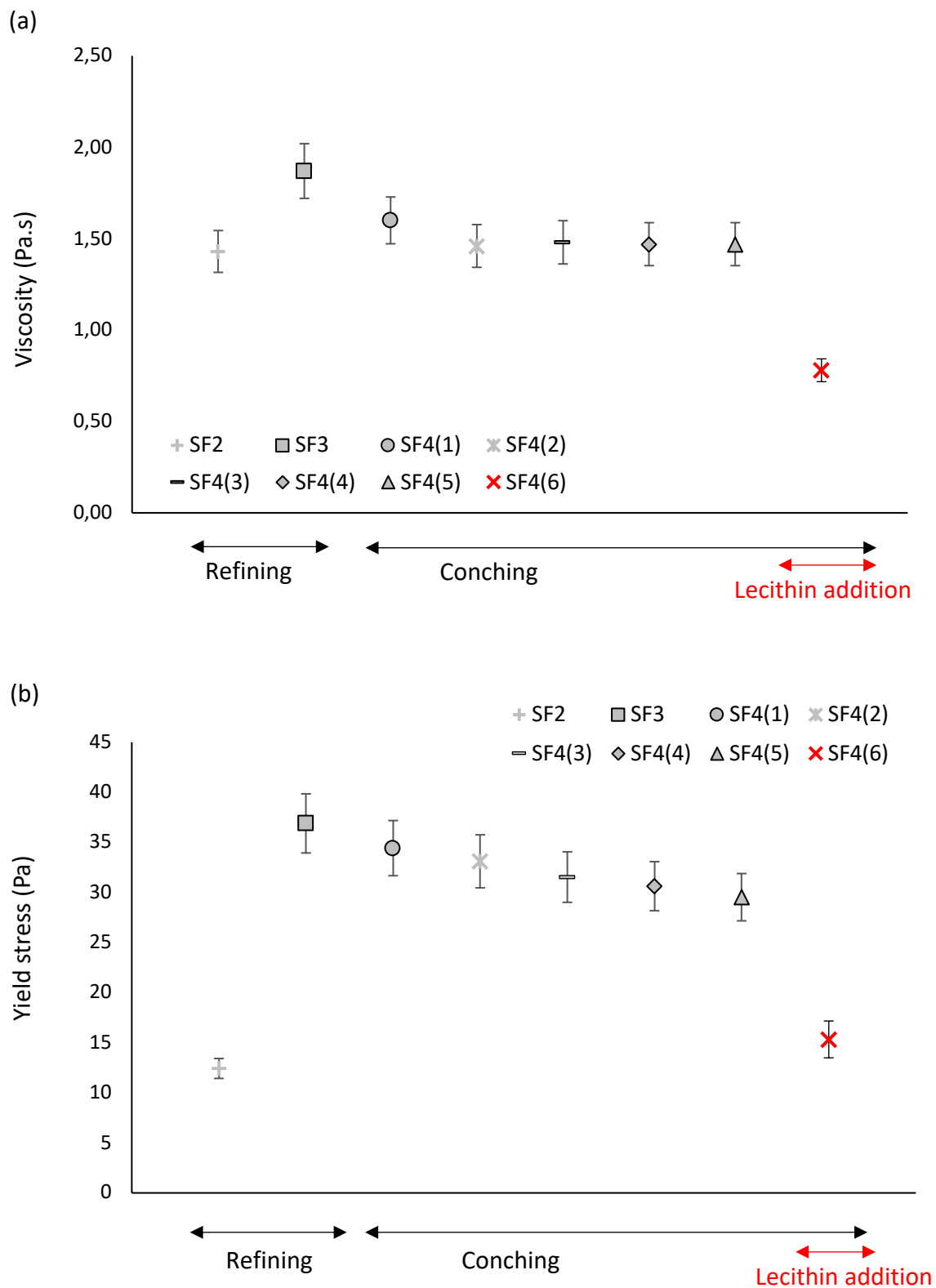


Figure 3-17. Evolution of the (a) viscosity and (b) yield stress of sweet fat samples over the production process. The data in red correspond to the sample containing lecithin.

We finally observe from Figure 3-17 that the evolution of the rheological parameters has the same trend than the evolution of the maximum packing fraction, which suggests that there is a correlation between the rheological properties and morphological properties of sugar suspension samples. We detail this correlation and its origin in chapter 4.

3.4.2 Sugar and cocoa suspension (dark chocolate (DC)) samples

We plot in Figure 3-18 the measured viscosity as a function of the shear rate for each dark chocolate samples and, in Figure 3-19, the fitted rheological parameters as a function of the production process except for DC1 due to an instability of the suspension during the measurement. We set the solid volume fraction at $\phi = 0.53$.

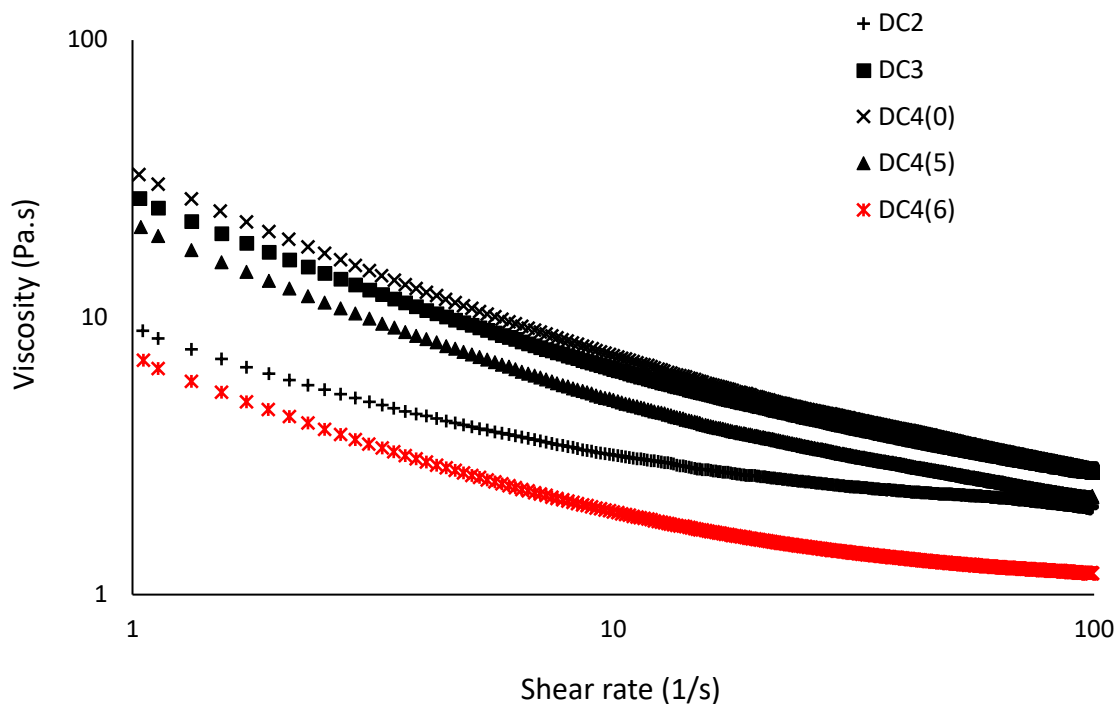


Figure 3-18. Flow curves of sugar and cocoa suspension (dark chocolate) samples. The data in red correspond to the sample containing lecithin.

As for sugar suspension samples, sugar and cocoa suspension samples exhibit a shear thinning behaviour with an increase of the rheological parameters during refining (from 2 Pa.s to 2.4 Pa.s for viscosity and from 14.3 Pa to 46.4 Pa for yield stress) followed by a decrease during conching (from 2.4 Pa.s to 1.1 Pa.s for viscosity and from 47.8 Pa to 9.1 Pa for yield stress). These results are in accordance with those of Glycerina and al. [11] mentioned in chapter 1. We recall that their study has showed that yield stress and viscosity increase from mixing (A) to refining (C) and decrease from refining (C) to conching and tempering (E).

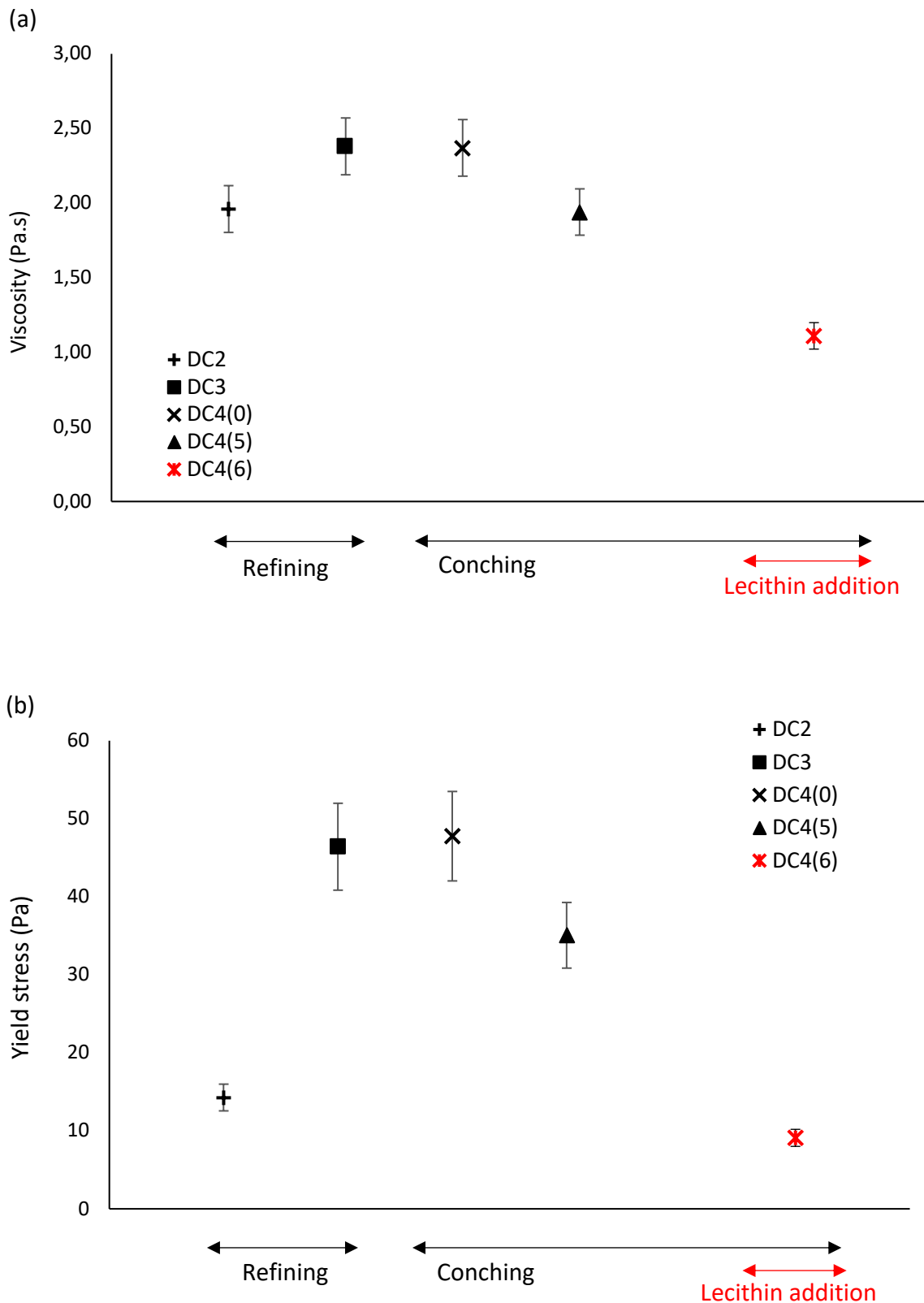


Figure 3-19. Evolution of the (a) viscosity and (b) yield stress of sugar and cocoa suspension (dark chocolate) samples over the production process. The data in red correspond to the sample containing lecithin.

We observe from Figure 3-19 that the evolution of the rheological parameters has the same trend than the evolution of the maximum packing fraction, which suggests that there is a correlation between the rheological properties and morphological properties of sugar and cocoa suspension samples. We detail this correlation and its origin in chapter 4.

Figure 3-19 also highlights that the lowest values of viscosity and yield stress are reached when lecithin is added as for sugar suspension samples. However, the decrease is more important for sugar and cocoa suspension than sugar suspension. In addition, the decrease of rheological parameters during the 5 first hours of conching (i.e., in absence of lecithin) is also more pronounced for sugar and cocoa suspension samples. These results suggest that there is a phenomenon occurring during the conching of sugar and cocoa suspension that is governing its rheological behaviour. The effect of this phenomenon is increased when lecithin is added.

3.4.3 Effect of moisture on the rheological behaviour of sugar and cocoa suspension

The decrease of the rheological parameters of sugar and cocoa suspension (dark chocolate) samples (Figure 3-19) during conching in absence of lecithin is more pronounced than for sugar suspension (sweet fat) samples (Figure 3-17). This behaviour can be owed partly to an evaporation of cocoa particles moisture. Indeed, Beckett [5] shows that, during the 6 hours of chocolate conching, the water content decreases by 0.6% by mass of chocolate and that, at the end of conching, the content is approximately 0.8% by mass of chocolate. Moreover, as mentioned in chapter 1, Haufmann et al. [12] have showed that the presence of water in cocoa suspensions leads to the formation of capillary bridges between the particles causing an increase of the rheological parameters of cocoa suspensions. Therefore, to highlight the effect of moisture content on sugar and cocoa suspension, we study the effect of moisture on cocoa suspensions made of fatted cocoa particles (Cocoa ($D_{50} = 9.2 \mu\text{m}$)) and cocoa butter.

We recall that the fatted cocoa powder (Cocoa ($D_{50} = 9.2 \mu\text{m}$)) used to produce dark chocolate suspension contains 4.5% water by mass of particles. We study 6 cocoa suspensions having a solid volume fraction $\phi = 0.43$. 3 suspensions in which we add water to increase the water content (3.9 %, 5.1% and 6.3% by total of suspension). 2 suspensions in which we decrease the water content (0.8% and 0% by total of suspension) by drying fatted cocoa particles (Cocoa ($D_{50} = 9.2 \mu\text{m}$)) at 50°C in the oven. The last suspension is the reference one containing 2.7% water by mass of suspension. We plot in Figure 3-20 (a) the measured viscosity as a function of the shear rate for the 5 cocoa suspensions studied. We observe that the yield stress and viscosity are increasing with the water content. Figure 3-20 (b) shows that our results are in accordance with those of Haufmann et al. [12].

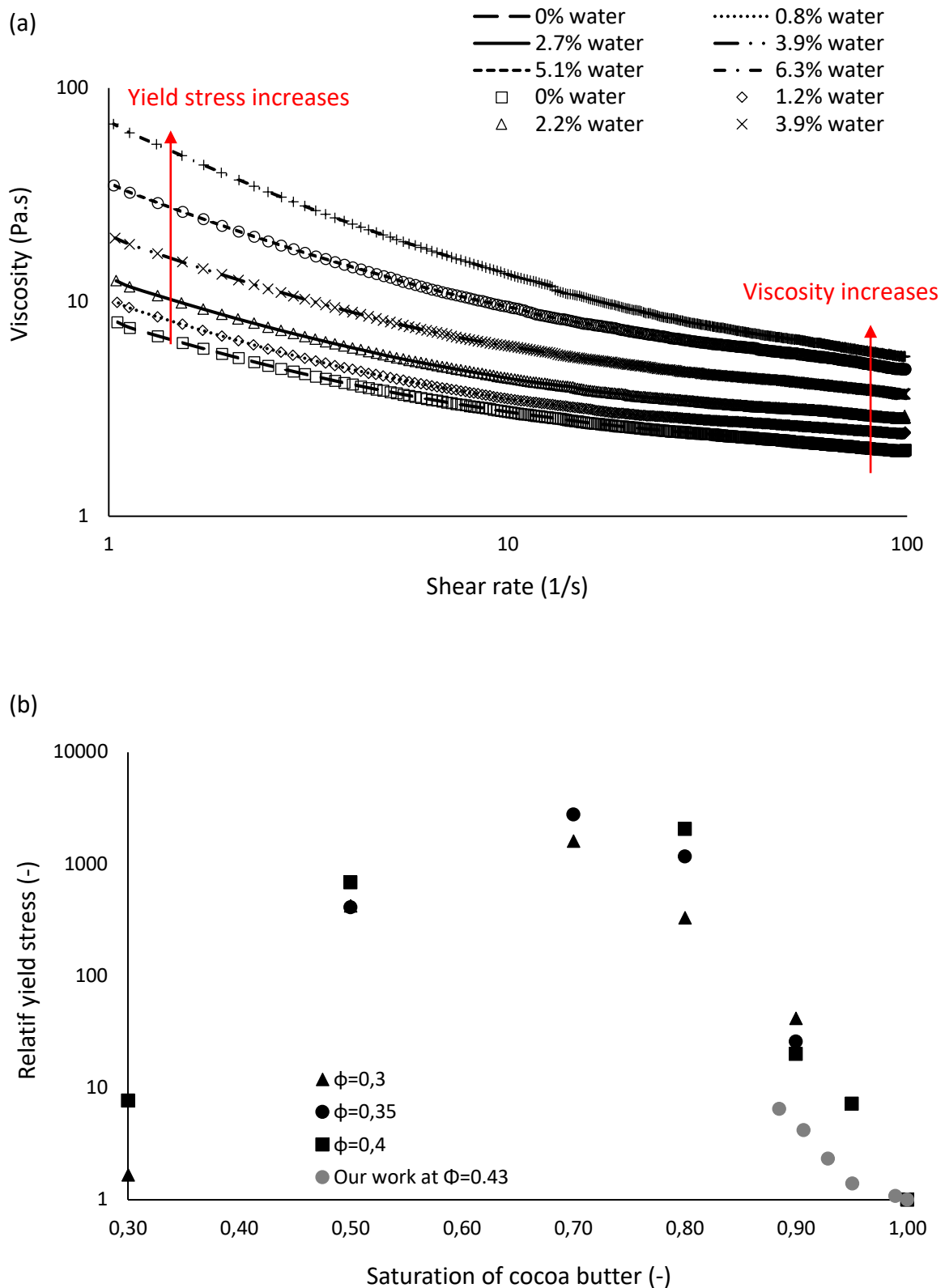
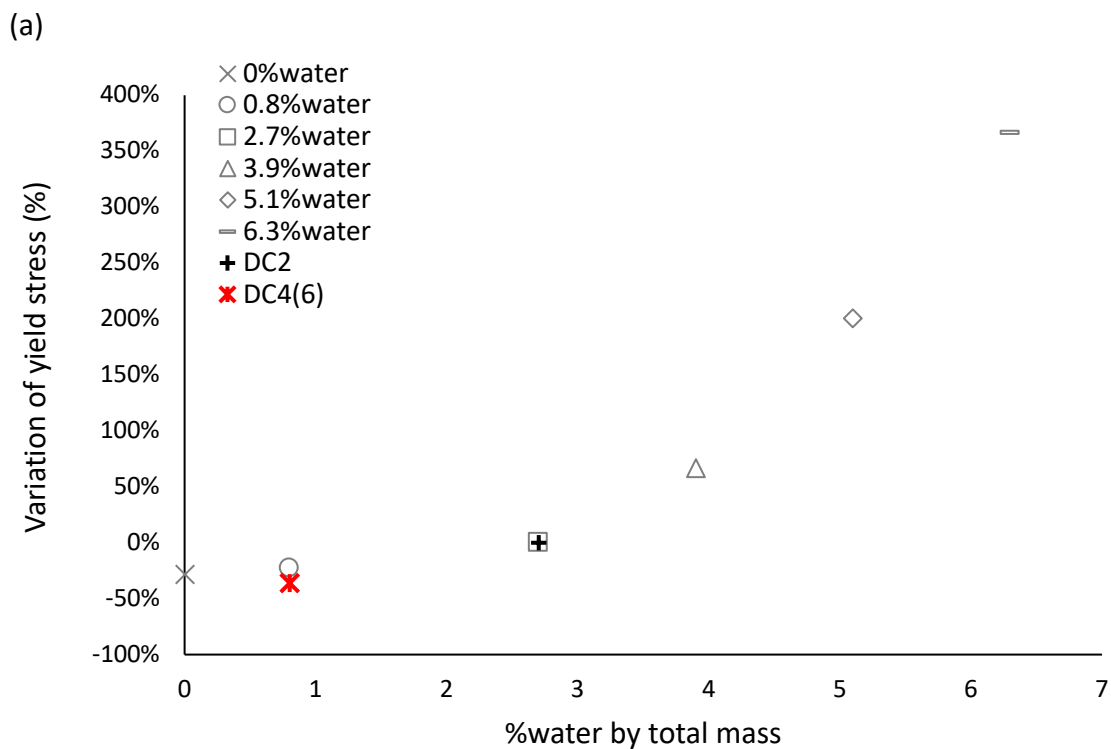


Figure 3-20. Flow curves of the (a) 5 cocoa suspensions studied in presence and absence of water and (b) normalized yield stress as a function of saturation of the preferentially wetting fluid for cocoa dispersions extracted from [12].

Chapter 3: Effect of chocolate production process on the morphological properties of the particles and rheological properties of the suspension

Based on [5], we know that, at the end of conching, we should have approximately 0.8% water by mass of chocolate. We therefore plot in Figure 3-21 the variation of yield stress and viscosity when the water content goes from 2.7% to 0.8% for cocoa suspensions and sugar and cocoa suspension samples (i.e., from DC2 to DC4(6)). We observe that the variation in viscosity and yield stress when the water content decreases is more pronounced for sugar and cocoa suspension than cocoa suspensions. Yield stress varies by 36% for sugar and cocoa suspension and by 22% for cocoa suspensions. Whereas viscosity varies by 43% and 15% for sugar and cocoa suspension and cocoa suspensions respectively. From these results, we can conclude that a decrease of water content during the conching of dark chocolate could only partly explain the decrease of viscosity observed during conching. Therefore, additionally to water evaporation and lecithin addition, another phenomenon must contribute to the decrease of the viscosity and yield stress during the conching.



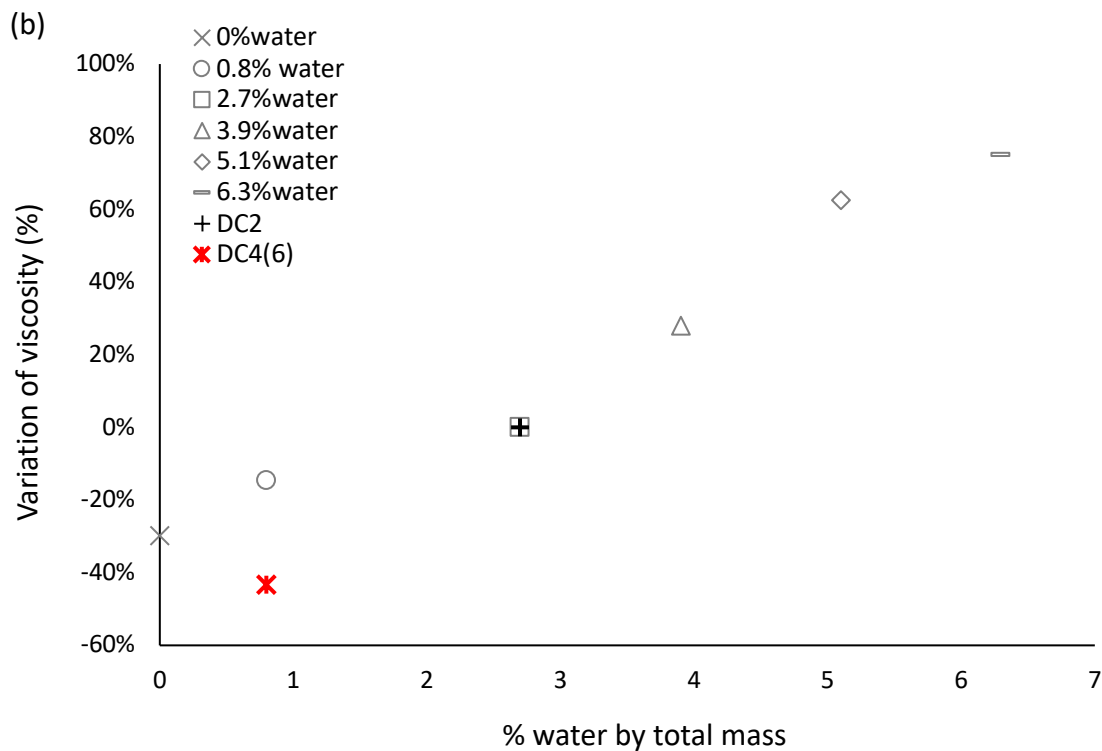


Figure 3-21. Variation of (a) yield stress and (b) viscosity for cocoa suspensions and sugar and cocoa suspension. The data in red correspond to the sample containing lecithin.

3.4.4 Ground and non-ground cocoa masses

We plot in Figure 3-22 the viscosity as a function of the shear rate for ground and non-ground cocoa mass. We observe that the viscosity decreases whereas the yield stress increase with the grinding. Herein we also notice that the effect of grinding on the rheological parameters is the same than on the morphological properties, which implies that there must be a correlation between both properties. We detail this correlation and its origin in chapter 4.

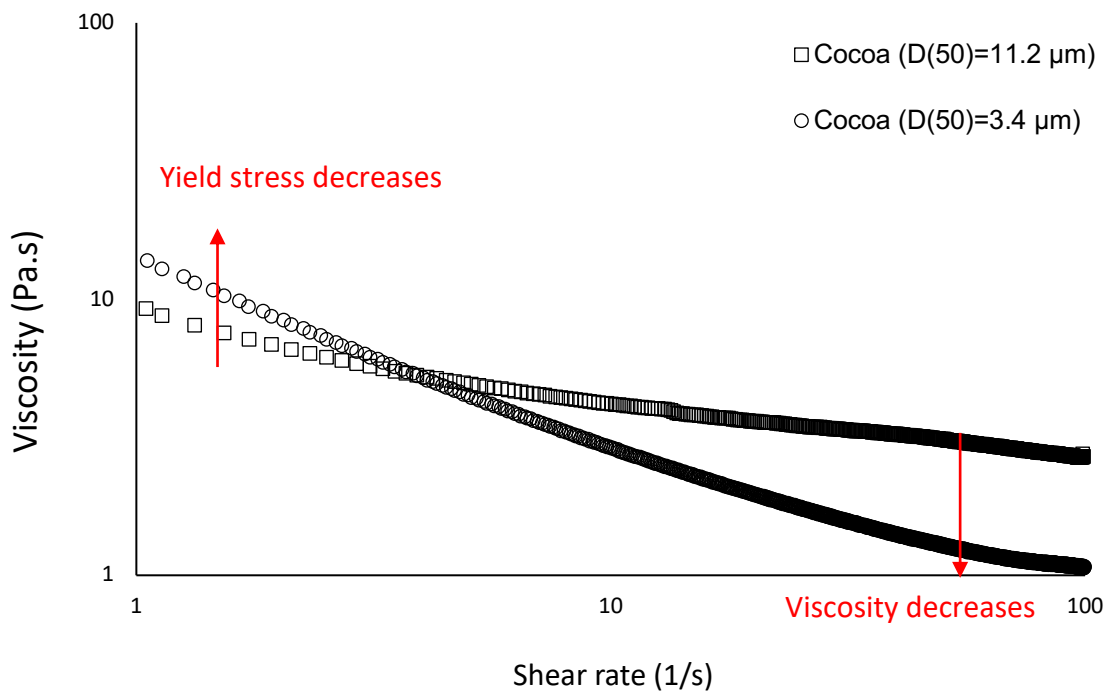


Figure 3-23. Viscosity (a) and yield stress (b) of cocoa suspensions.

3.5 Conclusion

In this chapter, we analyzed the influence of production process on particle size distribution, particle shape, maximum packing fraction and rheological behavior of dark chocolate and sweet fat samples. We also studied the effect of grinding on particle size distribution, particle shape, maximum packing fraction and rheological behavior of cocoa mass.

We demonstrated for dark chocolate and sweet fat samples that the refining steps of the production process leads to a decrease of the particle size and the maximum packing fraction. We also observed, during this step, an increase of the sample's viscosity and yield stress. Regarding the shape parameter (i.e., maximum packing fraction of each particle size class of a powder), it increases for dark chocolate and decreases for sweet fat samples. We also show that the conching step do not influence the particle size distribution. It leads to an increase the shape parameter and the maximum packing fraction and to the decrease of the viscosity and yield stress. We showed that the grinding of cocoa mass causes a decrease of its particle size distribution and viscosity, and an increase of its maximum packing fraction, particle shape parameter and yield stress.

We highlighted the fact that the evolution of the maximum packing fraction over the production process could be explained by the evolution of particle size distribution and shape parameter of the particles. For sweet fat samples, the particle size and/or particle shape

Chapter 3: Effect of chocolate production process on the morphological properties of the particles and rheological properties of the suspension

parameter control the maximum packing fraction during mixing and refining processes whereas only the shape parameter seems to control the maximum packing fraction during conching. For dark chocolate samples, the maximum packing fraction is controlled by the particle size during the mixing and refining processes and the shape parameter is governing the maximum packing fraction during the conching process.

Finally, we demonstrated that the presence of lecithin and water in the system can also influence the maximum packing fraction and rheological parameters of the samples over the production process. Indeed, we showed that lecithin increases drastically the maximum packing fraction when the suspension contains sugar particles by aligning the latter. The presence of water causes an increase of the viscosity and yield stress.

References:

- [1] Baixauli, R.; Sanz, T.; Salvadora, A.; Fiszmana, S. M. *Food Hydrocolloids* 2007, 21, 230–236.
- [2] Glicerina, V.; Balestra, F.; Dalla Rosa, M.; Romani, S. *Food Bioprocess Technol.* 2015, 8, 770-776.
- [3] Glicerina, V.; Balestra, F.; Dalla Rosa, M.; Roman S. *J. Food Eng.* 2015, 145, 45-50.
- [4] Gaonkar, A. G. *Journal of the American Oil Chemistry Society* 1989, 66, 1090-1092.
- [5] Beckett, S.T. (2010) *The Science of Chocolate*. London: RSC Publishing.
- [6] Anese, M.; Shtylla I.; Torreggiani, D.; Maltini, D. *Thermochimica Acta* 1996, 275, 131-137.
- [7] Ahmed, J.; Ramaswamy, H.S. *Journal of Food Engineering* 2006, 74, 376–382.
- [8] Atkinson, K.E. (1989). *An Introduction to Numerical Analysis* (2nd ed.). New York: John Wiley & Sons.
- [9] de Larrard, F. *Concrete Mixture Proportioning: a scientific approach*, E&FN SPON: An imprint of Routledge, London and New-York, 1999.
- [10] Bournonville, B. *Influence de la granulométrie des particules sur la rhéologie des suspensions concentrées*, Rapport interne, LMSGC, Champs sur Marne, 2003.
- [11] Glicerina, V.; Balestra, F.; Dalla Rosa, M.; Bergenstal, B.; Tornberg, E.; Roman, S. *Journal of Food Science* 2014, 79, 1359-1365.
- [12] Hoffmann, S.; Koos, E.; Willenbacher, N. *Food Hydrocolloids* 2014, 40, 44-52.

**Chapter 4: Correlation between the
morphological and rheological
parameters**

Table of contents

4.1	Studied suspensions	126
4.1.1	Sugar suspensions: sweet fat samples	126
4.1.2	Sugar and cocoa suspensions: dark chocolate samples.....	128
4.1.3	Cocoa suspensions.....	129
4.1.3.1	Composition.....	129
4.1.3.2	Particle size distribution.....	130
4.1.3.3	Maximum packing fraction.....	132
4.2	Influence of particle morphological properties on viscosity.....	133
4.2.1	Experimental results	133
4.2.1.1	Effect of the solid volume fraction of sugar suspensions (sweet fat) and sugar and cocoa suspensions (dark chocolate)	133
4.2.1.2	Effect of the substitution of coarse cocoa particles by fine cocoa particle ..	135
4.2.1.3	Effect of the maximum packing fraction of sugar suspensions (sweet fat), cocoa suspensions and sugar and cocoa suspensions (dark chocolate).....	136
4.2.1.4	Effect of emulsifier on sugar suspensions (sweet fat), cocoa suspensions and sugar and cocoa suspensions (dark chocolate).....	137
4.2.2	Outcome of the influence of the morphological properties on viscosity.....	139
4.3	Influence of the morphological properties on yield stress.....	140
4.3.1	Effect of the solid volume fraction of sugar suspensions (sweet fat) and sugar and cocoa suspensions (dark chocolate)	140
4.3.2	Effect of the substitution of coarse cocoa particles by fine cocoa particles..	142
4.3.3	Effect of the maximum packing fraction of the sugar suspensions (sweet fat), cocoa and sugar suspensions (dark chocolate) and cocoa suspensions.....	142
4.3.4	Effect on yield stress of the particle size distribution of the sugar suspensions (sweet fat), cocoa and sugar suspensions (dark chocolate) and cocoa suspensions.....	145
4.4	Summary.....	148
4.5	Conclusion.....	149
	References.....	149

The literature study summarized in chapter 1 suggested that exploiting the principles of the rheology of particulate suspensions is a promising method to decrease the fat content in chocolate while keeping a constant viscosity. It is known from the literature of suspensions rheology that the viscosity of a concentrated suspension mainly depends on the relative solid volume fraction (i.e., the solid volume fraction to maximum packing fraction ratio (ϕ/ϕ_{max})) [1, 2]. We recall that maximum packing fraction depends on particle size distribution and particle shape and can therefore be optimized to control chocolate suspension viscosity. It should be kept in mind that this method allows for the control of chocolate rheology without significant changes to the overall chocolate formulation, which is always beneficial from a manufacturer's perspective [3-6].

In this chapter, we are highlighting the fact that the samples studied in this thesis are indeed following the principle of the rheology of concentrated suspensions. To this end, we study in this chapter quantitatively (as opposed to the qualitative approach of the previous chapter) the correlation between the morphological and rheological properties measured in the previous chapter for sugar suspensions (sweet fat samples) and cocoa and sugar suspensions (dark chocolate samples and cocoa suspensions that we present in this chapter. In the following, we first recall the morphological and rheological properties of all studied suspensions. We then correlate the viscosity of the suspensions to their relative packing fraction and fit all viscosity data with Krieger-Dougherty equation. We finally correlate the yield stress of the suspensions to their morphological properties and highlighted a relation between the yield stress, the particle size distribution and the maximum packing fraction.

4.1 Studied suspensions

In this section, we recall the composition of the suspensions studied in the previous chapter, namely the suspensions composed only of sugar particles (refer as sweet fat) and the suspensions composed of cocoa and sugar particles (refer as dark chocolate). In addition to these suspensions, we also study in this section the morphological properties of cocoa suspensions that we formulate from the ground (Cocoa ($D_{50}= 11.2 \mu\text{m}$)) and non-ground (Cocoa ($D_{50}= 3.4 \mu\text{m}$)) cocoa masses studied in the previous chapter.

4.1.1 Sugar suspensions: sweet fat samples

We recall that in the previous chapter, we studied the rheological behaviour of 8 samples of sugar (sweet fat) suspensions at $\phi = 0.53$. In addition to this volume fraction, we are studying the rheological behavior at 3 other solid volume fractions ($\phi = 0.48$, $\phi = 0.45$ and $\phi = 0.41$) herein. The composition of the samples at each solid volume fraction is summarized in Table 4-1.

Chapter 4: Correlation between the morphological and rheological parameters

	Sugar particles (% mass)	Cocoa butter (% mass)	Lecithin (%mass)	Solid volume fraction \emptyset
SF1-After mixing	56.6	43.4	0	0.53
SF2-After 1 st refining	56.6	43.4	0	0.53
SF3-After 2 nd refining	56.6	43.4	0	0.53
SF4(1)-After 1h of conching	56.2	43.8	0	0.53
SF4(2)-After 2h of conching	56.2	43.8	0	0.53
SF4(3)-After 3h of conching	56.2	43.8	0	0.53
SF4(4)-After 4h of conching	56.2	43.8	0	0.53
SF4(5)-After 5h of conching	56.2	43.8	0	0.53
SF4(6)-End of conching	56	43.6	0.4	0.53

	Sugar particles (% mass)	Cocoa butter (% mass)	Lecithin (%mass)	Solid volume fraction \emptyset
SF1-After mixing	53.6	46.4	0	0.48
SF2-After 1 st refining	53.6	46.4	0	0.48
SF3-After 2 nd refining	53.6	46.4	0	0.48
SF4(1)-After 1h of conching	53.2	46.8	0	0.48
SF4(2)-After 2h of conching	53.2	46.8	0	0.48
SF4(3)-After 3h of conching	53.2	46.8	0	0.48
SF4(4)-After 4h of conching	53.2	46.8	0	0.48
SF4(5)-After 5h of conching	53.2	46.8	0	0.48
SF4(6)-End of conching	53	46.6	0.4	0.48

	Sugar particles (% mass)	Cocoa butter (% mass)	Lecithin (%mass)	Solid volume fraction \emptyset
SF1-After mixing	50.9	49.1	0	0.45
SF2-After 1 st refining	50.9	49.1	0	0.45
SF3-After 2 nd refining	50.9	49.1	0	0.45
SF4(1)-After 1h of conching	50.5	49.5	0	0.45
SF4(2)-After 2h of conching	50.5	49.5	0	0.45
SF4(3)-After 3h of conching	50.5	49.5	0	0.45
SF4(4)-After 4h of conching	50.5	49.5	0	0.45
SF4(5)-After 5h of conching	50.5	49.5	0	0.45
SF4(6)-End of conching	50.4	49.3	0.3	0.45

	Sugar particles (% mass)	Cocoa butter (% mass)	Lecithin (%mass)	Solid volume fraction \emptyset
SF1-After mixing	48.4	51.6	0	0.41
SF2-After 1 st refining	48.4	51.6	0	0.41
SF3-After 2 nd refining	48.4	51.6	0	0.41
SF4(1)-After 1h of conching	48.1	51.9	0	0.41
SF4(2)-After 2h of conching	48.1	51.9	0	0.41
SF4(3)-After 3h of conching	48.1	51.9	0	0.41
SF4(4)-After 4h of conching	48.1	51.9	0	0.41
SF4(5)-After 5h of conching	48.1	51.9	0	0.41
SF4(6)-End of conching	48	51.7	0.3	0.41

Table 4-1. Composition of the sugar (sweet fat) suspensions samples at different solid volume fraction.

4.1.2 Sugar and cocoa suspensions: dark chocolate samples

Similarly, to the sugar suspensions, we studied in the previous chapter the rheological behaviour of 6 samples of sugar and cocoa (dark chocolate) suspensions at $\phi = 0.53$. In addition to this volume fraction, we are studying the rheological behavior at 3 other solid volume fractions ($\phi = 0.48$, $\phi = 0.45$ and $\phi = 0.41$) herein. The composition of the samples at each solid volume fraction is summarized in Table 4-2.

	Sugar particles (% mass)	Cocoa particles (% mass)	Cocoa butter (% mass)	Lecithin (% mass)	Solid volume fraction ϕ
DC1-After mixing	47.6	17	35.4	0	0.53
DC2-After 1 st refining	47.6	17	35.4	0	0.53
DC3-After 2 nd refining	47.6	17	35.4	0	0.53
DC4(0)-Beginning of conching	47.6	16.9	35.5	0	0.53
DC4(5)-After 5h of conching	47.6	16.9	35.5	0	0.53
DC4(6)-End of conching	47.4	16.9	35.3	0.4	0.53

	Sugar particles (% mass)	Cocoa particles (% mass)	Cocoa butter (% mass)	Lecithin (% mass)	Solid volume fraction ϕ
DC1-After mixing	44.7	15.9	39.4	0	0.48
DC2-After 1 st refining	44.7	15.9	39.4	0	0.48
DC3-After 2 nd refining	44.7	15.9	39.4	0	0.48
DC4(0)-Beginning of conching	44.7	15.8	39.5	0	0.48
DC4(5)-After 5h of conching	44.7	15.8	39.5	0	0.48
DC4(6)-End of conching	44.5	15.8	39.3	0.4	0.48

	Sugar particles (% mass)	Cocoa particles (% mass)	Cocoa butter (% mass)	Lecithin (% mass)	Solid volume fraction ϕ
DC1-After mixing	42	15	43	0	0.45
DC2-After 1 st refining	42	15	43	0	0.45
DC3-After 2 nd refining	42	15	43	0	0.45
DC4(0)-Beginning of conching	42	14.9	43.1	0	0.45
DC4(5)-After 5h of conching	42	14.9	43.1	0	0.45
DC4(6)-End of conching	41.7	14.8	43.1	0.4	0.45

	Sugar particles (% mass)	Cocoa particles (% mass)	Cocoa butter (% mass)	Lecithin (% mass)	Solid volume fraction ϕ
DC1-After mixing	39.7	14.1	46.2	0	0.41
DC2-After 1 st refining	39.7	14.1	46.2	0	0.41
DC3-After 2 nd refining	39.7	14.1	46.2	0	0.41
DC4(0)-Beginning of conching	39.7	14.1	46.2	0	0.41
DC4(5)-After 5h of conching	39.7	14.1	46.2	0	0.41
DC4(6)-End of conching	39.5	14.1	46	0.4	0.41

Table 4-2. Composition of the sugar and cocoa (dark chocolate) suspensions samples at different solid volume fraction.

4.1.3 Cocoa suspensions

4.1.3.1 Composition

9 cocoa suspensions are formulated by mixing different proportions of Cocoa ($D_{50} = 3.4 \mu\text{m}$) (ranging from 10% to 90% with an increment of 10%) with Cocoa ($D_{50} = 11.2 \mu\text{m}$). Additionally, another cocoa mass having cocoa particles of mean diameter of $10.8 \mu\text{m}$ (Cocoa ($D_{50} = 10.8 \mu\text{m}$)) is ground for 6 hours to give Cocoa ($D_{50} = 2.8 \mu\text{m}$). 9 other cocoa are formulated from Cocoa ($D_{50} = 10.8 \mu\text{m}$) and Cocoa ($D_{50} = 2.8 \mu\text{m}$). The difference between the two grinding is the size of the beads used, which is of 1 mm for Cocoa ($D_{50} = 11.2 \mu\text{m}$) grinding whereas it is $500 \mu\text{m}$ for Cocoa ($D_{50} = 10.8 \mu\text{m}$) grinding. The solid volume fraction of all cocoa suspensions is 0.39. The composition of these suspensions is summarized in Table 4-3.

(a)	Cocoa particles (% total mass of suspension)		Cocoa butter (% total mass of suspension)
	Cocoa ($D_{50} = 11.2 \mu\text{m}$)	Cocoa ($D_{50} = 3.4 \mu\text{m}$)	
Cocoa ($D_{50} = 11.2 \mu\text{m}$) + Cocoa ($D_{50} = 3.4 \mu\text{m}$) (1)	45	4.6	50.4
Cocoa ($D_{50} = 11.2 \mu\text{m}$) + Cocoa ($D_{50} = 3.4 \mu\text{m}$) (2)	36.8	9.2	50.4
Cocoa ($D_{50} = 11.2 \mu\text{m}$) + Cocoa ($D_{50} = 3.4 \mu\text{m}$) (3)	32.2	13.8	50.4
Cocoa ($D_{50} = 11.2 \mu\text{m}$) + Cocoa ($D_{50} = 3.4 \mu\text{m}$) (4)	27.6	18.4	50.4
Cocoa ($D_{50} = 11.2 \mu\text{m}$) + Cocoa ($D_{50} = 3.4 \mu\text{m}$) (5)	23	23	50.4
Cocoa ($D_{50} = 11.2 \mu\text{m}$) + Cocoa ($D_{50} = 3.4 \mu\text{m}$) (6)	18.4	27.6	50.4
Cocoa ($D_{50} = 11.2 \mu\text{m}$) + Cocoa ($D_{50} = 3.4 \mu\text{m}$) (7)	13.8	32.2	50.4
Cocoa ($D_{50} = 11.2 \mu\text{m}$) + Cocoa ($D_{50} = 3.4 \mu\text{m}$) (8)	9.2	36.8	50.4
Cocoa ($D_{50} = 11.2 \mu\text{m}$) + Cocoa ($D_{50} = 3.4 \mu\text{m}$) (9)	4.6	45	50.4

(b)	Cocoa particles (% total mass of suspension)		Cocoa butter (% total mass of suspension)
	Cocoa ($D_{50} = 11.2$ μm)	Cocoa ($D_{50} = 3.4$ μm)	
Cocoa ($D_{50} = 10.8 \mu\text{m}$) + Cocoa ($D_{50} = 2.8 \mu\text{m}$) (1)	45	4.6	50.4
Cocoa ($D_{50} = 10.8 \mu\text{m}$) + Cocoa ($D_{50} = 2.8 \mu\text{m}$) (2)	36.8	9.2	50.4
Cocoa ($D_{50} = 10.8 \mu\text{m}$) + Cocoa ($D_{50} = 2.8 \mu\text{m}$) (3)	32.2	13.8	50.4
Cocoa ($D_{50} = 10.8 \mu\text{m}$) + Cocoa ($D_{50} = 2.8 \mu\text{m}$) (4)	27.6	18.4	50.4
Cocoa ($D_{50} = 10.8 \mu\text{m}$) + Cocoa ($D_{50} = 2.8 \mu\text{m}$) (5)	23	23	50.4
Cocoa ($D_{50} = 10.8 \mu\text{m}$) + Cocoa ($D_{50} = 2.8 \mu\text{m}$) (6)	18.4	27.6	50.4
Cocoa ($D_{50} = 10.8 \mu\text{m}$) + Cocoa ($D_{50} = 2.8 \mu\text{m}$) (7)	13.8	32.2	50.4
Cocoa ($D_{50} = 10.8 \mu\text{m}$) + Cocoa ($D_{50} = 2.8 \mu\text{m}$) (8)	9.2	36.8	50.4
Cocoa ($D_{50} = 10.8 \mu\text{m}$) + Cocoa ($D_{50} = 2.8 \mu\text{m}$) (9)	4.6	45	50.4

Table 4-3. Composition of the cocoa suspensions formulated from (a) Cocoa ($D_{50} = 11.2 \mu\text{m}$) + Cocoa ($D_{50} = 3.4 \mu\text{m}$) and from (b) Cocoa ($D_{50} = 10.8 \mu\text{m}$) + Cocoa ($D_{50} = 2.8 \mu\text{m}$).

4.1.3.2 Particle size distribution

From the measured particle size distributions of Cocoa ($D_{50} = 11.2 \mu\text{m}$), Cocoa ($D_{50} = 10.8 \mu\text{m}$), Cocoa ($D_{50} = 3.4 \mu\text{m}$) and Cocoa ($D_{50} = 2.8 \mu\text{m}$) shown in Figure 4-1, and by knowing their volume fraction in each suspension, we calculate the particle size distributions of all cocoa suspensions by following the protocol developed in chapter 2. Table 4-4 shows the characteristics diameters and polydispersity of the particles composing each suspension. As expected, we observe that the successive addition of fine cocoa particles decreases the overall particle size distribution of the suspension and thus increases the polydispersity.

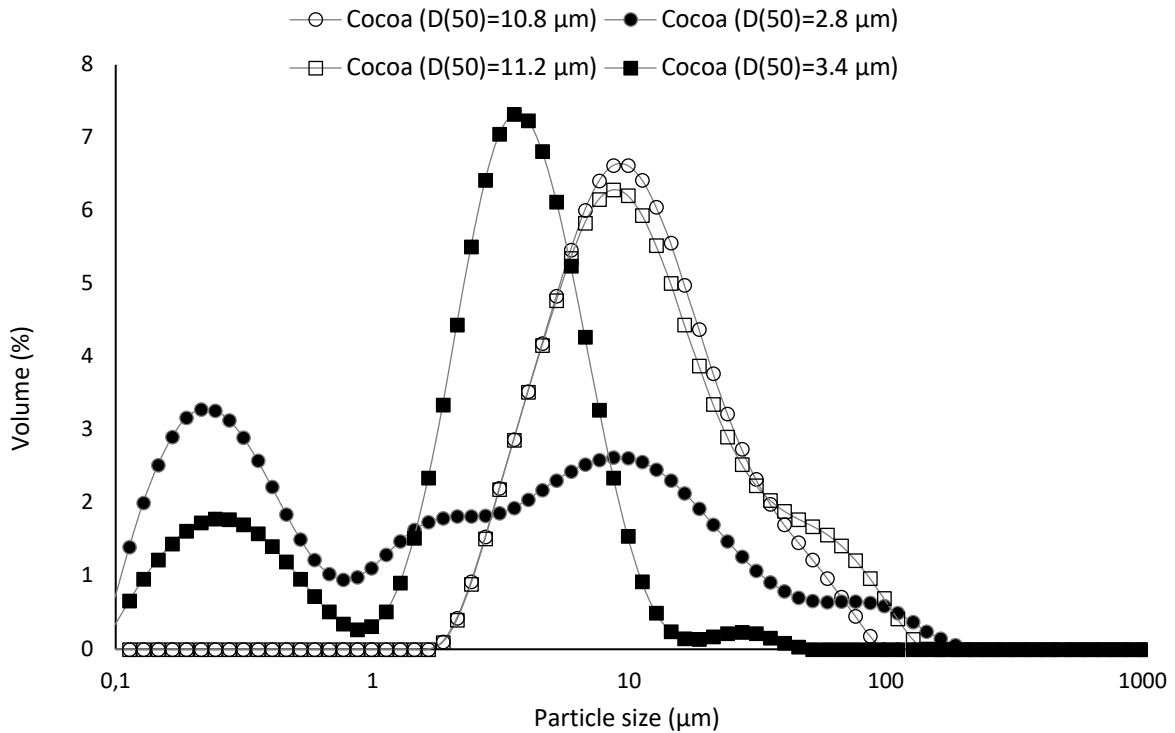


Figure 4-1. Particle size distribution of Cocoa ($D_{50} = 11.2 \mu\text{m}$), Cocoa ($D_{50} = 10.8 \mu\text{m}$), Cocoa ($D_{50} = 3.4 \mu\text{m}$) and Cocoa ($D_{50} = 2.8 \mu\text{m}$).

(a)	D_{10} (μm)	D_{50} (μm)	D_{90} (μm)	$\frac{D_{90}}{D_{10}}$
Cocoa ($D_{50} = 11.2 \mu\text{m}$) + Cocoa ($D_{50} = 3.4 \mu\text{m}$) (1)	3.93	10.4	41.6	10.6
Cocoa ($D_{50} = 11.2 \mu\text{m}$) + Cocoa ($D_{50} = 3.4 \mu\text{m}$) (2)	3.53	9.57	37.9	10.7
Cocoa ($D_{50} = 11.2 \mu\text{m}$) + Cocoa ($D_{50} = 3.4 \mu\text{m}$) (3)	3.12	8.80	34.1	10.9
Cocoa ($D_{50} = 11.2 \mu\text{m}$) + Cocoa ($D_{50} = 3.4 \mu\text{m}$) (4)	2.72	8.02	30.3	11.1
Cocoa ($D_{50} = 11.2 \mu\text{m}$) + Cocoa ($D_{50} = 3.4 \mu\text{m}$) (5)	2.31	7.25	26.6	11.5
Cocoa ($D_{50} = 11.2 \mu\text{m}$) + Cocoa ($D_{50} = 3.4 \mu\text{m}$) (6)	1.90	6.48	22.8	12
Cocoa ($D_{50} = 11.2 \mu\text{m}$) + Cocoa ($D_{50} = 3.4 \mu\text{m}$) (7)	1.50	5.70	19.1	12.7
Cocoa ($D_{50} = 11.2 \mu\text{m}$) + Cocoa ($D_{50} = 3.4 \mu\text{m}$) (8)	1.09	4.93	15.3	14
Cocoa ($D_{50} = 11.2 \mu\text{m}$) + Cocoa ($D_{50} = 3.4 \mu\text{m}$) (9)	0.69	4.15	11.5	16.7

(b)	D_{10} (μm)	D_{50} (μm)	D_{90} (μm)	$\frac{D_{90}}{D_{10}}$
Cocoa ($D_{50}= 10.8 \mu\text{m}$) + Cocoa ($D_{50}= 2.8 \mu\text{m}$) (1)	3.86	10	32.4	8.4
Cocoa ($D_{50}= 10.8 \mu\text{m}$) + Cocoa ($D_{50}= 2.8 \mu\text{m}$) (2)	3.41	9.23	31.9	9.4
Cocoa ($D_{50}= 10.8 \mu\text{m}$) + Cocoa ($D_{50}= 2.8 \mu\text{m}$) (3)	2.95	8.44	31.4	10.6
Cocoa ($D_{50}= 10.8 \mu\text{m}$) + Cocoa ($D_{50}= 2.8 \mu\text{m}$) (4)	2.49	7.66	30.9	12.4
Cocoa ($D_{50}= 10.8 \mu\text{m}$) + Cocoa ($D_{50}= 2.8 \mu\text{m}$) (5)	2.03	6.87	30.4	14.9
Cocoa ($D_{50}= 10.8 \mu\text{m}$) + Cocoa ($D_{50}= 2.8 \mu\text{m}$) (6)	1.57	6.09	29.9	19.1
Cocoa ($D_{50}= 10.8 \mu\text{m}$) + Cocoa ($D_{50}= 2.8 \mu\text{m}$) (7)	1.12	5.30	29.4	26.3
Cocoa ($D_{50}= 10.8 \mu\text{m}$) + Cocoa ($D_{50}= 2.8 \mu\text{m}$) (8)	0.66	4.51	28.9	43.8
Cocoa ($D_{50}= 10.8 \mu\text{m}$) + Cocoa ($D_{50}= 2.8 \mu\text{m}$) (9)	0.20	3.73	28.4	142

Table 4-4. Characteristic diameters and polydispersity ratio of the cocoa suspensions formulated from (a) Cocoa ($D_{50}= 11.2 \mu\text{m}$) + Cocoa ($D_{50}= 3.4 \mu\text{m}$) and from (b) Cocoa ($D_{50}= 10.8 \mu\text{m}$) + Cocoa ($D_{50}= 2.8 \mu\text{m}$).

4.1.3.3 Maximum packing fraction

We plot in Figure 4-2 the measured maximum packing fraction as a function of the mass proportion of fine cocoa particles for both cocoa suspensions. We recall that the maximum packing fractions are measured following the centrifugation protocol developed in chapter 2. We observe that the more the suspension contains fine cocoa particles, the higher is the maximum packing fraction. We also observe that the increase of maximum packing fraction is more important for Cocoa ($D_{50}= 11.2 \mu\text{m}$) + Cocoa ($D_{50}= 3.4 \mu\text{m}$) suspensions than Cocoa ($D_{50}= 10.8 \mu\text{m}$) + Cocoa ($D_{50}= 2.8 \mu\text{m}$) suspensions. This suggests that the finer the cocoa particles, the more they improve the maximum packing fraction. We conclude from these observations that the presence of fine cocoa particles in a system leads to an increase of the maximum packing fraction.

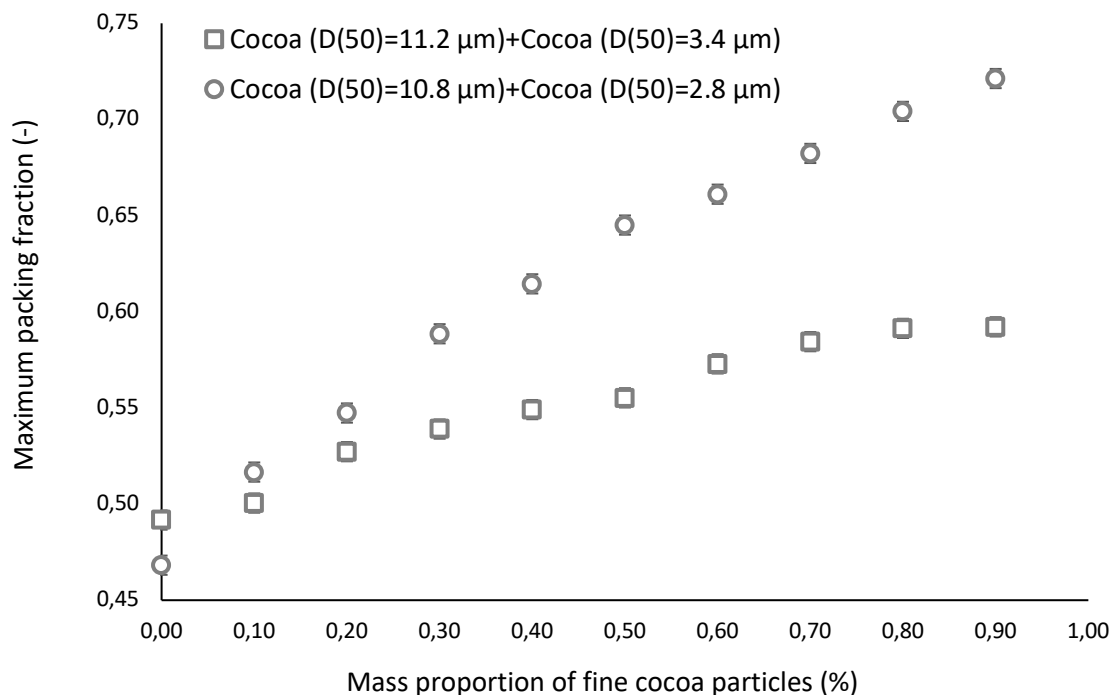


Figure 4-2. Measured maximum packing fractions of the cocoa suspensions formulated from Cocoa ($D_{50} = 11.2 \mu\text{m}$) + Cocoa ($D_{50} = 3.4 \mu\text{m}$) and from Cocoa ($D_{50} = 10.8 \mu\text{m}$) + Cocoa ($D_{50} = 2.8 \mu\text{m}$).

4.2 Influence of particle morphological properties on viscosity

4.2.1 Experimental results

4.2.1.1 Effect of the solid volume fraction of sugar suspensions (sweet fat) and sugar and cocoa suspensions (dark chocolate)

As previously mentioned in chapter 1, the rheological behaviour of a suspension is dependent on the solid volume fraction (ϕ). We thus study the influence of this parameter on the viscosity of sugar (sweet fat) suspensions and sugar and cocoa (dark chocolate) at solid volume fraction $\phi = 0.53$, $\phi = 0.48$, $\phi = 0.45$ and $\phi = 0.41$.

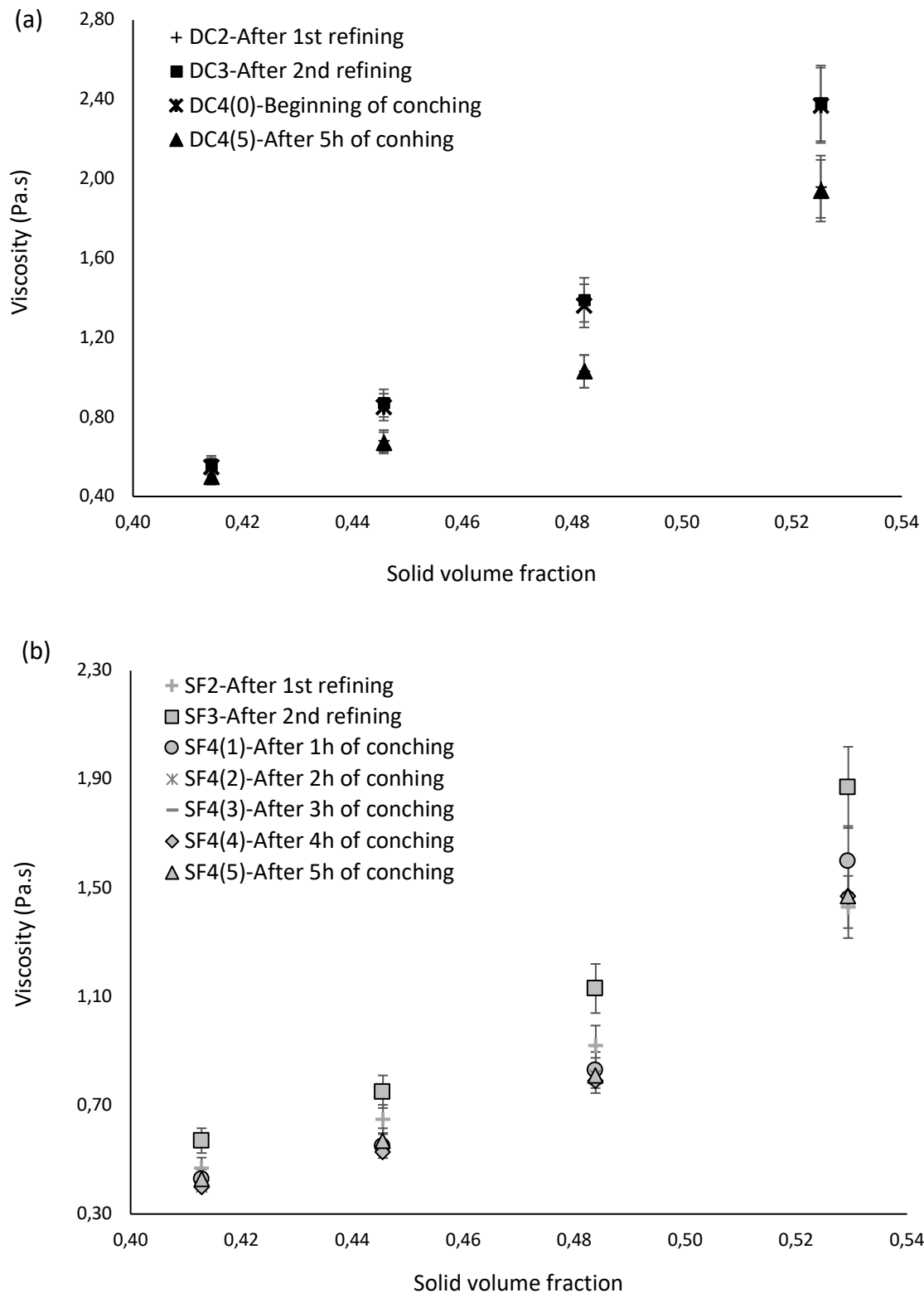


Figure 4-3. Evolution of viscosity at different solid volume fractions for (a) sugar and cocoa (dark chocolate) suspension samples and (b) sugar (sweet fat) suspension samples.

We plot in Figure 4-3 the measured viscosity as a function of the solid volume fraction for the flocculated samples (i.e., samples that do not contain lecithin) of sugar (sweet fat) and cocoa

and sugar (dark chocolate) suspensions. As expected, we observe that for both suspensions, the viscosity increases when the solid volume fraction increases. We also observe that the viscosity of these samples does not only depend on their solid volume fraction since they are not forming one only curve. The first observation is in good agreement with those obtained by [7, 8] while studying the effect of fat content on chocolate. Moreover, this dependence of the solid volume fraction on viscosity has also been shown for other food products [9-11]. The second observation is also in good agreement with literature [1] since as mentioned in chapter 1, the viscosity of a suspension does not only depend on the solid volume fraction but depends on the solid volume fraction to maximum packing fraction ratio.

4.2.1.2 Effect of the substitution of coarse cocoa particles by fine cocoa particles

We plot in Figure 4-4 the viscosity as a function of the mass proportion of fine cocoa particles. We observe that the viscosity decreases when the mass proportion of fine cocoa particles increases for both cocoa suspensions. We also observe that the decrease of viscosity is more important for Cocoa ($D_{50}= 10.8 \mu\text{m}$) + Cocoa ($D_{50}= 2.8 \mu\text{m}$) suspensions than Cocoa ($D_{50}= 11.2 \mu\text{m}$) + Cocoa ($D_{50}= 3.4 \mu\text{m}$) suspensions.

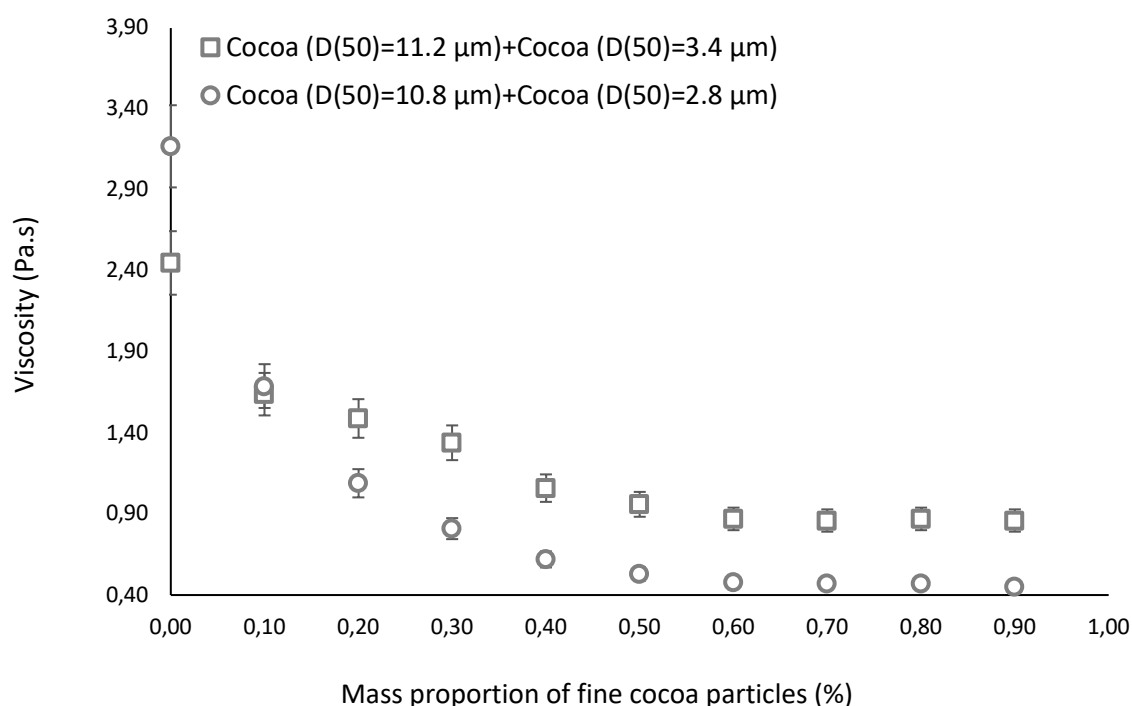


Figure 4-4. Measured viscosity of the cocoa suspensions formulated from Cocoa ($D_{50}= 11.2 \mu\text{m}$) + Cocoa ($D_{50}= 3.4 \mu\text{m}$) and from Cocoa ($D_{50}= 10.8 \mu\text{m}$) + Cocoa ($D_{50}= 2.8 \mu\text{m}$) as a function of mass proportion of fine cocoa particles. The solid volume fraction is constant and equals to 0.39.

4.2.1.3 Effect of the maximum packing fraction of sugar suspensions (sweet fat), cocoa suspensions and sugar and cocoa suspensions (dark chocolate)

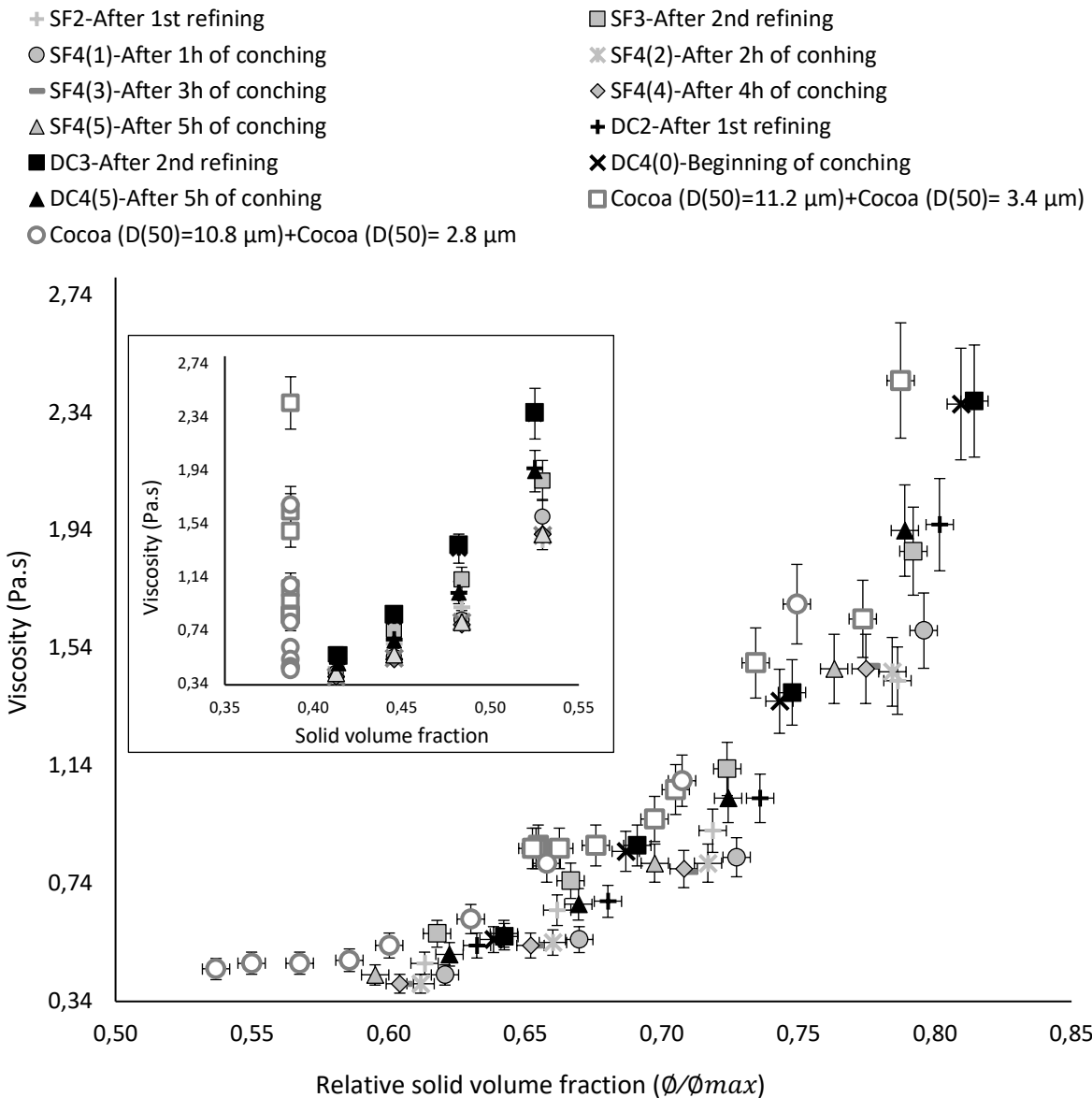


Figure 4-5. Viscosity as function of the relative solid volume fraction (ϕ/ϕ_{max}) for sugar and cocoa (dark chocolate) suspensions, sugar (sweet fat) suspensions and cocoa (Cocoa (D_{50} = 11.2 μm) + Cocoa (D_{50} = 3.4 μm) and Cocoa (D_{50} = 10.8 μm) + Cocoa (D_{50} = 2.8 μm)) suspensions. Insert: viscosity as a function of the solid volume fraction for sugar and cocoa (dark chocolate) suspensions, sugar (sweet fat) suspensions and cocoa (Cocoa (D_{50} = 11.2 μm) + Cocoa (D_{50} = 3.4 μm) and Cocoa (D_{50} = 10.8 μm) + Cocoa (D_{50} = 2.8 μm)) suspensions.

We plot in Figure 4-5 the measured viscosity as a function of the relative solid volume fraction (ϕ/ϕ_{max}) for sugar and cocoa (dark chocolate) suspensions, sugar (sweet fat) suspensions and cocoa suspensions. As expected and predicted by Krieger-Dougherty equation [1], we observe that the viscosity of all of these suspensions is following the same curve that we will refer to as “master” curve in the following. This confirms that the viscosity only depends on

the relative solid volume fraction (ϕ/ϕ_{max}). This correlation between viscosity and relative solid volume fraction can also explain the evolution of the viscosity of sugar and cocoa suspensions and sugar suspensions during the production process highlighted in the previous chapter.

4.2.1.4 Effect of emulsifier on sugar suspensions (sweet fat), cocoa suspensions and sugar and cocoa suspensions (dark chocolate)

We now study the influence of emulsifier on the dependency of the suspension's viscosity on the relative solid volume fraction (ϕ/ϕ_{max}). To that end, we add in Figure 4-5 the viscosity of the samples containing lecithin in sweet fat and dark chocolate (SF4(6) and DC4(6) respectively) as well as the viscosity of all dark chocolate and sweet fat samples that are deflocculated with PGPR. We recall that samples SF4(6) and DC4(6) contain 0.5% lecithin by total mass of suspension and that 1.5% PGPR by total mass of solid particles is necessary to deflocculate the samples. The curve obtained from all data is shown in Figure 4-6. We observe that in presence of emulsifier the sample's viscosity seems to follow the master curve. However, as known from literature [12], a decrease of the viscosity is also observed for these samples in presence emulsifier.

These results suggest that the industrial addition of lecithin does not affect the dependency of the viscosity on the relative solid volume fraction (ϕ/ϕ_{max}) implying that all industrial chocolate products should follow the master curve independently of the presence of emulsifier or not.

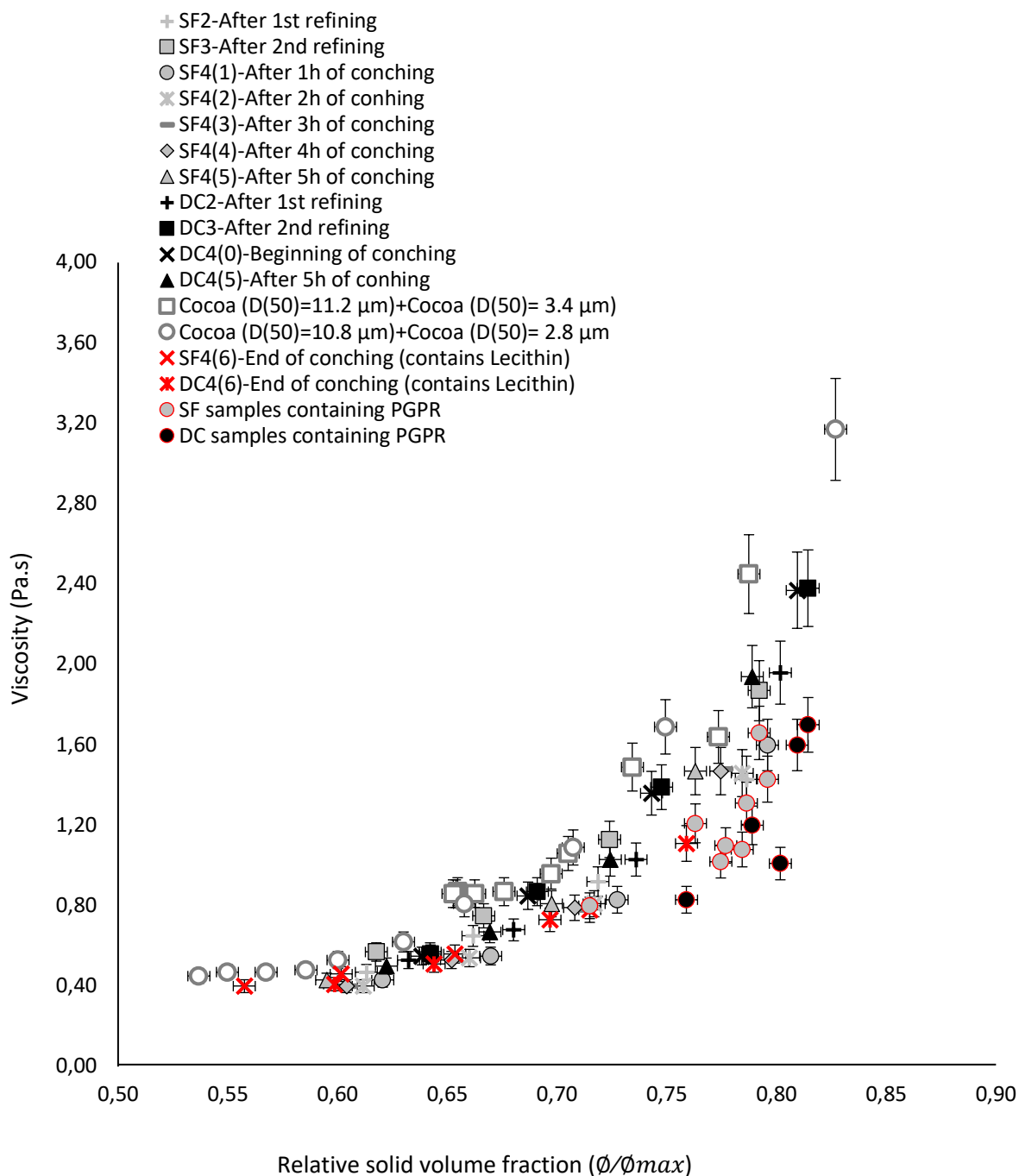


Figure 4-6. Viscosity as function of the relative solid volume fraction (ϕ/ϕ_{max}) for flocculated and deflocculated samples of sugar and cocoa (dark chocolate) suspensions, sugar (sweet fat) suspensions and cocoa (Cocoa ($D_{50}= 11.2 \mu\text{m}$) + Cocoa ($D_{50}= 3.4 \mu\text{m}$) and Cocoa ($D_{50}= 10.8 \mu\text{m}$) + Cocoa ($D_{50}= 2.8 \mu\text{m}$)) suspensions.

4.2.2 Outcome of the influence of the morphological properties on viscosity

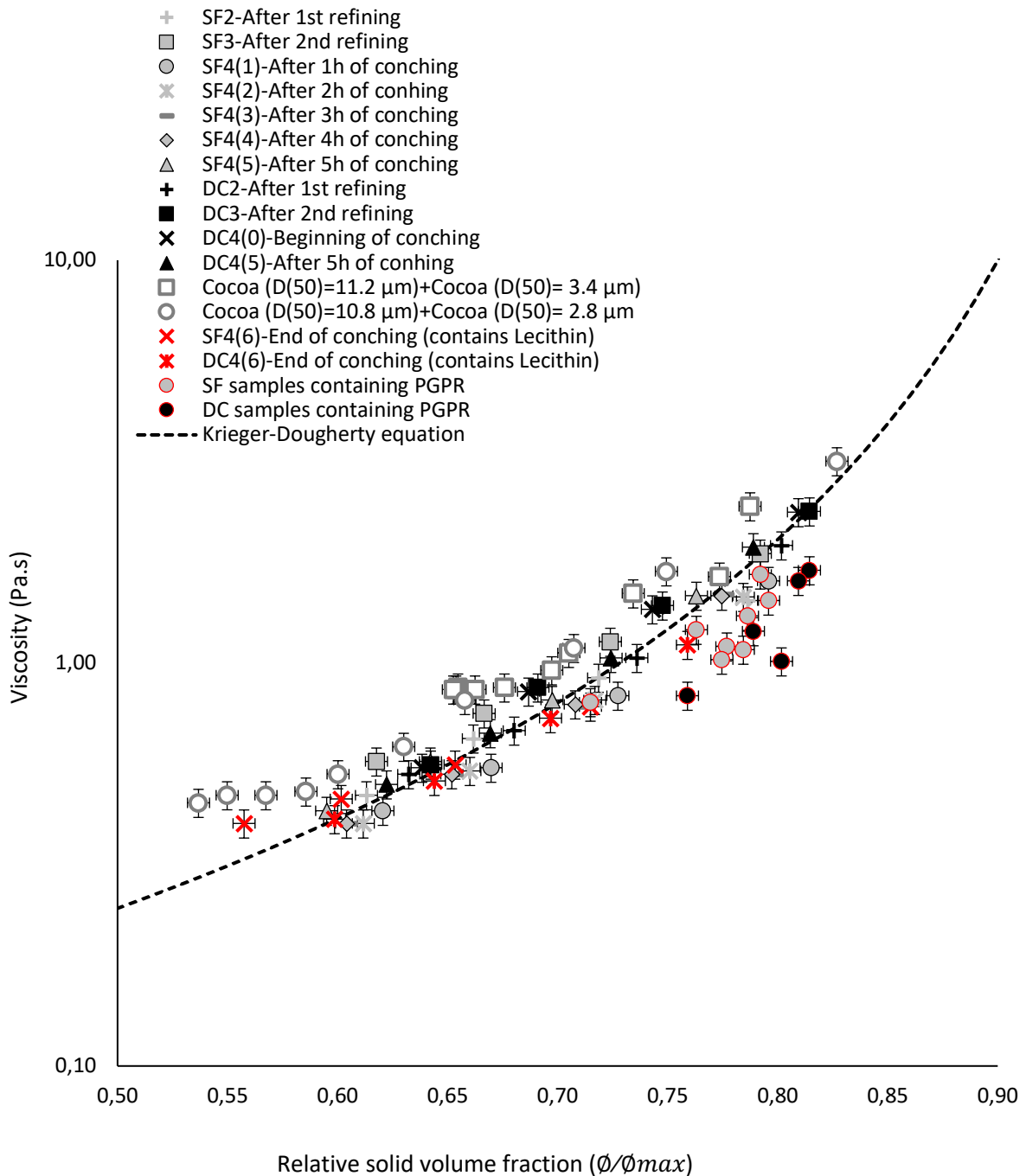


Figure 4-7. Viscosity as function of the relative solid volume fraction on maximum packing fraction (ϕ/ϕ_{max}) for flocculated and deflocculated samples of sugar and cocoa (dark chocolate) suspensions, sugar (sweet fat) suspensions and cocoa (Cocoa ($D_{50}= 11.2 \mu\text{m}$) + Cocoa ($D_{50}= 3.4 \mu\text{m}$) and Cocoa ($D_{50}= 10.8 \mu\text{m}$) + Cocoa ($D_{50}= 2.8 \mu\text{m}$)) suspensions. Krieger-Dougherty equation: $\mu = \mu_0 (1 - \phi/\phi_{max})^{-2.3}$. $\mu_0 = 0.05 \text{ Pa.s}$ is the viscosity of the cocoa butter.

We plot in Figure 4-7 the master curve fitted by Krieger-Dougherty equation. We find that the fit is perfectly matching the master curve when the exponent q (that we recall is a constant depending on the particle shape) is equal to 2.3. This value of q found is in good agreement with literature [13] where it was shown that for concentrated suspensions composed of non-elongated particles, the value of q is around 2. Moreover, these results are also in good agreement with those of Fang et al. [14] who showed that the viscosity of cocoa suspension composed of cocoa powder suspended in cocoa butter follows a generalized Quemada model [2] (i.e., a derived model from Krieger-Dougherty equation in which the exponent q is equal to 2) and Rao et al. [15] who found that the viscosity of starch granules are also well described by Quemada model.

We finally conclude from all viscosity results that the viscosity of chocolate suspensions (i.e., cocoa, sugar and cocoa and sugar suspensions) can be controlled via the relative solid volume fraction. It can also be predicted by Krieger-Dougherty equation. The results also suggest that the viscous hydrodynamic dissipations occurring between the particles in sugar and cocoa suspensions, sugar suspensions and cocoa suspensions govern the viscous dissipation. However, we know from literature [16] that when the solid volume fraction approaches a critical value, the direct contacts between the particles increase. We thus suggest that the fact that we find an exponent a little bit above 2 could be explained by the increase of the contribution of direct contacts on viscous hydrodynamic dissipations.

4.3 Influence of the morphological properties on yield stress

4.3.1 Effect of the solid volume fraction of sugar suspensions (sweet fat) and sugar and cocoa suspensions (dark chocolate)

We plot in Figure 4-8 the evolution of the yield stress as a function of the solid volume fraction of sugar and cocoa (dark chocolate) suspensions and sugar (sweet fat) suspensions. We observe that the yield stress of these samples evolves like their viscosity i.e., it increases when the solid volume fraction increases and is not only dependent on the solid volume fraction.

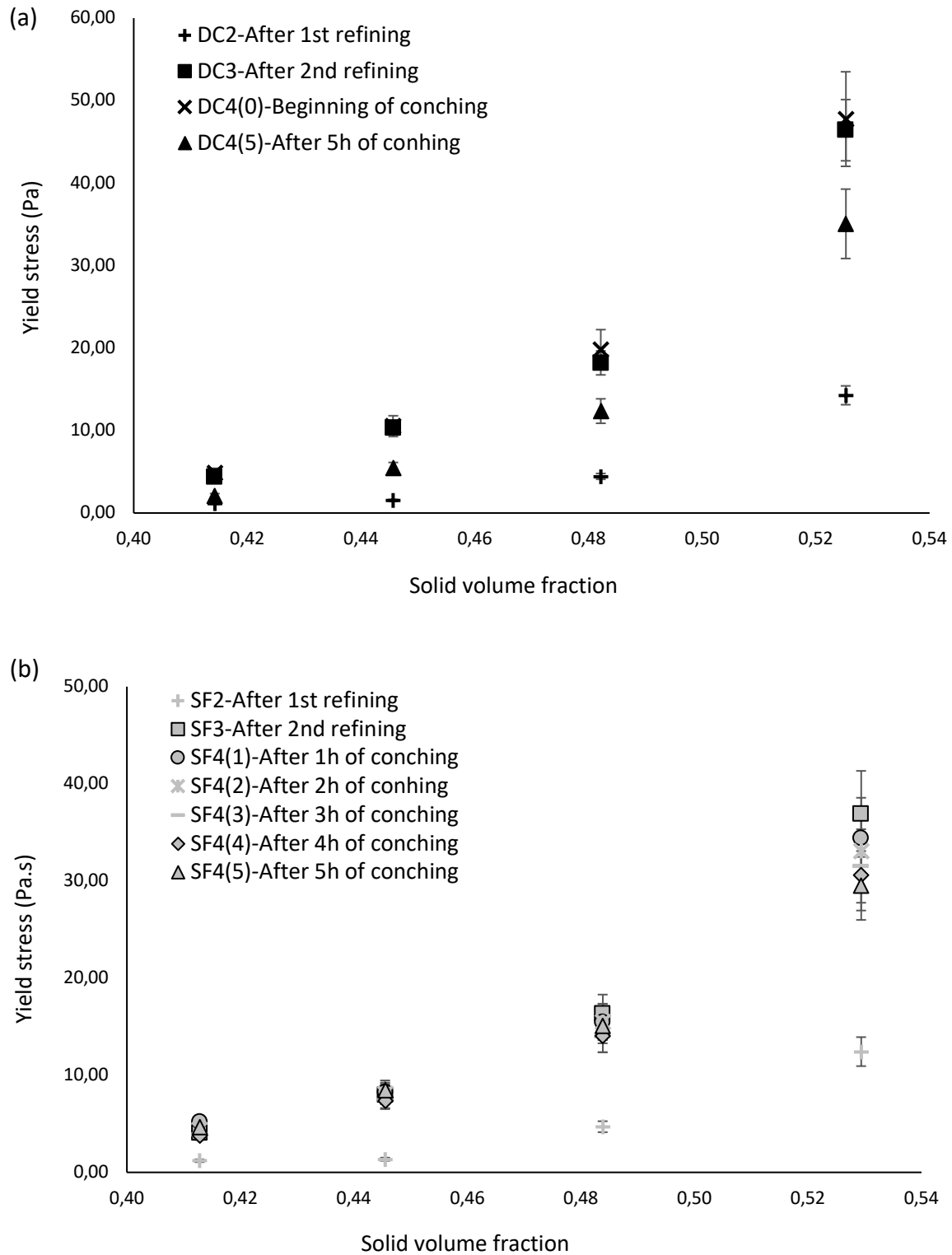


Figure 4-8. Evolution of the yield stress at different solid volume fractions for (a) sugar and cocoa (dark chocolate) suspensions and (b) sugar (sweet fat) suspensions.

4.3.2 Effect of the substitution of coarse cocoa particles by fine cocoa particles

We plot in Figure 4-9 the yield stress as a function of the mass proportion of fine cocoa particles. We observe that the yield stress decreases when the mass proportion of fine cocoa particles increases from 0% to 30% and then increases when the mass proportion increases from 40% to 100%. We recall that the maximum packing fraction increases when the mass proportion of fine cocoa particles increases (see Figure 4-2). According to literature [17], at a constant solid volume fraction, yield stress decreases when the maximum packing fraction increases. Therefore, the increase of yield stress observed above 30% of substitution could be owed to the decrease of suspension mean size. We will verify this suggestion on the next sections.

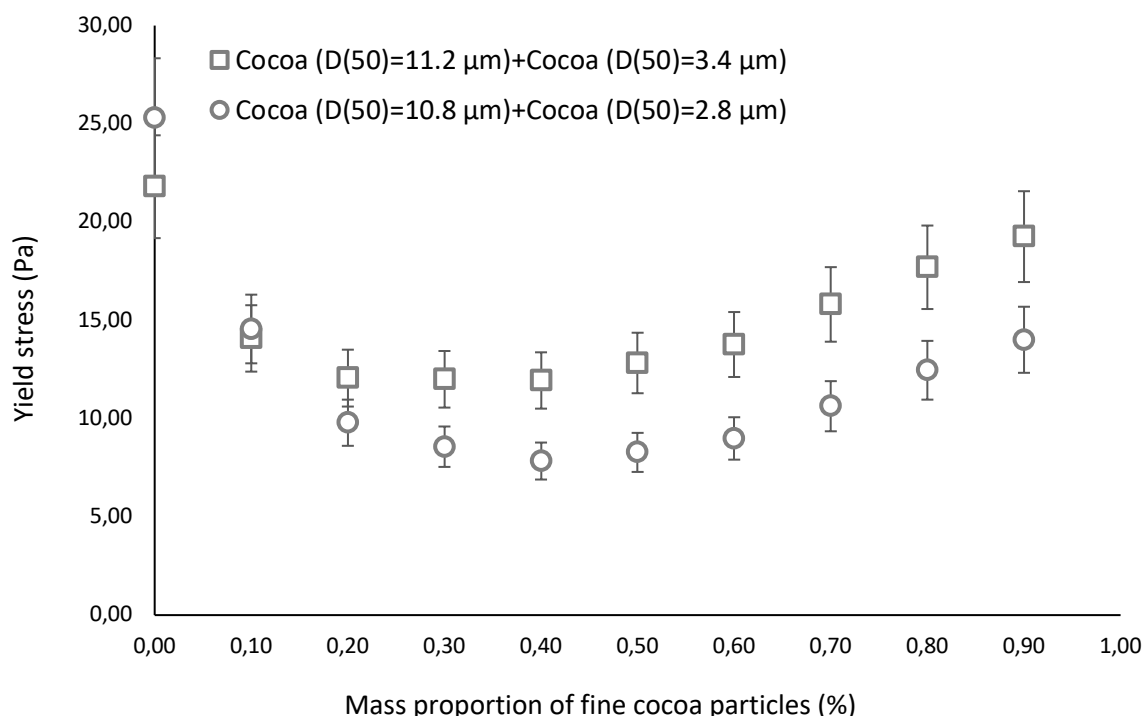
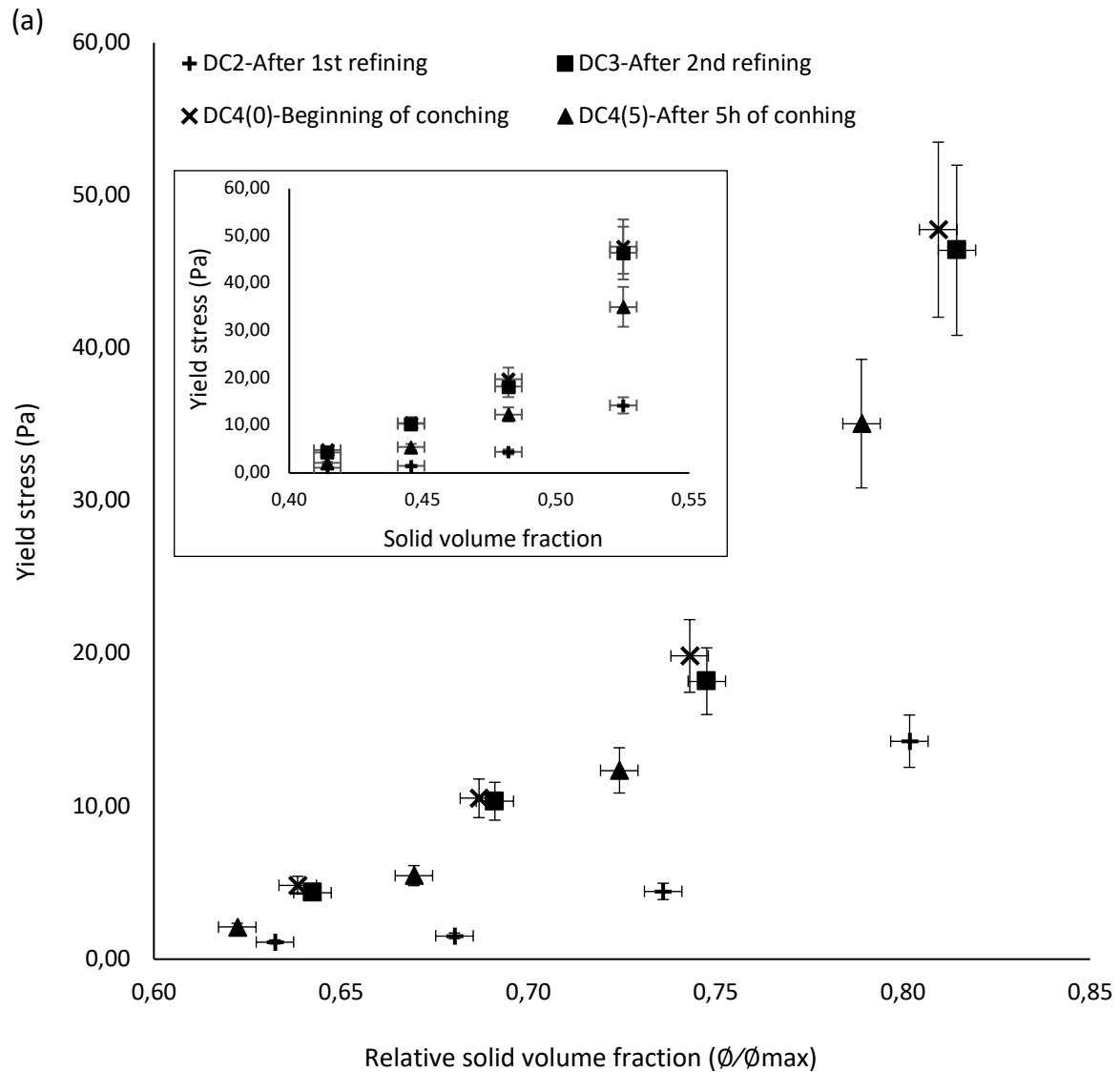


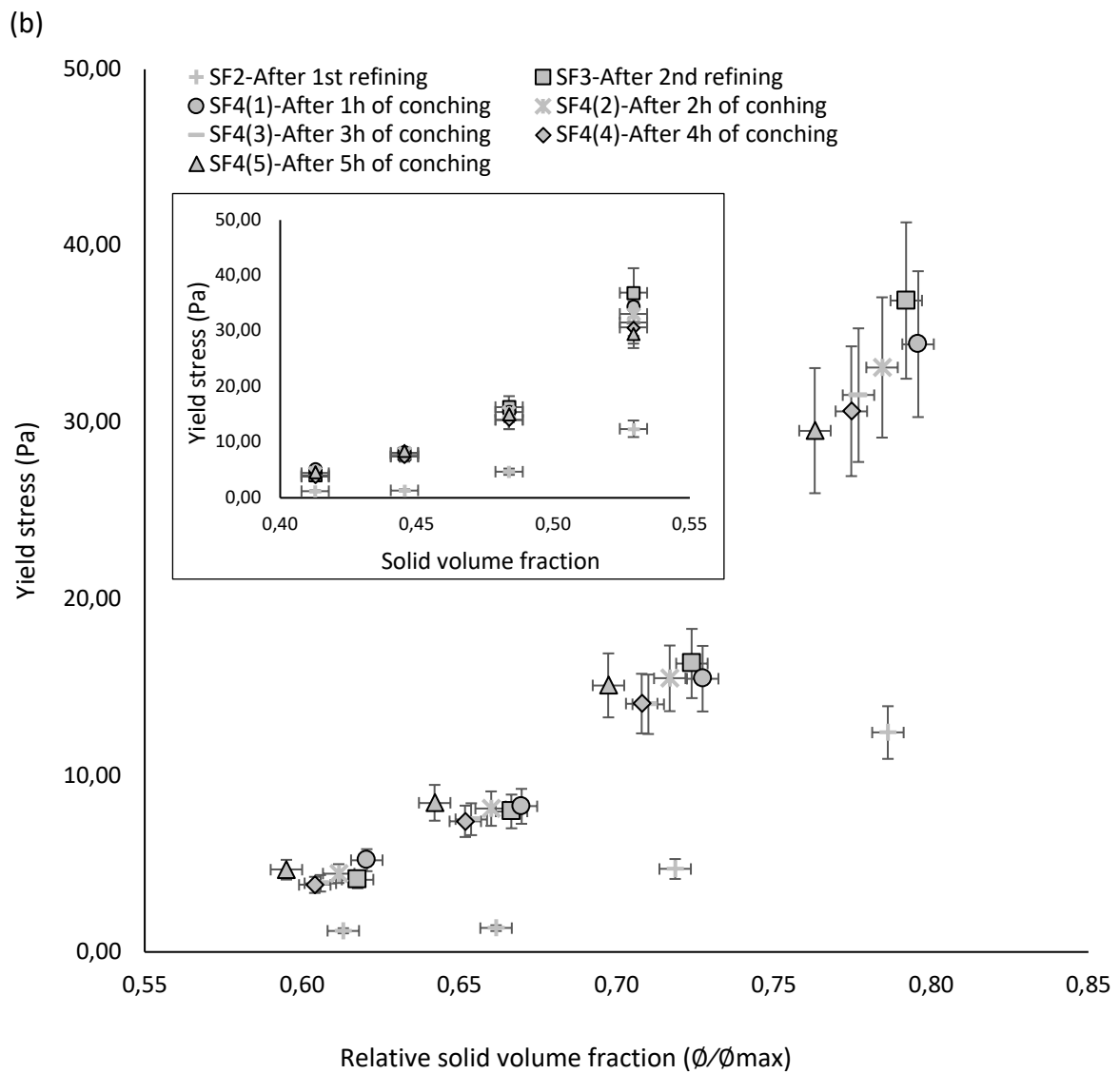
Figure 4-9. Measured viscosity of the cocoa suspensions formulated from Cocoa ($D_{50} = 11.2 \mu\text{m}$) + Cocoa ($D_{50} = 3.4 \mu\text{m}$) and from Cocoa ($D_{50} = 10.8 \mu\text{m}$) + Cocoa ($D_{50} = 2.8 \mu\text{m}$). The solid volume fraction is constant and equals to 0.39.

4.3.3 Effect of the maximum packing fraction of the sugar suspensions (sweet fat), cocoa and sugar suspensions (dark chocolate) and cocoa suspensions

We plot in Figure 4-10 the yield stress as a function of the relative solid volume fraction (Φ/Φ_{max}) for sugar and cocoa (dark chocolate) suspensions, sugar (sweet fat) suspensions, and cocoa suspensions. We observe that contrary to the viscosity, all yield stress values are

not following a master curve. Indeed, for dark chocolate and sweet fat samples, we observe that all data seem to form a master curve except those of SF2 and DC2 samples, which have particles of size much larger than the other samples (see chapter 3). This suggests that additionally to the relative solid volume fraction (ϕ/ϕ_{max}), the yield stress of the samples is also depending on their particle size. The same conclusion can be done for cocoa suspensions.





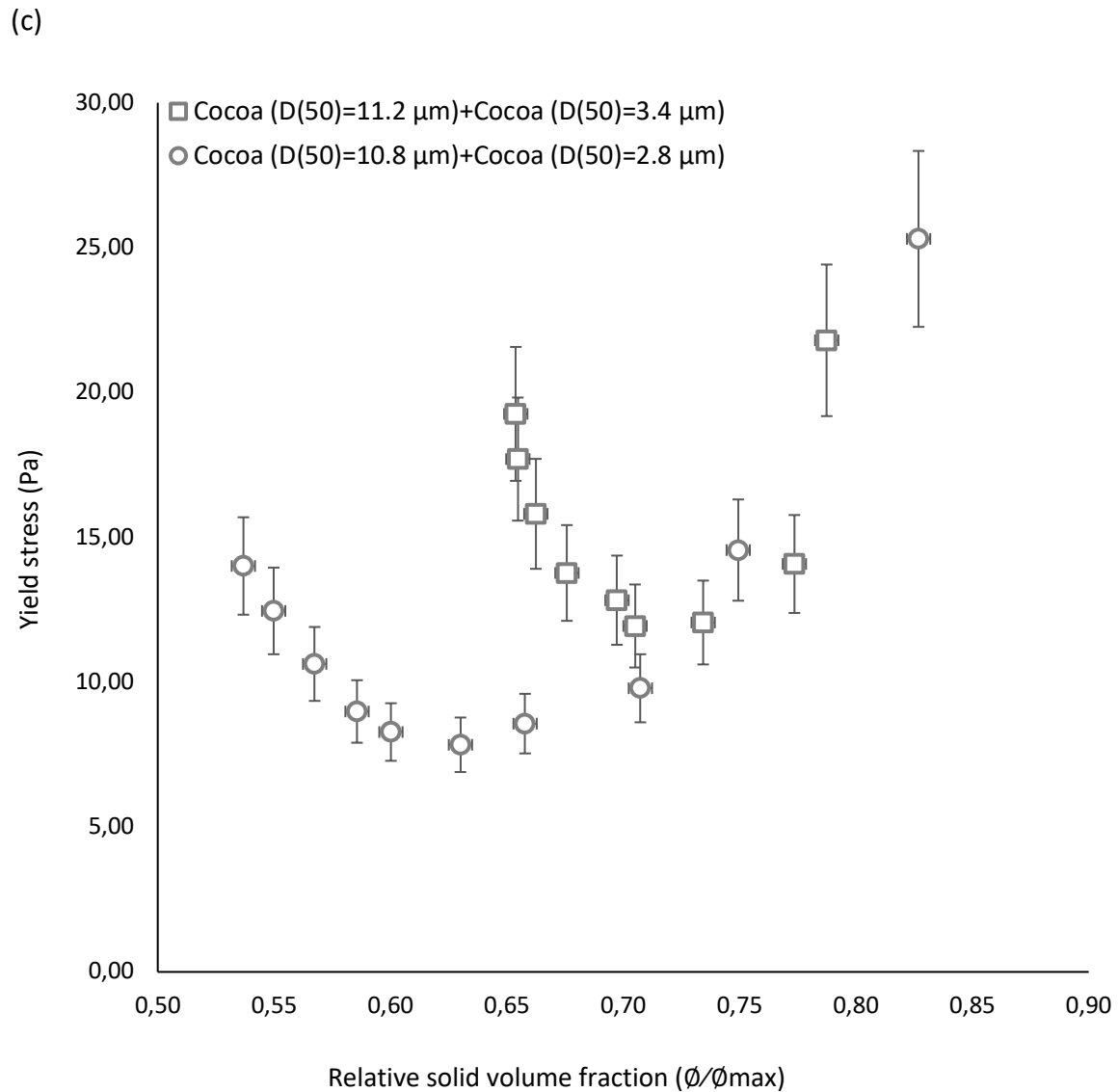
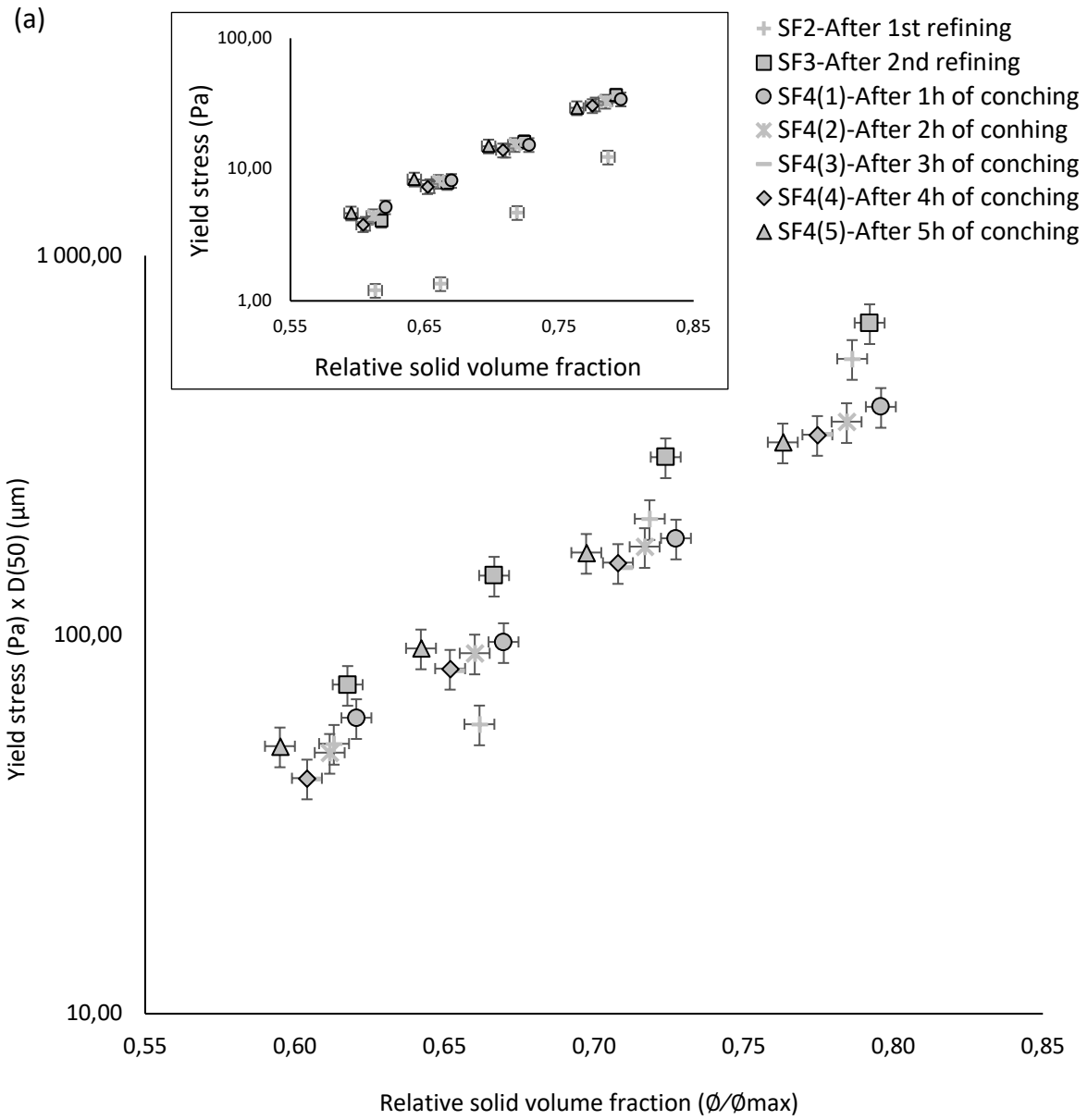
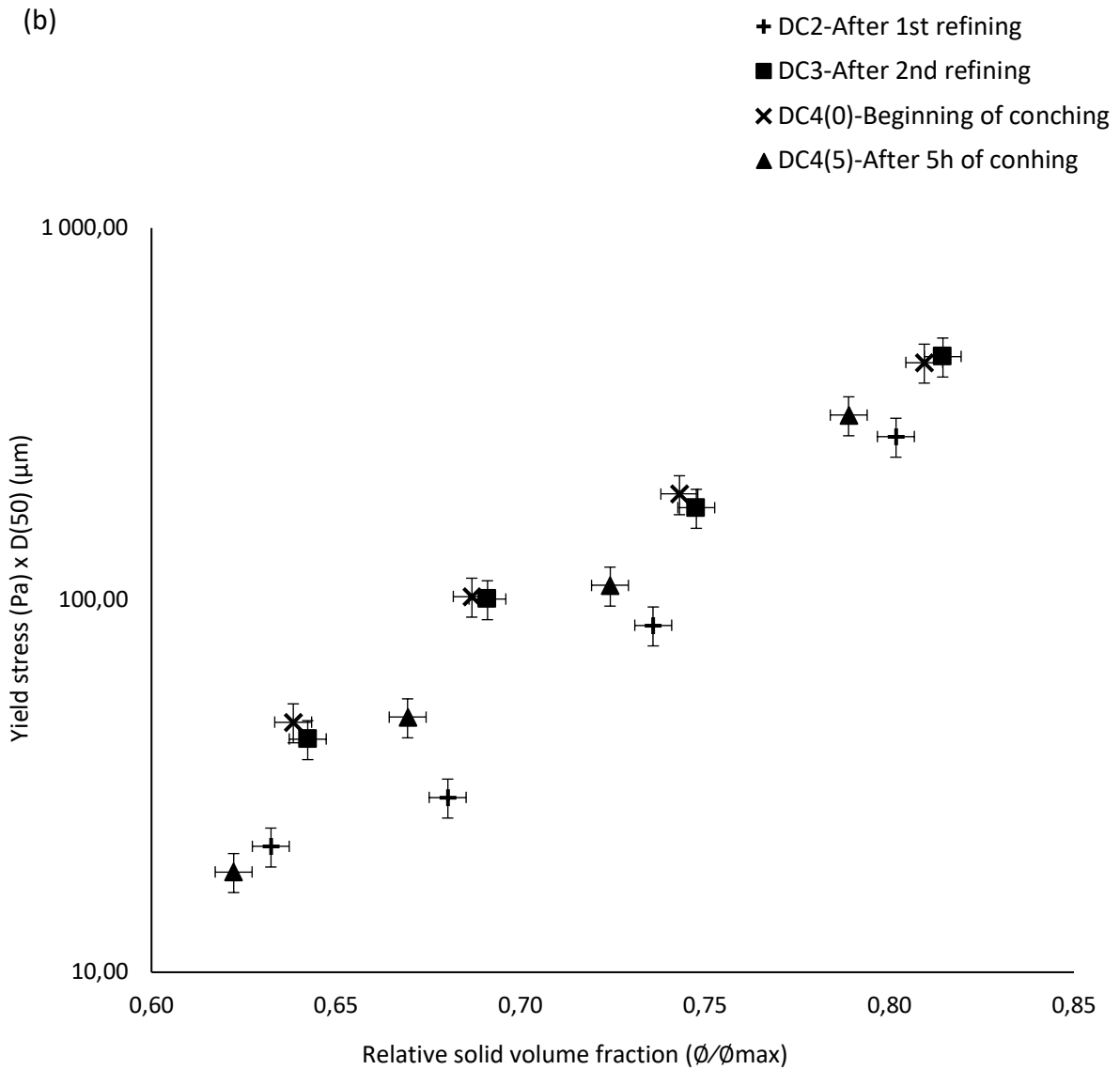


Figure 4-10. Yield stress as a function of the relative solid volume fraction for (a) sugar and cocoa (dark chocolate) suspensions, (b) sugar (sweet fat) suspensions and (c) cocoa ($D_{50}=11.2 \mu\text{m}$) + Cocoa ($D_{50}=3.4 \mu\text{m}$) and from Cocoa ($D_{50}=10.8 \mu\text{m}$) + Cocoa ($D_{50}=2.8 \mu\text{m}$) suspensions.

4.3.4 Effect on yield stress of the particle size distribution of the sugar suspensions (sweet fat), cocoa and sugar suspensions (dark chocolate) and cocoa suspensions

We plot in Figure 4-11 the yield stress multiplied by the mean diameter of the corresponding suspension as a function of the relative solid volume fraction (ϕ/ϕ_{max}). We note that all data follow a master curve and suggest that the yield stress is inversely proportional to the mean diameter of the suspension. The dependency of the yield stress on the particle size highlighted herein is in good agreement with literature [18] as shown in chapter 1.





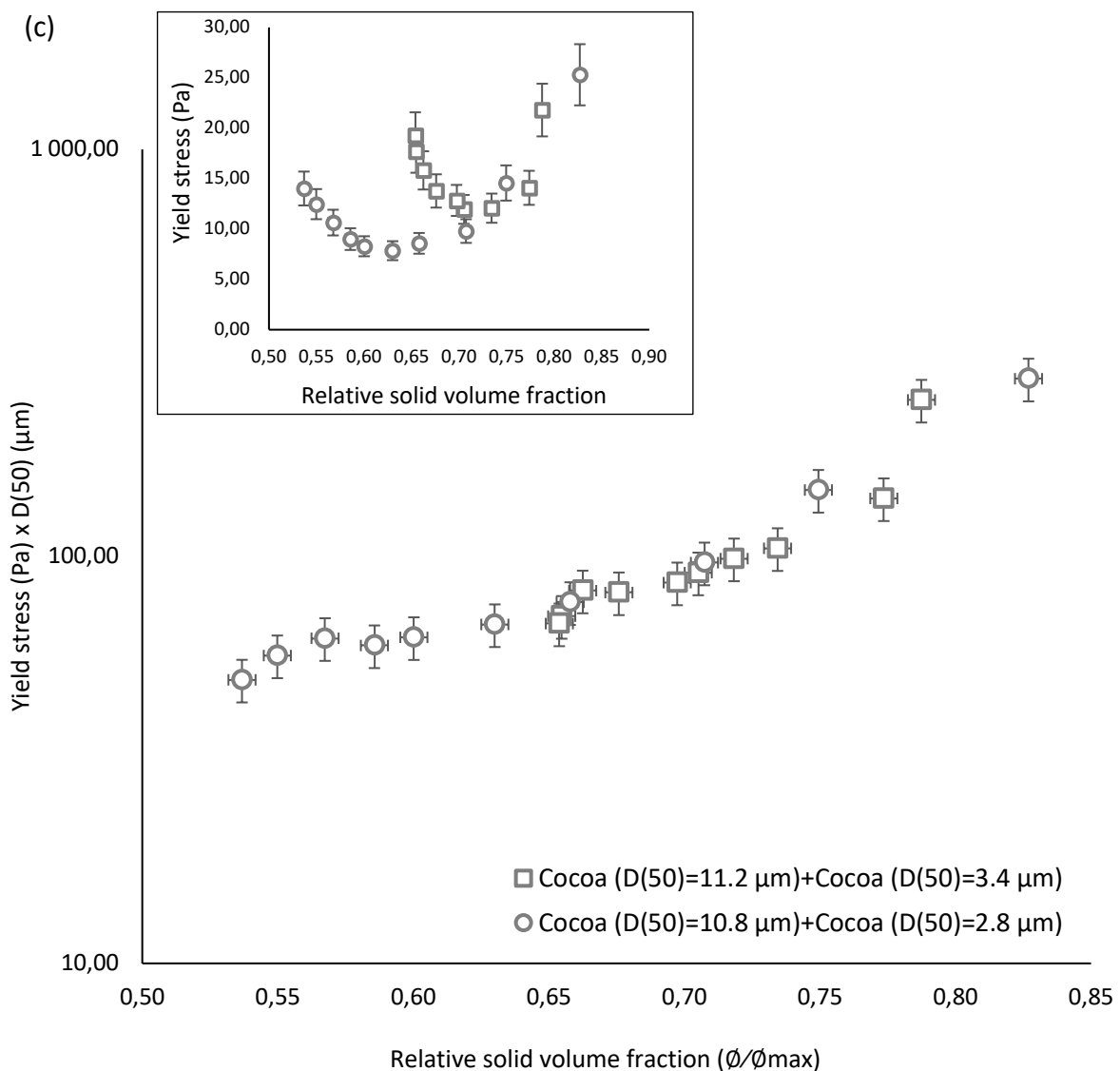


Figure 4-11. Yield stress as a function of the relative solid volume fraction (ϕ/ϕ_{max}) by taking into account the particle mean diameter (D_{50}) of (a) sugar (sweet fat) suspensions, (b) sugar and cocoa (dark chocolate) suspensions and (c) cocoa (Cocoa ($D_{50}= 11.2 \mu\text{m}$) + Cocoa ($D_{50}= 3.4 \mu\text{m}$) and Cocoa ($D_{50}= 10.8 \mu\text{m}$) + Cocoa ($D_{50}= 2.8 \mu\text{m}$)) suspensions. Insert: Yield stress as a function of the relative solid volume fraction (ϕ/ϕ_{max}) of (a) sugar (sweet fat) suspensions, (b) sugar and cocoa (dark chocolate) suspensions and (c) cocoa (Cocoa ($D_{50}= 11.2 \mu\text{m}$) + Cocoa ($D_{50}= 3.4 \mu\text{m}$) and Cocoa ($D_{50}= 10.8 \mu\text{m}$) + Cocoa ($D_{50}= 2.8 \mu\text{m}$)) suspensions.

4.4 Summary

Based on the results described above, we can summarize the relation between the viscosity (μ), solid volume fraction (ϕ) and maximum packing fraction (ϕ_{max}) as follows:

$$\mu = \mu_0 \times f(\phi/\phi_{max}) \tag{4 - 1}$$

With μ_0 the viscosity of the interstitial fluid.

The relation between the yield stress (τ), the particle mean diameter (D_{50}), solid volume fraction (ϕ) and maximum packing fraction (ϕ_{max}) as follows:

$$\tau = 1/D_{50} \times f(\phi/\phi_{max}) \quad (4 - 2)$$

4.5 Conclusion

In this chapter, we have studied 3 suspensions containing sugar particles alone, cocoa particles alone and a mixture of cocoa and sugar particles. We have demonstrated that the rheological parameters of all these suspensions are well correlated to the morphological ones.

We have concluded from our results that the viscosity of chocolate suspension is mainly governed by viscous hydrodynamic dissipations. We have demonstrated that the viscosity depends only on the relative solid volume fraction and can be predicted by Krieger-Dougherty equation for sugar suspensions.

The yield stress of sugar suspensions, cocoa suspensions and sugar and cocoa suspensions depends on the solid volume fraction on maximum packing fraction ratio and is inversely proportional to their particle mean diameters.

We have showed that the evolution of viscosity during the production process described in chapter 3 could be explained by the evolution of maximum packing fraction. Moreover, we have showed that the evolution of yield stress during the production process described in chapter 3 could be explained by the evolution of maximum packing fraction and particle size

References:

- [1] Krieger, I.M.; Dougherty, T.J. A mechanism for non-Newtonian flow in suspensions of rigid spheres. *Transaction of the Society of Rheology*, 1959, 3, 137-152.
- [2] Quemada, D. Rheology of concentrated disperse systems and minimum energy dissipation principle. *Rheologica Acta*, 1977, 16, 82-94.
- [3] Mongia, G.; Ziegler, G.R. The role of particle size distribution of suspended solids in defining the flow properties of milk chocolate. *Int. J. Food Properties*, 2000, 3, 137-147.
- [4] Kaiser, J.M.; Purwo, S. U.S. Patent WO 99/45789, 2002.
- [5] Aguilar, C.A.; Rizvi, S.S.H.; Ramirez, J.F.; Inda, A. Rheological behavior of processed mustard. I: effect of milling treatment. *J. Texture Stud.* 1991, 22, 59-84.
- [6] Villagran, F.V.; McCabe, G.M.; Wong, V.Y.L. U.S. Patent 5490999, 1996.
- [7] Beckett, S.T. *The Science of Chocolate: Controlling the flow properties of liquid chocolate*; 2nd ed.; Royal Society of Chemistry: Cambridge, 2008, pp. 80-102.
- [8] De Graef, V.; Depypere, F.; Minnaert, M.; Dewettinck, K. Chocolate yield stress as measured by oscillatory rheology. *Food Research International*, 2011, 44, 2660-2665.
- [9] Ye, A., Hemar, Y., & Singh, H. Enhancement of coalescence by xanthan addition to oil-in-water emulsions formed with extensively hydrolysed whey proteins. *Food Hydrocolloids*, 2004, 18, 737-746.
- [10] Ercelebi, E. A., & Ibanoglu, E. Rheological properties of whey protein isolate stabilized emulsions with pectin and guar gum. *European Food Research and Technology*, 2009, 229, 281-286.
- [11] Soleimanpour, M.; Koocheki, A.; Kadkhodaei, R. Influence of main emulsion components on the physical properties of corn oil in water emulsion: effect of oil volume fraction, whey protein concentrates and *Lepidium perfoliatum* seed gum. *Food Research International*, 2013, 50, 457-466.
- [12] Arnold, G.; Schuldt, S.; Schneider, Y.; Friedrichs, J.; Babick, F.; Werner, C.; Rohm, H. *Colloids and Surfaces A: Physicochem. Eng. Aspects*, 2013, 418, 147-156.
- [13]
- [14] FANG, T.N.; TIU, C.; WU, X.; DONG, S. J. *Texture Studies* 1995, 26, 203-215.
- [15] Rao, M.A.; Tattiyakul, J. Granule size and rheological behavior of heated tapioca starch dispersions. *Carbohydrate Polymers* 1999, 38, 123-132.
- [16] Roussel, N.; Lemaitre, A.; Flatt, R.J.; Coussot, P. *Cement and Concrete Research* 2010, 40, 77-84.
- [17] Do, T-A.L.; Hargreaves, J.M.; Wolf, B.; Hort, J.; Mitchell, J.R. *Journal of Food Science* 2007, 72, 541-552.
- [18] Beckett, S.T. *The Science of Chocolate: Controlling the flow properties of liquid chocolate*; 2nd ed.; Royal Society of Chemistry: Cambridge, 2008, 80-102.

**Chapter 5: Compressible Packing Model:
optimization of cocoa and sugar particle
size distribution**

Table of contents

5.1	Compressible Packing Model.....	154
5.1.1	From virtual packing fraction.....	152
5.1.2	...to real packing fraction	159
5.2	Is CPM able to predict the maximum packing fraction of cocoa and sugar mixtures?.....	160
5.2.1	Methodology	160
5.2.2	Results and discussion	162
5.2.2.1	Experimental and predicted real maximum packing fractions	162
5.2.2.1.1	Binary mixtures.....	162
5.2.2.1.2	Ternary mixtures.....	164
5.2.2.2	Correlation between the predicted and experimental maximum packing fraction.....	167
5.3	Conclusion.....	168
	References.....	169

In order to optimize particle size distribution, particle packing models have been developed. The Greek Apollonios de Pergas has been the first one to propose a way of defining the highest possible particle packing. His work has been cited latter by Guyon and Troadec [1]. The Apollonian packing model is based on the assumption that it is possible to fill the void in a packing of spheres by choosing a sphere having the greatest possible size so that it touches all the neighbouring particles. However, in practice, as we have a limited set of materials due to price, availability, or performance, it is not possible to choose particles one by one to fill the voids and attain the Apollonian packing. In 1928, Furnas [2] developed one of the first theories on filling voids after finding that the heaping of ore chunks in the containers resulted in large disparities in volume. Various models aiming at improving the Furnas model have been proposed in literature [3-7]. However, all of them are mainly based on the particle size distribution of the material and do not take into account the particle shape.

As explained in chapter 1, assuming that particles are spheres or neglecting their shape is misleading and leads to wrong predictions of the maximum packing fraction. In this thesis, we use the compressible packing model (CPM) developed by François de Larrard [8] and that takes into account both the particle size distribution and the shape of the particles to estimate the maximum packing fraction. CPM is a semi-empirical model developed to describe the packing density achieved by a granular mixture namely concrete. The main principle of the model is that all size classes in the mixture interact with all other sizes classes in the mixture affecting the overall packing density. The model also assumes that for the same material, the shape of a particle is independent on the size classes. The shape coefficient is computed by taking into account the particle size distribution and the maximum packing fraction of each material.

The objective of this chapter is to demonstrate that an analytical particle packing model intended to construction and building materials can also be used for food materials. The best way of demonstrating that is to validate the model by showing that the predicted (by CPM) and measured (by centrifugation) maximum packing fractions of different cocoa/sugar mixtures as a function of their composition are equal. The parameters controlling the maximum packing fraction are presented in the first part of this chapter. In the second part, the principles of CPM are described. In the third part, the methodology followed to validate the model is detailed. Finally, the measured and predicted results are compared.

5.1 Compressible Packing Model

Compressible Packing Model (CPM) is actually an improvement of an old model developed by de Larrard and Storrval in 1986 [9] called the Linear Packing Model (LPM). What makes CPM a better packing model than LPM is the fact that it takes into account a packing index K , which depends on the experimental protocol packing. This index corresponds to the energy used to pack experimentally a system and therefore it makes it possible to have a predictive packing density that is representative of the real one measured experimentally. CPM allows to predict two type of packing namely the real maximum packing fraction and the virtual maximum packing fraction. The real maximum packing fraction corresponds to the random close packing described in chapter 2 (i.e., the packing of particles under a given amount of compaction energy), which itself corresponds to the experimental maximum packing fraction called ϕ_{max} in this thesis. In the following, $\phi_{max\ predicted}$ will refer to the real maximum packing fraction predicted by CPM and ϕ_{max} to real maximum packing fraction measured experimentally. The virtual maximum packing fraction as defined by de Larrard represents the highest maximum packing fraction that can be attainable for a given mixture considering that there is a perfectly ordered packing (i.e., each particle is placed one by one near to each other). It corresponds to the ordered packing density described in chapter 2 and we will refer to it as $\phi_{virtual}$. In CPM, the real maximum packing fraction predicted ($\phi_{max\ predicted}$) is obtained from the virtual maximum packing fraction ($\phi_{virtual}$) thanks to the packing index K . Another important parameter that CPM takes into account are the particulate interactions generally occurring when two or more powders are mixed together. De Larrard [8] refer to these particulate interactions as geometrical interactions. They defined three possible geometrical interactions and concluded that the most common one is what is called the partial interaction. This interaction can be defined as the interaction occurring between two particles having different size diameters not so far from each other. In the following, we will only focus on binary and polydisperse mixture whose particles interact partially to describe how the virtual maximum packing fraction and the predicted real maximum packing fraction are calculated in CPM. More details about the two other particulate interactions (no interaction and total interaction) can be found in de Larrard book [8].

5.1.1 From virtual packing fraction...

The prediction of the virtual maximum packing fraction ($\phi_{virtual}$) for a given mixture depends on the particle size distribution by volume (i.e., each size class and its corresponding volume fraction) of each of its components, their experimental maximum packing fraction (ϕ_{max}), the experimental packing index K , and the geometrical interactions occurring between the particles.

Let's take the example of a binary mixture composed of component 1 (coarse particles) and component 2 (fine particles) to demonstrate how CPM works. Component 1 and 2 have

respectively d_1 and d_2 as particle diameters. CPM assumes that there is at least one dominant diameter in such mixture. Therefore, two different configurations can be distinguished. In the first configuration, the coarse particles diameter is dominant. When one fine particle is inserted into the coarse particles packing, and if the fine particle is not small enough to fill the space between the coarse particles, there is a loosening of the coarse particles packing which induces a de-structuring of the latter. This de-structuring phenomenon is usually referred as “loosening effect” (Figure 5-1(a)). In the second configuration where the fine particles dominate, when one coarse particle is inserted into the fine particles packing, an increase of the porosity in the vicinity of its surface is observed, leading to another kind of de-structuring phenomenon called “wall effect” (Figure 5-1(b)). Both effects depend on the geometrical interactions between particles of different size and are considered a linear function of the maximum packing fraction of the dominant component.

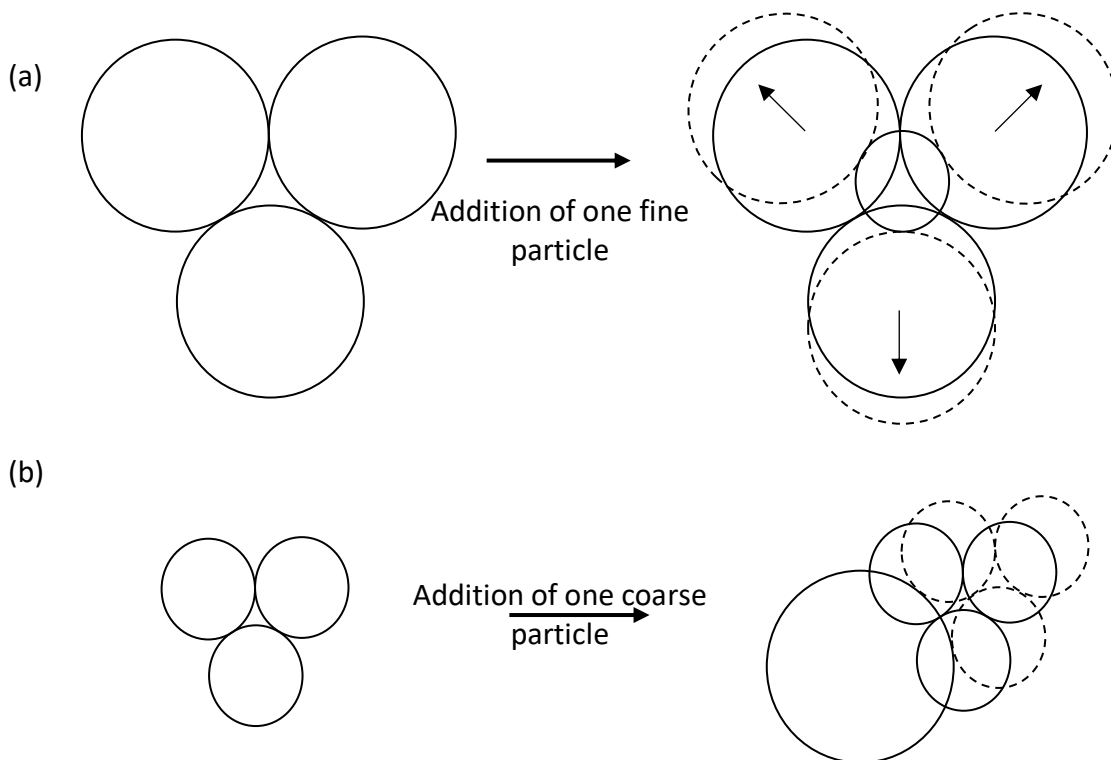


Figure 5-1. Representation of the (a) loosening and (b) wall effects taken into account in the compressible packing model (adapted from [10]).

In the following, we are detailing how de Larrard include the effects described above in the virtual maximum packing fraction calculation by studying the same binary system than previously (with $d_1 \geq d_2$) and in which partial interaction between particles arise. In de Larrard approach, the virtual maximum packing fraction of a binary mixture can be defined as:

$$\phi_{virtual} = \phi_1 + \phi_2$$

where ϕ_1 and ϕ_2 are the partial volumes (i.e., the volume occupied by each component taking into account the presence of the other component). In the following, y_1 and y_2 represent the volume fractions of component 1 and 2 respectively. β_1 and β_2 represent the residual packing fractions of each component taken separately.

By definition:

$$y_1 = \frac{\phi_1}{\phi_1 + \phi_2}$$

$$y_2 = \frac{\phi_2}{\phi_1 + \phi_2}$$

$$y_1 + y_2 = 1$$

When there is a partial interaction between particles, a loosening effect will happen when the coarse particles are dominant while a wall effect will be observed when the fine particles are dominant. Therefore, to calculate the virtual maximum packing fraction, the loosening and wall effects coefficients ($a_{1,2}$ and $b_{1,2}$ respectively) are taken into account.

The loosening effect leads to a decrease of the partial volume ϕ_1 due to the presence of fine particles. And as said previously, this effect is a linear function of the partial volume ϕ_2 because we supposed that the fine particles are sufficiently distant from each other. So, in this case, the virtual maximum packing fraction $\phi_{virtual}$ equals to:

$$\phi_{virtual(1)} = \phi_{virtual}$$

$$\phi_{virtual(1)} = \phi_1 + \phi_2$$

$$\phi_{virtual(1)} = \beta_1 (1 - a_{1,2}\phi_2) + \phi_2$$

$$\phi_{virtual(1)} = \beta_1 + (\phi_1 + \phi_2)(1 - a_{1,2}\beta_1) + y_2$$

$$\phi_{virtual} = \phi_{virtual(1)} = \frac{\beta_1}{1 - y_2(1 - a_{1,2}\beta_1/\beta_2)}$$

The wall effect leads to a reduction of the volume occupied by the fine particles. Here again, we will assume that the reduction is a linear function of the real maximum packing fraction ϕ_{max1} if the coarse particles are sufficiently distant from each other. We then write:

$$\phi_{virtual(2)} = \phi_{virtual}$$

$$\phi_{virtual(2)} = \phi_1 + \phi_2$$

$$\phi_{virtual(2)} = \phi_1 + \beta_2 \left(1 - \frac{\phi_1}{1 - \phi_1} b_{1,2}\right) (1 - \phi_1)$$

$$\phi_{virtual(2)} = \beta_2 + y_1 (\phi_1 + \phi_2) (1 - \beta_2 (1 + b_{1,2}))$$

$$\phi_{virtual(2)} = \frac{\beta_2}{1 - y_1 (1 - \beta_2 + b_{1,2} \beta_2 (1 - 1/\beta_1))}$$

whatever the dominant diameter, $\phi_{virtual(1)}$ and $\phi_{virtual(2)}$ may be calculated. Therefore, we can state that for any case:

$$\phi_{virtual} \leq \phi_{virtual(1)}$$

$$\phi_{virtual} \leq \phi_{virtual(2)}$$

Then:

$$\phi_1 \leq \beta_1$$

$$\phi_2 \leq \beta_2 (1 - \phi_2)$$

These last inequalities are called the impenetrability constraint relative to component 1 and 2 by de Larrard. Therefore, we can conclude from these previous statements, with no more concern about which component is dominant, that:

$$\phi_{virtual} = \inf(\phi_{virtual(1)}; \phi_{virtual(2)})$$

The boundary conditions for the coefficients $a_{1,2}$ and $b_{1,2}$ are:

$$a_{1,2} = b_{1,2} = 0 \text{ when } \frac{d_2}{d_1} \ll 1 \text{ (no interaction between the particles)}$$

$$a_{1,2} = b_{1,2} = 1 \text{ when } \frac{d_2}{d_1} = 1 \text{ (total interaction between the particles)}$$

The evolution of the virtual maximum packing fraction ($\phi_{virtual}$) considering the particulate interactions is represented in Figure 5-2. When there is no or partial interaction, the virtual maximum packing fraction increases until reaching an optimal value and then decreases. Nevertheless, we want to specify that there is not always an optimum when two or more classes are mixed together.

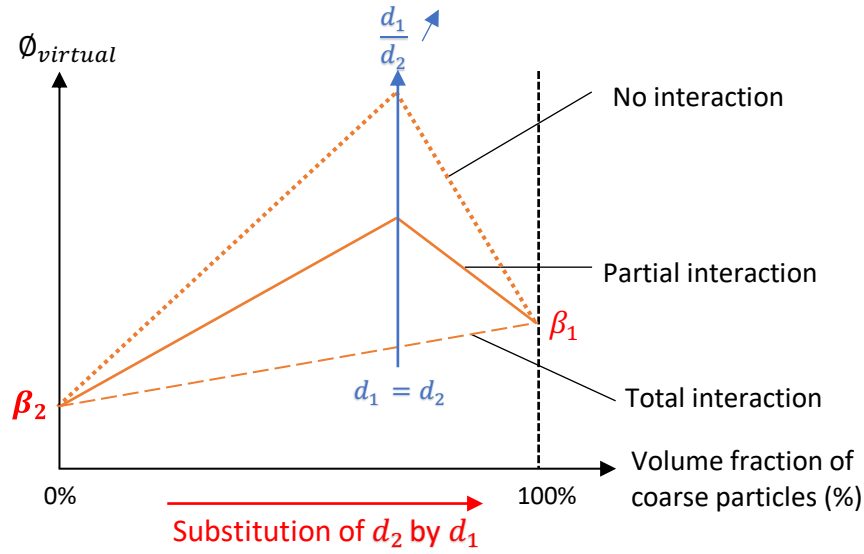


Figure 5-2. Evolution of the virtual maximum packing fraction of a binary mixture.

Let's now consider the general case of a ternary mixture in which $d_1 \geq d_2 \geq d_3$. Let's assume that 2 is the dominant component and that 1 exert a wall effect on those of 2 while 3 is exerting a loosening effect on 2. Therefore,

$$\phi_{virtual} = \phi_1 + \phi_2 + \phi_3$$

$$y_1 = \frac{\phi_1}{\phi_1 + \phi_2 + \phi_3}$$

$$y_2 = \frac{\phi_2}{\phi_1 + \phi_2 + \phi_3}$$

$$y_3 = \frac{\phi_3}{\phi_1 + \phi_2 + \phi_3}$$

$$y_1 + y_2 + y_3 = 1$$

If we follow the same approach as previously, we can conclude that:

$$\phi_2 = \beta_2 \left(1 - a_{2,3} \frac{\phi_3}{1 - \phi_1} - b_{2,1} \frac{\phi_1}{1 - \phi_1} \right) (1 - \phi_1)$$

Then,

$$\phi_{virtual} = \phi_{virtual(2)}$$

$$\phi_{virtual} = \frac{\beta_2}{1 - \left(1 - \beta_2 (1 + b_{2,1}) \right) y_1 - (1 - a_{2,3}) y_3}$$

$$\phi_{virtual} = \frac{\beta_2}{1 - \left(1 - \beta_2 + b_{2,1}\beta_2 (1 - 1/\beta_1)\right)y_1 - (1 - a_{2,3}\beta_2/\beta_3)y_3}$$

Thanks to the linearity of the equations describing loosening and wall effects, we can easily generalize the equation giving the virtual maximum packing fraction for a polydisperse mixture of n components of different sizes. When i is dominant in a polydisperse mixture, the most general equation for the virtual packing fraction is:

$$\phi_{virtual} = \frac{\beta_i}{1 - \sum_{j=1}^{i-1} (1 - \beta_i + b_{ij}\beta_i (1 - 1/\beta_j))y_j - \sum_{j=i+1}^n \left(1 - \frac{a_{ij}\beta_i}{\beta_j}\right)y_j}$$

With:

$$a_{ij} = \sqrt{1 - \left(1 - \frac{d_j}{d_i}\right)^{1.02}}$$

$$b_{ij} = \sqrt{1 - \left(1 - \frac{d_i}{d_j}\right)^{1.5}}$$

5.1.2 ...to real packing fraction

We are now considering the real packing fraction of a binary mixture. As already said, there is a packing index K which allows to deduce the real maximum packing fraction from the virtual maximum packing fraction. In de Larrard approach, the expression of the packing index K for a binary mixture is:

$$K = \frac{\frac{y_1}{\beta_1}}{\frac{1}{\phi_{max\ predicted}} - \frac{1}{\phi_{virtual(1)}}} + \frac{\frac{y_2}{\beta_2}}{\frac{1}{\phi_{max\ predicted}} - \frac{1}{\phi_{virtual(2)}}}$$

For a polydisperse mixture with a dominant component i , the expression of the packing index K becomes:

$$K = \sum_{i=1}^n K_i = \sum_{i=1}^n \frac{\frac{y_i}{\beta_i}}{\frac{1}{\phi_{max\ predicted}} - \frac{1}{\phi_{virtual(1)}}}$$

For monodisperse mixture:

$$K = \frac{1}{\frac{\beta}{\phi_{\max predicted}} - 1}$$

We summarize in Table 5-1 some K values determined by de Larrard [8].

Packing Techniques	Spill	Stitching with a rod	Vibration	Vibration + Compression (10 kPa)	« Boulettes » method	Virtual
<i>K</i>	4.1	4.5	4.75	9	6.7	∞

Table 5-1. Values of the packing index *K* for different packing methods [8].

5.2 Is CPM able to predict the maximum packing fraction of cocoa and sugar mixtures?

5.2.1 Methodology

Three cocoa masses (Cocoa ($D_{50} = 11.2 \mu\text{m}$), Cocoa ($D_{50} = 3.4 \mu\text{m}$), Cocoa ($D_{50} = 2.6 \mu\text{m}$)) fatted cocoa powder (Cocoa ($D_{50} = 9.2 \mu\text{m}$)), and sugar particles (Sugar ($D_{50} = 436 \mu\text{m}$) and Sugar ($D_{50} = 58.6 \mu\text{m}$)) are used to conduct the experiments required to validate the model. We recall that Cocoa ($D_{50} = 3.4 \mu\text{m}$) is obtained after 6 hours of Cocoa ($D_{50} = 11.2 \mu\text{m}$) grinding. Cocoa ($D_{50} = 2.6 \mu\text{m}$) is the product resulting of another cocoa mass grinding. We chose these materials because their granulometry is included in the particle size distributions range of the conventional chocolate products. Additionally, they are usually used as raw materials to produce dark chocolate, except the ground cocoa masses. We formulate 3 binary (Mixture 1, Mixture 2 and Mixture 3) and 2 ternary (Mixture 4 and Mixture 5) mixtures from these materials.

The methodology followed to validate the model can be divided into three steps:

- Step 1: Measure experimentally the particle size distribution and the real maximum packing fraction ϕ_{\max} of each material by following the protocols developed in chapter 2. The particle size distribution and experimental maximum packing fraction ϕ_{\max} measured as well as the experimental packing index *K* will be used as input data to estimate the virtual maximum packing fraction ϕ_{virtual} and the predicted real maximum packing fraction $\phi_{\max predicted}$ with the compressible packing model. The experimental real maximum packing fractions of the materials are summarized in Table 5-2 and their particle size distributions are represented in Figure 5-3.
- Step 2: Measure experimentally the real maximum packing fraction ϕ_{\max} of each binary and ternary mixtures.

- Step 3: Estimate the predicted real maximum packing fraction $\phi_{max\ predicted}$ of each mixture using the model and compared them to the experimental real maximum packing fraction ϕ_{max} . If the predicted and experimental real maximum packing fraction are well correlated, it suggests that CPM can be used as model to predict the maximum packing fraction of cocoa and sugar mixtures.

In order to be able to use CPM in a practical way, we program it using excel as software. The steps of the software programming will not be detailed here since it has been developed by following de Larrard approach which is clearly described in his book [8].

Experimental maximum packing fraction, ϕ_{max}	
Cocoa ($D_{50} = 11.2 \mu\text{m}$)	0.49 ± 0.005
Cocoa ($D_{50} = 3.4 \mu\text{m}$)	0.59 ± 0.01
Cocoa ($D_{50} = 2.6 \mu\text{m}$)	0.59 ± 0.01
Cocoa ($D_{50} = 9.2 \mu\text{m}$)	0.49 ± 0.005
Sugar ($D_{50} = 58.6 \mu\text{m}$)	0.63 ± 0.005
Sugar ($D_{50} = 436 \mu\text{m}$)	0.62 ± 0.005

Table 5-2. Experimental maximum packing fractions of the materials.

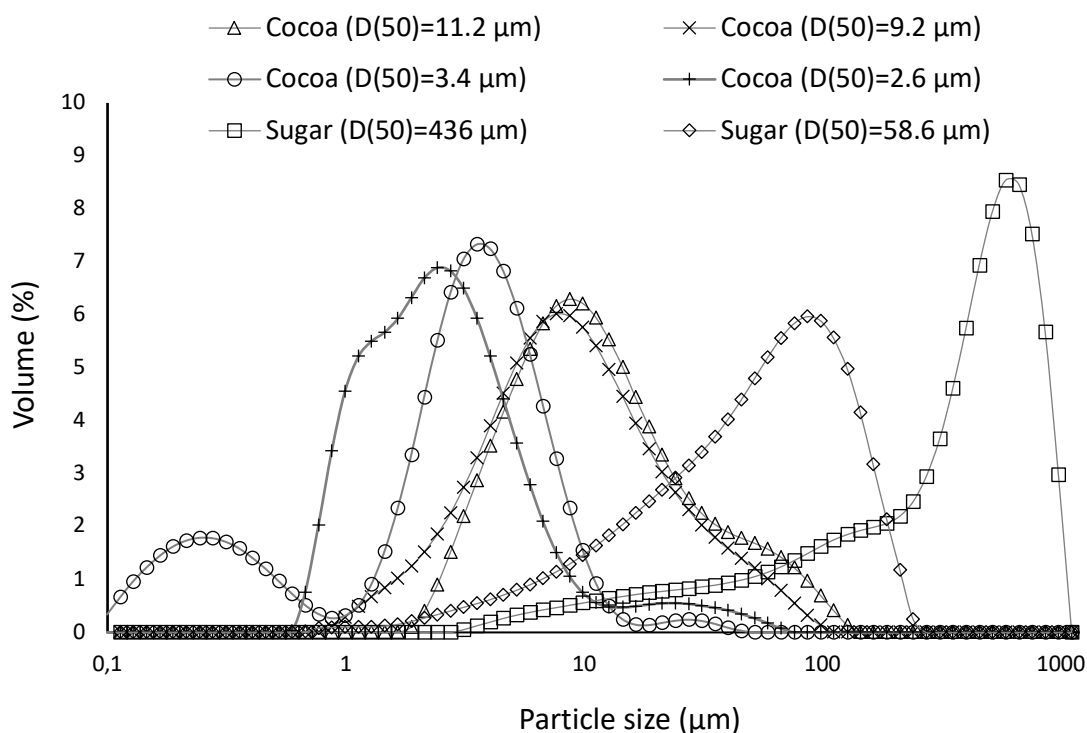


Figure 5-3. Particle size distribution of the materials used to formulate the binary and ternary mixtures.

5.2.2 Results and discussion

5.2.2.1 Experimental and predicted real maximum packing fractions

5.2.2.1.1 Binary mixtures

11 combinations are studied for each binary mixture. Their composition is summarized in Table 5-3. In these combinations, a proportion (ranging from 0 to 100% with a successive increment of 10%) of one component is substituted by the other component. The materials designate component 1 and 2 for each mixture are presented in Table 5-4.

	Volume fraction (% by total volume of solid particles)		Total volume fraction
	Component 1	Component 2	
Combination 1	0	1	1
Combination 2	0.1	0.9	1
Combination 3	0.2	0.8	1
Combination 4	0.3	0.7	1
Combination 5	0.4	0.6	1
Combination 6	0.5	0.5	1
Combination 7	0.6	0.4	1
Combination 8	0.7	0.3	1
Combination 9	0.8	0.2	1
Combination 10	0.9	0.1	1
Combination 11	1	0	1

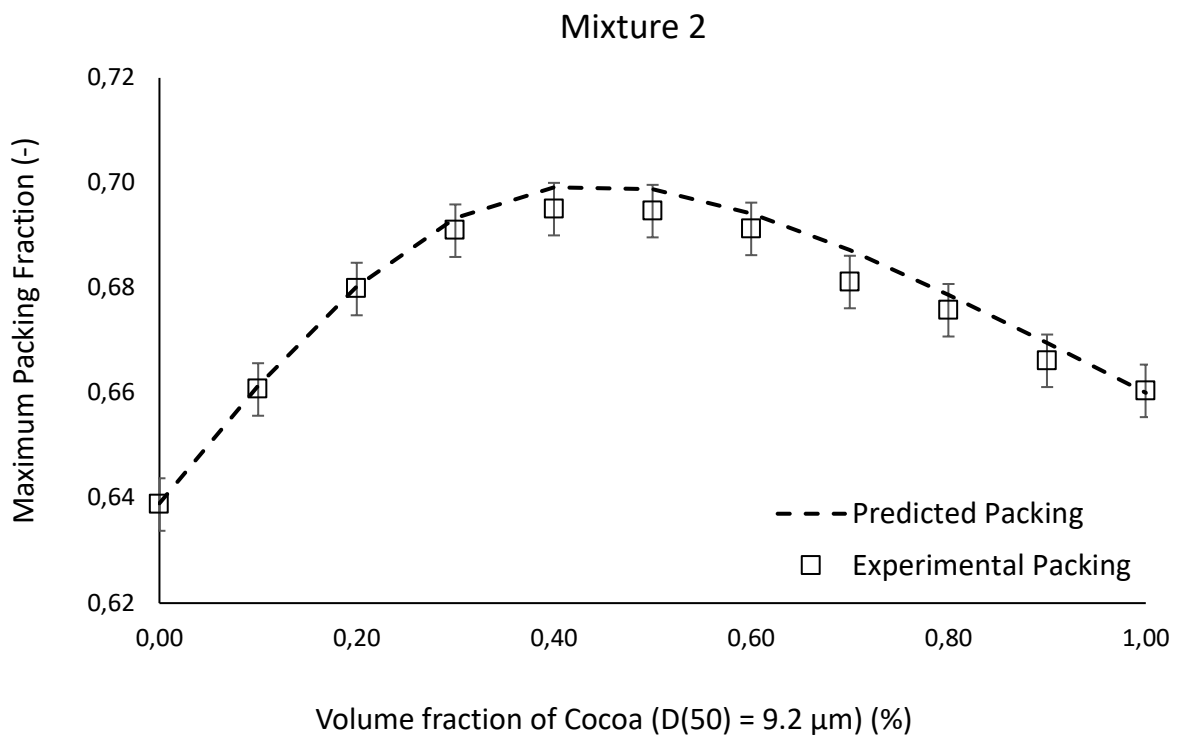
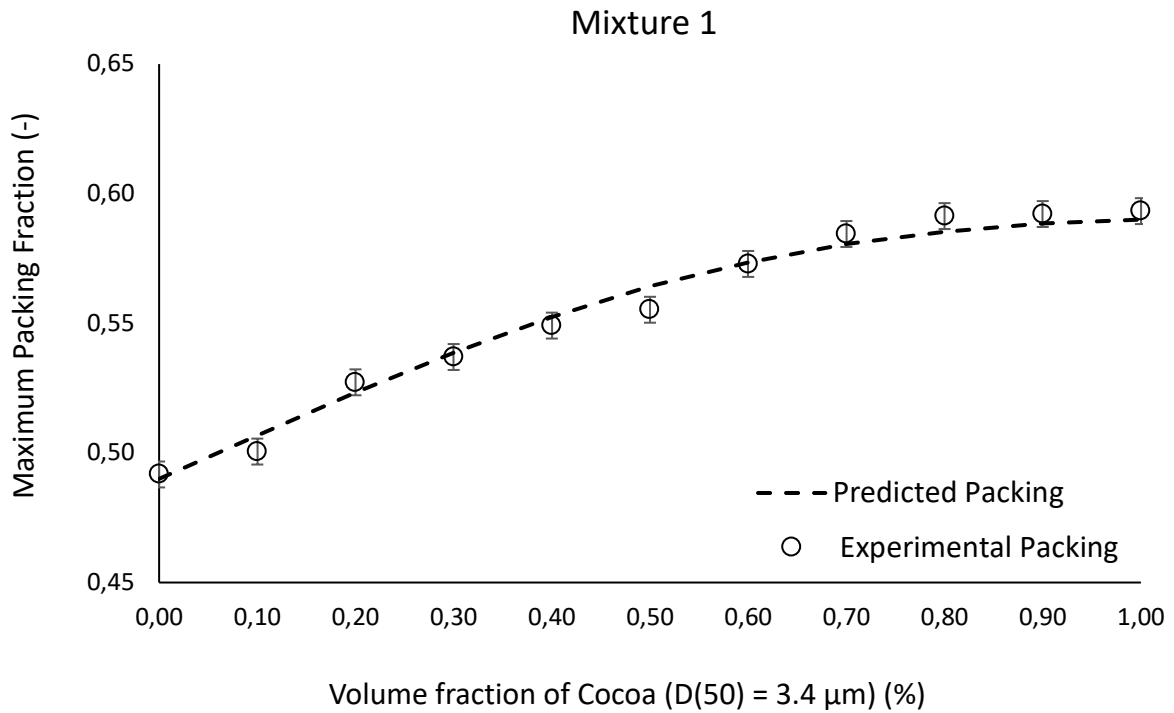
Table 5-3. List of the 11 combinations.

	Component 1	Component 2
Mixture 1	Cocoa ($D_{50} = 3.4 \mu\text{m}$)	Cocoa ($D_{50} = 11.2 \mu\text{m}$)
Mixture 2	Cocoa ($D_{50} = 9.2 \mu\text{m}$)	Sugar ($D_{50} = 58.6 \mu\text{m}$)
Mixture 3	Cocoa ($D_{50} = 9.2 \mu\text{m}$)	Sugar ($D_{50} = 436 \mu\text{m}$)

Table 5-4. Components 1 and 2 of each binary mixture.

We plot in Figure 5-4 the measured and predicted real maximum packing fractions of each binary mixture. We observe that the predicted maximum packing fractions have the same evolution than the measured maximum packing fractions. For mixtures 2 and 3, the evolution of the measured and predicted maximum packing fractions has a “bell” shape and in both cases, there is an optimal maximum packing fraction reached for combination 5. Whilst for mixture 1, the predicted and measured maximum packing fractions increase with the proportion of Cocoa ($D_{50} = 11.2 \mu\text{m}$) substituted by Cocoa ($D_{50} = 3.4 \mu\text{m}$). We must also specify that different values of packing index have been tried in order to find the one giving

the best correlation between the measured maximum packing fraction (ϕ_{max}) and the predicted maximum packing fraction ($\phi_{max\text{predicted}}$). The right packing index is equal to 9. This is in good agreement with de Larrard prediction about the value of packing index to use when a compressive method such as centrifugation is used to pack a system.



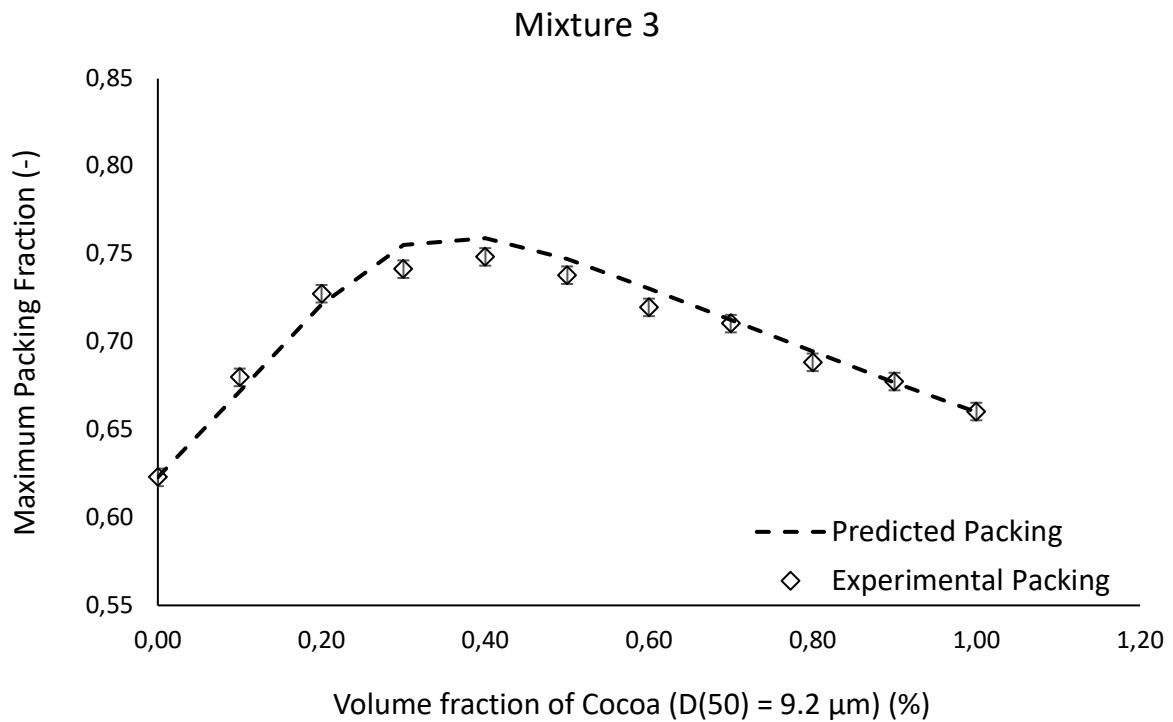


Figure 5-4. Measured and predicted real maximum packing fractions of the binary mixtures.

5.2.2.1.2 Ternary mixtures

We choose one of the dark chocolate recipes used by Cargill to formulate the ternary mixtures. This recipe contains 47.7% sugar particles, 19.6% cocoa particles and 32.3% fat by total mass of chocolate. The mass proportion of the solid particles in this recipe amounts to 71% sugar particles and 29 % cocoa particles by total mass of solid particles (i.e., 65% sugar and 35% cocoa by total volume of solid particles respectively). 11 combinations are also studied for both ternary mixtures. The proportion of sugar particles is kept constant in the 11 combinations of mixture 4 whereas it is the proportion of cocoa particles that remains constant for mixture 5. The composition and the components of both ternary mixtures are summarized in Table 5-5 and 5-6 respectively.

Chapter 5: Compressible Packing Model: optimization of cocoa and sugar
particle size distribution

	Volume fraction (by total volume of solid particles)			Total volume fraction
	Cocoa ($D_{50} =$ 9.2 μm)	Cocoa ($D_{50} =$ 2.6 μm)	Sugar ($D_{50} =$ 58.6 μm)	
Combination 1	0.35	0	0.65	1
Combination 2	0.315	0.035	0.65	1
Combination 3	0.28	0.07	0.65	1
Combination 4	0.245	0.105	0.65	1
Combination 5	0.21	0.14	0.65	1
Combination 6	0.175	0.175	0.65	1
Combination 7	0.14	0.21	0.65	1
Combination 8	0.105	0.245	0.65	1
Combination 9	0.07	0.28	0.65	1
Combination 10	0.035	0.315	0.65	1
Combination 11	0	0.35	0.65	1

Table 5-5. List of mixture 4 combinations and components.

	Volume fraction (by total volume of solid particles)			Total volume fraction
	Cocoa ($D_{50} =$ 9.2 μm)	Sugar ($D_{50} =$ 436 μm)	Sugar ($D_{50} =$ 58.6 μm)	
Combination 1	0.35	0	0.65	1
Combination 2	0.35	0.065	0.585	1
Combination 3	0.35	0.13	0.52	1
Combination 4	0.35	0.195	0.455	1
Combination 5	0.35	0.26	0.39	1
Combination 6	0.35	0.325	0.325	1
Combination 7	0.35	0.39	0.26	1
Combination 8	0.35	0.455	0.195	1
Combination 9	0.35	0.52	0.13	1
Combination 10	0.35	0.585	0.065	1
Combination 11	0.35	0.65	0	1

Table 5-6. List of mixture 5 combinations and components.

We plot in Figure 5-5 the experimental and predicted real maximum packing fractions of both ternary mixtures. As for binary mixtures, we observe that the predicted maximum packing fractions have the same evolution than the experimental maximum packing fractions. We observe that the successive additions of Sugar ($D_{50} = 436 \mu\text{m}$) and Cocoa ($D_{50} = 2.6 \mu\text{m}$) increase both maximum packing fractions of mixtures 4 and 5 respectively. However, we can

also observe for mixture 4 that from combination 7 to 11, the increase of the experimental and predicted maximum packing fractions is negligible compared to mixture 5.

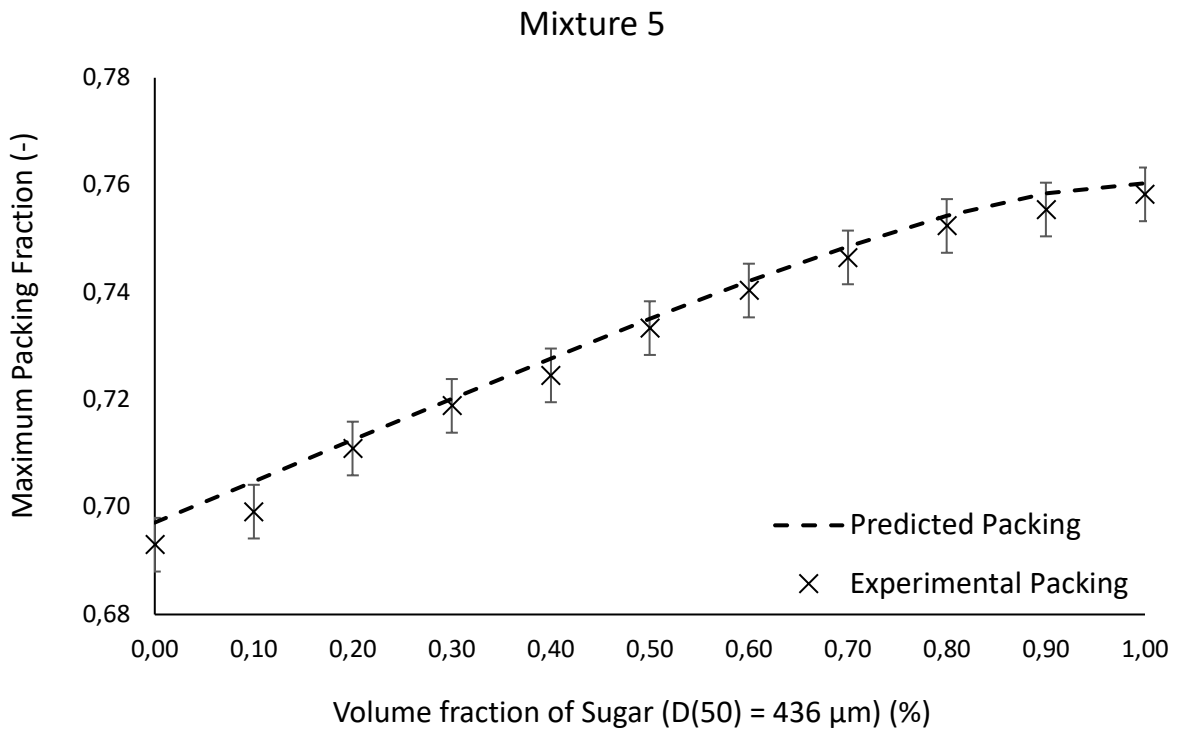
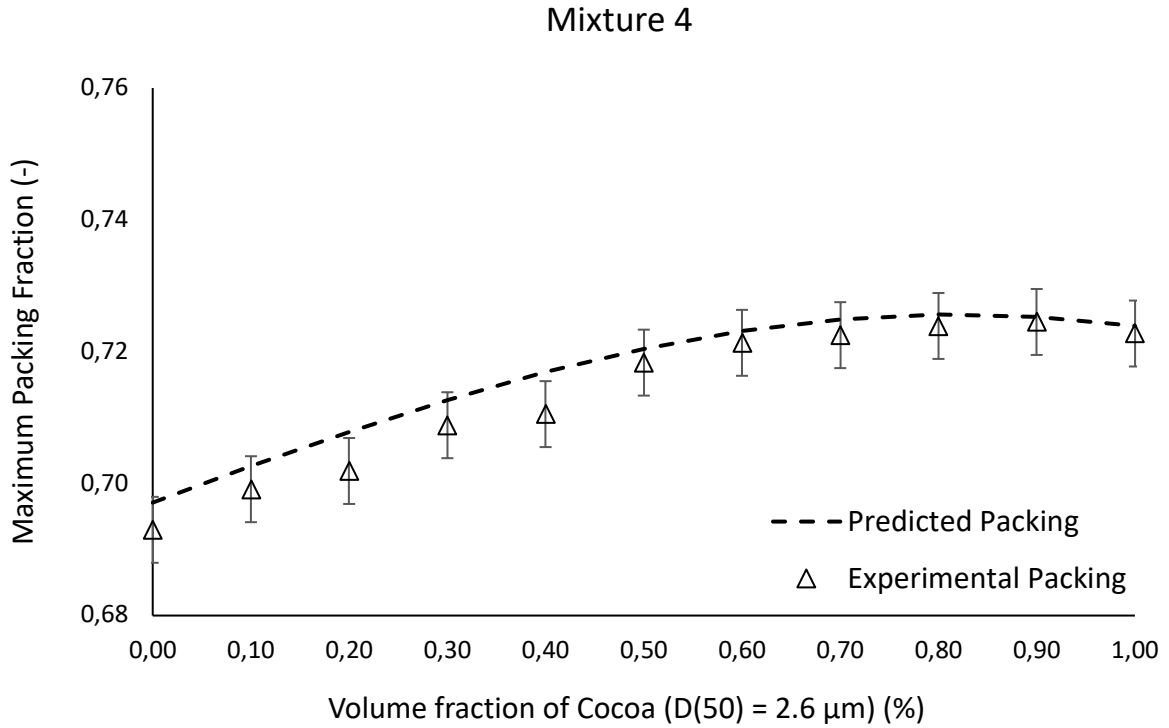
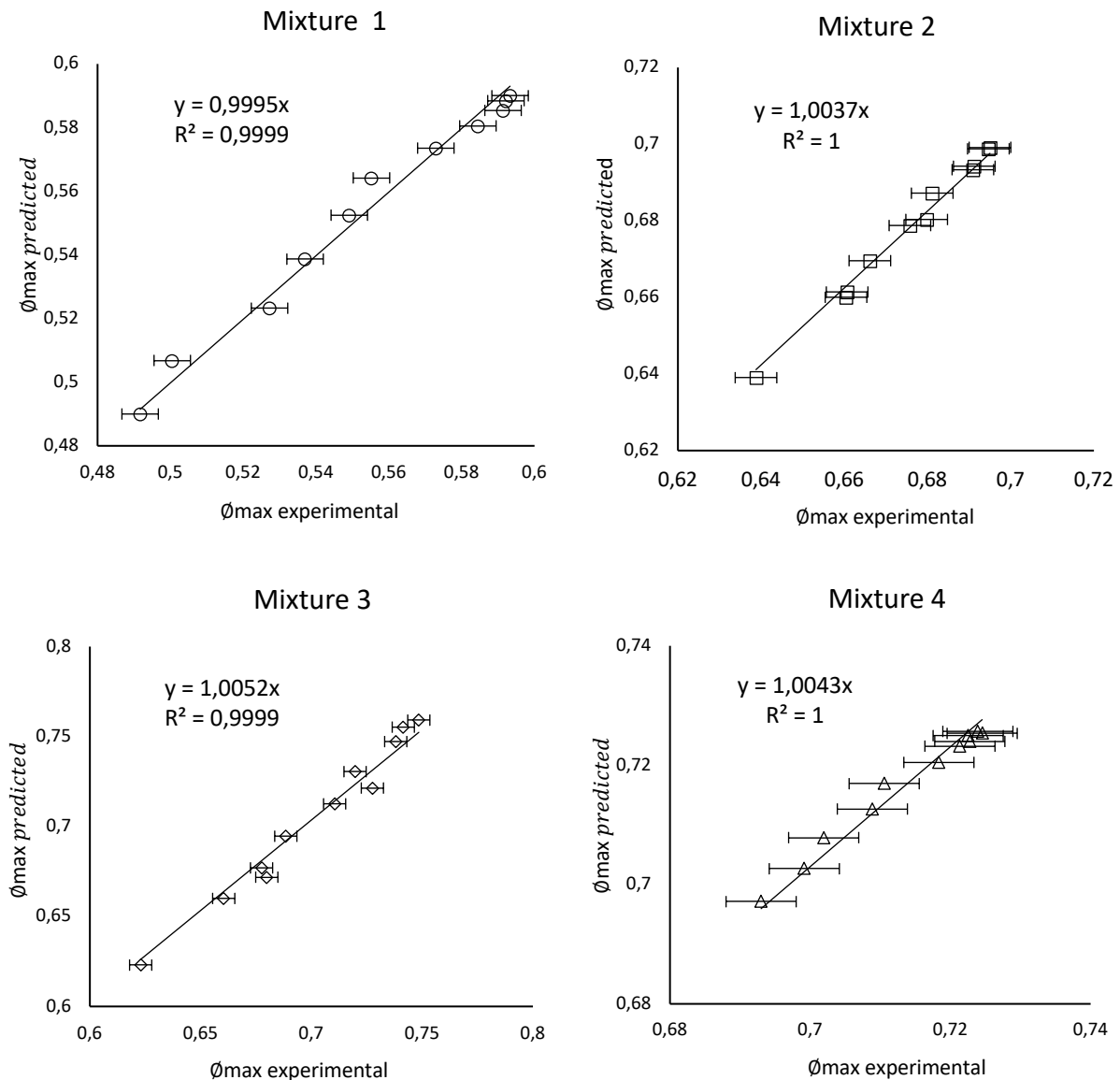


Figure 5-5. Experimental and predicted real maximum packing fractions of the ternary mixtures.

5.2.2.2 Correlation between the predicted and experimental maximum packing fraction

We plot in Figure 5-6 the predicted maximum packing fraction as a function of the experimental maximum packing fraction of the binary and ternary mixtures. We observe a good correlation between both maximum packing fractions with a mean error in absolute value of 0.2% (Mixtures 3 and 5), 0.3% (Mixture 4), 0.4% (Mixture 1) and 0.6% (Mixture 2). The correlation rate increases between 96% (Mixture 4) and 99% (Mixtures 1 and 5). These results confirm that the compressible packing model is a relevant packing model to use for the prediction of the maximum packing fraction of sugar and cocoa suspensions.



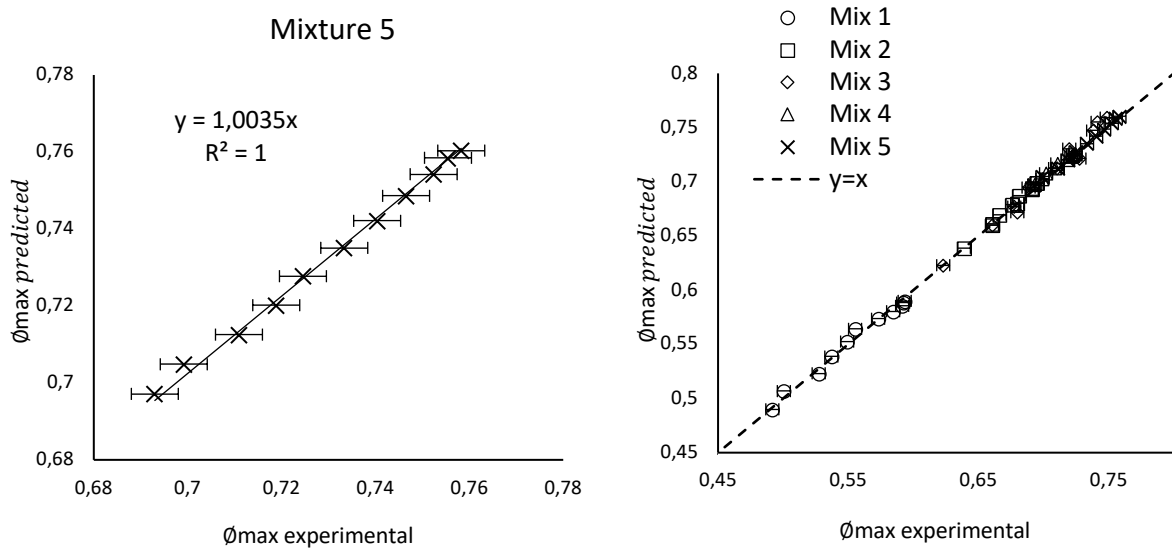


Figure 5-6. Correlation between the predicted and experimental maximum packing fractions.

5.3 Conclusion

In this chapter, we have demonstrated that the compressible packing model can be used to predict the maximum packing fraction of chocolate products. Indeed, there is an accuracy of 98% between the real maximum packing fraction predicted by CPM and the experimental maximum packing fraction measured by centrifugation. The validation of this theoretical model will allow us to predict the maximum packing fraction of different combinations and optimize particle size distribution in order to reduce the quantity of fat without changing the rheological behaviour.

References:

- [1] Guyon, E. ; Troadec, J.P. (1994) Du sac de billes au tas de sable. Editions Odile Jacob, Paris.
- [2] Furnas, C. *Ind. Eng. Chem.* 1930, 23, 1052-1058.
- [3] Andreasen, A.H.M. *Kolloid-Zeitschrift* 1930, 50, 217-228.
- [4] Powers, T.C. The properties of fresh concrete. New York, N.Y.: Wiley, 1968.
- [5] Funk, J.E.; Dinger, D.R. Predictive process control of crowded particulate suspensions: Applied to ceramic manufacturing, Springer, 1994.
- [6] Ouchiyama, N.; Tanaka, T. *Ind. Eng. Chem. Fundam.* 1981, 20, 66-71.
- [7] Ouchiyama, N.; Tanaka, T. *Ind. Eng. Chem. Fundam.* 1986, 25, 125-129.
- [8] de Larrard, F. Concrete Mixture Proportioning: a scientific approach, E&FN SPON: An imprint of Routledge, London and New-York, 1999.
- [9] Storvall, T.; de Larrard, F.; Buil, M. Linear Packing Density Model of Grain Mixtures, Powder Technology, 1986, 48, 1-12.
- [10] Chateau, X. Particle packing and the rheology of concrete. In: Roussel, N. (Ed.), Understanding the Rheology of Concrete, Woodhead Publishing, 2012.

**Chapter 6: Industrial applications:
formulation of reduced-fat content
chocolate and emulsifier free chocolate**

Table of contents

6.1	Chocolate suspensions studied.....	172
6.1.1	Conventional dark chocolates.....	173
6.1.2	Reference dark chocolates.....	174
6.2	Application 1: reduced-fat chocolate.....	179
6.3	Application 2: emulsifier free chocolate.....	186
6.4	Correlation between the viscosity and relative solid volume fraction of the reduced-fat chocolates, emulsifier free chocolates, sugar suspensions, sugar and cocoa suspensions cocoa suspensions and commercially available dark chocolates.....	192
6.5	Conclusion.....	195

The aim of this chapter is to implement what have been demonstrated in chapter 4, namely that it is possible to control the rheology of chocolate by controlling the relative solid volume fraction (ϕ/ϕ_{max}) and the mean particle size. To that end, we focus on the formulation of reduced-fat chocolates and emulsifier free chocolates by optimizing the particle size distribution of 4 industrial dark chocolate applications. The 4 applications are moulding, extrusion, enrobing and ice cream.

In the first application, we formulate reduced-fat chocolates by adding “fine” cocoa particles of size well below the particle size range of conventional chocolate. In the second application, we formulate emulsifier free chocolates by adding “coarse” sugar particles, the size of which is well above the particle size range in conventional chocolate. As predicted by the compressible packing model (CPM) and confirmed by experimental measurements, the addition of these particles leads to the increase of the maximum packing fraction.

Our results show that it is possible to decrease the fat content (i.e., increase the solid volume fraction) while adding fine particles and maintaining a constant relative solid volume fraction (ϕ/ϕ_{max}) and constant viscosity. Regarding the yield stress, as showed in chapter 4, the addition of fine particles in a suspension leads to its increase. However, by keeping the solid relative solid volume fraction constant, our results show that the increase in yield stress is moderated and acceptable in practice.

As shown in chapter 4, contrary to the fine particles, the addition of coarse particles leads to a decrease in yield stress. Therefore, our results show that it is possible to formulate an emulsifier-free chocolate without increasing the fat content of the suspension. Indeed, by only increasing the maximum packing fraction of a suspension by adding coarse particles, it is possible to formulate an emulsifier-free chocolate without increasing the viscosity and yield stress.

In the first part of this chapter, we present the reference dark chocolate formulated from the recipes used by Cargill to produce the 4 industrials dark chocolate applications. Then, we present the two projects conducted and, finally, we plot the viscosity and yield stress of the reduced-fat chocolates and emulsifier free chocolates on the master curves obtained in chapter 4.

6.1 Chocolate suspensions studied

In this section, we are presenting 4 conventional dark chocolates (extrusion, moulding, enrobing and ice cream) produced by Cargill using an industrial plant and 4 reference dark chocolates formulated in our laboratory by mixing all the required ingredients together and following the same recipe than Cargill to produce their 4 conventional dark chocolates. To ensure that our formulated reference dark chocolates have morphological and rheological properties as close as possible to those of Cargill, we formulate them using cocoa and sugar

particles having a particle size distribution similar to the 4 conventional chocolate particle size distribution. We recall that the mixing protocol followed is the one described in chapter 2. In the following, we will refer to the 4 conventional dark chocolates provided by Cargill as reference dark chocolates and we will refer to the 4 chocolates formulated in our laboratory as reformulated reference dark chocolates.

6.1.1 Conventional dark chocolates

The ingredients proportion, solid volume fraction (ϕ), measured maximum packing fraction (ϕ_{max}) of the conventional dark chocolates (extrusion, moulding, enrobing and ice cream) are summarized in Table 6-1.

Samples	Extrusion		Moulding		Enrobing		Ice cream	
	%m	%v	%m	%v	%m	%v	%m	%v
Sugar particles	58.5	46.7	47.7	36.3	40.6	29.7	39.5	28.2
Cocoa particles	15.2	16	19.6	19.7	20.1	19.4	15	14.1
Cocoa butter	25.8	36.6	32.3	43.5	38.7	50.1	45	57.1
Lecithin	0.50	0.70	0.40	0.50	0.60	0.80	0.50	0.60
ϕ	0.63		0.56		0.49		0.42	
ϕ_{max} (± 0.005)	0.74		0.70		0.68		0.66	

Table 6-1. Composition of the conventional dark chocolates. %m represents the mass proportion of each ingredient by total mass of chocolate and %v represents the volume proportion by total volume of chocolate.

We plot in Figure 6-1 the particle size distribution by volume of the conventional dark chocolates and the particle size distribution by volume of the final product (DC4(6)) resulting from the cocoa and sugar (dark chocolate) suspensions production studied in chapter 3 and 4. We observe that the conventional dark chocolates have the same particle size distribution with a mean diameter of 9 μm . As also shown in Figure 6-1, we observe herein that their particle size distributions are also similar to the one of final product collected at the end of the conching of cocoa and sugar (dark chocolate) suspensions. This suggests that we can reformulate the conventional dark chocolates in laboratory by using fatted cocoa powder (Cocoa ($D_{50} = 9.2 \mu\text{m}$)) and sugar (sweet fat) suspensions samples collected during conching.

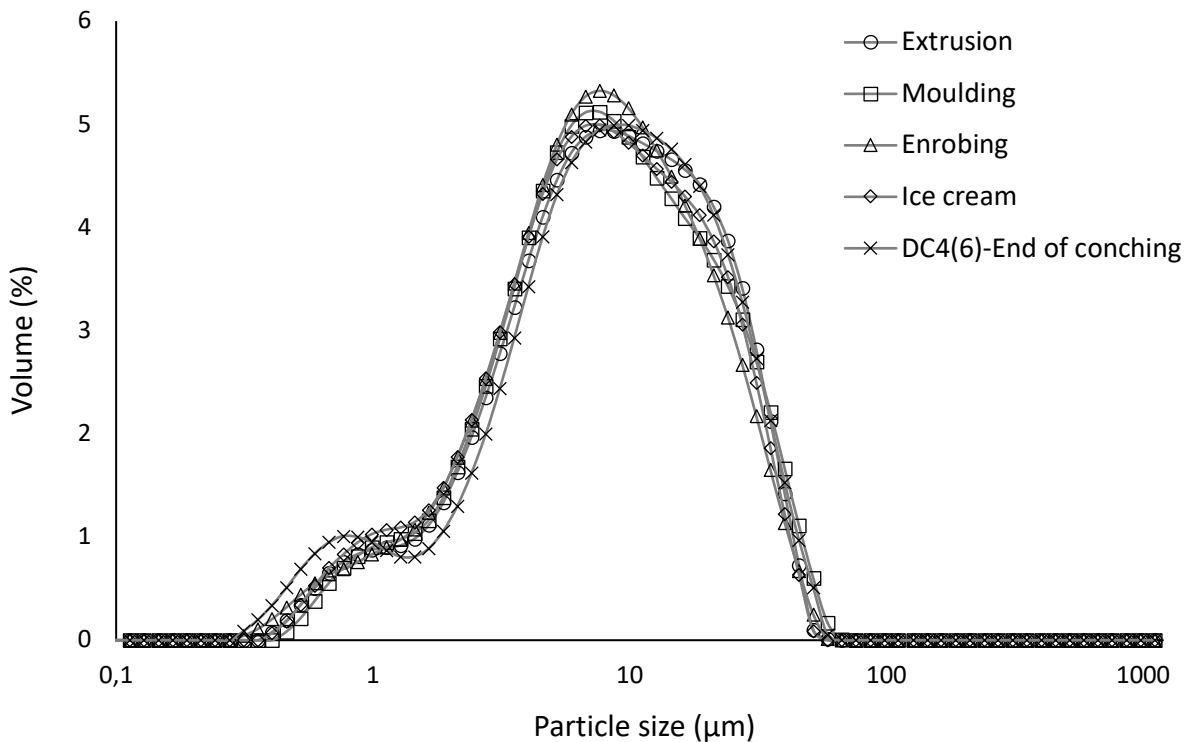


Figure 6-1. Particle size distribution by volume of the 4 conventional dark chocolates (extrusion, moulding, enrobing and ice cream) and the final product (DC4(6)) resulting from the cocoa and sugar (dark chocolate) suspensions production studied in chapter 3 and 4.

6.1.2 Reference dark chocolates

As previously suggested, the conventional dark chocolates could be formulated in laboratory by using fatted cocoa powder (Cocoa ($D_{50} = 9.2 \mu\text{m}$)) and sugar (sweet fat) suspensions samples collected during conching. Indeed, as showed in chapter 3, we recall that it is possible to predict the measured particle size distribution of sugar and cocoa suspensions during conching step from the particle size distribution of Cocoa ($D_{50} = 9.2 \mu\text{m}$) and the measured particle size distribution of sugar suspensions during conching step. We should also specify that we can use any sugar suspensions samples collected during conching to reformulate the reference dark chocolates since we demonstrated in chapter 3 that their particle size distribution remains unchanged during conching. We thus choose to use the sweet fat sample collected after 5 hours of conching (SF4(5)) for the formulation.

We plot in Figure 6-2 the particle size distribution by volume of the sugar (sweet fat) suspensions sample and fatted cocoa powder (Cocoa ($D_{50} = 9.2 \mu\text{m}$)) used to reformulate the 4 reference chocolates in our laboratory.

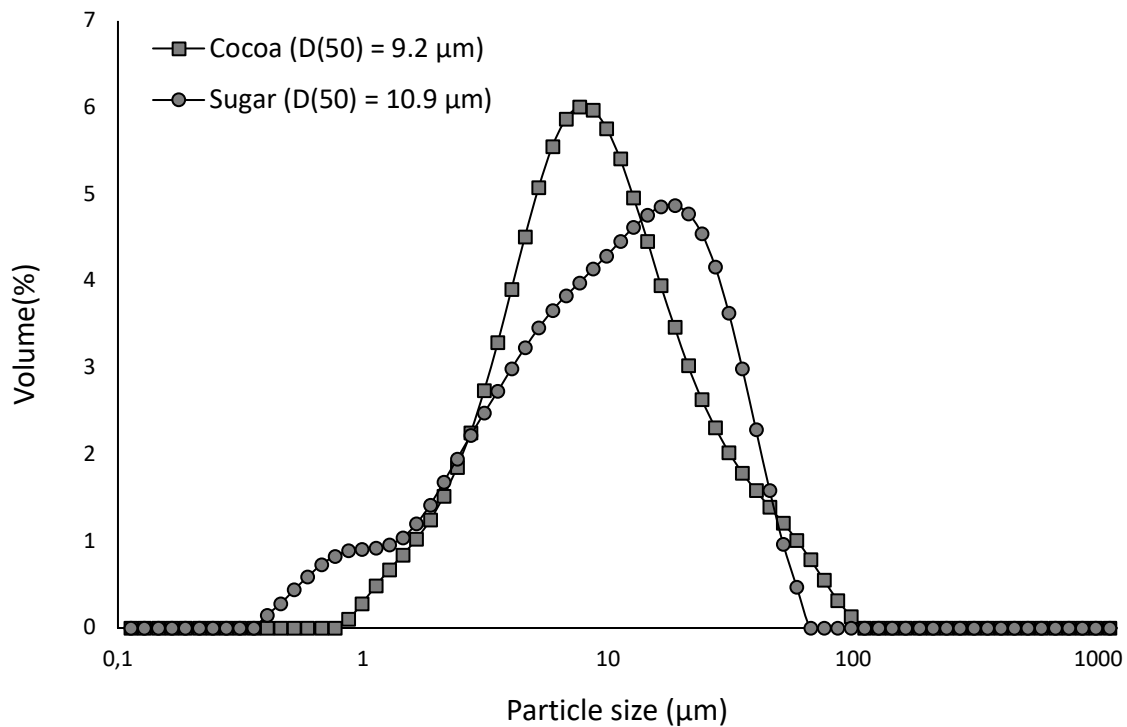
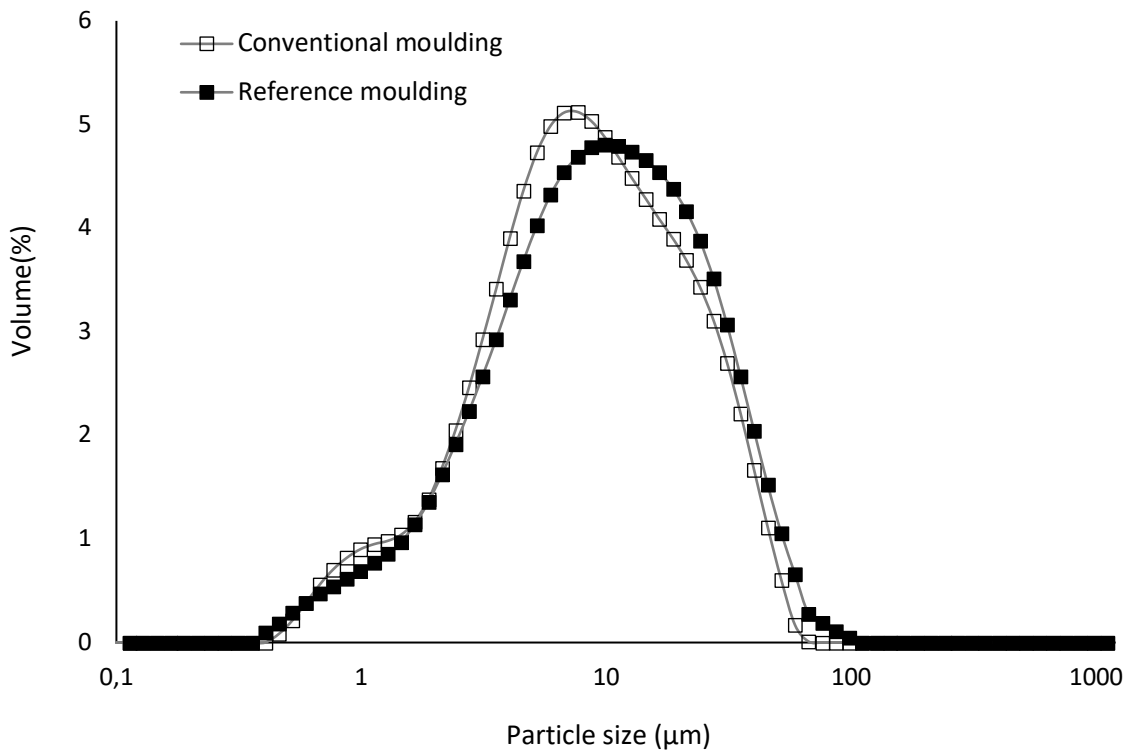
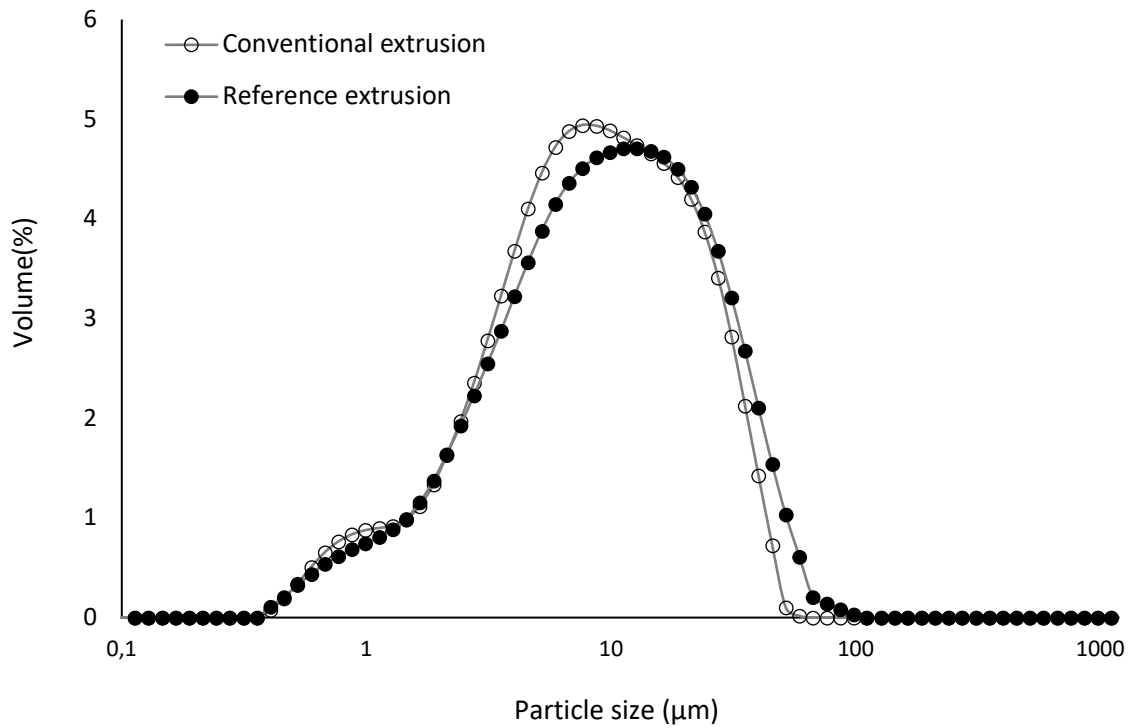


Figure 6-2. Particle size distribution of fatted cocoa powder (Cocoa ($D_{50} = 9.2 \mu\text{m}$)) and sugar (sweet fat) suspensions sample (SF4(5)) used to reformulate the reference dark chocolates.

We plot in Figure 6-3 the measured particle size distribution by volume of the conventional dark chocolates (previously shown in Figure 6-1) and the calculated particle size distribution by volume of the reference dark chocolates. We recall that it is possible to calculate the particle size distribution by using the protocol described in chapter 2. As expected, we observe that the measured and calculated particle size distributions are approximately the same. In the following, when we refer to extrusion, moulding, enrobing and Ice cream, it will be to designate the reference dark chocolates formulated in the laboratory.



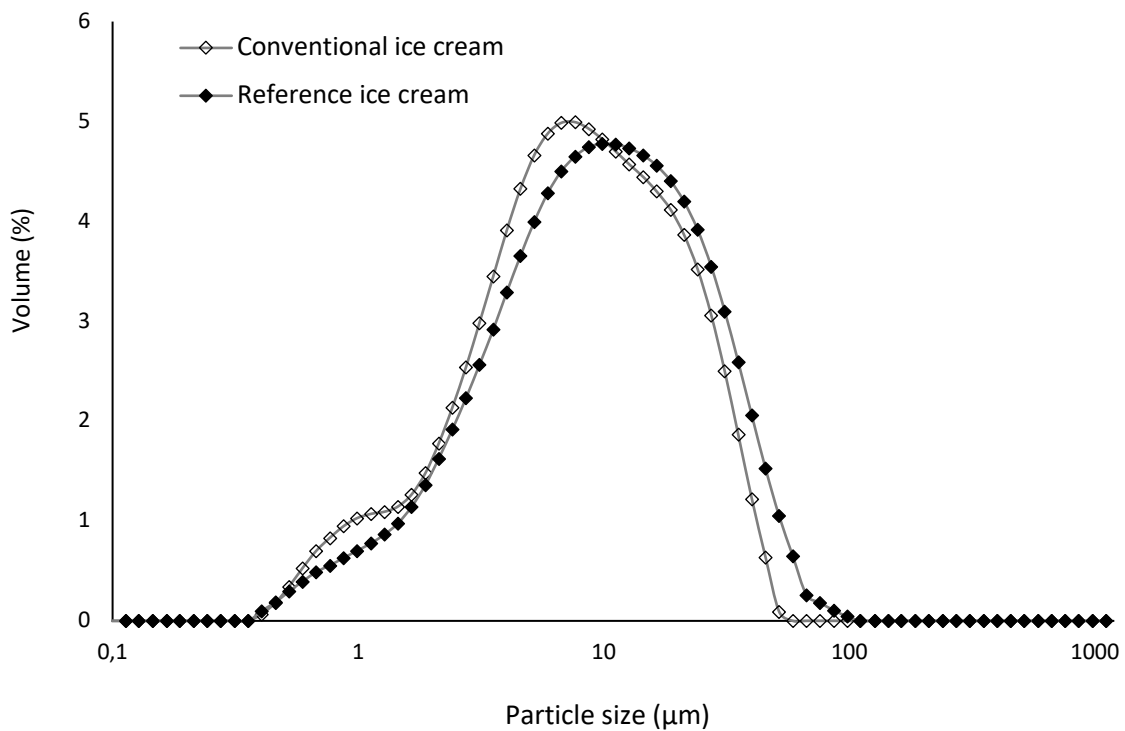
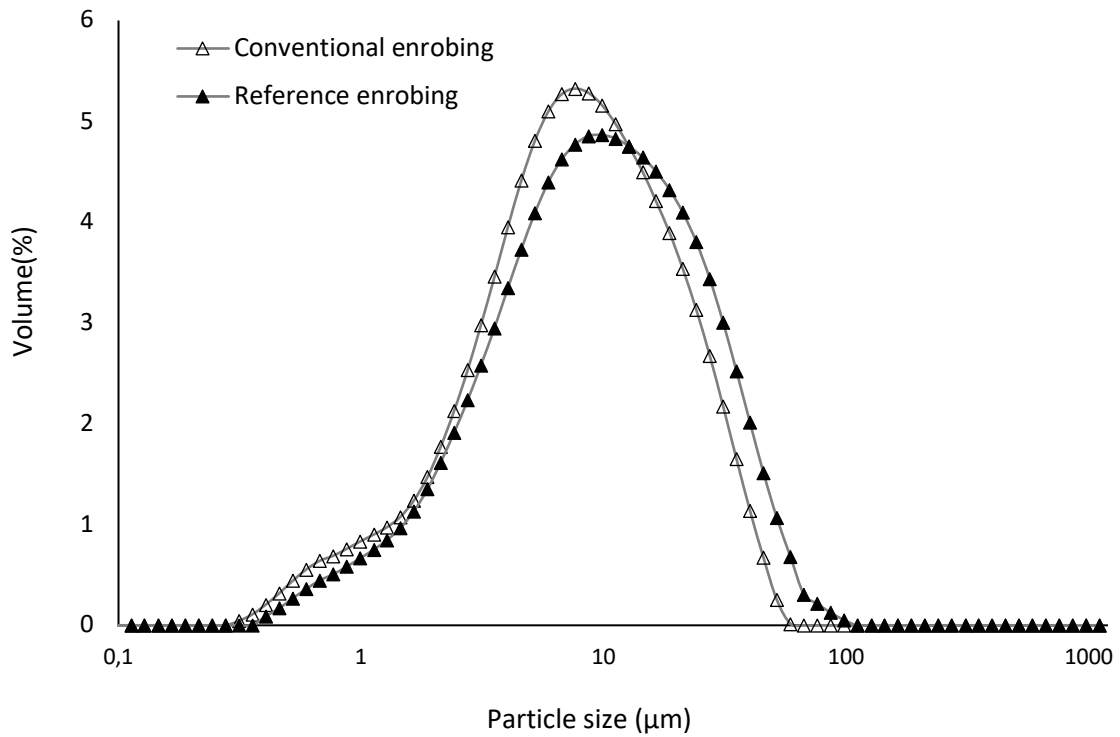


Figure 6-3. Particle size distribution of the conventional dark chocolates (unfilled data points) and the reference dark chocolates (filled data points).

We plot in Figure 6-4 the viscosity as a function of shear rate and present in Table 6-2 the measured maximum packing fraction of the reference dark chocolates. As expected, they exhibit a shear-thinning behaviour and their viscosity and yield stress decrease when the fat amount increases. Regarding the measured maximum packing fraction, we observe that they are following the same trend than those of the conventional dark chocolates.

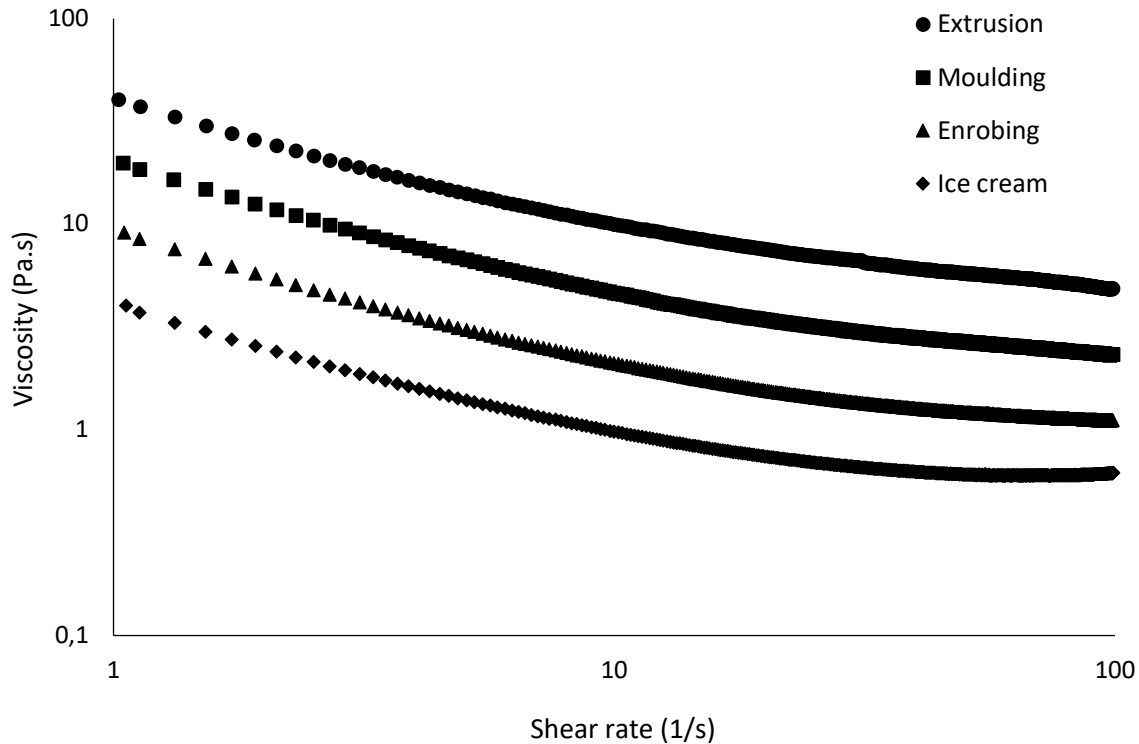


Figure 6-4. Flow curves of the reference dark chocolates (Extrusion, Moulding, Enrobing and Ice cream). The solid volume fraction of the reference dark chocolates is in Table 6-1.

	Extrusion	Moulding	Enrobing	Ice cream
$\phi_{max} (\pm 0.005)$	0.72	0.69	0.69	0.68

Table 6-2. Measured maximum packing fraction of the reformulated reference dark chocolates.

We then plot in Figure 6-5 the measured viscosity as a function of the relative solid volume fraction (ϕ/ϕ_{max}) for the 4 reference dark chocolates. We observe that the viscosity of the reference dark chocolates is forming one curve. This suggests that, as expected and shown in previous chapters, the viscosity of these samples only depends on the relative solid volume fraction and, therefore, the fat content of the reference dark chocolates can be decreased at constant viscosity by controlling their relative solid volume fraction (ϕ/ϕ_{max}).

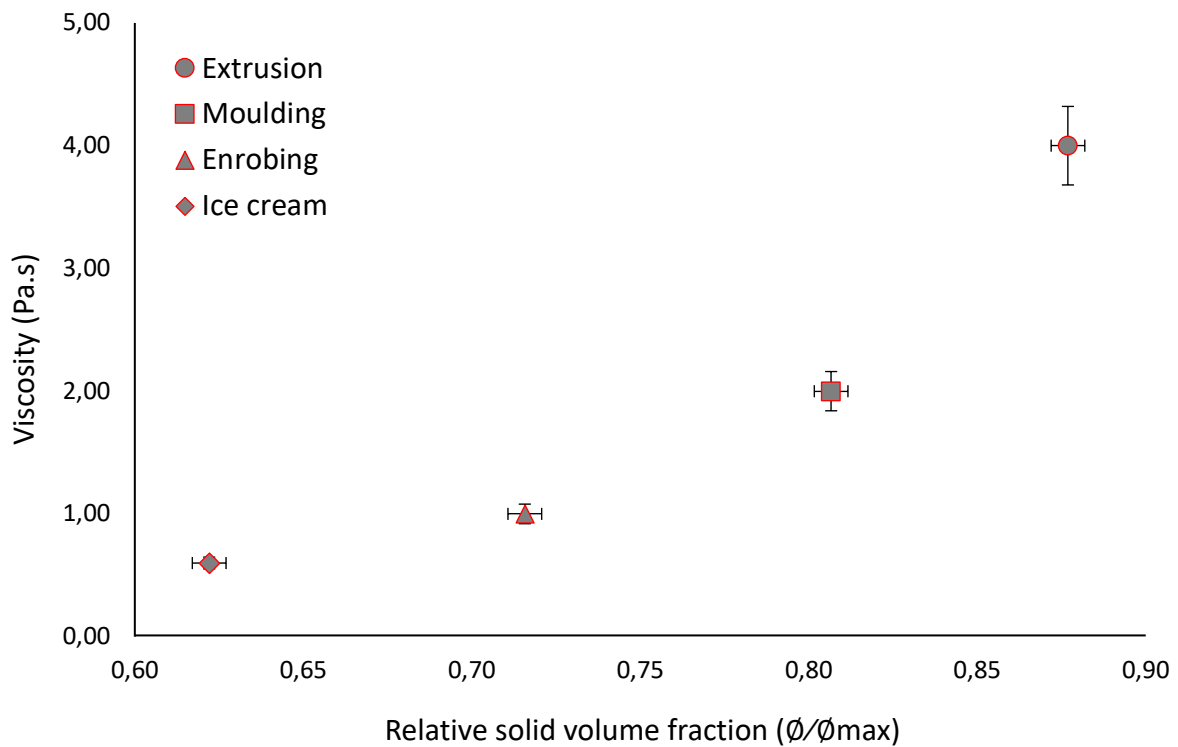


Figure 6-5. Viscosity as function of the relative solid volume fraction (ϕ/ϕ_{max}) of the reference dark chocolates.

6.2 Application 1: reduced-fat chocolate

The purpose of this application is to optimize the particle size distribution of the reference dark chocolates (extrusion, moulding, enrobing and Ice cream) by substituting “coarse” cocoa particles (Cocoa ($D_{50}= 9.2 \mu\text{m}$)) by “fine” cocoa particles (Cocoa ($D_{50}= 2.6 \mu\text{m}$)) and thus, increasing the maximum packing fraction. The particle size distributions of Cocoa ($D_{50}= 2.6 \mu\text{m}$), Cocoa ($D_{50}= 9.2 \mu\text{m}$) and Sugar ($D_{50}= 10.9 \mu\text{m}$) used to produce reduced-fat chocolates are represented in Figure 6-6. A representation of the optimization realised in this application is presented in Figure 6-7.

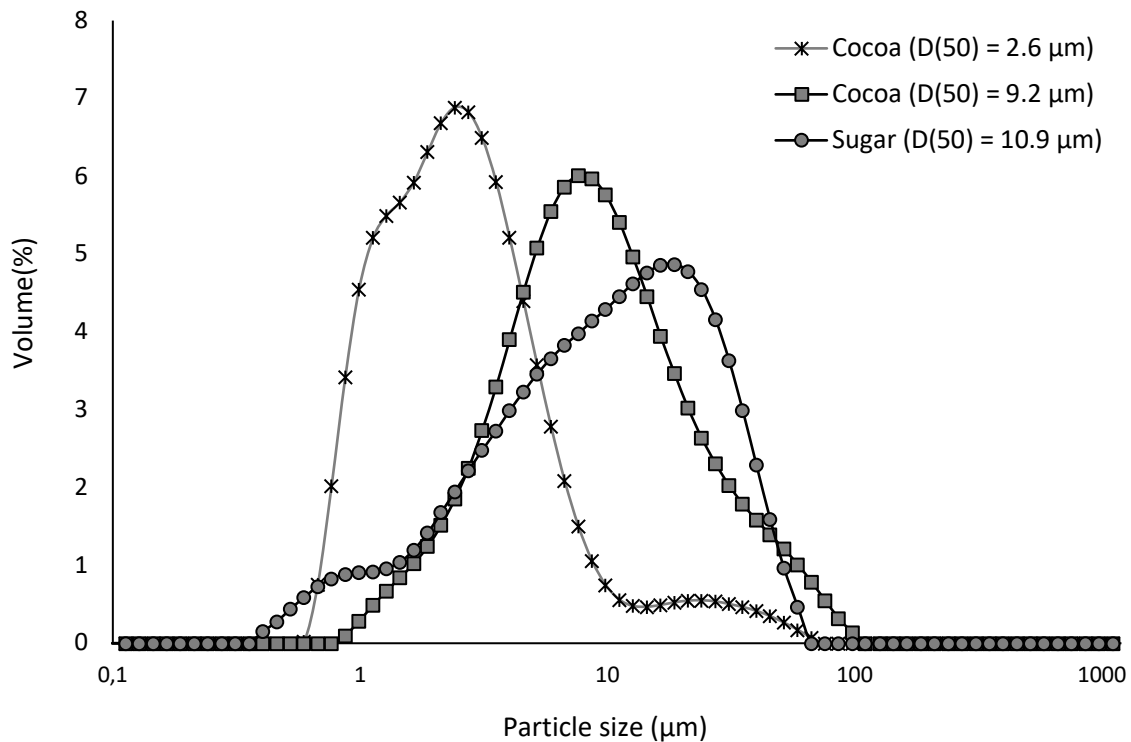


Figure 6-6. Particle size distribution of the solid particles used to formulate reduced-fat chocolates.

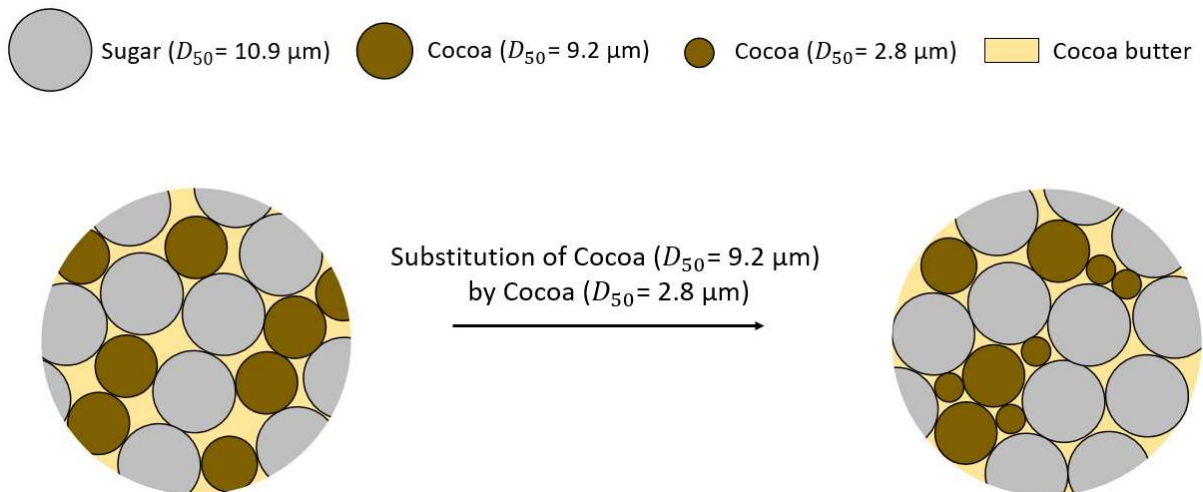


Figure 6-7. Representation of the substitution of coarse cocoa particles by fine cocoa particles in order to optimize the particle size distribution of the reference dark chocolates.

The first step of this application is the prediction of the evolution of the maximum packing fraction when substituting in the reference dark chocolates different proportions (ranging from 0 to 100% with a successive increment of 10%) of Cocoa ($D_{50} = 9.2 \mu\text{m}$) by Cocoa ($D_{50} = 2.6 \mu\text{m}$) by compressible packing model (CPM). We plot in Figure 6-8 the predicted maximum packing fraction as a function of the mass proportion of Cocoa ($D_{50} = 2.6 \mu\text{m}$). As expected,

the maximum packing fraction increases with the proportion of Cocoa ($D_{50} = 2.6 \mu\text{m}$) in each case. In this project, we study 6 reduced-fat chocolate formulations: 2 reduced-fat chocolate formulation containing 100% of Cocoa ($D_{50} = 2.6 \mu\text{m}$) that are Enrobing (0-100) and Ice cream (0-100) and 4 reduced-fat chocolate formulations containing 50% Cocoa ($D_{50} = 9.2 \mu\text{m}$) and 50% Cocoa ($D_{50} = 2.6 \mu\text{m}$) that are Extrusion (50-50), Moulding (50-50), Enrobing (50-50) and Ice cream (50-50). We are not studying Extrusion (0-100) and Moulding (0-100) because it is impossible to study their rheological properties as the addition of fine cocoa particles leads to a considerable increase of yield stress.

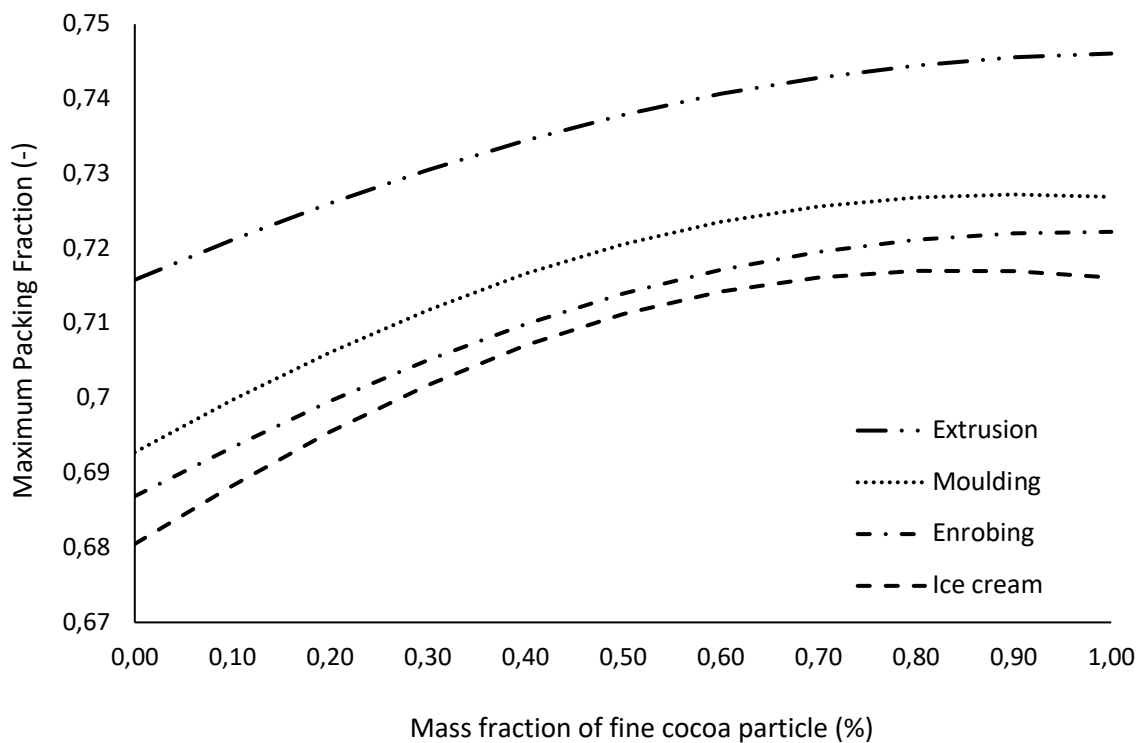


Figure 6-8. Evolution of the maximum packing fraction of the reference dark chocolates in presence of fine cocoa particles (Cocoa ($D_{50} = 2.6 \mu\text{m}$)) predicted by compressible model packing (CPM).

The second step of this project is the estimation of the solid volume fraction, at which we should prepare the reduced-fat chocolates so that they have the same relative solid volume fraction than the reference dark chocolates. We specify herein that the relative mass proportion of solid particles (i.e., mass proportion of cocoa particles to mass proportion of sugar particles ratio) in the reduced-fat chocolate is the same than in the reference dark chocolates and that only the total amount of fat changes. The composition of reduced-fat chocolate (0-100) and reduced-fat chocolate (50-50) is summarized in Table 6-3.

Chapter 6: Industrial applications: formulation of reduced-fat content
chocolate and emulsifier free chocolate

	Sugar (d=10.9 µm) (% by total mass)	Cocoa particles (% by total mass)		Cocoa butter (% by total mass)	Lecithin (% by total mass)	Predicted Solid volume fraction	Relative mass proportion of solid particles $\left(\frac{mass_{cocoa}}{mass_{sugar}}\right)$	Predicted relative solid volume fraction $\left(\frac{\phi}{\phi_{max}}\right)$
		Cocoa (d=9.2 µm)	Cocoa (d=2.6 µm)					
Extrusion	58.5	15.2	0	25.8	0.5	0.63	0.26	0.88
Extrusion (0-50)	59.6	7.8	7.8	24.3	0.5	0.64	0.26	0.88
Moulding	47.7	19.6	0	32.3	0.4	0.56	0.41	0.81
Moulding (50-50)	49	10.1	10.1	30.4	0.4	0.58	0.41	0.81
Enrobing	40.6	20.1	0	38.7	0.6	0.49	0.50	0.72
Enrobing (50-50)	42	10.4	10.4	36.6	0.6	0.51	0.50	0.72
Enrobing (0-100)	42.2	0	21	36.2	0.6	0.52	0.50	0.72
Ice cream	39.5	15	0	45	0.5	0.42	0.38	0.62
Ice cream (50-50)	40.7	7.7	7.7	43.4	0.5	0.44	0.38	0.62
Ice cream (0-100)	41.1	0	15.6	42.8	0.5	0.45	0.38	0.62

Table 6-3. Composition of the reference dark chocolate chocolates (Extrusion, Moulding, Enrobing and Ice cream), the reduced-fat dark chocolates (50-50) (Extrusion (50-50), Moulding (50-50), Enrobing (50-50) and Ice cream (50-50)) and the reduced-fat dark chocolates (0-100) (Enrobing (0-100) and Ice cream (0-100)).

Moreover, estimating the solid volume fraction of both reduced-fat dark chocolates (50-50) and reduced-fat dark chocolates (0-100) studied allow to predict the relative mass loss of fat as follows:

$$\text{Relative mass loss of fat (\%)} = 100 \times \frac{\text{Mass of fat}_{\text{reformulated reference}} - \text{Mass of fat}_{\text{reduced-fat chocolate (50-50)}}}{\text{Mass of fat}_{\text{reformulated reference}}}$$

$$\text{Relative mass loss of fat (\%)} = 100 \times \frac{\text{Mass of fat}_{\text{reformulated reference}} - \text{Mass of fat}_{\text{reduced-fat chocolate (0-100)}}}{\text{Mass of fat}_{\text{reformulated reference}}}$$

We plot in Figure 6-9 the predicted mass loss of fat of the reference dark chocolates as a function of the mass proportion of Cocoa ($D_{50} = 2.6 \mu\text{m}$). We observe that the relative mass loss of fat is of 6% by total mass of fat for Extrusion (50-50) and Moulding (50-50) and of 4% and 5% for Ice cream (50-50) and Enrobing (50-50) respectively. The relative mass loss is of 7% and 8% for Enrobing (0-100) and Ice cream (0-100) respectively.

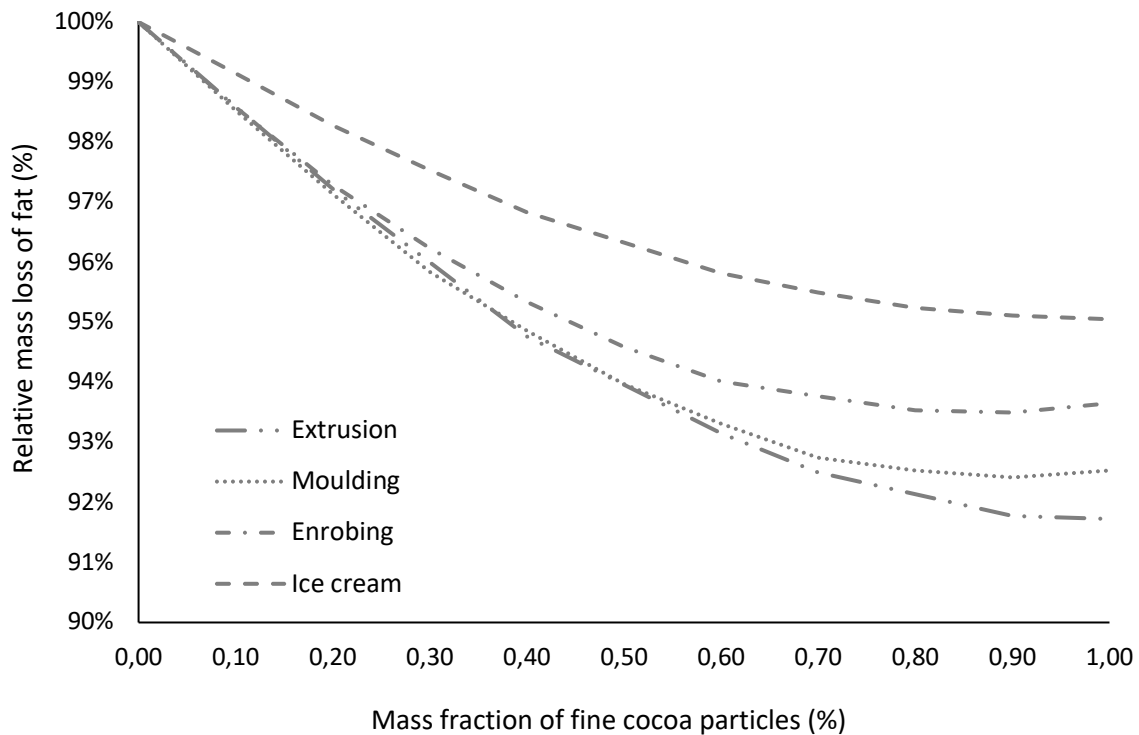


Figure 6-9. Predicted relative mass loss of fat for the reference dark chocolates when fine cocoa particles (Cocoa ($D_{50} = 2.6 \mu\text{m}$)) is added.

The final step of this project is the measurement of the rheological properties of the reduced-fat dark chocolates (50-50) (Extrusion (50-50), Moulding (50-50), Enrobing (50-50) and Ice cream (50-50)) and the reduced-fat dark chocolates (0-100) (Enrobing (0-100) and Ice cream (0-100)) in order to compare them to the rheological properties of the reference dark chocolates (Extrusion, Moulding, Enrobing and Ice cream).

We plot in Figure 6-10 the viscosity as a function of the solid volume fraction of the reference dark chocolates, the reduced-fat dark chocolates (50-50) and the reduced-fat dark chocolates (0-100). As expected, we observe that the change in viscosity is negligible when the solid volume fraction increases since we are maintaining the relative solid volume fraction (ϕ/ϕ_{max}) constant. These observations confirm as expected that the total fat amount of the reference dark chocolates can be decreased at constant viscosity by optimizing their particle size distribution and improving their maximum packing fraction. By plotting the viscosity as a function of the relative solid volume fraction (ϕ/ϕ_{max}) in Figure 6-11, we observe that both

reduced-fat chocolates (50-50) and reduced-fat chocolates (0-100) are also following the master curve formed by the reference dark chocolates.

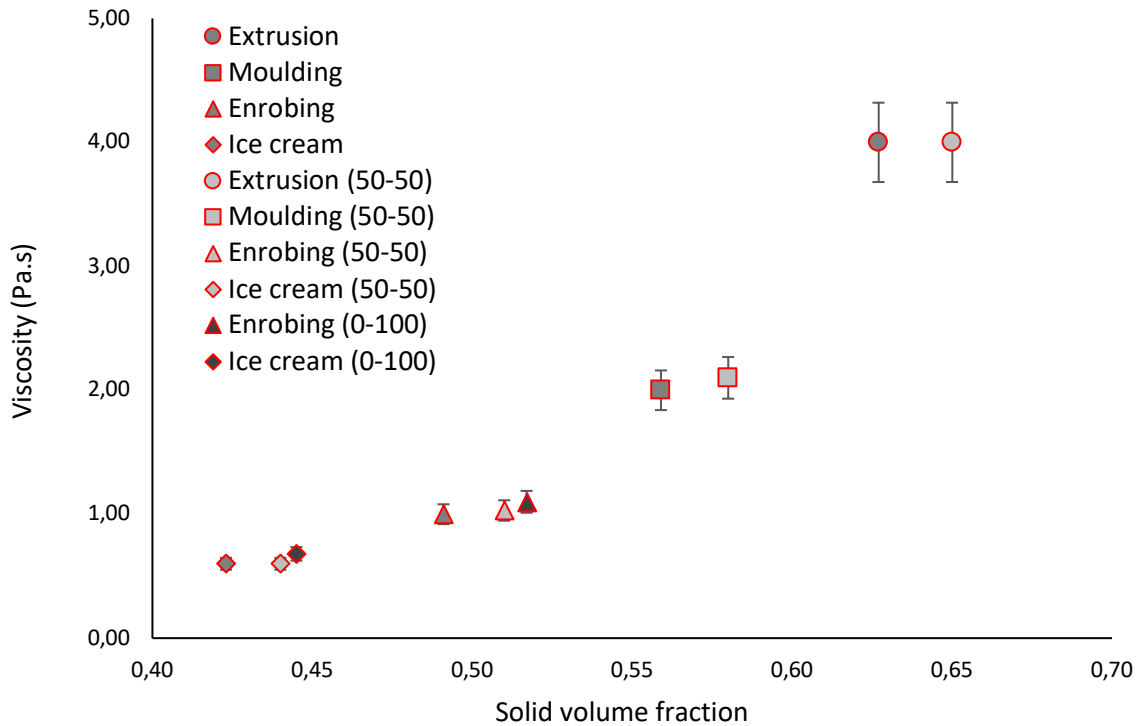


Figure 6-10. Measured viscosity as a function of the solid volume fraction of the reference dark chocolates, reduced-fat chocolates (50-50) and reduced-fat chocolates (0-100).

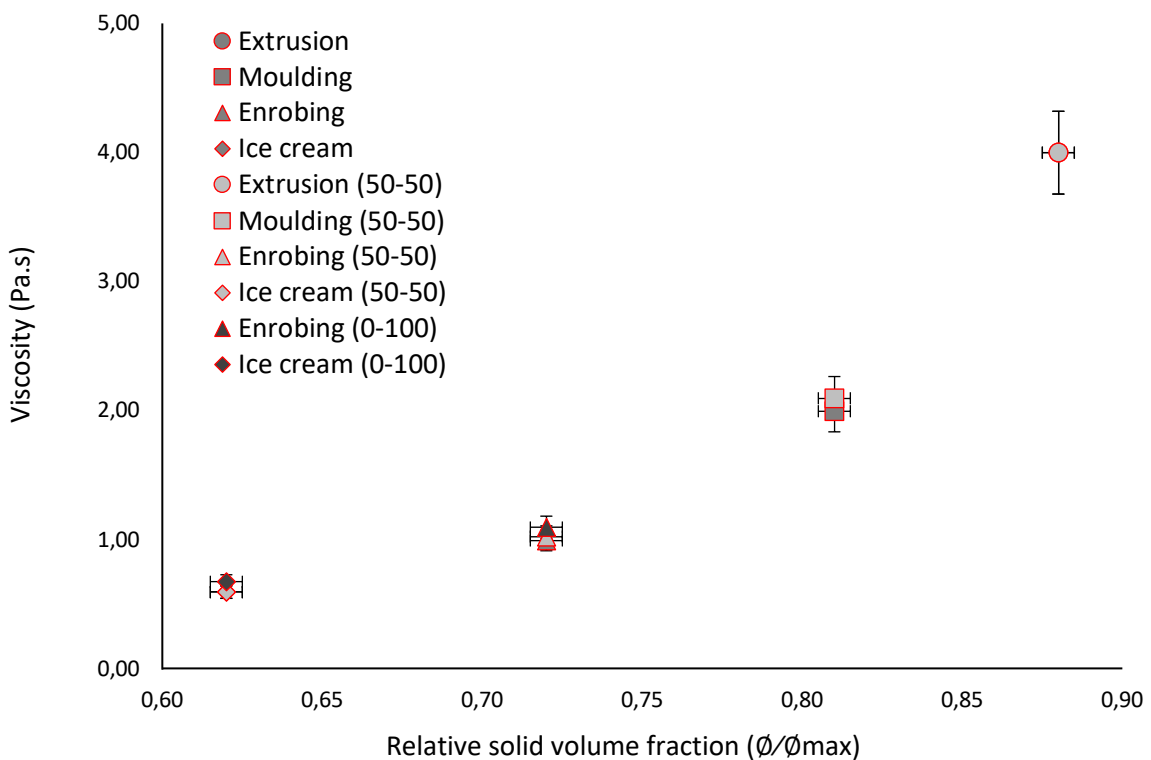


Figure 6-11. Measured viscosity as a function of the relative solid volume fraction of the reference dark chocolates (Extrusion, Moulding, Enrobing and Ice cream), reduced-fat chocolates (50-50) (Extrusion (50-50), Moulding (50-50), Enrobing (50-50) and Ice cream (50-50)) and reduced-fat chocolates (0-100) (Extrusion (0-100), Moulding (0-100), Enrobing (0-100) and Ice cream (0-100)).

Regarding the effect of the addition of fine cocoa particles on yield stress, we plot in Figure 6-12 the yield stress of the reference dark chocolates, reduced-fat chocolates (50-50) and reduced-fat chocolates (0-100) as function of the relative solid volume fraction. We observe that reduced-fat chocolates (50-50) and reduced-fat chocolates (0-100) display higher yield stresses than the reference dark chocolates. We suggest that this increase is owed to the decrease of these chocolates' particle size distribution due to the presence of Cocoa ($D_{50} = 2.6 \mu\text{m}$) since we showed in chapter 4 that yield increase when the particle size decreases. This increase could be moderated by the addition of an emulsifier in the system, a component that is far cheaper than fat.

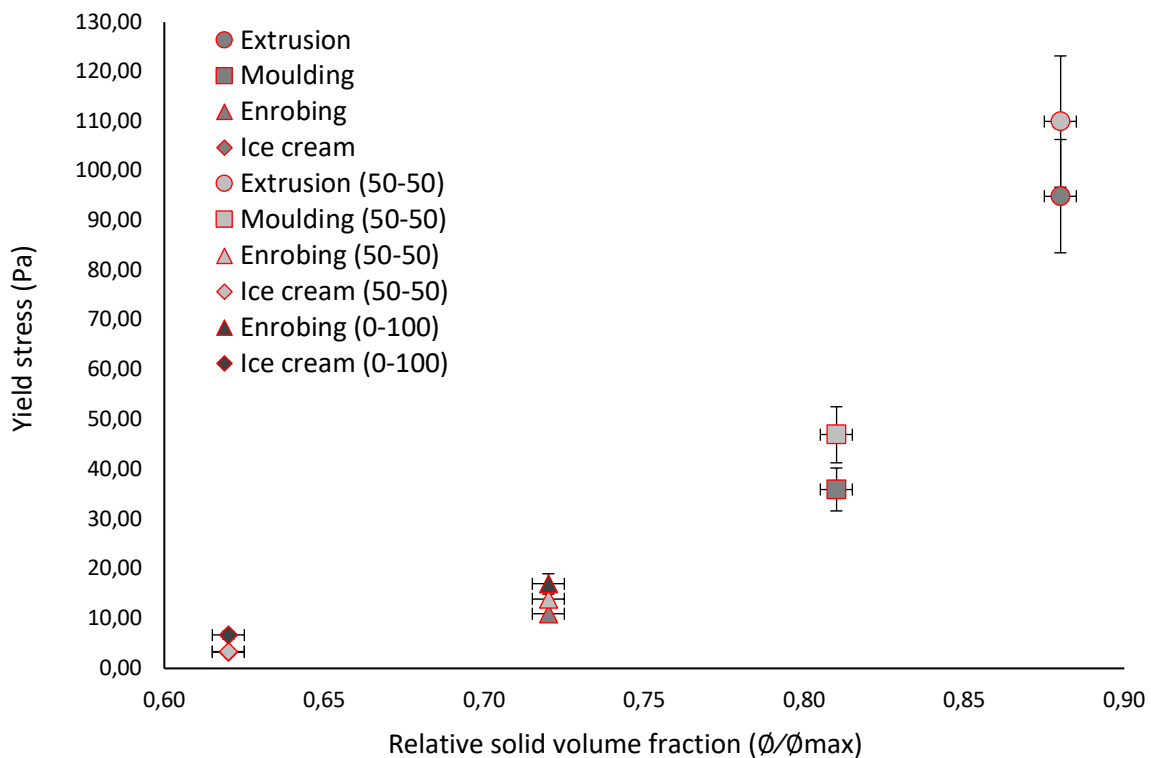


Figure 6-12. Measured yield stress as a function of the relative solid volume fraction of the reference dark chocolates (Extrusion, Moulding, Enrobing and Ice cream), reduced-fat chocolates (50-50) (Extrusion (50-50), Moulding (50-50), Enrobing (50-50) and Ice cream (50-50)) and reduced-fat chocolates (0-100) (Extrusion (0-100), Moulding (0-100), Enrobing (0-100) and Ice cream (0-100)).

Finally, by plotting the experimental relative mass loss of fat and the predicted relative mass loss of fat in Figure 6-13, we observe that they are in good agreement. All of these observations confirm what have been demonstrated in chapters 4 and 5 namely that it is possible to decrease the fat content of dark chocolate at constant viscosity by improving the maximum packing fraction. Moreover, the CPM allows to predict accurately the maximum packing fraction and therefore, the decrease in the fat content.

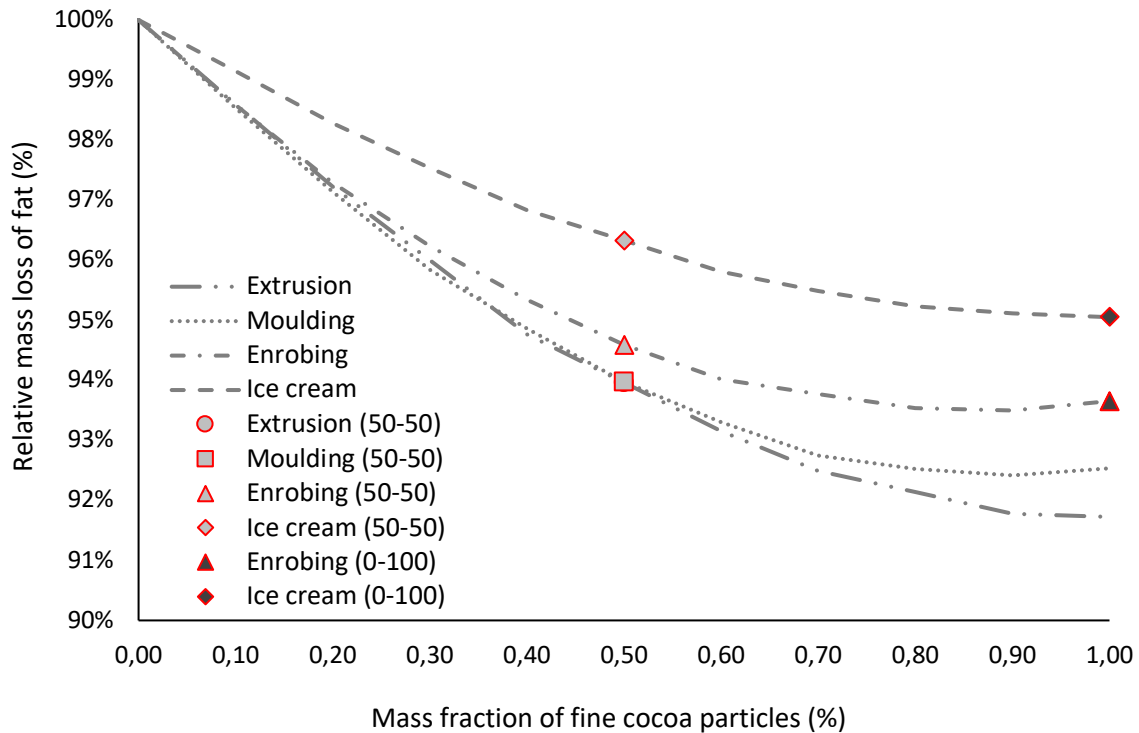


Figure 6-13. Predicted relative mass loss of fat of reference dark chocolates (Extrusion, Moulding, Enrobing and Ice cream) and experimental relative mass loss of fat of the reduced-fat dark chocolates (50-50) (Extrusion (50-50), Moulding (50-50), Enrobing (50-50) and Ice cream (50-50)) and the reduced-fat dark chocolates (0-100) (Enrobing (0-100) and Ice cream (0-100)).

6.3 Application 2: emulsifier free chocolate

This second project consists of the optimization of the particle size distribution of one reference dark chocolate (extrusion) by substituting “fine” sugar particles (Sugar ($D_{50} = 8.3 \mu\text{m}$)) by “coarse” sugar particles (Sugar ($D_{50} = 146 \mu\text{m}$)) and thus, increasing the maximum packing fraction. The particle size distribution of the solid particles used in this project is represented in Figure 6-14. We choose to only study extrusion as reference dark chocolate in this project because it is the only application in which the addition of coarse particles does not change the textural properties of the final product and the mouthfeel sensation of the

consumer. A representation of the optimization realised in this project is presented in Figure 6-15.

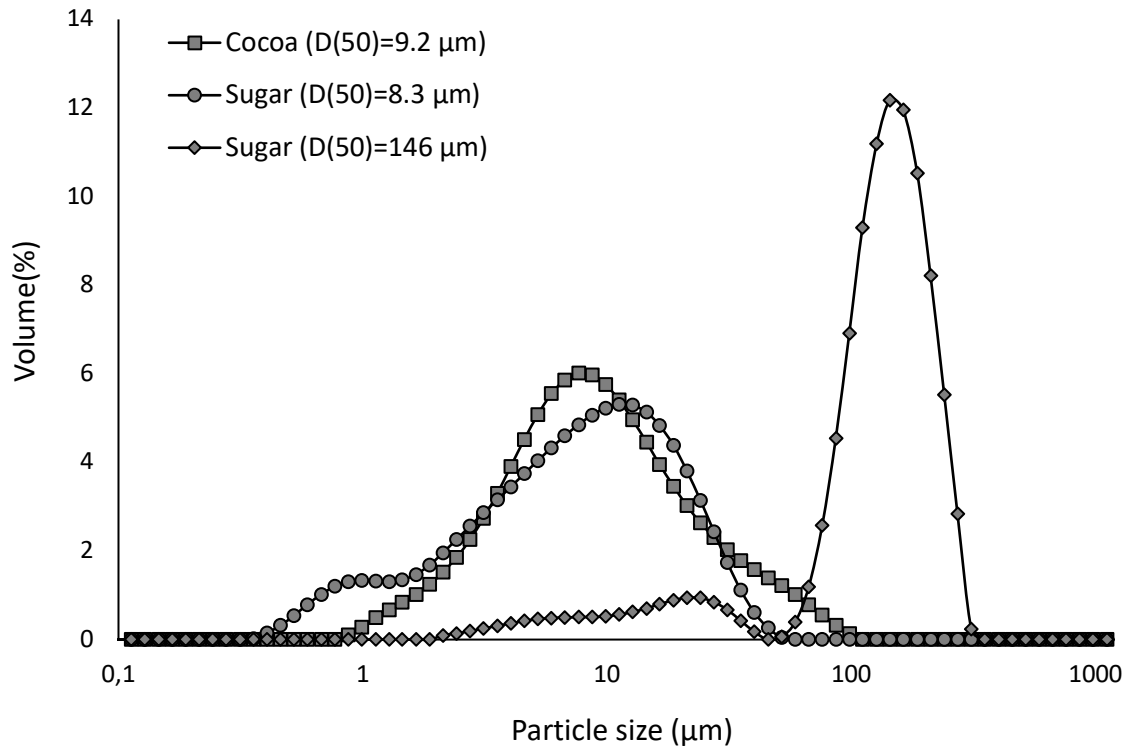


Figure 6-14. Particle size distribution of the particles used to produce emulsifier free chocolate.

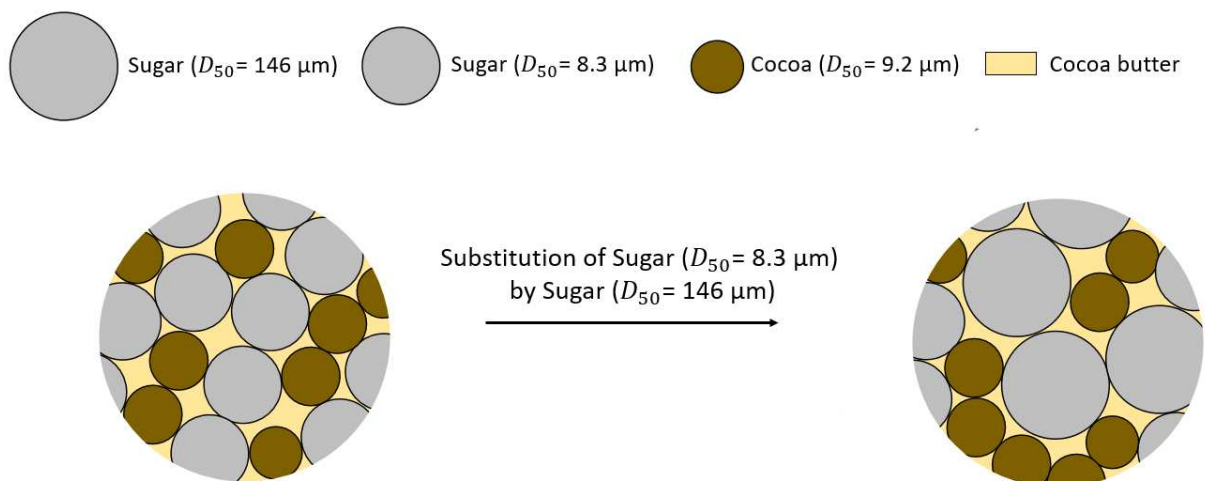


Figure 6-15. Representation of the substitution of fine sugar particles by coarse sugar particles in order to optimize the particle size distribution of the reference extrusion chocolate.

The first step of this project is the study of the effect of the addition of coarse sugar particles on viscosity and yield stress. To that end, we substitute 50% Sugar (D₅₀=8.3 µm) by Sugar

($D_{50} = 436 \mu\text{m}$). We should also specify that we do not keep the relative solid volume fraction constant between the reference extrusion chocolate and the substituted extrusion chocolate (i.e., we study both at the same solid volume fraction, $\phi = 0.63$) and that both reference and substituted extrusion chocolate contain the same amount of emulsifier (see Table 6-4). In the following, we will refer to the substituted extrusion chocolate and reference extrusion chocolate as Emulsifier-Extrusion (50-50) and Emulsifier-Extrusion respectively. The composition of both Emulsifier-Extrusion (50-50) and Emulsifier-Extrusion is presented in Table 6-4.

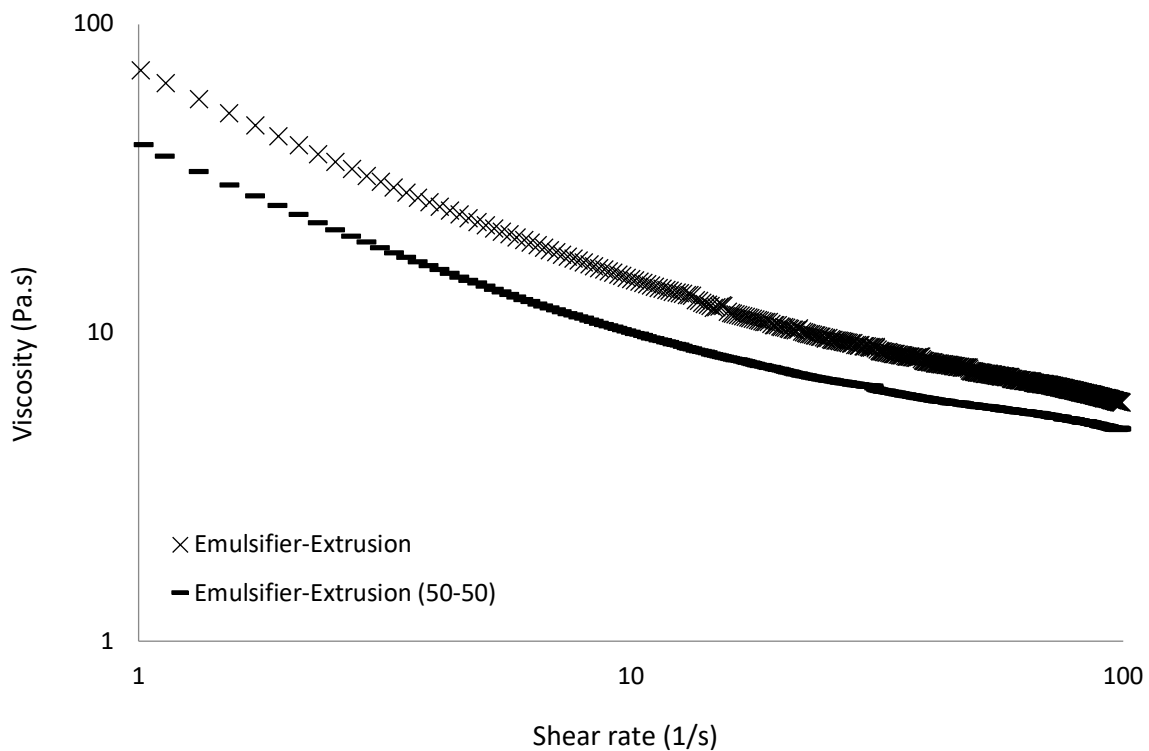


Figure 6-16. Flow curves of Emulsifier-Extrusion and Emulsifier-Extrusion (50-50).

We plot in Figure 6-16 the flow curve of Emulsifier-Extrusion (50-50) and Emulsifier-Extrusion. We observe that the addition of coarse sugar particles leads to a decrease of viscosity and yield stress for the same proportion of emulsifier. This observation suggests that it should be possible to formulate an emulsifier free extrusion chocolate having rheological properties as close as possible to those of reference extrusion chocolate by optimizing the particle size distribution of the reference extrusion chocolate.

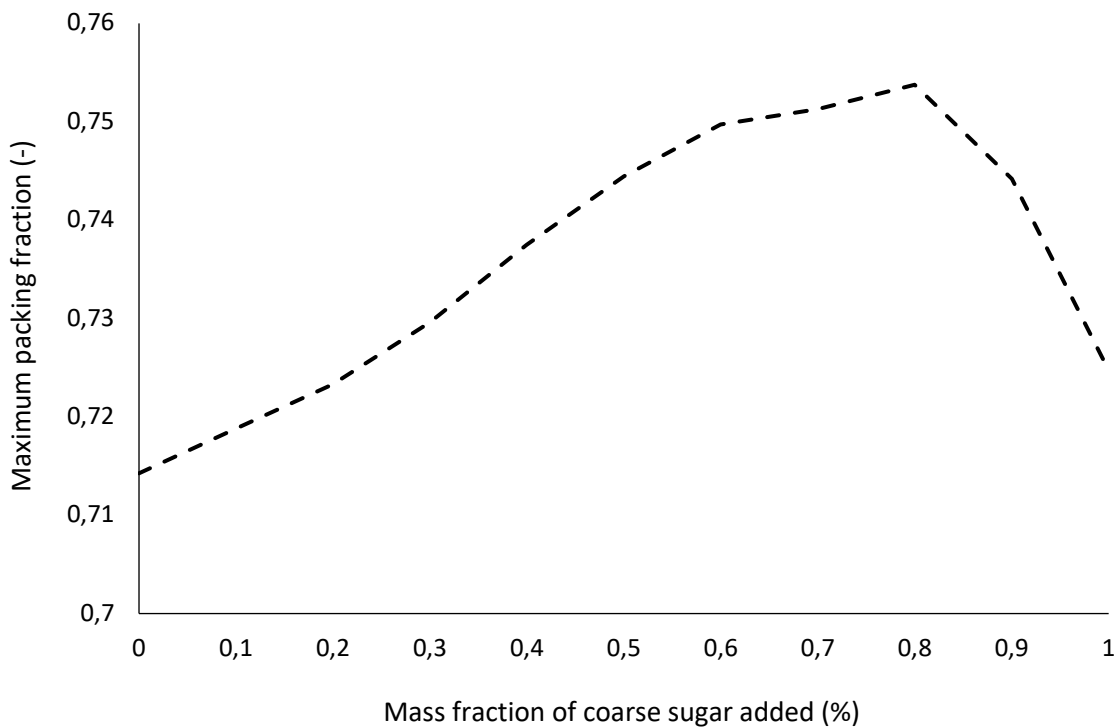


Figure 6-17. Evolution of the maximum packing fraction of reference extrusion chocolate in presence of Sugar ($D_{50}= 146 \mu\text{m}$) predicted by compressible model packing (CPM).

The second step of this project is the prediction of the evolution of the maximum packing fraction of reference extrusion (Emulsifier-Extrusion) chocolate when Sugar ($D_{50}= 8.3 \mu\text{m}$) is substituted by Sugar ($D_{50}= 146 \mu\text{m}$). We plot in Figure 6-17 the predicted maximum packing fraction as a function of the mass proportion of coarse sugar particles (Sugar ($D_{50}= 146 \mu\text{m}$)). We observe that there is an optimum when 80% Sugar ($D_{50}= 8.3 \mu\text{m}$) is substituted by Sugar ($D_{50}= 146 \mu\text{m}$). This optimum implies that the particle size distribution of reference extrusion chocolate is fully optimized when 80% of coarse particles is added. We thus study 3 emulsifier free chocolates: one composed of 80% Sugar ($D_{50}= 146 \mu\text{m}$) and 20% Sugar ($D_{50}= 8.3 \mu\text{m}$) by total mass of sugar particles, a second one composed of 60% Sugar ($D_{50}= 146 \mu\text{m}$) and 40% Sugar ($D_{50}= 8.3 \mu\text{m}$) and a last one composed of 40% Sugar ($D_{50}= 146 \mu\text{m}$) and 60% Sugar ($D_{50}= 8.3 \mu\text{m}$). We will refer to these 3 emulsifier free chocolates as Emulsifier Free-Extrusion (20-80), Emulsifier Free-Extrusion (40-60) and Emulsifier Free-Extrusion (60-40) respectively. The composition of the emulsifier free chocolates is summarized in Table 6-4.

Chapter 6: Industrial applications: formulation of reduced-fat content
chocolate and emulsifier free chocolate

	Cocoa ($D_{50}=9.2$ μm) (% by total mass)	Sugar particles (% by total mass)		Cocoa butter (% by total mass)	Lecithin (% by total mass)	Solid volume fraction (ϕ)	Predicted maximum packing fraction (ϕ_{max})	Relative mass proportion of solid particles $\left(\frac{\text{mass}_{\text{cocoa}}}{\text{mass}_{\text{sugar}}}\right)$	Predicted relative solid volume fraction $\left(\frac{\phi}{\phi_{\text{max}}}\right)$
		Sugar ($D_{50}=8.3$ μm)	Sugar ($D_{50}=146$ μm)						
Emulsifier - Extrusion	15.2	58.6	0	25.8	0.5	0.63	0.72	0.26	0.88
Emulsifier- Extrusion (50-50)	15.2	29.3	29.3	25.8	0.5	0.63	0.74	0.26	0.85
Emulsifier Free- Extrusion (60-40)	15.2	35.3	23.5	26	0	0.63	0.74	0.26	0.85
Emulsifier Free- Extrusion (40-60)	15.2	23.5	35.3	26	0	0.63	0.75	0.26	0.84
Emulsifier Free- Extrusion (20-80)	15.2	11.8	47	26	0	0.63	0.75	0.26	0.83

Table 6-4. Composition of the Emulsifier-Extrusion (Emulsifier-Extrusion and Emulsifier-Extrusion (50-50)) chocolates and the Emulsifier Free-Extrusion (Emulsifier Free-Extrusion (20-80), Emulsifier Free-Extrusion (40-60) and Emulsifier Free-Extrusion (60-40)) chocolates.

The final step of this project is the measurement of the rheological properties of the Emulsifier-Extrusion (Emulsifier-Extrusion (50-50) and Emulsifier-Extrusion) chocolates and the Emulsifier Free-Extrusion (Emulsifier Free-Extrusion (20-80), Emulsifier Free-Extrusion (40-60) and Emulsifier Free-Extrusion (60-40)) chocolates. We plot in Figure 6-18 the viscosity and yield stress as a function of the relative solid volume fraction of these chocolates.

As expected, we observe that both Emulsifier Free-Extrusion (60-40) and (40-60) samples exhibit higher viscosity and yield stress compared to those of the reference extrusion chocolate (Emulsifier-Extrusion) since they are not containing emulsifier. These results suggest that the substitution of 40% or 60% fine sugar by coarse sugar is not sufficient to compensate the absence of emulsifier.

Chapter 6: Industrial applications: formulation of reduced-fat content chocolate and emulsifier free chocolate

However, we note that for Emulsifier Free-Extrusion (20-80), the viscosity remains unchanged and the yield stress decrease compared to the viscosity and yield stress of the reference extrusion chocolate (Emulsifier-Extrusion). This results suggest that the substitution of 80% fine sugar by coarse sugar is more than sufficient to compensate the absence of emulsifier.

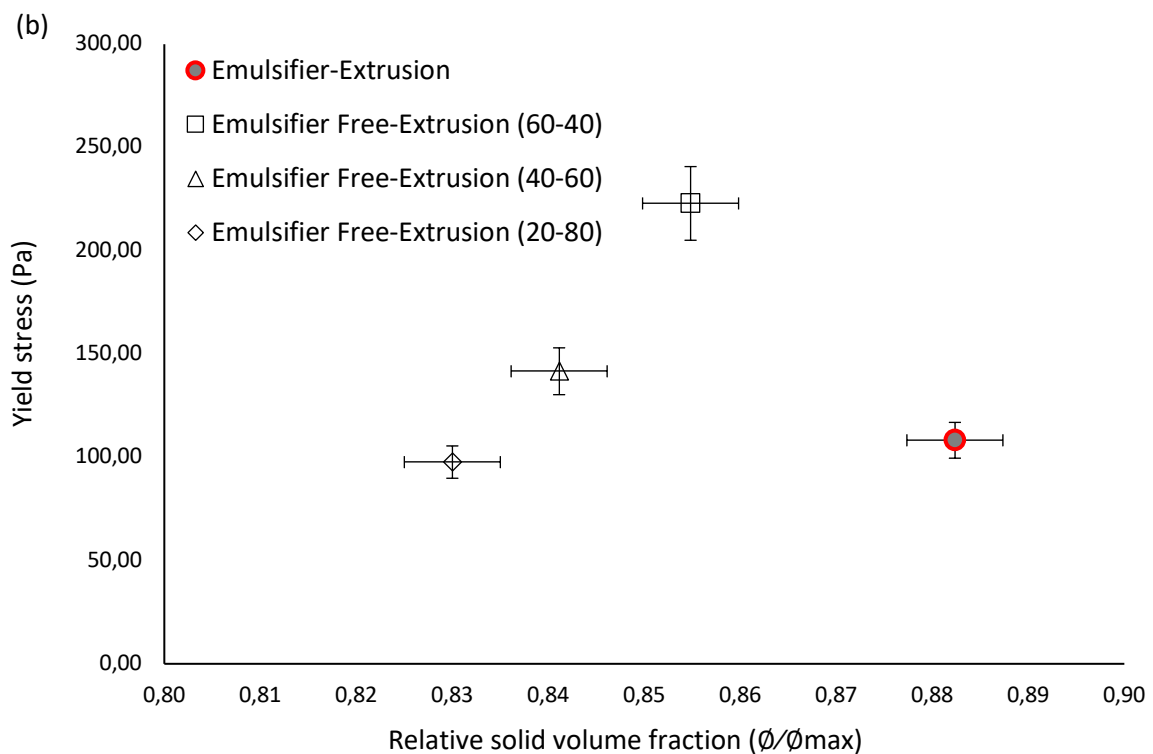
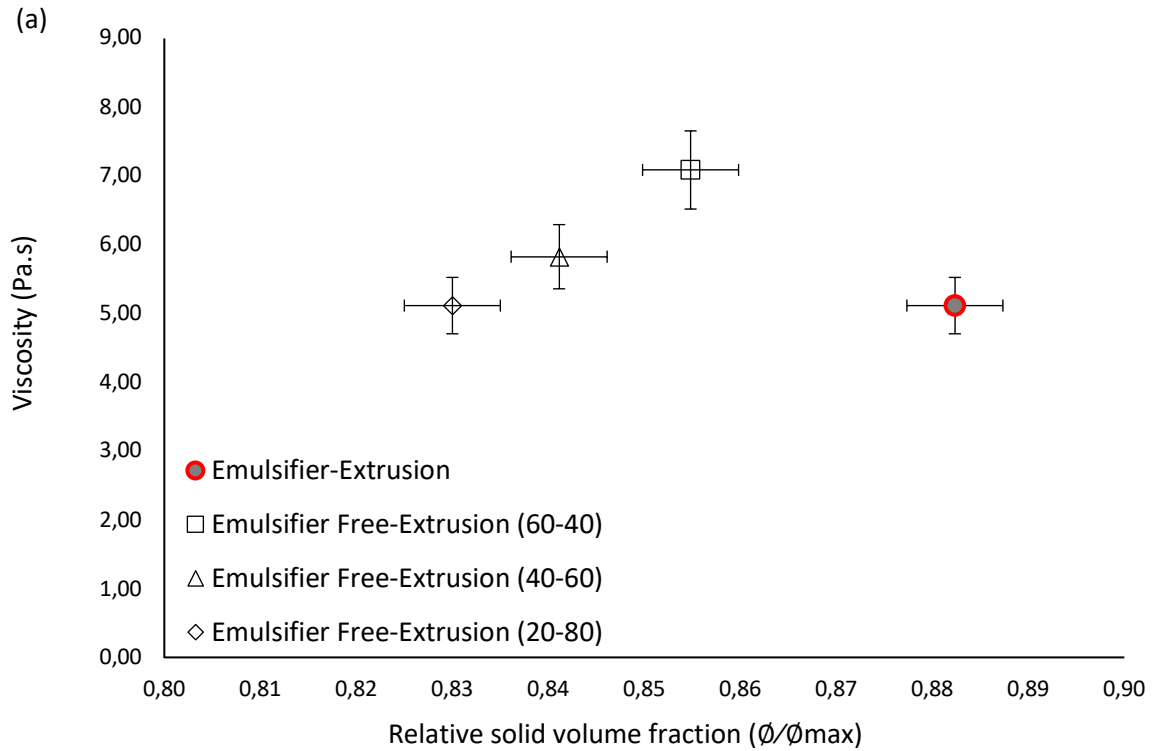


Figure 6-18. (a) Measured viscosity and (b) measured yield stress as a function of the relative solid volume fraction of the Emulsifier-Extrusion (50-50) and the Emulsifier Free-Extrusion (Emulsifier Free-Extrusion (20-80), Emulsifier Free-Extrusion (40-60) and Emulsifier Free-Extrusion (60-40)) chocolates.

6.4 Correlation between the viscosity and relative solid volume fraction of the reduced-fat chocolates, emulsifier free chocolates, sugar suspensions, sugar and cocoa suspensions cocoa suspensions and commercially available dark chocolates

We compare in this section the measured viscosity of sugar suspensions, sugar and cocoa suspensions, cocoa suspensions, reduced-fat chocolates, emulsifier free chocolates, and commercially available dark chocolates (i.e., Jacques, Delicata and 365 Essential). The composition and properties of the 3 dark chocolates are summarized in Table 6-5.

We recall that sugar suspensions, sugar and cocoa suspensions, cocoa suspensions have been studied in chapter 3 and 4.

We conclude from this figure that the viscosity of the suspensions studied in the two projects depend on the relative solid volume fraction and can be predicted by Krieger-Dougherty equation as the viscosity of the suspensions studied in chapters 3 and 4. Regarding the dark chocolates purchased in supermarket, we observe that the viscosity of Delicata is perfectly following the master curve suggesting that the master curve highlighted in this thesis can be applied to industrial dark chocolates found in supermarket. However, we observe that the viscosities of Jacques and 365 Essential are lower than the other viscosities. We suggest that a wrong estimation of the solid volume fraction of Jacques and 365 Essential as well as the presence of lecithin could explain the fact that the viscosities of Jacques and 365 Essential are lower. Indeed, we estimate the solid volume fraction of Jacques, Delicata and 365 Essential from the imprecise information about the mass proportions of the ingredients on their packaging.

Chapter 6: Industrial applications: formulation of reduced-fat content
chocolate and emulsifier free chocolate

Samples	Jacques	Delicata	365 Essential
Sugar particles (%by total mass)	48.3	41.6	49.8
Cocoa particles (%by total mass)	19.8	21.5	17.7
Cocoa butter (%by total mass)	31.4	36.4	32
Lecithin (%by total mass)	0.51	0.51	0.51
Solid volume fraction (ϕ)	0.57	0.52	0.56
Maximum packing fraction ($\phi_{max} (\pm 0.005)$)	0.64	0.64	0.67
Relative solid volume fraction	0.89	0.81	0.84
Measured viscosity (Pa.s)	2.68	1.70	2.57
Measured yield stress (Pa)	50.7	24.1	35.9

Table 6-5. Composition of the 3 dark chocolates (Jacques, Delicata and 365 Essential) bought in supermarket.

Chapter 6: Industrial applications: formulation of reduced-fat content chocolate and emulsifier free chocolate

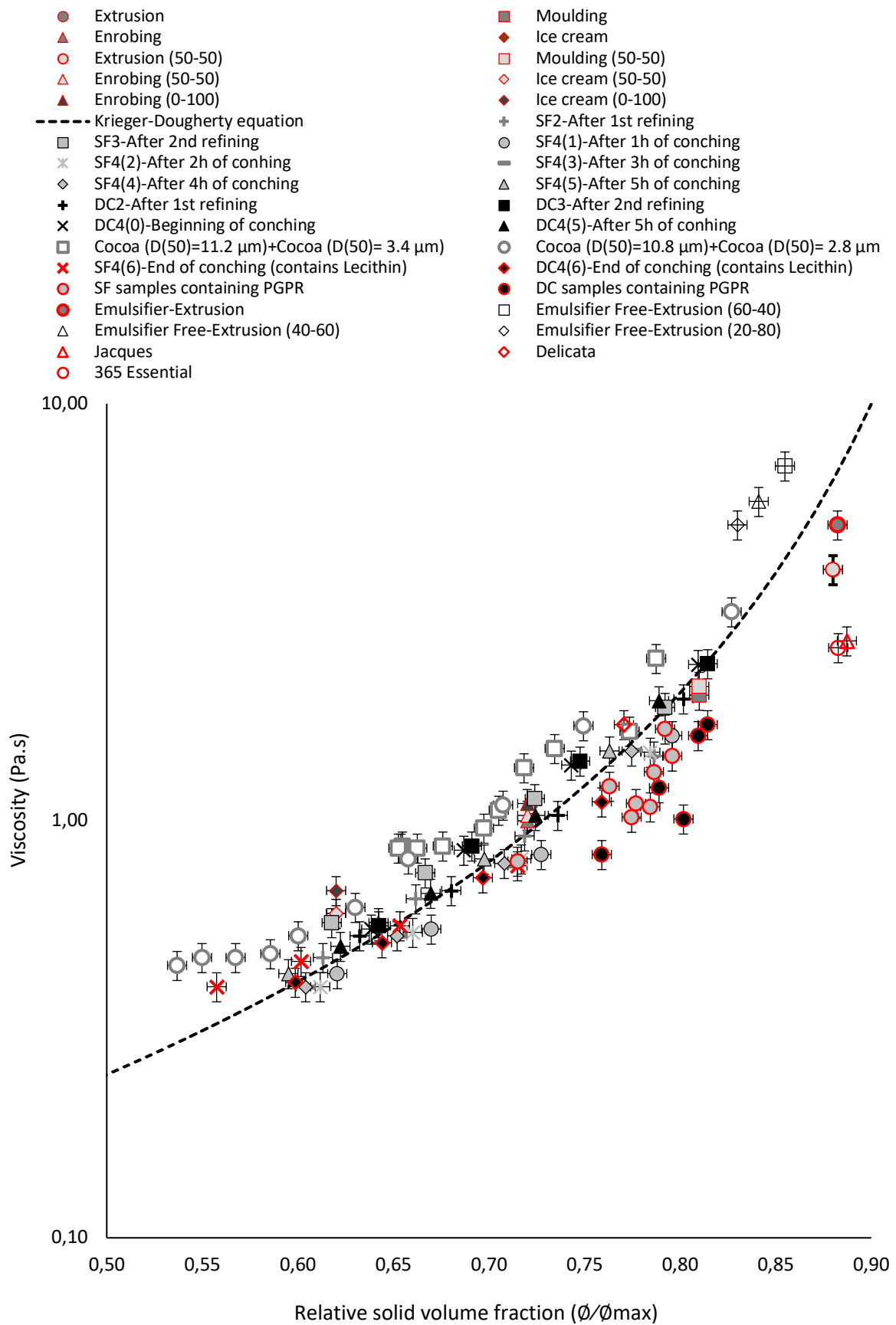


Figure 6-19. Measured viscosity as a function of the relative solid volume fraction of sugar (sweet fat) suspensions, sugar and cocoa (dark chocolate) suspensions, cocoa (Cocoa ($D_{50}= 11.2 \mu\text{m}$) + Cocoa ($D_{50}= 3.4 \mu\text{m}$) and Cocoa ($D_{50}= 10.8 \mu\text{m}$) + Cocoa ($D_{50}= 2.8 \mu\text{m}$)) suspensions, the reference dark chocolates (Extrusion, Moulding, Enrobing and Ice cream), the reduced-fat chocolates (Extrusion (50-50), Moulding (50-50), Enrobing (50-50), Ice cream (50-50), Enrobing (0-100) and Ice cream (0-100)), the Emulsifier-Extrusion, the emulsifier free chocolates (Emulsifier Free-Extrusion (20-80), Emulsifier Free-Extrusion (40-60) and Emulsifier Free-Extrusion (60-40)) and the supermarket dark chocolates (Jacques, Delicata and 365 Essential).

6.5 Conclusion

We have demonstrated in this chapter that it is possible to decrease the fat content of chocolate suspension while keeping the viscosity constant by optimizing the particle size distribution of chocolate suspension through the addition of fine cocoa particles. We have also demonstrated that the addition of these fine particles leads to an increase of the yield stress that can be moderated by the addition of emulsifier.

We have showed in this chapter that emulsifier free chocolate can be formulated while keeping the viscosity unchanged by adding coarse sugar particles to optimize the particle size distribution of chocolate suspension. The addition of coarse sugar particle leads to a decrease of the yield stress.

Finally, we have showed that the viscosity of all chocolate suspensions studied in this thesis depends on the relative solid volume fraction and can be predicted by Krieger-Dougherty equation.

Conclusions and Perspectives

Conclusions and Perspectives

We have showed in this thesis that the rheological behaviour of melt chocolate can be tuned through an accurate control of the morphological and packing properties of sugar and cocoa powder.

In the first chapter, we have described the interactions within chocolate suspensions, the parameters governing the rheological behaviour of chocolate suspensions and the effect of other components such as water and emulsifier on the rheological behaviour. We have also presented the main production processing steps.

In the second chapter, we have described the experimental protocols developed to study the morphological, physical and rheological properties of the chocolate suspensions. We have showed that the envelope density of cocoa particles can be determined by a drying-protocol measurement. By means of laser granulometry, we have also showed that the particle size distribution of binary mixture such as chocolate suspensions must be measured using an average of the optical indexes of both cocoa and sugar solid particles and only in a deflocculated state. Moreover, we have used centrifugational loading to measure the maximum packing fraction of our deflocculated materials and proposed a protocol, which limits the particle size separation artefact. Finally, we have showed that the thixotropic behavior of chocolate suspensions can be neglected with the developed rheological protocol and that Bingham equation can be used to accurately fit the measured flow curves.

In the third chapter, we have studied the effect of the production process on particle size distribution, particle shape, maximum packing fraction and rheological behavior of sugar and cocoa suspensions (representative of a chocolate suspension) and sugar suspensions. We have also studied the effect of grinding on particle size distribution, particle shape, maximum packing fraction and rheological behavior of cocoa mass.

We have demonstrated that the refining process leads to a decrease in both the mean particle size and maximum packing fraction of both model suspensions. We have also showed that the conching process do not influence the particle size distribution but leads to an increase in the maximum packing fraction and, therefore, to a decrease in viscosity and yield stress.

By comparing the evolution of the particle size distribution of dark chocolate and sugar over the process, our results have suggested that only the particle size distribution of sugar evolve through the production process while the particle size distribution of cocoa remains roughly constant.

Finally, we have demonstrated that the presence of lecithin and water in the system can also influence the rheological parameters of the samples over the production process. Indeed, the addition of lecithin at the end of the process has led to a decrease of both yield stress and viscosity (that still needs to be further elucidated) while the evaporation of water during the process has contributed to the decrease of both yield stress and viscosity.

In the fourth chapter, we have demonstrated that the rheological parameters of all suspensions studied in chapter 3 (sugar suspensions and sugar and cocoa suspensions) are well correlated to the morphological ones over the production process. We also correlated the morphological and rheological properties of cocoa suspensions that were subjected to a grinding process.

Our results have showed that the viscosity of these suspensions is mainly governed by viscous hydrodynamic dissipations. We have demonstrated that the viscosity depends only on the relative solid volume fraction and can be predicted by Krieger-Dougherty equation.

The yield stress of sugar suspensions, cocoa suspensions and sugar and cocoa suspensions also depends on the solid volume fraction on maximum packing fraction ratio but is inversely proportional to the suspension particles mean diameter.

Finally, we have showed that the evolution of viscosity during the production process can only be explained by the evolution of maximum packing fraction. Moreover, we have showed that the evolution of yield stress during the production process can be explained by the evolution of maximum packing fraction along with particle size.

In the fifth chapter, we have demonstrated that the compressible packing model can be used to predict the maximum packing fraction of chocolate products. Indeed, there is an accuracy of 98% between the maximum packing fraction predicted by the model and the experimental packing fraction measured by centrifugation. The validation of this theoretical model has allowed for the prediction of the maximum packing fraction of different material powders combinations and for the optimization of particle size distribution in order to decrease the quantity of fat without changing the rheological behaviour. We have also demonstrated that the highest maximum packing fractions are reached when fine cocoa particles and/or coarse sugar particles are added into sugar and cocoa suspensions.

In the sixth and final chapter, we have demonstrated that it is possible to decrease the fat content of chocolate suspension while keeping the viscosity constant by optimizing the particle size distribution of chocolate suspension through the addition of fine cocoa particles. We have also demonstrated that the addition of these fine particles leads to an increase of the yield stress that can be moderated by the addition of emulsifier.

We have showed that an accurate control of particle mean size and maximum packing fraction by adding coarse sugar particles allows for the removal of the emulsifiers from chocolate without increasing the fat content of the suspension and without affecting the viscosity and yield stress.

As a perspective of this work, it would be interesting to incorporate finer particles in order to further decrease the fat amount of chocolate suspensions. It would also be interesting to study white and milk chocolates, which contain soft and deformable dairy products. Moreover, studying how these dairy products influence the maximum packing fraction and the rheological behaviour would be essential.

In this work, we have chosen to only focus on cocoa and sugar particles and have thus not studied the impact of other food powders on the optimization of the maximum packing fraction of chocolate. Finding other food powders that can be incorporated in chocolate to optimize their packing fraction would be another way for formulating reduced-fat chocolate or emulsifier free chocolate.

Finally, studying the shape of the particles by imaging and correlating them with the shape parameter obtained from the Compressible Packing Model should also be interesting in order to confirm the results of this thesis. It would also be important to complete this work by studying the mechanism of action of emulsifiers and the consequences of their presence on the morphological and rheological properties of chocolate.